THE UNIVERSITY OF CHICAGO

ROLE OF TRANSCRIPTION FACTORS AND INTERCALATED DISC PROTEINS IN ARRHYTHMOGENESIS

A DISSERTATION SUBMITTED TO

THE FACULTY OF THE DIVISION OF THE BIOLOGICAL SCIENCES

AND THE PRITZKER SCHOOL OF MEDICINE

IN CANDIDACY FOR THE DEGREE OF

DOCTOR OF PHILOSOPHY

INTERDISCIPLINARY SCIENTIST TRAINING PROGRAM:

BIOPHYSICAL SCIENCES

BY

WENLI DAI

CHICAGO, ILLINOIS

AUGUST 2020

Table of Contents

List of Figures

Acknowledgements

I would like to thank my thesis advisor, Dr. Christopher Weber for being a fantastic mentor throughout the past four years. He has been tremendously supportive and provided invaluable mentorship in scientific thinking and writing, conducting experiments, and career guidance. Further, I'm grateful for the opportunity to have worked with Dr. Weber because it has truly been a fun experience.

I would also like to thank my second thesis advisor, Dr. Francisco Bezanilla, and my thesis committee members, Dr. Eric Beyer and Dr. Ivan Moskowitz, for their continued support through the course of my graduate studies. I am very thankful that each of you has welcomed me into your own labs, helped to improve my science and shape my PhD experience.

A big thank you to my lab mates, especially Dr. Le Shen for being a tremendous mentor, Dr. Ye Li for all of her help and her friendship, Dr. Elizabeth Lee for being a tremendous friend and graduate school guide, Dr. Rajiv Nadadur, for being a friend and mentor on many of these projects. I'm also grateful to my programs the ISTP and the Biophysics program, especially Dr. Alison Anastasio, Dr. Kristin McCann, Dr. Michele Wittels, and Dr. Juliana Feder for their support throughout my time and helping to make sure everything went as smoothly as it possible could.

Finally, I couldn't have done this without the support of my friends and family. I'm deeply grateful for my parents, Dr. Songtao Dai and Jixian Zhang for all of their sacrifices to allow me to be where I am today. I owe my interest in science and medicine to them. I'm also extremely thankful for, Dr. Brett Aiello, for being the most supportive, kind, and loving partner I could ask for.

Abstract

Healthy cardiac conduction and function relies on the coordinated electrical activity of distinct populations of cardiomyocytes. Disruption of cell-cell conduction results in cardiac arrhythmias and cardiomyopathies, a leading cause of morbidity and mortality worldwide. We investigated the mechanisms of arrhythmia formation from several angles. Recent genetic studies have highlighted a major heritable component and identified numerous loci associated with risk of arrhythmias such as atrial fibrillation, including transcription factor genes *TBX5* and *GATA4*. We defined a novel calcium-dependent mechanism of atrial fibrillation following transcription factor *Tbx5* insufficiency. We then examined the coregulatory relationship between *Tbx5* and *Gata4* in maintaining atrial rhythm and found that AF pathophysiology caused by *Tbx5* haploinsufficiency, including was rescued by *Gata4* haploinsufficiency. In addition to transcription factors, many other proteins, particularly those important for electrical and physical coupling between cells can regulate cardiac conduction. We show inducible loss of the intercalated disc protein ZO-1 in cardiomyocytes of adult mice impedes AV node conduction and modestly affects ejection fraction.

Chapter I: Introduction

Cardiac arrhythmias and their societal impact

Cardiac arrhythmia, or abnormal rhythm, is a common and dangerous condition that is associated with numerous negative outcomes including stroke, myocardial infarction, and death[1, 2]. Our understanding of arrhythmias has grown tremendously over the past few decades with the advent of new technologies such as genome wide association studies (GWAS) to identify potential genes that regulate processes involved in arrhythmia development, followed by use of transgenic animal models to examine the mechanistic underpinnings of genetic regulation[3]. However, there is tremendous complexity in the genetic regulatory networks and their consequences on cardiomyocyte action potential generation, calcium handling, and cell-cell communication. By dissecting this complex network and examining in depth the role of individual players as well as their interplay, we aim to develop a deep understanding of how cardiac rhythm is maintained and conversely, how and why arrhythmias occur. Addressing gaps in knowledge in disease mechanisms will be critical to guide the development of more effective arrhythmia therapeutics.

The heart is a unique organ because it is composed of cells, cardiomyocytes, connected in a functional syncytium which allows for rapid and coordinated conduction of electrical signal, which then drives contraction[4, 5]. Within the heart, specialized cells in the conduction system generate spontaneous action potentials, a property referred to as automaticity. Not all conduction cells have the same rate of action potential generation, which enables depolarization of the heart to occur in an organized and unidirectional manner[6, 7]. In a normal rhythm cycle (sinus rhythm), depolarizing signal is initiated at the sinoatrial (SA) node, which has the highest rate of automaticity, travels through the atria, arrives at the atrioventricular node, where there is a delay,

through the His-Purkinje fibers (which has the lowest rate of automaticity), and ending in ventricular depolarization[8]. The timing and sequence of depolarization in conduction system cells determine the rate and rhythm of atrial and ventricular contractions. Arrhythmias can occur when any part of the conduction pathway is disrupted. For example, loss of conduction within the SA node, which serves as the pacemaker of the heart, can result in slowed heart rate, bradyarrhythmias, while loss of conduction within the AV node can result in prolongation of the delay between atrial and ventricular depolarization[9]. Further, if the SA node is functionally compromised and has decreased automaticity, other regions of the conduction system can take over as the main pacemaker, leading to abnormal patterns of depolarization[10]. Since there are many mechanisms that can underlie the development of cardiac arrhythmias, there is a diversity of clinical presentations including abnormally slow heart rate, bradyarrhythmias, abnormally fast heart rate, tachyarrhythmias and irregular rhythms such as skipped, premature or extra beats.

Atrial fibrillation overview

Cardiac arrhythmias are often characterized by their location as atrial and ventricular arrhythmias as they can have different presentations and treatments. Atrial arrhythmias include atrial fibrillation (AF), atrial flutter, sick sinus syndrome, and sinus tachycardia and bradycardia, of which atrial fibrillation is the most common, affecting more than 33 million people worldwide[2, 8]. AF is characterized by rapid and irregular electrical activity, resulting in incomplete and asynchronous contractions, which prevent blood in the atria from fully emptying into the ventricle. Increased dwell time of blood within the atria results in increased likelihood of thrombi formation, leading to stroke, myocardial infarction, and heart failure. AF presents a significant challenge to the health care industry as it complicates overall health care management and can increase a patient's treatment cost five-fold[11]. On average, the cost per patient in the first

year following their AF diagnosis was in the order of 18,000 dollars and the total annual cost to treat AF patients in the US is on the order of 26 billion dollars[2, 12]. AF is a highly significant and growing public health concern.

Treatments for atrial fibrillation generally begins with anti-arrhythmic drugs to control the rate and rhythm of the heart along with anti-coagulants to prevent stroke. The efficacy of anti-arrhythmic drugs is significantly increased if it is administered immediately after the onset of AF and at a high dosage [13]. If the AF cannot be kept under control pharmacologically, usually if the patient has experienced AF longer than 7 days, cardioversion and ablation therapy are the next line of treatments[14, 15]. Cardioversion consists a discharge of electrical current to simultaneously depolarize all cardiomyocytes during the QRS complex in order to restore sinus rhythm and is often coupled with anti-arrhythmic drugs[16]. In ablation treatment, the AF focal points are identified and removed by applying extreme heat or cold to induce scarring[14]. However, these treatments are often not long-term solutions and the side effects can be severe. For example, a significant side effect of anti-arrhythmic drugs is an increased chance of ventricular arrhythmias, which can be immediately life-threatening, particularly in cases where patients develop coronary artery disease or heart failure in addition to the AF[17]. The complication rate for ablation therapy remains between 2-4%, and complications include perforation resulting in cardiac tamponade, emboli formation, vasculature damage, and creation of new reentry circuits leading to atrial flutter[18, 19]. Further, some patients eventually do not respond to either pharmacologic treatments or ablation[20]. At the moment, there is still a knowledge gap that limits the ability to personalize a treatment course to the individual patient. One of the main barriers in the betterment of AF therapies is the limited understanding of the mechanisms underlying AF and the ability to identify the specific causes of disease in an

individual patient[21]. By connecting genetic data with mechanistic insight and clinical trials, we hope to increase the potential improved treatments.

While the studies that follow do not directly examine ventricular arrhythmias, it is important to note that ventricular fibrillation is considered one of the most severe rhythm disorders. Ventricular fibrillation, like AF is characterized by irregular electrical activity and incomplete contraction. However, since ventricular contraction is required to supply blood to the body, ventricular fibrillation is an emergency. The mechanisms underlying ventricular fibrillation continues to be a topic of extensive study.

Trigger mechanisms in arrhythmias

Much work has been done to understand the cellular mechanisms that underlie cardiac arrhythmias, and in our current understanding, arrhythmias are characterized by the presence of an abnormal myocardial substrate and formation of an ectopic trigger. Abnormal substrate refers to altered electrical conduction between cardiomyocytes. Ectopic trigger refers to initiation of electrical activity at regions outside of the sinoatrial node. Reentry loops occur with increased frequency when there is both a substrate and trigger. The development of reentry circuits is prevented in healthy cardiac tissue by the brief inactivation of cells immediately after activation, forcing depolarization to occur in the forward direction. This inactivation time is known as a refractory period. However, when obstacles are present that block forward conduction, the depolarizing wave front may circle back around to reactivate the initial area after the refractory period ends, creating a reentry circuit[8, 22, 23].

Ectopic triggers are predominantly caused by abnormal depolarization of a cardiomyocyte during the action potential. The action potential of a cardiomyocyte is dependent on its location, but overall, there are several unifying characteristics. At the beginning of each

depolarization cycle, cardiomyocytes are at a resting membrane potential. During phase 0 of the action potential, there is a rapid influx of sodium ions results in a fast depolarization, which is then followed by repolarization stages during which there is a balance between potassium ions leaving the cells (repolarizing current) and calcium and sodium entry into the cell, depolarizing current. Over the course of repolarization, sodium and calcium channels inactivate, and potassium current becomes dominant and the cell returns to its resting membrane potential[24]. Membrane depolarization is coupled to cardiomyocyte contraction via the second messenger calcium in a process referred to as excitation-contraction coupling. Initial depolarization of the cell by sodium influx triggers the opening of voltage-gated L-type calcium channels, allowing extracellular calcium to flow down a steep electrochemical gradient into the cell. This initial calcium entry is sensed by ryanodine receptors, and triggers release of a large burst of calcium from the sarcoplasmic reticulum into the cytosol via a calcium induced calcium release mechanism. Free intracellular calcium binds to troponin C, thus removing myosin inhibition and allowing for contraction to occur. During the relaxation phase, calcium must be removed from the cytosol through return into the sarcoplasmic reticulum through SERCA protein or extrusion from the cell through sodium calcium exchanger at the plasma membrane. Decrease of intracellular calcium triggers dissociation of calcium from troponin C, reversing contraction[25]. The flux of calcium into and back out of the cytosol is called a calcium transient, and the rising and falling phases follow the action potential depolarization and repolarization.

Ectopic activity is often categorized into early afterdepolarizations (EADs) and delayed afterdepolarizations (DADs). EADs are characterized by the slowing or reversing of repolarization during the plateau or repolarization phase (phases 2 and 3), with phase 2 EADs being more commonly associated with prolonged APs. Increased depolarization drive, decreased

repolarization drive, or a combination of both during the plateau phase of the AP can promote EAD formation. High depolarization drive can be caused by increases in late sodium, L-type calcium, or inward NCX current while reduced repolarization drive can be caused by decreased potassium currents. Often, increase in depolarizing force from one source causes a positive feedback loop that promotes continued depolarization. For example, depolarization via late sodium current can reopen L-type calcium channels, which results in further depolarization and higher calcium levels in the cytosol, which leads to increased activity of NCX[26, 27]. EADs can occur in the context of shortened APs if intracellular calcium concentration is high when the membrane has repolarized to the equilibrium potential for NCX, driving calcium extrusion and sodium influx into the cells, resulting in depolarization[28]. In contrast to EADs which occur during phase 2 and 3 of repolarization, DADs occur after the cardiomyocyte has fully repolarized. Similar to EADs associated with short APDs, DADs are thought to be triggered by high intracellular calcium levels coupled with spontaneous calcium release from the sarcoplasmic reticulum, leading to activation of NCX, nonselective cationic channels, calcium activated chloride channel, with NCX being the predominant contributor to depolarization[23, 29].

EADs and DADs are associated with triggered activity, or the generation of abnormal spontaneous action potentials. In dog Purkinje fibers, phase 2 EADs could propagate to neighboring cells with shorter action potentials, triggering either an EAD or a triggered event[30]. In canine atrial preparations, late phase 3 EADs were observed to induce triggered activity with takeoff potentials between -60 and -75mv[31]. EAD triggered APs can occur either in the original cardiomyocyte through reactivated L-type calcium and inward NCX mediated AP upstroke, or in neighboring cells at their resting membrane potential through activation of fast sodium channels. “EAD islands” can also be created due to coupling between cells such that at a small distance

coupled cells share the same AP characteristics, but synchronization decreases over distance. When EADs trigger APs within these EAD islands, these APs may propagate into neighboring regions to trigger EADs in those regions[32].

Substrate mechanisms in arrhythmias

As previously mentioned, cardiac myocardium forms a syncytium in which individual cells are tightly coupled to its neighboring cells. This serves as a critical mechanism by depolarizing current from an EAD or DAD from one cell is distributed across many neighboring cells, preventing, thus diluting its potential to prevent repolarization in a large group of cells, a concept called source-sink mismatch[32, 33]. Thus, in order to generate a spontaneous depolarization of a 2D tissue nearly 7000 contiguous EAD-generating cardiomyocytes would be necessary. However, in cases when there is a substrate for reentry present, only 40 EAD generating cells would be required[34, 35]. Examples of arrhythmogenic substrate include reduced conduction speed via decreased gap junction conductance, intercalated disc abnormalities, fibrosis, reduced repolarization reserve, and any structural and functional obstacles that impede propagation in the appropriate path[36]. Several studies have shown loss of connexins and other intercalated disc proteins result in decreased conduction velocity[37]. Additionally, functional obstacles could include changes that alter conduction or refractoriness properties of the tissue through the presence of EADs and DADs. For example, low-level depolarization of the membrane by DADs can inactivate sodium channels, leading to inactivated regions dispersed among excitable neighboring cells, creating a local conduction block. EADs and prolonged action potentials may result in heterogeneity of the refractory period, also promoting local conduction block[38]. These examples demonstrate that triggers and substrates may not be separate, but rather pathologic changes such as calcium handling alterations can serve as both.

Genetic basis for atrial fibrillation

Work beginning nearly eight decades ago has generated a body of literature demonstrating a role of genetics in atrial fibrillation[3, 39]. In fact, if a patient has AF, there is over a thirty percent chance that they will also have at least one close relative who also has arrhythmias[40-42]. The earliest studies were in families where AF, but not heart disease was commonly found. Using linkage studies, a number of genetic loci have been identified, including in KCNQ1, KCNE1, KCNJ,GJA,CNAN,SCN5,SCN10,CACNA,NPPA[43]. Most of these genes encode for ion channels or junctional channels, with the exception of atrial natriuretic peptide precursor. While these mutations had a strong effect in individuals, they were often rare mutants, which made determining their relevance to the general population difficult to ascertain. With the advent of GWAS technology, a new perspective on the role of genetic modulation of AF risk was beginning to take form. Using GWAS methods, the whole genome could be surveyed in a large population of people to identify loci that had lower effect size, but were more prevalent in the population. Subsequently, several key ideas were generated. First, a new class of genetic loci important in AF development was identified: developmental transcription factors such as TBX5, PITX2, GATA4-6, NKX2.5, ZFHX3,PRRX1[44]. Second, studies linking these transcription factors to a direct mechanism for AF development, revealed regulatory roles of these transcription factors in the expression of ion channels and calcium handling moieties as well as complex interactions between multiple transcription factors[43, 45-50]. Third, new work has highlighted the role of microRNAs (miRNAs) in the regulation of both AF relevant transcription factors as well as on genes encoding channels directly[51]. Further, the combination of new knowledge of these genetic risk factors along with traditional clinically known risk factors such as diabetes, hypertension, cardiomyopathy among others, has provided support of a ‘multi-hit’

hypothesis, where underlying genetic risk factors, which could have a lower effect size on their own, when combined with other genetic risk factors or with other clinical risk factors result in AF[43, 44]. We discuss the first two points in greater detail in the following chapters.

MiRNAs are a class of small noncoding RNAs that perform post-transcriptional repression of target genes of more than sixty percent of all protein-coding genes[52]. There is increasing evidence that miRNAs are regulators of cardiac rhythm and that alterations in miRNA expression can result in AF. Altered miRNA expression patterns in the heart and circulating in the blood have been observed in both patients with AF and animal models[51]. Further, studies altering individual miRNAs have revealed several mechanism by which miRNAs may regulate cardiac rhythm. MiRNAs play a role in the regulation of potassium channels. For example, inhibition of miR-26 increased inward rectifier current (I_{K1}) and increased incidence of AF in mice[53]. Further, miRNAs can regulate calcium handling, as shown by canine and murine miR-328 overexpression models which show decreased L-type calcium current and increased AF susceptibility[54]. Additionally, alteration in miRNA expression can also induce structural remodeling, leading to atrial fibrosis, and thus providing an arrhythmogenic substrate[51, 55]. Currently, there are still many miRNAs identified by microarray analysis (comparing AF patients to those with sinus rhythm) for which we do not yet understand the mechanism of action.

Tbx5 model of atrial fibrillation

Previous work from the Moskowitz lab demonstrated the importance of T-box transcription factor-5, TBX5, in maintaining cardiac rhythm[47]. TBX5 has been studied in the context of development, and is known to be critical for limb and cardiac development, as patients with mutations in TBX5, resulting in haploinsufficiency, develop Holt- Oram syndrome,

characterized by defects in the cardiac septation and formation of the cardiac conduction system. TBX5 is expressed throughout most of the heart, but is much more abundant in the atria compared to the ventricle[56]. Recently, *Tbx5* variants have been implicated in increased AF risk by several GWAS[57, 58]. A mouse model of *Tbx5* knockout was generated to directly examine its role on AF development. Adult specific *Tbx5* knockout in mice resulted in the development of spontaneous and sustained AF and isolated atrial cardiomyocytes from these mice have a prolonged AP and increased incidence of EADs and DADs. RNA-sequencing of *Tbx5* knockout atria revealed decreases in *Ryr2* and *Atp2a2*, and presence of calcium chelating agent, BAPTA, inside the pipette normalized the AP, providing evidence of calcium mishandling[47].

In the first chapter of this dissertation, we test the hypothesis that TBX5 is critical for cellular calcium homeostasis, and that the disruption in normal calcium handling causes AP prolongation and ectopic activity, resulting in AF generation. We demonstrate that *Tbx5* deficient atrial cardiomyocytes have simultaneous decreased SERCA mediated SR calcium uptake, and increased NCX mediated calcium efflux, and increased calcium influx through L-type calcium channel. To demonstrate that these changes provide the mechanistic underpinnings for the AP abnormalities, we normalized SERCA function by removing its inhibition through phospholamban removal and found that AP duration and triggered events could be rescued. Further, tbx5 knockout mice with normalized SERCA function no longer developed AF. In summary, we provide a novel calcium dependent mechanism underlying *Tbx5* dependent AF risk.

Tbx5 interaction with transcription factor Gata4 in regulation of AF risk

Along with TBX5, a number of other transcription factors have been implicated in AF[3]. It is noteworthy that several of these transcription factors are also critical for cardiac development,

providing evidence for the idea of gene regulatory networks that regulate cardiac rhythm throughout life. Previously, the Moskowitz lab identified a gene regulatory network comprised of *Tbx5, Pitx2*, and downstream membrane effector genes[47]. PITX2 has been shown to be critical for atrial septum and SA development. Although *Pitx2* was one of the first AF susceptibility loci to be identified, understanding the mechanism by which it regulates cardiac rhythm remains difficult as both decreased and increased expression levels results in increased AF risk and PITX2 has multiple targets[59, 60]. However, several studies have demonstrated that reduction of PITX2 in mice results in higher AF susceptibility and atrial cardiomyocytes show decreased ap duration[59, 61, 62]. It is however noteworthy that Nadadur et. Al. discovered that in *Tbx5* knockout mice, *Pitx2* was significantly reduced, and AF susceptibility and AP abnormalities could be rescued by P*itx2* haploinsufficiency. Further, *Scn5a, Gja1, Dsp, Ryr2,* and *Atp2a2* were found to be coregulated by *Tbx5* and *Pitx2* but in opposite directions. These data suggested an incoherent feed-forward loop that is driven by *Tbx5*, but modulated by *Pitx2*. Overall, this demonstrates the complexity of the gene regulatory network that maintains cardiac rhythm, and suggests that examination of transcription factor interactions in the adult atrium can be very valuable.

In the second chapter of this dissertation, we examine test the hypothesis that cardiogeneic transcription factor genes *Tbx5, Gata4,* and *Nkx2.5* interact to maintain atrial rhythm. We discover that *Gata4* and *Tbx5* coregulate *Ryr2* and *Atp2a2* in opposite directions. *Tbx5* haploinsufficiency driven AF and AP abnormalities were normalized by *Gata4* haploinsufficiency. Specifically, *Gata4* haploinsufficiency rescues SERCA activity in *Tbx5* haploinsufficient cardiomyocytes. Interestingly, we found *Gata4* and *Tbx5* activated an *Atp2a2* enhancer, but *Gata4* suppressed activation of a *Ryr2* enhancer by *Tbx5*. *Nkx2.5* was not found to have an effect on AF susceptibility either individually or in combination with *Gata4* or *Tbx5*. In

summary, we add the antagonistic interaction between *Gata4* and *Tbx5* to the complex gene regulatory network regulating atrial rhythm.

Independent effects of altering downstream intercalated disc in arrhythmogenesis

One thrust of arrhythmia substrate research is elucidating the structure and function of the intercalated disc. The intercalated disc is a complex structure that links adjacent cardiomyocytes electrically and structurally, allowing the heart to function as a syncytium. The intercalated disc contains a number of key components including gap junctions, which facilitate rapid ion and small molecule exchange between cells, adherens junctions, which facilitate maintenance of cell shape during the contraction relaxation cycle, and desmosomes, which provide significant structural support[37]. Adherens junctions are composed predominantly of N-cadherin, which connects two cells by homodimerizes with N-cadherin from the adjacent cell as well as linking to the actin cytoskeleton through beta-catenin[63]. Gap junctions are predominantly composed of connexins, which form a pore between two cells. In the ventricle connexin 43 is the predominant form while in the atria and conduction fibers, connexin 40, 30.2, and 45 play important roles[64, 65]. Recently, gap junctions protein connexin 43 has been shown to be necessary for sodium channel function and a new model of action potential generation and propagation being regulated jointly by ion channels and gap junction proteins is gaining more support[66]. Desmosomes provides structural support through desmoglein-2 and desmocollin-2 that link two cells and also link to plakophilin-2 and desmoplakin that connect to intermediate filaments[63]. Although previously thought to be completely distinct regions, recent evidence points towards the area composita model in which adherens junctions, gap junctions, desmosomes, along with ion channels are able to interact with one another[37]. In this model, scaffolding proteins such as ZO-1 are critical for linking different functional components to achieve one functional unit[67]. Overall, intercalated

disc proteins are critical for maintaining cell-cell communication and misregulation can result in arrhythmias, most commonly arrhythmogenic cardiomyopathy, characterized by arrhythmias in combination with fibrosis or structural alterations. Mutations associated with arrhythmogenic cardiomyopathy have been identified in a growing number of intercalated disc proteins spanning all of the components of the area composita[68].

While desmosome proteins were the first to be identified in arrhythmogenic cardiomyopathy probands, more recently mutations in adherens junction, gap junction, and scaffolding proteins have also been implicated[69]. Among those is tight junction protein, ZO-1, which has been studied extensively in epithelia and endothelia, but until recently not much was known about its role in the heart. In epithelia, ZO-1 was the first protein to be identified as a main tight junction component, where it binds to claudins and JAM family proteins to maintain barrier function. Loss of ZO-1 results in loss of tight junctions and consequently breakdown of the barrier capability[70]. In line with its role as a scaffolding protein, ZO-1 has multiple domains which allow for binding to other proteins, namely the PDZ, GUK, and SH3 domains. Additionally, ZO-1 can bind F-actin directly through its actin binding domain, allowing to be a modulator of mechanotranduction[71]. Similarly, in endothelial cells, ZO-1 facilitates mechanotranduction and angiogenesis and its loss results in disruption of the tight junction and redistribution of junctional proteins such as vinculin and pak2[72].

ZO-1 is localized to intercalated discs in cardiac tissue, where it has been shown to regulate both gap junction and adherens junction organization[37]. The second PDZ domain of ZO-1 interacts with the carboxyl terminus of connexins and ZO-1 has been shown to regulate the size and localization of gap junctions in the perinexus of the intercalated disc, the area surrounding a region with a high density of gap junctions[73, 74]. ZO-1 binding with connexin in the perinexus

region prevents association with the connexins of the neighboring cell. Thus, disruption of ZO-1 binding to connexin at the edge of a gap junction plaque actually increases gap junction size even in animal models[75]. Despite this, introducing a dominant-negative ZO-1 construct resulted in both decreased gap junction and adherens junction size at the intercalated disc with pronounced reduction of Cx43, N-cadherin, and ZO-1 complexes. This indicates that ZO-1 regulation of the gap junction is not simply through its direct interactions with connexin, but also through its interactions with other proteins particularly in the adherens junction regions[76]. ZO-1 is able to reside in complexes with N-cadherin, connexins, vinculin, coxsackie and adenovirus receptor, and alpha-catenin thus positioning it to be a scaffolding protein that can link gap junction and adherens junction regions[73, 77-80]. Further, ZO-1 can also mediate the trafficking of connexins to the gap junction. Studies showing loss of connexin 43 and N-cadherin independently result in loss of ZO-1, further suggest that adaptor proteins are a vital part of the large protein complexes formed at the intercalated disc. Thus, isolating the independent role of such adaptor proteins in the adult heart could provide valuable insight into how the structure and function of the intercalated disc is maintained.

In the third chapter of the dissertation, we aim to test the hypothesis that ZO-1 is required for intercalated disc functioning and cell-cell conduction. We generated a cardiac specific, inducible ZO-1 deletion model in mice, allowing us to examine how loss of ZO-1 affects cardiac conduction and function in adulthood. ZO-1 knockout mice show atrioventricular bock with moderate reduction of ejection fraction accompanied by decreased connexin 40 expression in the AV node. Interestingly, ventricular conduction was not decreased although connexin 43 was decreased in the ventricular tissue. Genetic dissection of the location specific role of ZO-1 by comparing whole heart, conduction system, and AV node distal deletion of *Tjp1* showed AV

node dysfunction in both whole heart and conduction system knockout of ZO-1, but not when it was deleted distal to the AV node. Ejection fraction reduction was observed only in the whole heart deletion model. In summary, we find that ZO-1 plays an important role in localizing connexins to the intercalated disc and maintaining conduction in the AV node.

Chapter II: A calcium transport mechanism for atrial fibrillation

Note: The following section titled "A calcium transport mechanism for atrial fibrillation" is reproduced verbatim, with the exception of figure renumbering from my published article (Dai et al., eLife 2019;8:e41814). This material is distributed under the terms of the CC BY-NC 4.0 Unported license (https://creativecommons.org/licenses/by-nc/4.0/).

Authors: Wenli Dai*, Brigitte Laforest*, Leonid Tyan, Kaitlyn M. Shen, Rangarajan D. Nadadur, Francisco J. Alvarado, Stefan Mazurek, Sonja Lazarevic, Margaret Gadek, Yitang Wang, Ye Li, Hector H. Valdivia, Le Shen, Michael T. Broman, Ivan P. Moskowitz§ and Christopher R. Weber§

*These authors contributed equally to this work

§ Co-corresponding authorship

Abstract

Risk for Atrial Fibrillation (AF), the most common human arrhythmia, has a major genetic component. The T-box transcription factor TBX5 influences human AF risk and adult-specific *Tbx5*-mutant mice demonstrate spontaneous AF. We report that TBX5 is critical for cellular Ca^{2+} homeostasis, providing a molecular mechanism underlying the genetic implication of TBX5 in AF. We show that cardiomyocyte action potential (AP) abnormalities in *Tbx5*-deficient atrial cardiomyocytes are caused by a decreased sarcoplasmic reticulum (SR) Ca^{2+} ATPase (SERCA2)-mediated SR calcium uptake which was balanced by enhanced trans-sarcolemmal calcium fluxes (calcium current and sodium/calcium exchanger), providing mechanisms for triggered activity. The AP defects, cardiomyocyte ectopy, and AF caused by TBX5 deficiency were rescued by phospholamban removal, which normalized SERCA function. These results directly link transcriptional control of SERCA2 activity, depressed SR Ca^{2+} sequestration, enhanced trans-sarcolemmal calcium fluxes, and AF, establishing a mechanism underlying the genetic basis for a Ca^{2+}-dependent pathway for AF risk.

Introduction

Atrial fibrillation (AF) is the most common arrhythmia in humans, characterized by irregularly irregular atrial electrical activity, resulting in asynchronous atrial contraction. AF is a global problem, affecting more than 33 million people and approximately 25% of Americans over the age of forty[1, 81]. AF is associated with significant morbidity and mortality due to thromboembolic events, heart failure, and sudden cardiac death. AF also significantly complicates overall health care management, with AF patients costing 5 times more to treat than patients without AF[82]. The total annual cost to treat AF patients in the US is on the order of 26 billion dollars[81]. AF is a highly significant and growing public health concern.

A genetic basis for AF risk has been described in the last decade. Large community-based cohort studies indicate that heritability provides between 40 and 62% of AF risk[81, 83]. An emerging paradigm describes AF as a multifactorial disease with genetic predisposition that will determine the propensity of secondary clinical insults to cause AF. This model highlights the importance of understanding the molecular mechanisms underlying the genetic predisposition to AF. Genome-wide association studies (GWAS) studies have identified common risk variants and familial mutations at the T-box transcription factor 5 (TBX5) locus that result in increased risk for AF[84, 85]. Adult-specific *Tbx5* knockout mice demonstrate primary spontaneous and sustained AF, providing evidence supporting the genetic implication at this locus. GWAS have also implicated multiple genes involved in cardiomyocyte calcium handling, including *Atp2a2*, encoding the sarcolemmal calcium ATPase SERCA2, and *sln* and *pln*, encoding direct binding SERCA2 inhibitors sarcolipin and phospholamban, respectively. We have previously demonstrated that these cardiomyocyte calcium control genes are direct TBX5 targets[47]. These observations suggested that tight transcriptional control of SERCA2 activity may be central to

atrial rhythm robustness and that variation in SERCA2 expression and activity may contribute to AF risk.

The cellular mechanisms causing the irregular electrical activity in AF are believed to include an abnormal myocardial substrate and formation of an ectopic trigger. Abnormal substrate refers to altered electrical conduction between cardiomyocytes. Ectopic trigger refers to cardiomyocyte ectopy, or initiation of electrical activity at regions outside of the sinoatrial node. Both of these cellular phenomena are observed in *Tbx5* adult-specific mutant mice and have been associated with abnormal cellular calcium handling[86-98]. We described the TBX5-dependent gene regulatory network essential for atrial rhythm control and identified downstream ion channels and transporters potentially important to rhythm control[47, 99].Triggered activity in the form of early and delayed afterdepolarizations (EADs and DADs) observed in Tbx5-deficient atrial cardiomyocytes could be rescued by heavy buffering of cytoplasmic calcium[47]. *Tbx5*-dependent calcium handling has thereby emerged as a potential mediator of the myocardial physiologic abnormalities resulting in AF.

We sought to define the Tbx5-dependent cellular mechanisms responsible for abnormal calcium-dependent electrical activity. We found that *Tbx5*-dependent AF is associated with abnormal sarcoplasmic reticulum (SR) calcium uptake due to depressed SERCA2 expression, depressed SERCA function, and increased phospholamban expression. Decreased SR calcium uptake is compensated by increased Ca^{2+} extrusion from cardiomyocytes via sodium-calcium exchanger (NCX) current (I_{NCX}), which provides a mechanism for TBX5-dependent action potential (AP) prolongation and the propensity for triggered cellular ectopy. In the setting of enhanced NCX mediated Ca^{2+} efflux and depressed SR uptake, compensatory increases in L-type calcium current (I_{CaL}) balance calcium extrusion to maintain steady state calcium

homeostasis. Together these calcium handling alterations contribute to AP prolongation and triggered activity,

We further demonstrated that calcium handling abnormalities, AP alterations, and triggered activity are all normalized by knockout of phospholamban, which prevents *Tbx5*-dependent AF. These results establish a direct link between depressed SR Ca^{2+} sequestration, enhanced NCX activity, and AF. This model suggests that targeting calcium handling pathways may be a treatment rationale for a subpopulation of AF patients.

Materials and methods

Reagent type (species) or resource	**Designation**	**Source or reference**	**Identifiers**	**Additional information**
Genetic reagent (M. musculus)	*Tbx5*$^{fl/fl}$ (*Tbx5*^{tm1Jse})	PMID: 11572777, 27582060	MGI:2387850	Dr. Jonathan G Seidman (Harvard)
Genetic reagent (M. musculus)	*Pln*$^{-/-}$ (*Pln*^{tm1Egk})	PMID: 8062415	MGI:2158357	Dr. Evangelia Kranias (University of Cincinnati)
Genetic reagent (M. musculus)	*Rosa26*^{CreERT2} (*Gt(ROSA)26Sor*$^{tm1(cre/ERT2)Tyj}$)	PMID: 17251932, 27582060	MGI:3790674	Dr. Tyler Jacks (Massachusetts Insititute of Technology)
Antibody	Mouse anti-RyR2	ThermoFisher	Cat. #: MA3-925	WB (1:2000)
Antibody	Mouse anti-SERCA2	ThermoFisher	Cat. #: MA3-919	WB (1:1000)
Antibody	Mouse anti-NCX	ThermoFisher	Cat. #: MA3-926	WB (1:1000)
Antibody	Mouse anti-PLN	Badrilla	Cat. #: A010-14	WB (1:5000)
Antibody	Rabbit anti-pT17-PLN	Badrilla	Cat. #: A010-13	WB (1:5000)

Antibody	Rabbit anti-pS16-PLN	Badrilla	Cat. #: A010-12	WB (1:5000)
Antibody	Rabbit anti-Cav1.2	Alomone	Cat. #: ACC-003	WB (1:200)
Antibody	Mouse anti-GAPDH	Millipore	Cat. #: MAB374	WB (1:10000)
Antibody	Goat anti-mouse-HRP	Thermofisher	Cat. #: 31437	WB (1:5000)
Antibody	Goat anti-rabbit-HRP	Thermofisher	Cat. #: 31463	WB (1:5000)
Chemical compound, drug	Fluo-4 AM	Thermofisher	Cat. #: 14201	10 µM x 20 min
Chemical compound, drug	Nifedipine	Sigma	Cat. #: N7634	30 µM
Chemical compound, drug	Collagenase Type 2	Worthington Biochemical	Cat. # LS004177	1 g/L
Chemical compound, drug	Tamoxifen	MP Biomedicals	Cat#: 156738	2 mg/injection x 3 doses
Chemical compound, drug	Laminin	Invitrogen	Cat. #: 2039175	0.5 mg/ml
Chemical compound, drug	[3H]ryanodine	PerkinElmer	Cat. #: NET950250UC	
Chemical compound, drug	TRIzol	Invitrogen	Cat. #: 15596026	
Chemical compound, drug	Ryanodine	MP Biomedicals	SKU #:0215377001	
Chemical compound, drug	Caffeine	Sigma	Cat. #: C0750	10 mM

Software, algorithm	Clampex/Clampfit Data acquisition and analysis	Molecular Devices	Version 10.3.2.1	
Software, algorithm	LabChart for electrophysiology studies	ADInstruments	Version 5 and 8	
Software, algorithm	Buffering analyses using MaxChelator	Stanford	WEBMAXCLITE v1.15	Chris Patton, Stanford University
Software, algorithm	Western Blot quantification ImageJ	NIH	Version 1.48	
Software, algorithm	Hierarchical Statistical technique using R	R Core Team	Script from PMID: 29016722	Ken Macleod, Imperial College London
Commercial Assay or Kit	qScript cDNA synthesis kit	Quanta		
Commercial Assay or Kit	Power SYBR Green PCR Master Mix	Applied Biosystems		

Generation of mice: The *Tbx5*$^{fl/fl}$, *Pln*$^{-/-}$ and *Rosa26*^{CreERT2} lines have all been previously described and were kept in a mixed genetic background[100-102]. Double knockout mice were generated by crossing *Tbx5*$^{fl/fl}$*;R26*^{CreERT2} mice with germline *Pln*$^{-/-}$ mice. After two generations, we obtained *Tbx5*$^{fl/fl}$*;R26*^{CreERT2} mice with either loss of one (*Pln*$^{+/-}$) or both (*Pln*$^{-/-}$) copies of *Pln*. All experiments were done using age- and genetic strain-matched littermate controls. Tamoxifen was administered for three consecutive days at a dose of 0.167 mg/kg body weight by intraperitoneal injection at 6-10 weeks of age, as previously described[47]. All experiments were performed in accordance to The University of Chicago Institutional Animal Care and Use Committee (IACUC) approved protocol.

ECG recordings: 8- to 10- week-old mice were anesthetized using isoflurane, and telemetry transmitters (ETA-F10, Data Science International) were implanted in the back with leads tunneled to the right upper and left lower thorax, as previously described (Wheeler MT et al., JCI 2004). Baseline recordings were obtained for 24-hours after a post-implant recovery period of one day. ECG data was analyzed using LabChart 8 (AD Instruments).

Intracardiac electrophysiology studies: Detailed protocols for intracardiac electrograms have been previously described[47]. Briefly, 8- to 10- week-old mice were anesthetized with isoflurane and a vertical skin cut-down at the right jugular vein was performed. A 1.1-F octapolar catheter (EPR-800, Millar Instruments) was advanced in the right jugular vein to perform electrical stimulation. The catheter was connected to ADI BioAmp and PowerLab apparatus and signals were recorded using LabChart Software (ADInstruments). Atrial induction pacing was performed using burst pacing and the presence of at least three cycles of atrial tachycardia or fibrillation at least twice was considered positive.

$[Ca^{2+}]_i$ transient measurement: Langendorff perfusion with 2 mg/mL of Collagenase Type 2 (Worthington Biochemical) at 5 ml/min was used to isolate atrial cardiomyocytes. Cardiomyocytes were then plated on laminin coated glass bottom dishes for 30 minutes prior to incubation with 10 μM Fluo-4/AM (Molecular Probes/Invitrogen) in normal Tyrode's solution containing (in mM): 140 NaCl, 4 KCl, 10 glucose, 10 HEPES, and 1 $MgCl_2$, 1 $CaCl_2$ pH 7.4 using NaOH for 20 minutes at room temperature. Cells were perfused with prewarmed Tyrode for 10 minutes prior to imaging. Imaging was performed on an Olympus microscope with a 20x objective lens, a LAMBDA DG-4 power source with 488 nm excitation and 515 nm emission filters and a PMT (Microphotometer) to record whole cell signal. Electrical field stimulation (Grass stimulator; Astro-Med) was performed at 1 Hz. SERCA and NCX measurements were

performed by flowing sodium free Tyrode with 10 mM caffeine followed by sodium free Tyrode alone or Tyrode with caffeine respectively. Cells were returned to normal Tyrode in both cases at the end of the recording. $[Ca^{2+}]_i$ transients are presented as total fluorescence intensity normalized to resting fluorescence (F/F_0) obtained from steady-state resting conditions before field stimulation. $[Ca^{2+}]_i$ transients and sparks were acquired in line-scan mode (3 ms per scan; pixel size 0.12 μm) using a Zeiss confocal microscope.

Whole-cell electrophysiological recordings: APs and voltage clamp recordings were recorded using standard ruptured patch protocol[47]. We used current clamp mode with 0.5 nA × 2 ms current clamp pulses to measure APs. Voltage clamp mode was used to measure capacitance transients and to study $[Ca^{2+}]_i$ transients with fixed duration depolarizations. Cardiomyocytes are kept at 37 °C and perfused with Tyrode solution (140 NaCl, 4 KCl, 1 MgCl2, 1 CaCl2, 10 HEPES, 10 Glucose, and pH 7.4 with NaOH). Internal pipette solution composition was (in mM): 20 KCl, 100 K-glutamate, 10 HEPES, 5 MgCl2, 10 NaCl, 5 Mg-ATP, 0.3 Na-GTP. Patch pipettes (World Precision Instruments) were pulled to have a mean resistance of 3.5–5 MΩ. An Ag–AgCl pellet and 3M KCl agar bridge was used to ground the bath. Liquid junction potentials, were always corrected after cell rupture. External solution for I_{CaL} contained (in mM): 120 Tetraethylammonium-chloride, 10 CsCl, 10 Glucose, 10 HEPES, 1.5 $MgCl_2$, 1 $CaCl_2$, pH 7.4 with CsOH. Internal pipette solution contained (in mM): 100 Cs-methanesulfonate, 30 CsCl, 10 HEPES 5 EGTA, 2 $MgCl_2$, 5 Mg-ATP, pH 7.2 with CsOH. I_{CaL} was recorded during 200 ms voltage clamp pulses from a holding potential of -40 mV to test potentials ranging from -40 to +60 mV, with pulses applied every 2 s in 5 mV increments. Peak current amplitudes were normalized to the cell capacitance (C_m) and presented as current density (A/F). Steady-state inactivation of I_{CaL} was investigated using two-pulse protocol. Holding potential was -80 mV.

The first pulse depolarized membrane from -60 to 20 mV with 10 mV increments during 500 ms, the second pulse depolarized the membrane to 10 mV for 50 ms. The inactivation curves were fit to a Boltzmann distribution. Acquisition was performed using an Axopatch-200B amplifier connected to a Digidata1550A acquisition system (Axon Instruments, Foster City, CA, USA). In recording filtering at 2 kHz was performed using the amplifier Bessel and sampled at 10 kHz. Analysis was performed using pCLAMP10 (Axon Instruments) and a home written analysis code.

Western blots: Atrial tissue was collected and homogenized as described previously[103], in a buffer containing 0.9% NaCl, 10 mM Tris-HCl pH 6.8, 20 mM NaF and protease inhibitors. Equal amounts of protein, as determined by Bradford assay, were loaded. 50 µg of tissue homogenate, in Laemmli buffer, was separated by SDS-PAGE in 4-20% TGX or AnyKD precast gels (Bio-Rad). Proteins were transferred to PVDF membrane using the iblot2 transfer system (ThermoFisher) or wet transfer. Primary antibodies were as follows: anti-RyR2 (1:2000; MA3-925, ThermoFisher), SERCA2 (1:1000; MA3-919, ThermoFisher), NCX (1:1000; MA3-926, ThermoFisher), PLN (1:5000; A010-14, Badrilla), pT17-PLN (1:5000; A010-13, Badrilla), pS16-PLN (1:5000; A010-12, Badrilla), Cav1.2 (1:200; ACC-003, Alomone), GAPDH (1:10000; MAB374, Millipore). Secondary antibodies were: goat anti-mouse-HRP (1:5000; 31437, ThermoFisher) or goat anti-rabbit-HRP (1:5000; 31463, ThermoFisher). Secondary antibody concentrations were 5x higher when using the ibind Flex system. SuperSignal ECL reagent (ThermoFisher) was used to develop membranes followed by imaging with a ChemiDoc MP apparatus (Bio-Rad). Band intensities were quantified with the ImageLab software (Bio-Rad) or using ImageJ (NIH).

[^{3}H]Ryanodine binding assay: Binding assays were carried out following a protocol previously described[104]. Binding mixtures contained 100 µg of protein from homogenates prepared from pooled atria (5-7 mice), 0.2 M KCl, 20 mM Hepes (pH 7.4), 6.5 nM [^{3}H]ryanodine (PerkinElmer), 1 mM EGTA and enough $CaCl_2$ to set free [Ca^{2+}] between 10 nM (pCa^{2+} 8) and 100 µM (pCa^{2+} 4). The ratio between Ca^{2+} and EGTA was determined using MaxChelator (WEBMAXCLITE v1.15 http://maxchelator.stanford.edu/webmaxc/webmaxclite115.htm). Following a 2 hour incubation at 36ºC, reactions were filtered through Whatman GF/B Filters using a Brandel M24-R Harvester. [^{3}H]ryanodine binding was determined using a Beckman LS6500 scintillation counter and BioSafe II scintillation cocktail (RPI Corp). Non-specific binding was quantified in the presence of 2 µM unlabeled ryanodine (MP Biomedicals) and subtracted.

Quantitative real time PCR: Left atrial tissue of *Tbx5*$^{fl/fl}$*;R26*^{CreERT2} and *R26*^{CreERT2} mice was removed two weeks after receiving tamoxifen and RNA was isolated using a Trizol (Invitrogen) based method. Reverse transcription reaction was carried out using the qScript cDNA synthesis kit (Quanta) according to the manufacturer's protocol. Quantitative RT-PCR was performed using the Power SYBR Green PCR Master Mix (Applied Biosystems) and run on an Applied Biosystems AB7500 machine. Relative fold changes were calculated using the comparative threshold cycle method ($2^{-\Delta\Delta Ct}$), using glyceraldehyde-3-phosphate dehydrogenase (*Gapdh*) gene expression level as internal control.

PCR primers

Gene	F Primer	R Primer
Tbx5	GGCATGGAAGGAATCAAGGT	CTAGGAAACATTCTCCTCCCTGC
Ryr2	CAAATCCTTCTGCTGCCAAG	CGAGGATGAGATCCAGTTCC
Atp2a2	CTGGTGATATAGTGGAAATTGCTG	GGTCAGGGACAGGGTCAGTA
Pln	TTATGCCAGGACGGCAAAAG	CACTGTGACGATCACCGAAG
Sln	CTGAGGTCCTTGGTAGCCTG	GGTGTGTCAGGCATTGTGAG
Cacna1c	CTACAGAAACCCATGTGAGCAT	CAGCCACGTTGTCAGTGTTG
Ncx1	TTCTCATACTCCTCGTCATCG	TTGAGGACACCTGTGGAGTG
Calm1	TGGGAATGGTTACATCAGTGC	CGCCATCAATATCTGCTTCTCT
Calm2	ACGGGGATGGGACAATAACAA	TGCTGCACTAATATAGCCATTGC
Calm3	GATGGCACCATTACCACCAAG	CGCTGTCTGTATCCTTCATCTTT

Statistical analysis: Values are represented as mean ± standard error of the mean (± SEM). Statistical significance for quantitative metrics of APs, SERCA, NCX, SR load, I_{CaL}, spark frequency, and $[Ca^{2+}]_i$ transients were determined using hierarchical statistical methods[105]. Statistical significance for mRNA, and protein expression studies was determined using Student's t-test. Statistical significance of the nifedipine effect on AP duration was determined using two-tailed paired t-test. A two-tailed Fisher's exact test was used for statistical significance of count-based analysis of AF inducibility and EAD and DAD count. Statistical significance is designated as * $p<0.05$, ** $p<0.01$, and *** $p<0.001$.

Results

Cytoplasmic calcium is responsible for AP prolongation in Tbx5-mutant atrial cardiomyocytes.

We previously reported that *Tbx5* deficient atrial cardiomyocytes demonstrated AP prolongation and myocardial ectopy. We hypothesized that these defects were caused by cellular calcium handling abnormalities. We therefore surveyed the expression of known calcium handling genes in the adult-specific *Tbx5* knockout model. We assessed gene expression in

Tbx5$^{fl/fl}$;*R26*^{CreERT2} and control *R26*^{CreERT} mice at 10 weeks of age following tamoxifen (TM) treatment at 8 weeks of age. Consistent with previous observations, the adult *Tbx5*$^{fl/fl}$;*R26*^{CreERT2} but not control mice developed spontaneous AF, showing an irregularly irregular heartbeat, by telemetric electrocardiogram (ECG) recordings (Fig. 1A,B). As previously shown, APs and $[Ca]_i$ transients were prolonged in *Tbx5*$^{fl/fl}$;*R26*^{CreERT2} (Fig. 1C)[47]. We assessed expression of genes important to cellular calcium handling in the left atrium by quantitative PCR (Fig. 1D). mRNA transcripts for RyR2 (*Ryr2*) and SERCA2 (*Atp2a2*), two of the main determinants of sarcoplasmic reticulum (SR) calcium flux, were decreased by 61% and 71% respectively in *Tbx5*$^{fl/fl}$;*R26*^{CreER2} mice compared to *R26*^{CreER2} controls (p=0.026 and p=0.001 for *Ryr2* and *Atp2a2* respectively) consistent with previous studies[47]. In addition, phospholamban *(Pln)* mRNA expression was increased by 69% in *Tbx5*$^{fl/fl}$;*R26*^{CreER2} compared to *R26*^{CreER2} (p=0.023), which would be expected to further depress SERCA2 activity. There was no significant difference in mRNA expression of the alpha 1C subunit of the L-type calcium channel (*Cacna1c*), the cardiac sodium calcium exchanger (*Ncx1*), or of any of the calmodulins 1-3 (*Calm1, Calm2, Calm3*) (Fig. 1C). These data are consistent with the hypothesis that the myocardial electrophysiology deficits in the *Tbx5*-deficient AF model may be due to abnormal calcium handling.

We examined the relationship between myocardial electrophysiology deficits and calcium flux in *Tbx5*-mutant atria. In steady state, with each cardiomyocyte contraction cycle, calcium entering the cardiomyocyte (L-type calcium channel, I_{CaL}) is extruded from the cell (predominantly via inward I_{NCX}). Similarly, calcium leaving the SR via RyR2 release or SR leak pathways is taken back up into the SR via SERCA2. We examined the effect of altered TBX5-dependent gene expression on these aspects of cardiomyocyte calcium flux. Given the observed

changes in *Ryr2* and *Atp2a2* mRNA abundance, we hypothesized that AP prolongation in *Tbx5* deficient cardiomyocytes was due to calcium handling defects downstream of initial Ca^{2+} entry through I_{CaL}. To test this, we recorded APs in the presence and absence of the L-type Ca^{2+} channel blocker nifedipine. This approach blocks Ca^{2+} entry into the cell and indirectly removes the effect of Ca^{2+} entry on downstream Ca^{2+} handling pathways, including SR Ca^{2+} release/reuptake as well as the electrogenic effect of calcium transport out of the cell via inward I_{NCX}. 30 μM nifedipine completely inhibited L-type calcium current, preventing Ca^{2+} entry or release of SR calcium in control $R26^{CreERT2}$ and $Tbx5^{fl/fl};R26^{CreERT2}$ (Fig. 2-figure supplement 1). In control $R26^{CreERT2}$ atrial cardiomyocytes, the effect of nifedipine on AP duration was small, with 19 ± 4% shortening of APD90 (p=0.008) (Fig. 2A). However, in $Tbx5^{fl/fl};R26^{CreERT2}$ atrial cardiomyocytes, nifedipine had a profound effect: APD50 was shortened by 16 ± 6% and APD90 by 61 ± 6% (p= 0.02 and 0.007 respectively) (Fig. 2B, C). Western blot with densitometry analysis for $Ca_V1.2$ showed no significant difference in protein expression (Fig. 2D), in line with the qPCR data (Fig. 1D), consistent with no TBX5-driven direct transcriptional regulation of L-type calcium channels. However, peak I_{CaL} current was increased 92±34% (p=0.027) in $Tbx5^{fl/fl};R26^{CreERT2}$ atrial cardiomyocytes compared to control $R26^{CreERT2}$ (Fig. 2E, 2F). The inactivation kinetics at peak I_{CaL} were accelerated $Tbx5^{fl/fl};R26^{CreERT2}$ compared to control $R26^{CreERT2}$ (τ=26.7 ms *vs*. τ=40.0 ms; p= 0.05). Steady-state I_{CaL} inactivation was unchanged (Fig. 2-figure supplement 2). These data suggest that increased I_{CaL} may contribute to TBX5-loss associated AP prolongation and EADs. However, nifedipine also blocks SR Ca^{2+} release as well as downstream Ca^{2+} extrusion pathways, which also affect AP duration. Further, since late AP repolarization is dramatically prolonged (negative to -30 mV where I_{CaL} is largely

inactive) we hypothesized that *Tbx5*-deficiency disrupts Ca^{2+} handling pathways downstream of I_{CaL}.

Removal of Tbx5 results in decreased Ca^{2+} sparks and RyR2 expression, but no overall reduction in RyR2 open probability.

Because RyR2 is a critically important sarcolemmal calcium extrusion channel and *Ryr2* mRNA was downregulated in *Tbx5*-mutant atria, we investigated the *Tbx5* dependent regulation of RyR2 protein expression and function. RyR2 protein expression was significantly decreased in left atria of $Tbx5^{fl/fl};R26^{CreERT2}$ mice compared to $R26^{CreERT2}$ mice by western blot (Fig. 3A), consistent with the observed downregulation of *Ryr2* mRNA (Fig. 1B). We hypothesized that decreased RyR2 contributed to abnormal Ca^{2+} release from the SR and tested this by measuring local spontaneous RyR2-mediated Ca^{2+} release events (Ca^{2+} sparks) using confocal linescans (Fig. 3B). The frequency of Ca^{2+} sparks in $Tbx5^{fl/fl};R26^{CreERT2}$ atrial cardiomyocytes was decreased in comparison with $R26^{CreERT2}$ atrial cardiomyocytes at different pacing frequencies from 0 to 2 Hz (Fig. 3C). A decrease in calcium sparks can be due to either decreased RyR2 open probability or a reduced SR calcium load. To differentiate these possibilities, we first examined RyR2 function in the setting of reduced RYR2 expression by performing a [^{3}H]-ryanodine binding assay. [^{3}H]-ryanodine binding to RyR2 correlates with RyR2 open probability[86]. Despite reduced ryanodine receptor expression, overall ryanodine binding was unchanged over the majority of the physiological range of calcium values, with no shift in calcium sensitivity (Fig. 3D). This observation suggests that the alterations in spark frequency were not due to changes in total RyR2 open probability. Instead, it may be caused by diminished SR Ca^{2+} uptake, a SERCA-dependent property.

Adult-specific Tbx5 deficiency reduces SERCA activity and SR load while increasing sodium-calcium exchanger activity

We next focused on the balance of diastolic calcium efflux pathways as potential mediators of Ca^{2+} mishandling by measuring SR Ca^{2+} content and protein expression and function of SERCA2 and NCX1. We observed that SERCA2 protein expression was decreased while NCX1 protein expression was increased in $Tbx5^{fl/fl};R26^{CreERT2}$ in comparison with $R26^{CreERT2}$ atria (Fig. 4A,B). To define steady state SR Ca^{2+} content, we loaded cardiomyocytes with Fluo-4 AM and paced with a train of field stimuli to achieve a steady state Ca^{2+} content (Fig. 4C,D) and peak Ca^{2+} content and rate of Ca^{2+} removal were measured. The $[Ca^{2+}]_i$ transient peaks were unchanged, but $[Ca^{2+}]_i$ transient decay rates, corresponding to SR Ca^{2+} uptake and cellular Ca^{2+} extrusion, were slowed in $Tbx5^{fl/fl};R26^{CreERT2}$ compared to $R26^{CreERT2}$ atrial cardiomyocytes (Fig. 4E,F)[47], consistent with defective Ca^{2+} removal from the cytosol. We also measured $[Ca^{2+}]_i$ transients in voltage clamp mode using 40 ms square wave voltage clamp pulses from -80 to 0 mV (Fig. 4-figure supplement 1). Similar to the field stimulation experiments, $[Ca^{2+}]_i$ transient decay rates were slowed, but $[Ca^{2+}]_i$ transient peaks were decreased by 23 ± 4% (p=0.02) in $Tbx5^{fl/fl};R26^{CreERT2}$ cardiomyocytes compared to $R26^{CreERT2}$, which suggests that AP prolongation is essential to maintaining peak twitch $[Ca^{2+}]_i$. The latter experiment is also consistent with depressed SR loads in $Tbx5^{fl/fl};R26^{CreERT2}$ compared to $R26^{CreERT2}$ atrial myocytes.

We hypothesized that decreased SERCA2 expression caused decreased SR load. We examined SERCA activity by synchronizing the opening of RyR2 channels while preventing Ca^{2+} extrusion through NCX using caffeine containing, sodium-free, Tyrode solution. This provides a measurement of the maximum release of Ca^{2+} into the cytosol from the SR, a measure

of the SR Ca^{2+} load (Fig. 4C,D). SR $[Ca^{2+}]$ was reduced by 24±8% (p=0.0005) in *Tbx5*$^{fl/fl}$*;R26*^{CreERT2} compared with *R26*^{CreERT2} atrial cardiomyocytes (Fig. 4G). SERCA activity was assessed from $[Ca^{2+}]_i$ decay rate after SR release in the absence of external sodium (NCX inactive). Peak SERCA activity was reduced by 31± 9% (p=0.006) in *Tbx5*$^{fl/fl}$*;R26*^{CreERT2} compared with *R26*^{CreERT2} atrial cardiomyocytes (Fig 4C,H). NCX activity was assessed as the rate of change in $[Ca^{2+}]_i$ decay in Na^+ containing caffeine solution, preventing net SR uptake. Since NCX activity is depends on $[Ca]_i$, we plotted NCX as a function of the $[Ca]_i$ signal. NCX activity was ~60% higher in *Tbx5*$^{fl/fl}$*;R26*^{CreERT2} in comparison with *R26*^{CreERT2} atrial cardiomyocytes (Fig. 4D,I). Thus, removal of *Tbx5* causes decreased SR Ca^{2+} load and decreased SERCA function, but increased NCX mediated Ca^{2+} extrusion. Increased inward NCX activity promotes cardiomyocyte depolarization, providing a mechanism for prolonged APs and increased ectopy in *Tbx5* mutant atrial cardiomyocytes.

Genetic augmentation of SERCA activity and normalization of SR load eliminates susceptibility to AF.

We hypothesized that *Tbx5* deficiency reduces SERCA activity by decreasing SERCA2 protein expression (Fig 4A) and increasing expression of phospholamban (*Pln*), a negative regulator of SERCA2 (Fig. 1D). If these were the primary causes of decreased SERCA function in *Tbx5* mutant atria, reduced PLN or PLN phosphorylation (relieving inhibition of SERCA2) would be expected to normalize SERCA function. Western blot analysis showed that PLN expression was significantly increased in *Tbx5*$^{fl/fl}$*;R26*^{CreERT2} compared with *R26*^{CreERT2} atria (Fig. 5A). In addition, PLN phosphorylation was also increased at serine 16 in *Tbx5*$^{fl/fl}$*;R26*^{CreERT2} compared to *R26*^{CreERT2}. These data suggest PLN phosphorylation may be a compensatory mechanism in response to decreased SERCA expression and activity, but is insufficient to

normalize SERCA function (Figure 4). Thus, we hypothesized that reduction of *Pln* gene expression would be more effective in restoring SERCA function.

We assessed if *Pln* deficiency can affect SERCA function in a dose dependent manner by crossing the $Tbx5^{fl/fl};R26^{CreERT2}$ with germline *Pln* knockout mice ($Pln^{-/-};R26^{CreERT2}$)[102]. We compared SR load and SERCA function in adult-specific *Tbx5; Pln* double mutant mice versus *Tbx5* mutant mice. We measured SR load and SERCA function using caffeine-induced SR release in atrial cardiomyocytes from $R26^{CreERT2}$, $Tbx5^{fl/fl};R26^{CreERT2}$, $Pln^{-/-};R26^{CreERT2}$, $Tbx5^{fl/fl};Pln^{-/+};R26^{CreERT2}$ mice, and $Tbx5^{fl/fl};Pln^{-/-};R26^{CreERT2}$ mice. Control *Pln* deficient mice ($Pln^{-/-};R26^{CreERT2}$) had increased steady state SR load and SERCA activity relative to $R26^{CreERT2}$ (Fig. 5C, D). Interestingly, the decreased SR load and SERCA function observed in *Tbx5* mutant mice ($Tbx5^{fl/fl};R26^{CreERT2}$) was converted to elevated SR load and SERCA function after the removal of *Pln* ($Tbx5^{fl/fl};Pln^{-/-};R26^{CreERT2}$) (Fig. 5C,D). *Pln* loss alone increased peak twitch calcium. However, in the setting of combined *Tbx5; Pln* deficiency, peak twitch calcium and tau twitch were normalized to $R26^{CreERT2}$ values (Fig 5E, F).

We next tested the possibility that decreased SERCA function was the mechanism of TBX5-deficiency driven AP prolongation and triggered activity and that decreased *Pln* may rescue these defects. As we previously showed, $Tbx5^{fl/fl};R26^{CreERT2}$ atrial cardiomyocytes exhibited significantly prolonged APs and frequent EADs and DADs compared to $R26^{CreERT2}$ atrial cardiomyocytes (Fig. 6A,B)[47]. APs of $Pln^{-/-};R26^{CreERT2}$ atrial cardiomyocytes were similar to $R26^{CreERT2}$ controls (Fig. 6C). The prolonged AP duration observed $Tbx5^{fl/fl};R26^{CreERT2}$ was rescued in both $Tbx5^{fl/fl};Pln^{+/-};R26^{CreERT2}$ and $Tbx5^{fl/fl};Pln^{-/-};R26^{CreERT2}$ atrial cardiomyocytes (43 ± 10% and 38 ± 5% shorter than $Tbx5^{fl/fl};R26^{CreERT2}$ respectively; p=0.01,0.0007) (Fig. 6D,E). Along with normalization of AP duration, we observed significantly fewer EADs and DADs in

Tbx5$^{fl/fl}$;*Pln*$^{-/-}$;*R26*^{CreERT2} cardiomyocytes (Fig. 6F). The data demonstrate the importance of TBX5-driven SERCA activity on cellular electrophysiology and triggered activity in atrial cardiomyocytes and decreased *Pln* rescues both SERCA function and cardiomyocyte electrophysiological abnormalities in *Tbx5*-mutant mice.

The data above show reducing *Pln* gene dosage rescues calcium handling defects, AP prolongation and triggered activity observed in *Tbx5* mutant atrial cardiomyocytes. We hypothesized that normalizing these cardiomyocyte cellular defects would reduce AF susceptibility in *Tbx5* knockout mice (Fig. 7). We performed intracardiac burst pacing. All *Tbx5*$^{fl/fl}$; *R26*^{CreERT2} mice (6/6) paced into AF, compared to none of the *R26*^{CreERT2} (0/5) or *Pln*$^{-/-}$;*R26*^{CreERT2} littermate controls (0/7). Consistent with our hypothesis, AF susceptibility was significantly decreased in *Tbx5; Pln* compound knockouts: only 1/11 of *Tbx5*$^{fl/fl}$;*Pln*$^{-/-}$;*R26*^{CreERT2} paced into AF (Fig 7F). Thus, *Tbx5*-deficiency induced AF is due to calcium handling abnormalities, specifically decreased SR load and SERCA activity, and that modulation of the SERCA2 inhibitor, *Pln*, normalized SERCA activity and AF susceptibility caused by *Tbx5* loss.

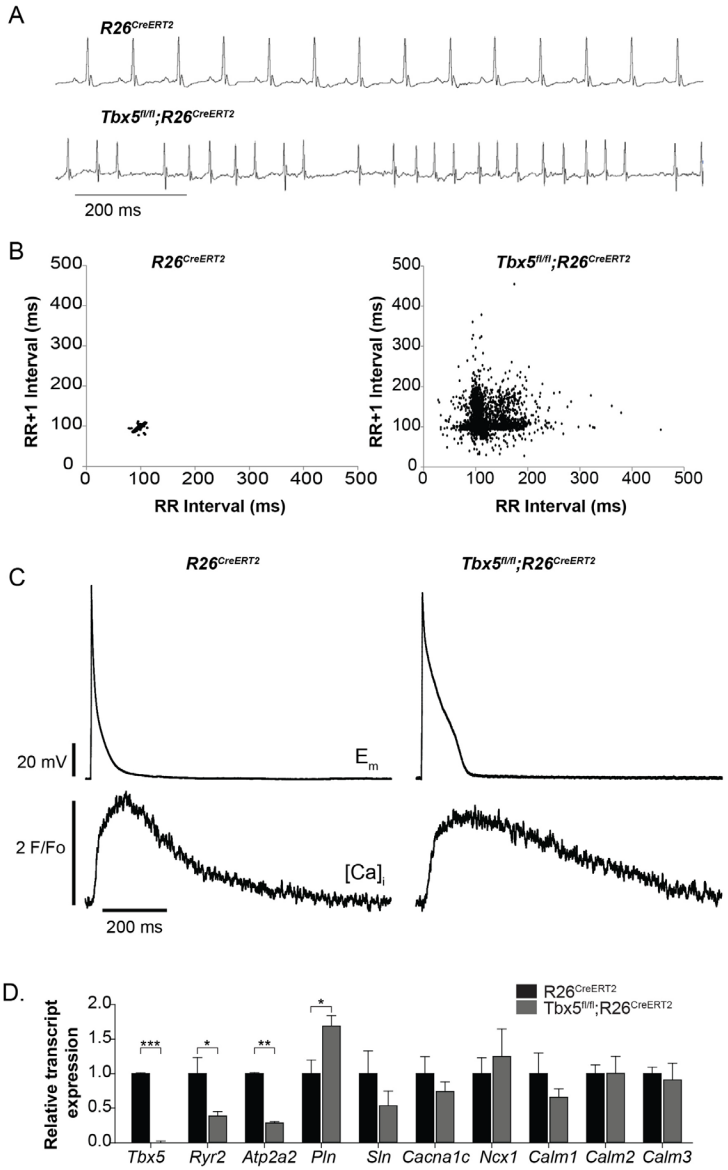

Figure 2-1. Atrial fibrillation in Tbx5fl/fl;R26CreERT2 mice is associated with altered expression of genes important to cellular calcium handling.

(**A**) *Tbx5$^{fl/fl}$;R26^{CreERT2}* mice developed spontaneous AF as assessed by surface ECG compared to *R26^{CreERT2}*. Traces are representative of 15 animals per genotype. (**B**) Poincaré plot shows irregularly irregular rhythm in *Tbx5$^{fl/fl}$;R26^{CreERT2}*, consistent with AF, compared to normal sinus rhythm in *R26^{CreERT2}* mice. Poincaré plots are each one representative animal of 15 animals per genotype. (**C**) Simultaneous AP and $[Ca]_i$ recordings show prolonged AP duration and slowed $[Ca^{2+}]_i$ transient decay in *Tbx5$^{fl/fl}$;R26^{CreERT2}* atrial cardiomyocytes compared to *R26^{CreERT2}*. Recordings are representative of simultaneous $[Ca]_i$ and E_m recordings (myocytes/mice; dual E_m and $[Ca]_i$ from 5/5 *R26^{CreERT2}* and 17/5*Tbx5$^{fl/fl}$;R26^{CreERT2}*, E_m-only from 23/9 *R26^{CreERT2}* and 20/9 *Tbx5$^{fl/fl}$;R26^{CreERT2}*, and $[Ca]_i$-only from 27/6 *R26^{CreERT2}* and 28/6 *Tbx5$^{fl/fl}$;R26^{CreERT2}*).(**D**) Quantitative PCR was performed on RNA isolated from left atrial tissue of 3-5 animals per genotype. mRNA expression of a panel of calcium handling genes potentially important for rhythm regulation was determined. *Ryr2* and *Atp2a2* expression were decreased and *Pln*

Figure 2-1, continued.

expression was increased in *Tbx5*$^{fl/fl}$*;R26*^{CreERT2} relative to *R26*^{CreERT2} atria. (*** $p<0.001$, **, $p<0.01$, *, $p<0.05$)

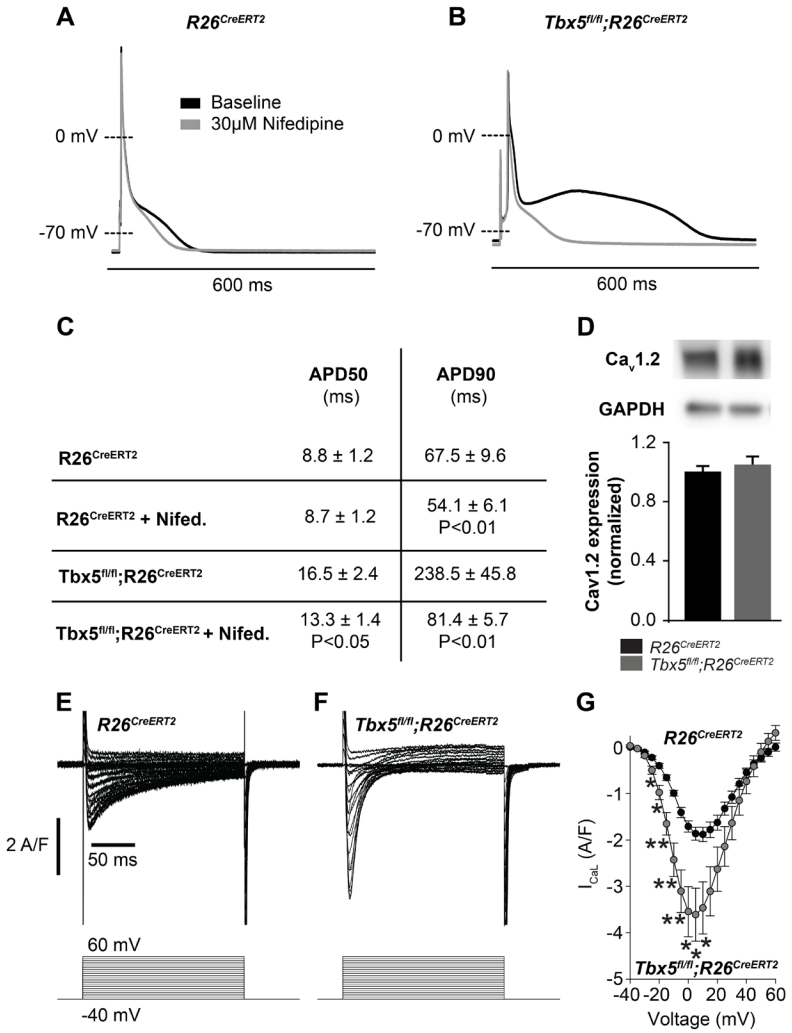

Figure 2-2. Calcium current blockade dramatically shortened the AP in *Tbx5$^{fl/fl}$;R26^{CreERT2}* atrial cardiomyocytes, consistent with the $[Ca]_i$ dependence of AP prolongation following TBX5 loss.

(**A***)* Representative recording of an AP from *R26^{CreERT2}* atrial cardiomyocytes before and after 30 μM nifedipine treatment. (**B**) Representative recording of a *Tbx5$^{fl/fl}$;R26^{CreERT2}* atrial cardiomyocytes before and after nifedipine treatment. (**C**) Paired APD properties before and after treatment with 30 μM nifedipine (myocytes/mice; n=8/3*Tbx5$^{fl/fl}$;R26^{CreERT2}* and n=6/4 *R26^{CreERT2})*. In *R26^{CreERT2}* cardiomyocytes, the effect of nifedipine on APD90 was small, but significant 19±4%. A much larger nifedipine effect was observed in *Tbx5$^{fl/fl}$;R26^{CreERT2}* cardiomyocytes. APD50 decreased by 16±5% and APD90 decreased by 61±6% in the presence of nifedipine. (**D**) Western blot of atrial tissue in 5 animals for each genotype showed protein expression for the alpha 1C subunit of the L-type calcium channel (Cav1.2) was unchanged. (normalized to GAPDH) (**E,F***)* Representative I_{CaL} recordings show Peak L-type calcium current was increased in *Tbx5$^{fl/fl}$;R26^{CreERT2}* cardiomyocytes compared to *R26^{CreERT2}* (G) Average IV relationship of L-type calcium current (myocytes/mice; n=22/7 *R26^{CreERT2}* and 20/5 *Tbx5$^{fl/fl}$;R26^{CreERT2}*). (*** p<0.001, **, p<0.01, *, p≤0.05)

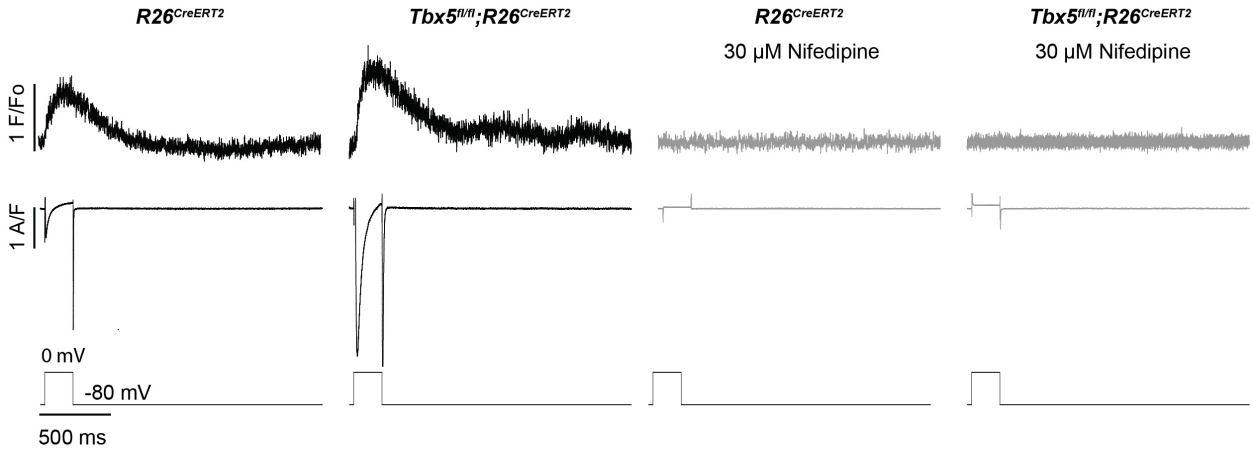

Supplemental Figure 2-2.1. L-type calcium current is sensitive to Nifedipine

30 uM Nifedipine blocks L-type calcium current and calcium-induced calcium release in *R26^{CreERT2} and Tbx5$^{fl/fl}$;R26^{CreERT2}* cardiomyocytes.

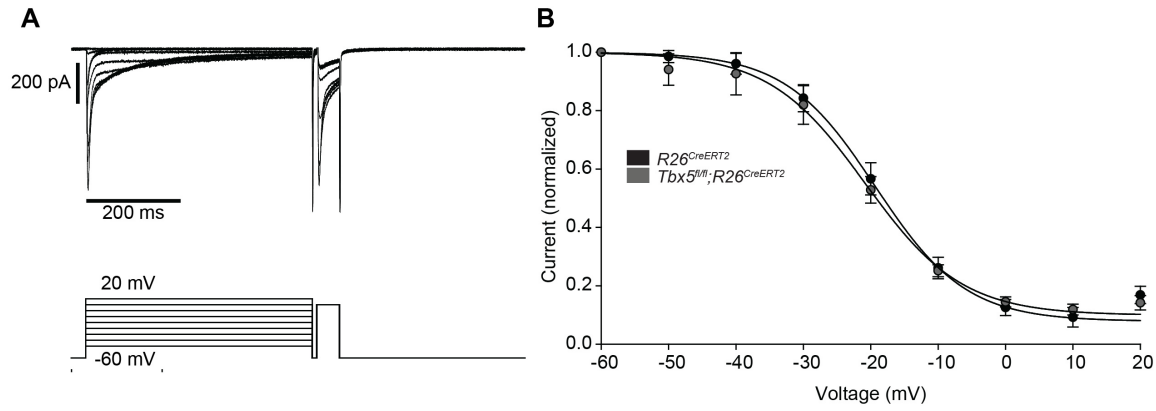

Supplemental Figure 2-2.2. L-type calcium channel inactivation unchanged

A. Protocol used to assess steady state inactivation of I_{CaL} (representative trace from *Tbx5$^{fl/fl}$;R26^{CreERT2}* cardiomyocytes) B. Steady state inactivation of I_{CaL} was the same in *R26^{CreERT2} and Tbx5$^{fl/fl}$;R26^{CreERT2}* cardiomyocytes. (myocytes/mice; Representative of 4/9 *R26^{CreERT2}* and 3/10 *Tbx5$^{fl/fl}$;R26^{CreERT2}*).

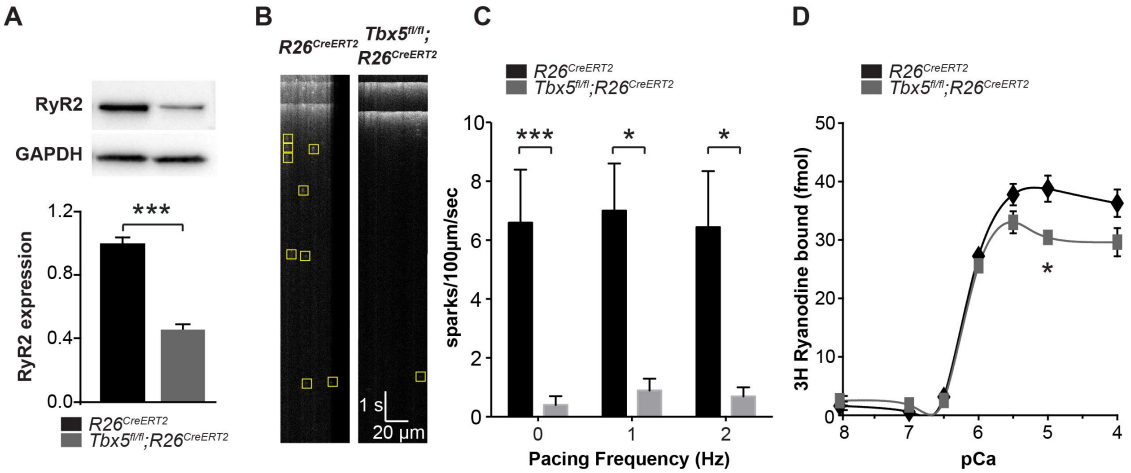

Figure 2-3. Spark frequency is reduced in *Tbx5$^{fl/fl}$;R26^{CreERT2}* atrial cardiomyocytes.

(**A)** Western blot from atrial tissue from 10 animals per genotype was used to measure RyR2 expression. RyR2 was significantly decreased in *Tbx5$^{fl/fl}$;R26^{CreERT2}* atria compared to *R26^{CreERT2}* atria (normalized to GAPDH). (**B**) Fluo-4 loaded cardiomyocytes demonstrated reduced spark frequency in *Tbx5$^{fl/fl}$;R26^{CreERT2}* compared to *R26^{CreERT2}* atrial cardiomyocytes (representative recordings). (**C**) Spark frequency was reduced at rest and after steady state pacing at different frequencies (myocytes/mice; n=12/4 *Tbx5$^{fl/fl}$;R26^{CreERT2}* and n=12/3 *R26^{CreERT2}*). (**D**) Ryanodine binding assay (without normalization) demonstrated no significant difference over the physiologic range of [Ca]ɨ in *Tbx5$^{fl/fl}$;R26^{CreERT2}* compared to *R26^{CreERT2}*. Each measure corresponds to an assay performed on pooled atria from 8-10 mice with 3 independent measures per condition (* $p<0.05$, ** $p<0.01$, *** $p<0.001$).

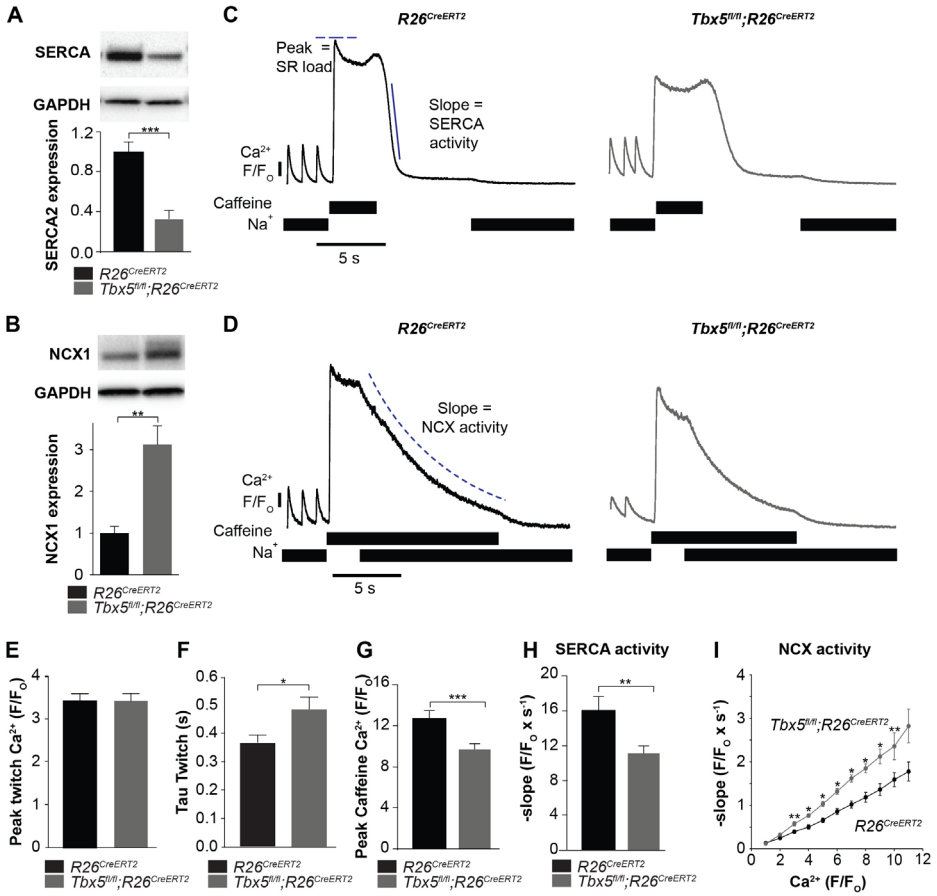

Figure 2-4. SERCA function is decreased while NCX function is increased in *Tbx5$^{fl/fl}$;R26^{CreERT2}* atrial cardiomyocytes.

(**A**) Expression of SERCA2 was significantly decreased while (normalized to GAPDH) (**B**) expression of NCX1 was significantly increased in *Tbx5$^{fl/fl}$;R26^{CreERT2}* atria compared to *R26^{CreERT2}* atria as measured by western blot in 10 animals per genotype. (normalized to GAPDH) (**C**) Application of Na^+ free caffeine solution after pacing to steady state at 1 Hz provided a measurement of SR load. In the absence of extracellular Na^+, $[Ca^{2+}]_i$ plateaued at high levels due to negligible role of non-NCX mediated extrusion in *R26^{CreERT2}* and *Tbx5$^{fl/fl}$;R26^{CreERT2}* atrial cardiomyocytes. Removal of caffeine in the absence of external Na^+ provided a measure of SERCA mediated SR calcium uptake (representative traces). (**D**) Restoration of external Na^+, in the presence of sustained extracellular caffeine provided a measure of NCX mediated calcium efflux (representative traces). (**E**) The peak of steady state twitch $[Ca^{2+}]_i$ transients was similar but (**F**) tau of $[Ca^{2+}]_i$ decay, determined from twitch $[Ca^{2+}]_i$ transients, was increased in *Tbx5$^{fl/fl}$;R26^{CreERT2}* compared to *R26^{CreERT2}* cardiomyocytes (myocytes/mice; n=27/6 *R26^{CreERT2}, n= 28/6 Tbx5$^{fl/fl}$;R26^{CreERT2})*. (**G**) SR load, determined from peak caffeine transients was decreased in *Tbx5$^{fl/fl}$;R26^{CreERT2}* compared to R26^{CreERT2} cardiomyocytes (myocytes/mice; n=34/*6 R26^{CreERT2}, n=32/6 Tbx5$^{fl/fl}$;R26^{CreERT2}*). (**H**) SERCA activity, determined from the maximal rate of calcium decay was diminished in *Tbx5$^{fl/fl}$;R26^{CreERT2}* compared to *R26^{CreERT2}* cardiomyocytes (myocytes/mice; n=29/*3 R26^{CreERT2}, n=32/3 Tbx5$^{fl/fl}$;R26^{CreERT2}*). (**I**) NCX activity (decay slope), was increased at all levels of calcium in *Tbx5$^{fl/fl}$;R26^{CreERT2}* cardiomyocytes (myocytes/mice; n= 35/*3 R26^{CreERT2}, n= 21/3 Tbx5$^{fl/fl}$;R26^{CreERT2})*. (* $p<0.05$, ** $p<0.01$, *** $p<0.001$)

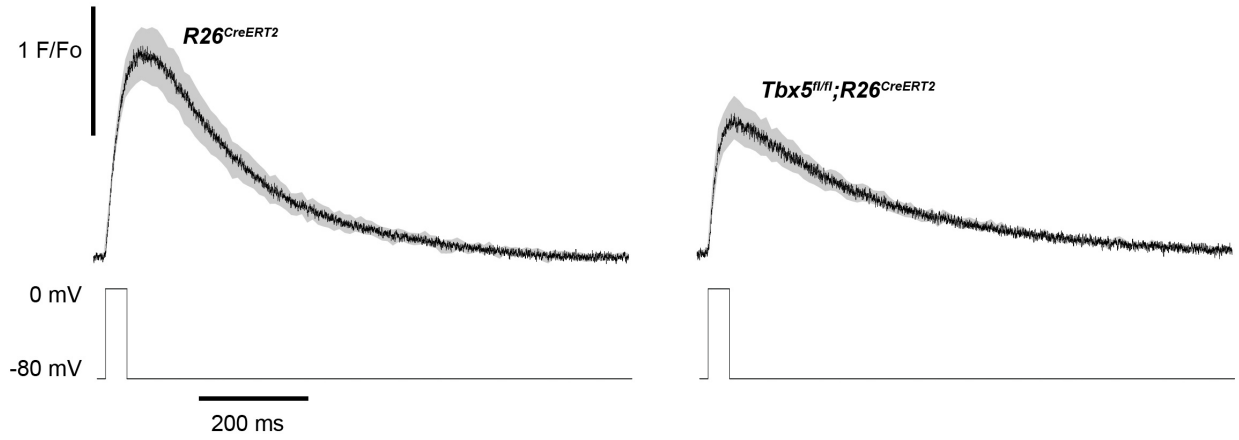

Supplemental Figure 2-4. Tbx5$^{fl/fl}$;R26^{CreERT2} myocytes have lower peak calcium following a square wave protocol.

$[Ca^{2+}]_i$ transients recorded using 40 ms voltage clamp pulses demonstrate 23 ± 4 % (p=.02) reduction in peak calcium in *Tbx5$^{fl/fl}$;R26^{CreERT2}* compared to *R26^{CreERT2}* atrial cardiomyocytes. While the decay kinetics of *Tbx5$^{fl/fl}$;R26^{CreERT2}* are slowed, there no differences in the initial rate of $[Ca^{2+}]_i$ rise (*R26^{CreERT2}* rise slope = 107 ± 11 F/F_o*s; *Tbx5$^{fl/fl}$;R26^{CreERT2}* rise slope = 108 ± 18 F/F_o*s, p=0.96). Average of all myocytes is shown in black with grey indicating standard error of mean (myocytes/mice; n=5/3 *R26^{CreERT2},* n= 13/5 *Tbx5$^{fl/fl}$;R26^{CreERT2})*.

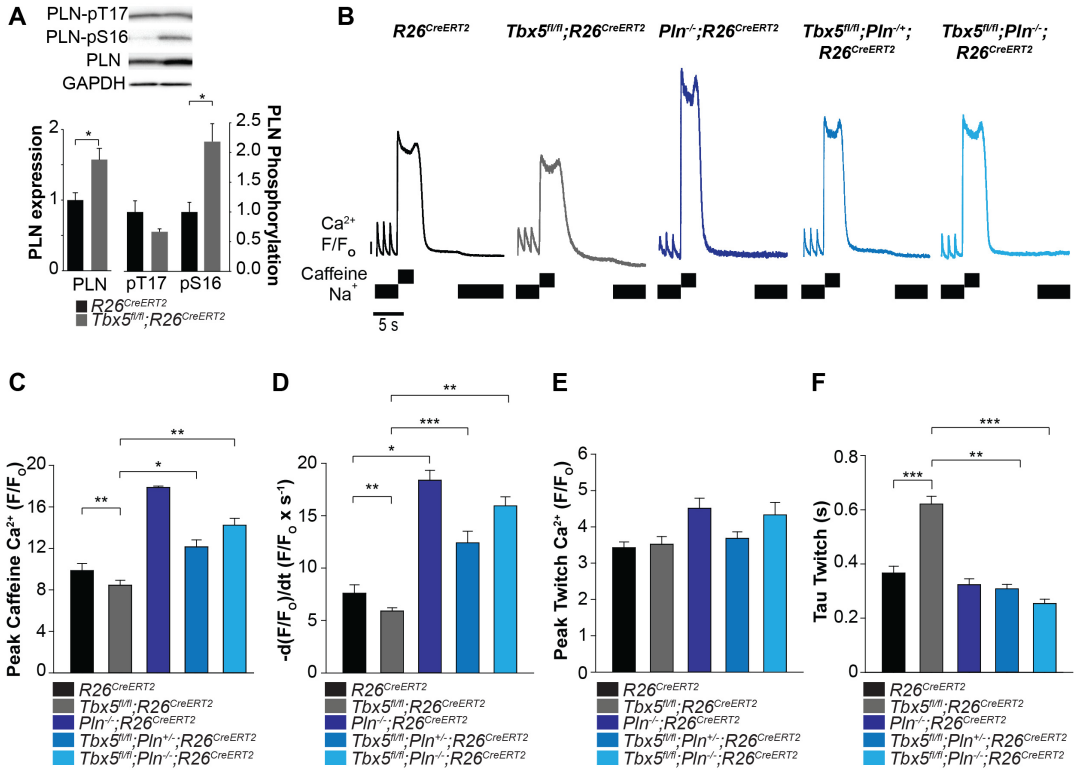

Figure 2-5. Phospholamban knockout normalized SERCA function in *Tbx5*$^{fl/fl}$*;R26*^{CreERT2}.

(**A**) PLN expression was increased in *Tbx5*$^{fl/fl}$*;R26*^{CreERT2} compared to *R26*^{CreERT2} as measured by western blot with 5 animals per genotype. PLN expression was normalized to GAPDH. The proportion of PLN S16, but not T17 phosphorylation was also increased (normalized to PLN). (**B**) Representative SR load and SERCA measurements in *R26*^{CreERT2}, *Tbx5*$^{fl/fl}$*;R26*^{CreERT2}, *Pln*$^{-/-}$*;R26*^{CreERT2}, *Tbx5*$^{fl/fl}$*;Pln*$^{-/+}$*;R26*^{CreERT2} and *Tbx5*$^{fl/fl}$*;Pln*$^{-/-}$*;R26*^{CreERT2} atrial cardiomyocytes were collected as described in Figure 4. (**C, D**) SR load and SERCA function were significantly higher in *Tbx5*$^{fl/fl}$*;Pln*$^{-/+}$*;R26*^{CreERT2} and *Tbx5*$^{fl/fl}$*;Pln*$^{-/-}$*;R26*^{CreERT2} compared to *Tbx5*$^{fl/fl}$*;R26*^{CreERT2} cardiomyocytes and comparable to *R26*^{CreERT2} cardiomyocytes. (**E**) $[Ca^{2+}]_i$ transient peaks were unchanged in *Tbx5*$^{fl/fl}$*;R26*^{CreERT2} ,*Tbx5*$^{fl/fl}$*;Pln*$^{-/+}$*;R26*^{CreERT2} and *Tbx5*$^{fl/fl}$*;Pln*$^{-/-}$*;R26*^{CreERT2}, but increased in *Pln*$^{-/-}$*;R26*^{CreERT2} cardiomyocytes. (**F**) $[Ca^{2+}]_i$ transient decay rate in *Tbx5*$^{fl/fl}$*;Pln*$^{-/+}$*;R26*^{CreERT2} and *Tbx5*$^{fl/fl}$*;Pln*$^{-/-}$*;R26*^{CreERT2} cardiomyocytes were normalized to that of *R26*^{CreERT2} cardiomyocytes (myocytes/mice; n=34/3 *R26*^{CreERT}, n=36/3 *Tbx5*$^{fl/fl}$*;R26*^{CreERT2}, n=30/3 *Pln*$^{-/-}$*;R26*^{CreERT2}, n=*21*/3 *Tbx5*$^{fl/fl}$*;Pln*$^{-/+}$*;R26*^{CreERT2}, *n=27*/3 *Tbx5*$^{fl/fl}$*;Pln*$^{-/-}$ atrial cardiomyocytes). (* $p<0.05$, ** $p<0.01$, *** $p<0.001$)

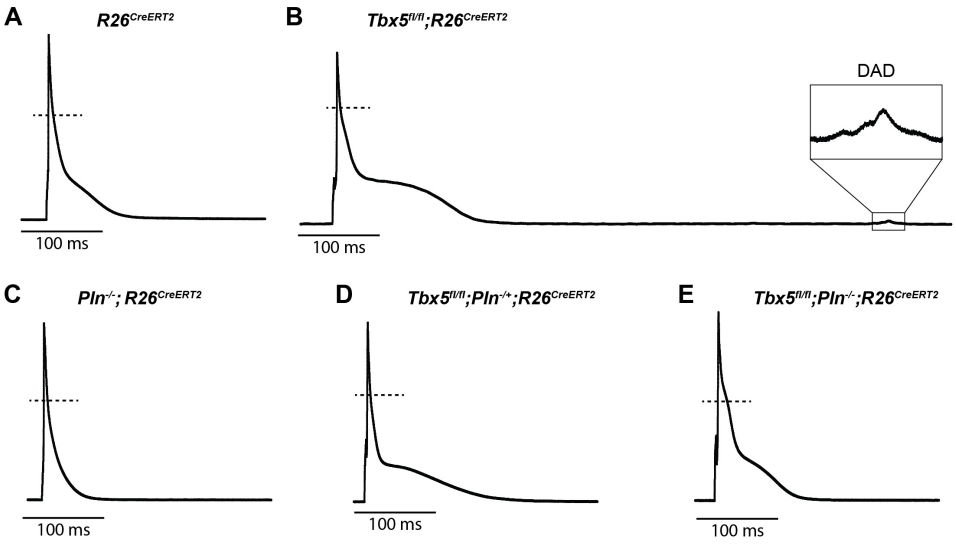

F

	RMP (mV)	AP Max(mV)	APD50 (ms)	APD90 (ms)	EAD	DAD
R26^{CreERT2}	-78.0 ± 1.4	57.6 ± 1.7	7.8 ± 0.6*	55.8 ± 5.1***	0/18*	0/18**
Tbx5$^{fl/fl}$;R26^{CreERT2}	-78.7 ± 1.3	50.5 ± 6.9	21.7 ± 3.9	144.4 ± 13.2	6/24	8/24
Pln$^{-/-}$; R26^{CreERT2}	-79.7 ± 2.0	56.5 ± 5.0	9.4 ± 0.8	50.5 ± 4.1***	1/12	4/12
Tbx5$^{fl/fl}$;Pln$^{-/+}$;R26^{CreERT2}	-79.9 ± 1.3	60.9 ± 2.8	7.9 ± 0.9	81.4 ± 13.1*	0/9	1/9
Tbx5$^{fl/fl}$;Pln$^{-/-}$;R26^{CreERT2}	-82.6 ± 0.6*	49.8 ± 3.5	17.0 ± 2.2	88.4 ± 6.9***	0/22*	1/22*

Figure 2-6. PLN knockout normalized AP duration and prevented triggered activity in *Tbx5$^{fl/fl}$;R26^{CreERT2}*.

Representative APs recorded from (**A**) *R26^{CreERT}*, (**B**)*Tbx5$^{fl/fl}$;R26^{CreERT2},* (**C**)*Pln$^{-/-}$;R26^{CreERT2}*, (**D**)*Tbx5$^{fl/fl}$;Pln$^{-/+}$;R26^{CreERT2},* (**E**)*Tbx5$^{fl/fl}$;Pln$^{-/-}$* atrial cardiomyocytes as described previously in Figure 2. (**F**) TBX5-loss dependent AP prolongation and frequency of triggered activity was normalized by phospholamban knockout (myocytes/mice: n=18/7 *R26^{CreERT}*, n=24/12 *Tbx5$^{fl/fl}$;R26^{CreERT2},* n=12/5 *Pln$^{-/-}$;R26^{CreERT2}*, n=9/3 *Tbx5$^{fl/fl}$;Pln$^{-/+}$;R26^{CreERT2}, and n=22*/3 *Tbx5$^{fl/fl}$;Pln$^{-/-}$*). (* p<0.05, ** p<0.01, *** p<0.001)

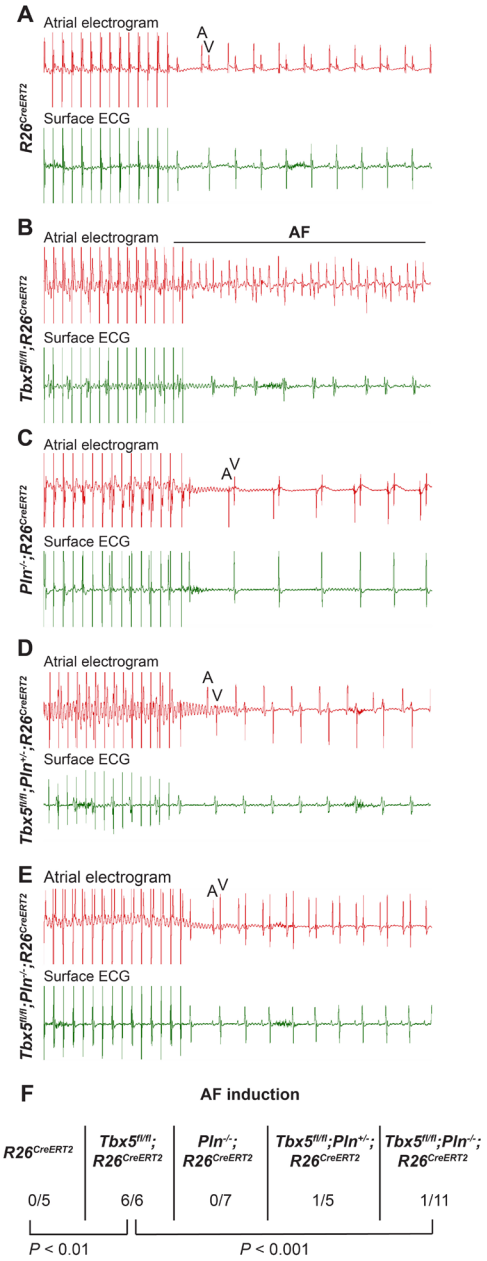

Figure 2-7. PLN deficiency protected against TBX5-loss associated AF.

Intra-atrial pacing was used to induce AF. Representative intracardiac atrial electrogram recordings and corresponding surface ECG are shown from (A) $R26^{CreERT2}$, (B)$Tbx5^{fl/fl}$;$R26^{CreERT2}$, (C)$Pln^{-/-}$;$R26^{CreERT2}$, (D)$Tbx5^{fl/fl}$;$Pln^{-/+}$;$R26^{CreERT2}$, (E)$Tbx5^{fl/fl}$;$Pln^{-/-}$;$R26^{CreERT2}$ atrial cardiomyocytes. A, atrial electrical signal; V, far field ventricular electrical signal. (F) AF was reproducibly demonstrated in 6/6 Tbx5 knockouts in contrast to 1/11 Pln/Tbx5 double knockouts, indicating rescue of atrial arrhythmogenesis. P values were determined by Fisher's exact test (n=5 $R26^{CreERT2}$, n=6 $Tbx5^{fl/fl}$;$R26^{CreERT2}$, n=7 $Pln^{-/-}$;$R26^{CreERT2}$, and n=5 $Tbx5^{fl/fl}$;$Pln^{-/+}$;$R26^{CreERT2}$, n=11 $Tbx5^{fl/fl}$;$Pln^{-/-}$ mice)

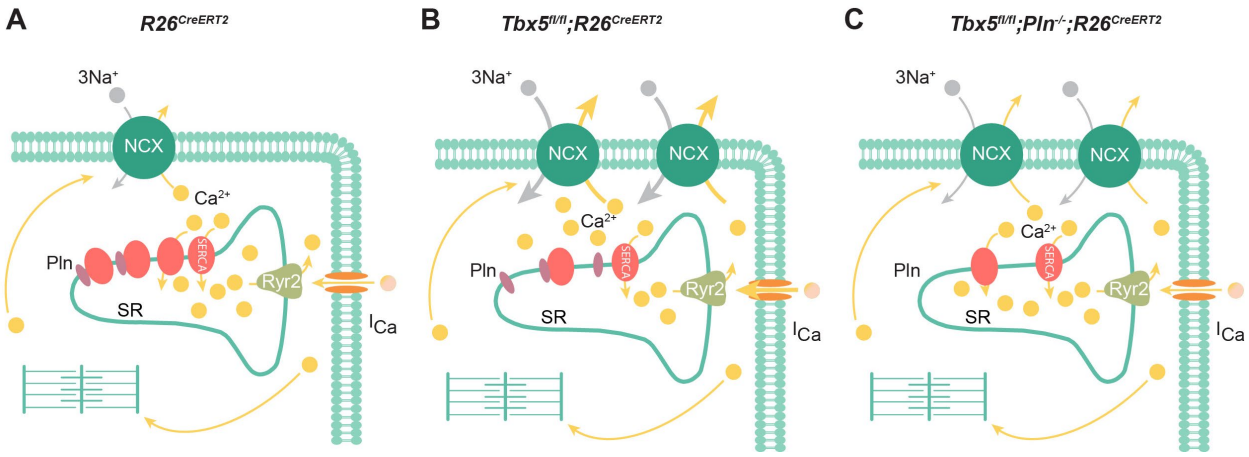

Figure 2-8. Model of TBX5-dependent calcium regulation in atrial cardiomyocytes.

(A) Excitation-contraction coupling of atrial cardiomyocytes is achieved through regulation of intracellular calcium handling. (B) Adult-specific *Tbx5*-knockout leads to decreased expression of SERCA2 and increased expression of PLN, leading to decreased SR Ca^{2+} load. In addition, removal of *Tbx5* is associated with increased NCX1 expression and activity, thereby increasing Ca^{2+} extrusion, which is balanced by increased L-type calcium entry. (C) Combined *Tbx5/Pln* knockout relieves repression of SERCA2. This results in normalization of SERCA activity and rescue of cardiomyocyte ectopy, triggered activity, and AF observed with *Tbx5* deficiency.

Discussion

AF initiation has been linked to calcium handling abnormalities in computational and *in vivo* disease models[106, 107]. Ectopic or triggered activity in the form of EADs and DADs are often due to calcium handling abnormalities that increase NCX activity and promote AF initiation[107]. However, the mechanism underlying genetic predispositions for AF remain poorly understood. Genetic variants and mutations at the *Tbx5* locus are associated with increased risk for human AF and *Tbx5*-mutant mice show both spontaneous and burst pacing-induced AF[47]. We report a calcium transport mechanism for *Tbx5* dependent ectopic activity. We show that TBX5 is a critical regulator of SERCA-mediated SR calcium handling and that *Tbx5*-deficient mice have increased NCX-mediated Ca^{2+} extrusion, balanced by increased I_{CaL} mediated Ca^{2+} influx. These calcium handling abnormalities provide a mechanism explaining the frequent triggered activity observed after TBX5 knockout. We show that decreasing phospholamban dosage can normalize TBX5-loss associated cellular calcium handling abnormalities, shorten AP duration, prevent triggered activity, and diminish AF susceptibility.

Decreased SERCA activity and SR load in TBX5-loss associated atrial fibrillation

We and others have hypothesized that ectopic triggers of AF can be due to abnormal atrial calcium handling. Here we define this relationship in a model of spontaneous AF[96, 108]. We analyzed the major calcium transport pathways in atrial myocytes and demonstrated that the critical calcium handling deficit associated with *Tbx5*-loss is depressed SERCA-mediated SR calcium uptake. We report significant reduction of SERCA2 protein expression and function, consistent with human paroxysmal or chronic AF[87, 88, 97, 98].

The mechanism causing cardiomyocyte depolarizations from depressed SERCA activity must be indirect, given that SERCA2 is localized to the intracellular SR membrane and therefore does not directly contribute to membrane potential itself. Instead, slowed SR calcium uptake from depressed SERCA activity provides higher cytosolic calcium driving force for calcium extrusion from the cell via electrogenic inward I_{NCX}.

Increased NCX activity in Tbx5- mutant atrial cardiomyocytes drives ectopic activity

We demonstrate increased NCX1 protein expression with *Tbx5* knockout, a finding also observed in human and other animal models of AF[91, 94, 96, 97]. Since protein expression, electrochemical driving force, and allosteric calcium regulation can all affect amplitude of inward I_{NCX}[109], we measured NCX activity following loss of *Tbx5*. NCX activity was significantly increased at all levels of calcium (Fig.4I). Thus, increased NCX function coupled with prolonged $[Ca^{2+}]_i$ transients, drives increased inward I_{NCX}, providing additional depolarizing current during the AP, contributing to its prolongation. While increased NCX function may partially compensate for the depressed SERCA function to bring down calcium levels, it may also promote calcium-induced delayed afterdepolarizations in the setting of inappropriately timed SR calcium release events. Previous modeling in ventricular cardiomyocytes predicted countervailing functions of SERCA and NCX[110], which we observed in *Tbx5* knockout mice. Our data further support that DADs, which are classically thought to relate to SR calcium overload can still occur with depressed SR loads in the appropriate context of depressed SERCA and elevated NCX function[87].

Modeling suggests that compensatory increases in L-type calcium current in the setting of depressed SERCA function could be required to maintain systolic and diastolic calcium levels[110].

In line with the modeling, we observed enhanced peak I_{CaL} with loss of *Tbx5*. This may account for early AP prolongation as well as EADs. It is interesting that peak $[Ca]_i$ is depressed using controlled square wave voltage clamp pulses (Fig. 4-figure supplement 1), which suggests that 40 ms is insufficient to maintain calcium entry in *Tbx5* knockout, even in the setting of enhanced I_{CaL}. However, in the setting of AP prolongation (Fig. 2E-G) peak twitch calcium levels are maintained. Additionally, the increase in calcium entering the cell through I_{CaL} during the AP would be expected to balance a net increase in NCX mediated calcium extrusion (Fig. 4I), a requirement for steady state $[Ca^{2+}]_i$ homeostasis. However, our observations that L-type calcium channel expression is TBX5-independent (Fig. 1D, 2D) and that genetically targeting only the Ca^{2+} efflux pathways in our model is sufficient to restore normal electrical activity (Fig. 5-7) suggest that the I_{CaL} change is not a primary TBX5-dependent effect. Furthermore, although I_{CaL} is increased, it quickly inactivates in TBX5 knockout cardiomyocytes (Fig. 2F). Together with our observation that nifedipine normalizes the APD, this supports that enhanced calcium entry impacts APD via secondary $[Ca]_i$ dependent mechanisms.

TBX5 loss results in reduced RyR2 expression

In addition to identifying the role of altered NCX and SERCA function, we assessed the importance of TBX5-driven RyR2 expression. *RYR2* is a known susceptibility locus for AF and *RYR2* mutations are correlated with AF. We observed that RyR2 protein expression was significantly depressed following *Tbx5* loss[3, 111]. Defective RyR2 function has also been associated with AF[89, 112]. Despite TBX5-dependent RyR2 expression, the ryanodine binding assay[113] suggested that RyR2 function is generally preserved over the physiologic range of calcium in *Tbx5*-mutant atria (Fig. 3D). This suggests a compensatory mechanism must occur allowing for preserved RyR2 open probability in the setting of depressed protein expression. For

example, CaMKII is a potential regulator of RyR2 function which could increase the open probability and thereby increase steady leakage or favor spontaneous local Ca^{2+} release events from the SR[89, 91, 114] in *Tbx5*-deficient mice. In line with such compensation, we could not detect any differences in the calcium rise kinetics during controlled square wave voltage clamp pulses (Fig.4-figure supplement 1). Nevertheless, RyR2 compensation in the setting of reduced expression could contribute to abnormal triggered activity in the setting of *Tbx5* loss, and is an important topic for further investigation.

Abnormalities of the TBX5/SERCA2/PLN regulatory axis drive AF formation.

We found that depressed SERCA function in TBX5 knockout was completely normalized with heterozygous or homozygous phospholamban knockout, which normalized AP duration, decreased frequency of afterdepolarizations, and reduced AF inducibility. This finding demonstrates the importance of SERCA2 to the pathophysiology of AF in the *Tbx5*-loss model. While phospholamban has been associated with AF by GWAS[3, 104], its functional role is less clear. Although PLN is predominantly found in the ventricle[115], we showed not only its expression is increased in the atria in the context of *Tbx5* loss, but also PLN participates in rheostatic control of SERCA activity in the atria, which is sufficient to protect against AF inducibility (Fig. 5-7). Our findings are further supported by patient studies. For example, in patients who experience post-operative AF, SERCA2 is significantly decreased in the atrial tissue[116], but those with PLN mutations have decreased AF susceptibility in the context of arrhythmogenic right ventricular cardiomyopathy[117]. Thus, AF is a heterogeneous disease and there can be variability in how the calcium handling proteins are expressed[118] in different disease settings. The genetic background of an individual may be a critical determinant of how calcium handling moieties are disrupted to result in AF.

In summary, the most important features of the *Tbx5*-dependent SERCA2 and PLN regulatory axis are reduced SR uptake and load (Fig. 8). In this setting, enhanced inward I_{NCX} and I_{CaL} contributes to AP prolongation, and, more importantly, to cardiomyocyte ectopy. Finally, we demonstrate PLN as a potential means to augment SERCA function, restoring normal atrial myocyte electrical activity and normal sinus rhythm in *Tbx5* knockout mice. Thus, the *Tbx5*- knockout model represents an excellent system to study pharmacologic rescue of SERCA activity, prevention of cardiomyocyte ectopy, and AF.

Broader implications for clinical treatment of AF

AF has become an increasingly common cause of morbidity and mortality, underlying over one-third of stroke cases and significantly increases the risk for heart failure[81]. Consequently, AF poses a significant socioeconomic burden. AF does not always exist in isolation, but rather in conjunction with other predisposing factors such as obesity, thyroid hormone alterations, or heart failure. Interestingly, disruptions in calcium handling proteins such the SERCA2-PLN regulatory axis are implicated as predisposing factors. In AF compounded by heart failure, decreased SERCA2 and phosphorylated PLN, and increased NCX1 expression were observed[119]. Decrease in phosphorylated PLN coupled with an increase in total PLN has been found in animal models of obesity, potentially increasing risk of AF[120, 121]. These findings suggest a need to evaluate an individual's genetic background as well as changes in calcium handling proteins when considering predisposing factors for AF.

Currently, there are few effective and targeted AF therapies, in part due to an incomplete understanding of the mechanisms underlying AF. Recent studies of specific genetic loci for AF susceptibility have opened new opportunities to identify specific mechanisms at play in

subpopulations of AF patients. Understanding these specific mechanisms may facilitate more effective personalized therapies to target specific atrial Ca^{2+} handling abnormalities. Our data is consistent with the knowledge that pharmacologic regulators of NCX1 or SERCA2 may normalize defects in cellular calcium handling in the atrium[86, 122-125]. For example, a selective NCX1 inhibitor, ORM-10103, was shown to prevent cellular Ca^{2+} handling abnormalities in ischemic ventricular cardiomyocytes, possibly by limiting calcium entry through outward I_{NCX}.[122, 126] The benefit of NCX inhibition might also be considered in human cases of AF with increased NCX activity. Further, resveratrol, which increases SERCA2 activity, has been shown to decrease AF, suggesting that targeting SERCA2 activity may be a viable therapeutic approach[127, 128]. In addition to providing specific insight into treating TBX5-loss associated AF, our findings may be more broadly applied. These data suggest that pharmacological treatment of AF may be improved by assessing for a defect in the TBX5-SERCA2-PLN axis followed by specifically targeting the defect to restore normal cardiomyocyte electrical activity. We expect this work and continued efforts to uncover mechanisms responsible for AF in subpopulations of patients will play a key role in advancing personalized therapeutics for AF.

Chapter III: Atrial fibrillation risk loci interact to modulate Ca^{2+}-dependent atrial rhythm homeostasis

Authors: Brigitte Laforest[*], Wenli Dai[*], Leonid Tyan, Sonja Lazarevic, Kaitlyn Shen, Margaret Gadek, Michael T. Broman, Christopher Weber[§] and Ivan P. Moskowitz[§]

*These authors contributed equally to this work

[§] Co-corresponding authorship

Abstract

Atrial Fibrillation (AF), defined by disorganized atrial cardiac rhythm, is the most prevalent cardiac arrhythmia world-wide. Recent genetic studies have highlighted a major heritable component and identified numerous loci associated with AF risk, including the cardiogenic transcription factor genes *TBX5, GATA4*, and *NKX2-5*. We report that *Tbx5* and *Gata4* interact with opposite sign for atrial rhythm control than for cardiac development. Using mouse genetics, we find that AF pathophysiology caused by *Tbx5* haploinsufficiency, including atrial arrhythmia susceptibility, prolonged action potential duration, and ectopic cardiomyocyte depolarizations were all rescued by *Gata4* haploinsufficiency. In contrast, *Nkx2-5* haploinsufficiency showed no combinatorial effect. The molecular basis of the TBX5/GATA4 interaction included normalization of intra-cardiomyocyte calcium flux and expression of calcium channel genes *Atp2a2* and *Ryr2*. Furthermore, GATA4 and TBX5 show antagonistic interactions on a *Ryr2* enhancer. Atrial rhythm instability caused by *Tbx5* haploinsufficiency was rescued by decreased dose of *Pln*, a SERCA inhibitor, consistent with a role for decreased sarcoplasmic reticulum calcium flux in *Tbx5*-

dependent AF susceptibility. This work defines a link between *Tbx5* dose, SR calcium flux, and AF propensity. The unexpected interactions between *Tbx5* and *Gata4* in atrial rhythm control suggest that evaluating specific interactions between genetic risk loci will be necessary for ascertaining personalized risk from genetic association data.

Introduction

Atrial fibrillation (AF) is the most common sustained cardiac arrhythmia, affecting more than 7 million Americans and 33 million people worldwide [2]. AF is characterized by an irregular pattern of atrial depolarization, resulting in rapid and disorganized atrial conduction and lack of effective atrial chamber contraction. The rhythm abnormality in AF manifests with circulatory deficits and systemic thromboembolism that greatly increase morbidity and mortality. Because age is an independent risk factor for AF, its prevalence is expected to rise significantly as the population ages. AF has become a major clinical and economic burden, owing to the limitations and side effects associated with current AF therapies. Although AF most often manifests in the context of pre-existing cardiac pathologies, such as hypertension and cardiomyopathy, idiopathic or lone AF forms indicated a heritable component [57]. Genome-wide association studies (GWAS) have to date identified over one hundred AF-associated loci, including many transcription factor (TF) loci, suggesting that transcriptional control of atrial rhythm is an important mediator of AF risk [3, 129].

Recent work has illuminated a role for abnormal cardiomyocyte calcium (Ca^{2+}) handling in the cellular pathophysiology of AF. The current paradigm of AF causation describes ectopic (triggered) atrial activity, mediated by early and delayed afterdepolarization (EAD and DAD) events, and a fibrillogenic substrate that propagates the abnormal triggers causing arrhythmia. EADs and DADs have been associated with abnormal cardiomyocyte Ca^2 handling, including RYR2 dysfunction, reduced SERCA2 (encoded by *ATP2A2*) activity, and/or increased Na^+/Ca^{2+} exchanger (NCX) activity [91, 97, 106, 130, 131]. How alterations of *RYR2*, *ATP2A2*, or *NCX* expression in AF models contributes to AF risk remains to be defined.

GWAS and familial inheritance have implicated transcription factor genes in AF pathogenesis, including the cardiogenic transcription factors (TFs) TBX5, GATA4 and NKX2-5

[57, 58]. Autosomal dominant mutations in the T-box TF *TBX5* cause Holt-Oram syndrome, characterized by upper limb malformations, congenital heart defects, cardiac conduction system abnormalities, and increased AF risk [132, 133]. In addition, GWAS has identified common risk variants associated with PR interval and increased AF susceptibility in intergenic or intronic regions of TBX5 [134-137]. Adult-specific *Tbx5* deletion in mice leads to spontaneous and sustained AF, characterized by slowed conduction and decrements in the expression of ion channels linked to AF [47]. TBX5 drives the atrial expression of *Pitx2*, and TBX5 and PITX2 co-modulate the expression of cardiac rhythm effector genes, including *Ryr2* and *Atp2a2*. These findings indicated that interactions between TBX5 and PITX2 provide tight control of an atrial rhythm gene regulatory network and that perturbation of this network triggered AF susceptibility [47]. This example suggested that cardiac TFs implicated in AF by genetic association may co-regulate a gene regulatory network for atrial rhythm homeostasis. GATA4 and NKX2-5 are particularly relevant candidates, given that they both interact physically and genetically with TBX5 during cardiac development. GATA4, a zinc finger transcription factor, plays critical roles in heart development and cardiomyocyte differentiation [138-140]. Several *GATA4* loss-of-function mutations have been reported to underlie AF susceptibility in humans [58, 141-143]. GATA4 is highly expressed in adult cardiomyocytes, however its specific role in atrial cardiac rhythm has not been investigated. *NKX2-5*, a homeodomain containing TF has been implicated in AF by GWAS and family studies [134, 144-146]. Common variants associated with PR prolongation, a marker for increased AF risk, have also been identified close to *NKX2-5* by GWAS [134]. Heterozygous mutations in *NKX2-5* are associated with a spectrum of congenital heart diseases (CHD) in humans and mice [147-151]. NKX2-5 also has been shown to regulate a number of target genes involved in the cardiomyocyte action potential, suggesting that it may play a direct role in AF predisposition [152].

Combinatorial interactions between TBX5, GATA4 and NKX2-5 are critical for heart development. TBX5, GATA4, and NKX2-5 physically interact and CHD-causing (but not CHD-sparing) mutations in TBX5 abrogate these interactions [153]. Mutations in *GATA4* that disrupt transcriptional cooperativity with TBX5 result in CHD and impaired cardiac gene expression, leading to aberrant chromatin states and gene expression [153, 154]. *Tbx5/Gata4* double heterozygous mice develop cardiac defects that are more severe than *Tbx5* or *Gata4* haploinsufficient mice alone, providing evidence for a cooperative interaction [155]. TBX5, NKX2-5 and GATA4 synergistically activate multiple cardiac enhancers and promoters [100, 153, 156-164]. Cooperative interactions between TBX5, NKX2-5 and GATA4 on cardiac gene expression may rely on interdependent binding of these factors genome-wide, enabling co-regulation of the cardiac differentiation program [165]. Removal of *Tbx5* or *Nkx2-5* in mouse ES cell cardiac differentiations or *GATA4* in human iPS cardiac differentiations resulted in inappropriate distribution of the other TFs to lineage-inappropriate sites, inducing ectopic gene regulation [154, 165]. This paradigm suggested that heterotypic interactions between these cardiogenic TFs may influence atrial rhythm control.

We investigated the combinatorial genetic interactions between the cardiogenic transcription factors *Tbx5*, *Gata4*, and or *Nkx2-5* in murine atrial rhythm control. We hypothesized that adult-specific combined *Tbx5*, *Gata4*, or *Nkx2-5* haploinsufficiency may alter AF susceptibility and illuminate AF pathophysiology. Surprisingly, we found that *Gata4* haploinsufficiency rescued the cardiac rhythm, cardiomyocyte electrophysiology, and molecular defects caused by *Tbx5* haploinsufficiency. In contrast, introducing *Nkx2-5* haploinsufficiency had no observed effect on the penetrance or severity of defects caused by *Tbx5* haploinsufficiency alone. *Gata4* haploinsufficiency rescued the calcium handling defects and *Ryr2* and *Atp2a2* gene expression deficits caused by *Tbx5* haploinsufficiency. We found that GATA4 negatively

modulated TBX5 activation of a *cis*-regulatory element at *Ryr2*. This observation indicated that GATA4 could repress TBX5-dependent transcriptional activation in some contexts, and provided a molecular model for the rescue of *Tbx5* haploinsufficiency by *Gata4* haploinsufficiency. We tested the hypothesis that rescue of *Tbx5* haploinsufficiency was mediated by rescue of calcium homeostasis. Introduction of haploinsufficiency for phospholamban (Pln), a SERCA inhibitor, into *Tbx5* haploinsufficient mice caused normalization of cardiac rhythm and rescue of SERCA activity. Rescue of the *Tbx5* haploinsufficient phenotype by *Gata4* deficiency illuminated a novel TF genetic interaction in atrial rhythm control and provided a molecular model for transcriptional control of cardiomyocyte calcium flux as a central component of atrial rhythm homeostasis.

Methods

Experimental Design: This study was designed to investigate the oligogenic interaction of TFs that have been linked to AF by GWAS studies. We used murine models of conditional *Tbx5* deletion, conditional *Gata4* deletion, conditional *Nkx2-5* deletion and germline *Pln* heterozygosity for their similarities to human AF phenotype. The number of mice per genotype depended on the experiments and is specified in figure legends. For animal studies, littermates were used as controls and mice were grouped when appropriate. Endpoints for studies were selected according the phenotype of adult *Tbx5* haploinsufficient mice. For single cell electrophysiology and calcium flux measurements, 3-5 mice per genotype were analyzed and a total of 10 cells were recorded for every mouse. All experiments, recordings and analysis were performed in a blinded fashion. Outliers were excluded if samples/replicates were >2 SDs from the population mean.

Transgenic mice: $Tbx5^{fl/fl}$, $Gata4^{fl/fl}$, $Nkx2\text{-}5^{fl/fl}$, $Pln^{+/-}$ and $Rosa26^{CreERT2}$ mice have all been previously described [100-102, 148, 166]. Mice were maintained on a mixed genetic background,

harboring one copy of the Cre recombinase. All experiments involving *Tbx5*, *Gata4, NKx2-5* and *Pln* heterozygotes and *Gata4/Tbx5*, *Tbx5/Nkx2-5*, *Gata4/Nkx2-5* and *Tbx5/Pln* compound heterozygotes and *Tbx5/Gata4/Nkx2-5* triple heterozygotes were performed 2 weeks after TM treatment, and age-matched littermate controls ($R26^{CreERT2}$) were used for comparison. 200 µl of tamoxifen (20 mg/ml in corn oil) was administered for three consecutive days by intraperitoneal injection at 6- to 8-weeks of age, as previously described [47].

Telemetry ECG recordings: Ambulatory ECG studies were performed on 8- to 10-weeks old mice. Mice were anesthetized using isoflurane, and telemetry transmitters (ETA-F10, Data Science International (DSI)) were implanted subcutaneously in the back with leads tunneled to the right upper and left lower thorax, as previously described [167]. After post-implant recovery period of one day, baseline recordings were collected by DSI telemetric physiological monitor system. *P* wave duration, PR interval and Poincare plots were calculated using Ponemah Physiology Platform (DSI) and custom Python script.

Intracardiac electrophysiology studies: Animals underwent catheter-based intracardiac recordings 2 weeks after receiving TM, as previously described [47]. Mice were anesthetized with isoflurane, and right atrial and ventricular electrograms as well as surface electrogram were recorded using a 1.1-F octapolar catheter (EPR-800, Millar Instruments) inserted via the right jugular vein. Programmed extra-stimulation protocols and burst pacing were used to induce atrial tachycardia and AF in animal subjects. Programmed right atrial extra-stimulation was carried out using S1 drive trains of 80 ms followed by 5 extra-stimulations at 50 ms each. Burst pacing was performed by applying a series of single extra-stimulus delivered at a constant pacing rate of 15-20 ppm (900-1200 bpm). Inducibility was considered positive if two or more series of atrial tachycardia and/or fibrillation was observed following burst pacing in the same animal.

Fibrillation was considered non inducible if zero or one cycle or irregular atrial rhythm was observed in the animal.

Echocardiography: Transthoracic echocardiography was performed two weeks post-TM treatment under inhaled isoflurane, delivered via a nose cone, as previously described [168]. Briefly, animals were imaged with a VisualSonics Vevo 770 machine (VisualSonics) using a 30-MHz high-frequency transducer. Body temperature was maintained using a heated imaging platform. 2-dimensional images were recorded in parasternal long- and short-axis projections, with guided M-mode recordings at the midventricular level in both views. M-mode echocardiographic images were obtained at the mid-papillary muscle level in the parasternal short-axis view and measurement calculated at the same level from M- and/or B-mode images of long- or short axis view. Left ventricular dimensions in both diastole and systole were measured form at least three different beats from each projection and averaged to calculate the left ventricular ejection fraction.

Calcium flux measurement: Single cell atrial cardiomyocytes were isolated by Langendorff perfusion with 2mg/mL of Collagenase Type 2 at 5 ml/min. Atrial myocytes were plated on laminin coated glass bottom dishes and incubated at room temperature for 30 minutes prior to incubation with Fluo-4/AM (Molecular Probes/Invitrogen). Cells were then incubated with 10 μM Fluo-4/AM for one hour in normal Tyrode's solution containing (in mM): 140 NaCl, 4 KCl, 10 glucose, 10 HEPES, and 1 $MgCl_2$, 1 $CaCl_2$, with pH 7.4 using NaOH, followed by a 10min perfusion wash with pre-warmed Tyrode. SERCA and NCX measurements were performed using an Olympus microscope with a x20 objective lens, a LAMBDA DG-4 power source with a 488 excitation and 515 excitation filters and a PMT (Microphotometer) to record whole cell signal, with electrical field stimulation (Grass stimulator; Astro-Med) at 1 Hz. SERCA and NCX

activities were measured as follow: sodium-free caffeine (10 mM) containing solution was applied in the absence of extracellular sodium and the cells returned to normal Tyrode at the end of the recording. In the presence of sodium- free caffeine Tyrode, the intracellular calcium remains elevated and the peak value is a measure of SR calcium load that was released into the cytosol.

Whole-cell electrophysiological recordings: Action potentials were recorded using the whole-cell patch-clamp method [47]. Whole-cell action potentials were recorded using an Axopatch-200B amplifier connected to a Digidata1550A acquisition system (Axon Instruments, Foster City, CA, USA). Atrial myocytes were isolated by Langendorff perfusion, plated on laminin coated glass bottom dishes and incubated at room temperature for 30 minutes prior to recordings. Tyrode solution (140 mM NaCl, 4 mM KCl, 1 mM MgCl2, 1 mM CaCl2, 10 mM HEPES, 10 mM Glucose, pH 7.4 with NaOH) was used to perfuse atrial cardiomyocytes during recordings at 37 °C. Internal pipette solution contained 20 mM KCl, 100 mM K-glutamate, 10 mM HEPES, 5 mM MgCl2, 10 mM NaCl, 5 mM Mg-ATP and 0.3 mM Na-GTP. Action potentials were triggered using 0.5 nA × 2 ms current clamp pulses following liquid junction potential correction. All recordings were filtered at a frequency of 2 kHz using a built-in Bessel filter and sampled at 10 kHz. Results were analyzed using pCLAMP10 (Axon Instruments).

Diastolic calcium measurements: Atrial myocytes were isolated by Langendorff perfusion, plated on laminin coated glass bottom dishes and incubated at room temperature for 30 minutes prior to staining with Fura-2 AM. Cells were then incubated with 1 μM Fura-2 AM for 10 minutes in normal Tyrode's solution. Diastolic calcium measurements were performed at a fluorescence emission of 510 nm and recorded using an Olympus IX81 Inverted Widefield Microscope. $[Ca]_i$ was calculated by the ratio of emissions following excitation at 340 nm and 380 nm.

Relative luciferase assays: HEK293T and HL-1 cells were co-transfected as described previously [47]. The *Atp2a2* and *Ryr2* cis-regulatory elements were amplified from C57/B6 mouse genomic DNA. The sequence was confirmed by sequencing and then cloned into the pGL4.23 enhancer luciferase response vector with a minimal promoter. Mutagenesis of the GATA4 binding motifs was performed by PCR cloning, confirmed by sequencing and then cloned into the pGL4.23 vector. Cells were co-transfected with the luciferase response vector and pRL control using lipofectamine 3000, then lysed and assayed following 48 hours using the Dual-Luciferase Reporter Assay system (Promega).

Quantitative real time PCR: Total RNA was extracted from the left atrial wall of 8- to 10-weeks adult mice (2 weeks after receiving TM) using Trizol (Invitrogen) combined with RNeasy mini-kit (Qiagen), according to the manufacturer's instructions. First-strand cDNA was synthesized using the qScript cDNA synthesis kit (Quanta) according to the manufacturer's protocol. Gene expression was assayed using the Power SYBR Green PCR Master Mix (Applied Biosystems) and run on an Applied Biosystems AB7500 machine in 96-well plates. Relative fold changes were calculated using the comparative threshold cycle method ($2^{-\Delta\Delta Ct}$) using Glyceraldehyde-3-phosphate dehydrogenase (*Gapdh*) as an internal control. Primer sequences used in this study are listed below.

	Primers	
Gene	**Forward**	**Reverse**
Tbx5	GGCATGGAAGGAATCAAGGT	CTAGGAAACATTCTCCTCCCTGC
Gata4	AAACGGAAGCCCAAGAACCTGAAT	GAGCTGGCCTGCGATGTCTAGGTG
Nkx2.5	ACATTTTACCCGGGAGCC	GGCTTTGTCCAGCTCCAC
Ryr2	CAAATCCTTCTGCTGCCAAG	CGAGGATGAGATCCAGTTCC
Atp2a2	CTGGTGATATAGTGGAAATTGCTG	GGTCAGGGACAGGGTCAGTA

Sln	CTGAGGTCCTTGGTAGCCTG	GGTGTGTCAGGCATTGTGAG
NCX	TTCTCATACTCCTCGTCATCG	TTGAGGACACCTGTGGAGTG
CamK2B	ACCCTCTACTTTCTCTCCTCC	ACTTTGGTGTCTTCGTCCTC
Pln	TTATGCCAGGACGGCAAAAG	CACTGTGACGATCACCGAAG
Cacna1c	CTACAGAAACCCATGTGAGCAT	CAGCCACGTTGTCAGTGTTG
Kcnj3	GCTGGCAACTACACTCCCTG	AACATGCAGCCGATGAGGAA
Kcnj5	TGTAAGAGCTCCGTGCTTGG	TGTGGAGATGTCTCGTGCTC
Kcna5	AAAATTGGAGACGATGACGG	ATGAGGCCCATCACTGTAGG
Kcnd3	GGGTGGCAGGCAGGTTAGA	CCTGCTGCTCCCGTCGTA
Kcnh2	ATGGCTCAGATCCAGGCAGTTA	CAAGGAGAGCGGTCAGGTAATG
Kcnk2	TGGCTACGGGTGATCTCTAAG	GCTGGAACTTGTCGTAGATCTC
Kcnn3	CAAGAATGCCGCCGCCAATGTC	CCAGGCTGCCAATCTGCTTTTC
Kcnq1	GAGGATAGGAGGCCAGACCA	AAGTACTGCATGCGCCTGAT

Statistical analysis: All data is represented as means ± standard error of the mean (± SEM). For comparison of conscious ECG parameters, action potential duration (APD50 and APD90), SR load and SERCA activity, a one-way ANOVA followed by post-hoc Tukey analysis was used to test significance. For gene expression studies and in vitro luciferase assays, a one-way ANOVA followed by internal student T-test was used to test significance. AF inducibility and triggered activity (from AP measurements) counts were analyzed with a Fisher's exact test (two-tailed).

Study approval: All animal experiments were performed in accordance with national and institutional guidelines and were approved by the University of Chicago Institutional Animal Care and Use Committee (IACUC) approved protocol.

Results

Reduced Gata4 rescues atrial arrhythmias caused by reduced Tbx5

We previously demonstrated that adult-specific *Tbx5* deletion or haploinsufficiency caused spontaneous AF or AF susceptibility, respectively, linking TBX5 dose with AF risk [47]. GATA4 and NKX2-5 physically and genetically interact with TBX5 during cardiac development, and all three cardiogenic TFs are strongly expressed in the adult atrium and are genetically linked to AF risk in humans (Figure 1A) [44, 57, 153, 155, 161, 165, 169]. We therefore hypothesized that GATA4 and NKX2-5 would genetically interact with TBX5 in adult atrial rhythm control. We employed a conditional knockout strategy to establish haploinsufficiency of *Gata4*, *Tbx5* and *Nkx2-5* singly or in combination in the adult mouse, affording normal gene dosage throughout development to circumvent early lethality or structural heart defects observed with each mouse model [100, 170-172]. We combined TF floxed alleles ($Gata4^{fl/fl}$; or $Tbx5^{f/l/fl}$ or $Nkx2\text{-}5^{fl/fl}$) with a tamoxifen (TM)-inducible *Cre* recombinase allele at the Rosa26 locus ($R26^{CreERT2}$) to generate adult compound haploinsufficient *Gata4/Tbx5* ($Gata4^{fl/+};Tbx5^{fl/+};R26^{CreERT2}$), *Gata4/Nkx2-5* ($Gata4^{fl/+};Nkx2\text{-}5^{fl/+};R26^{CreERT2}$) and *Tbx5/Nkx2-5* ($Tbx5^{fl/+};Nkx2\text{-}5^{fl/+};R26^{CreERT2}$) and triple haploinsufficient ($Tbx5^{fl/+};Gata4^{fl/+};Nkx2\text{-}5^{fl/+};R26^{CreERT2}$) mice [100, 148, 166]. All TF allelic combinations were generated and evaluated as littermates in a mixed genetic background. Mice were treated with TM at 6 weeks of age and loss of *Gata4*, *Tbx5* and/or *Nkx2-5* expression was confirmed in the left atrium of by qPCR 2 weeks following TM treatment (Figure 1B and Supplemental Figure 1A). Specifically, *Gata4* decrements were not observed in *Tbx5* or *Nkx2-5* single heterozygotes, indicating that TBX5 or NKX2-5 alone does not regulate expression of *Gata4* (Figure 1B and Supplemental Figure 1A). Similarly, *Tbx5* (or *Nkx2-5*) expression is not regulated by GATA4 or NKX2-5 (or TBX5) alone. However, a greater reduction in *Gata4* expression was observed in *Tbx5/Nkx2-5* compound heterozygotes compared to their respective single haploinsufficient

controls (P = 0.195 versus *Tbx5*$^{fl/+}$;*R26*^{CreERT2}, P = 0.038 versus *Nkx2-5*$^{fl/+}$;*R26*^{CreERT2}, respectively), suggesting that TBX5 and NKX2-5 may cooperatively regulate GATA4.

We first confirmed that atrial rhythm was sensitive to *Tbx5* dosage in these mixed background crosses by examining adult *Tbx5* heterozygotes (*Tbx5*$^{fl/+}$;*R26*^{CreERT2}). Significant prolongation of the *P*-wave duration, representing atrial depolarization (AF-associated finding in humans studies) was observed in *Tbx5*$^{fl/+}$;*R26*^{CreERT2} mice compared to control littermates 2 weeks after TM treatment by conscious ambulatory telemetry ECG (P = 0.0008) (Figure 1C). The PR interval, representing the period between initiation of atrial and ventricular depolarization, was unchanged in *Tbx5*$^{fl/+}$;*R26*^{CreERT2} compared to *R26*^{CreERT2} mice (P = 0.132) (Figure 1D), consistent with our previous publication [47]. We further interrogated propensity to atrial arrhythmias by catheter-directed intracardiac pacing. *Tbx5*$^{fl/+}$;*R26*^{CreERT2} adult mice were highly susceptible to AF induction, depicted by the irregular atrial electrogram, by intracardiac atrial pacing using either programmed single extra-stimulus or burst pacing. AF was reproducibly induced in 11 of 18 *Tbx5*$^{fl/+}$;*R26*^{CreERT2} mice but in 0 of 8 *R26*^{CreERT2} mice following atrial burst pacing (P=0.0074) (Figure 1E, F and I). Of these, 7 of 11 *Tbx5*$^{fl/+}$;*R26*^{CreERT2} mice displayed atrial tachycardia (AT) and/or AF episodes lasting >1,000 ms (P = 0.0128), with a mean duration of 15,963 ms. In addition, 4 of 11 *Tbx5* heterozygotes (P = 0.103) displayed rapid atrial irregular rhythm for <1,000 ms, with a mean duration of 678 ms. Remarkably, 5 of 11 *Tbx5*$^{fl/+}$;*R26*^{CreERT2} mice displayed spontaneous atrial arrhythmias in addition to induced irregular atrial rhythm (Supplemental Figure 2). *Tbx5*$^{fl/+}$;*R26*^{CreERT2} mice showed normal cardiac function two weeks post-TM treatment, with no difference in left ventricular ejection fraction compared to *R26*^{CreERT2} adult mice (Supplemental Figure 3). These findings establish that *Tbx5* haploinsufficiency causes atrial conduction deficits and increased AF risk.

Atrial rhythm was not sensitive to adult-specific *Gata4* or *Nkx2-5* haploinsufficiency. Adult-specific *Gata4* (*Gata4*$^{fl/+}$;*R26*^{CreERT2}) or *Nkx2-5* (*Nkx2-5*$^{fl/+}$;*R26*^{CreERT2}) haploinsufficiency caused no abnormalities of *P*-wave duration ($P = 0.928$ *R26*^{CreERT2} versus *Gata4*$^{fl/+}$;*R26*^{CreERT2} and $P = 0.08$ *R26*^{CreERT2} versus *Nkx2-5*$^{fl/+}$;*R26*^{CreERT2}) or PR interval ($P = 0.956$ *R26*^{CreERT2} versus *Gata4*$^{fl/+}$;*R26*^{CreERT2} and $P = 0.985$ *R26*^{CreERT2} versus *Nkx2-5*$^{fl/+}$;*R26*^{CreERT2}) by conscious ambulatory telemetry ECG and showed no sign of beat-to-beat variability by Poincaré analysis in comparison to *R26*^{CreERT2} control littermates ($P = 0.946$ *R26*^{CreERT2} versus *Gata4*$^{fl/+}$;*R26*^{CreERT2} and $P = 0.992$ *R26*^{CreERT2} versus *Nkx2-5*$^{fl/+}$;*R26*^{CreERT2}) (Figure 1C, D, Supplemental Figure 1). Unlike reduced *Tbx5* dosage, *Gata4* or *Nkx2-5* haploinsufficient mice were not vulnerable to atrial arrhythmias by pacing induction (Figure 1F, G and I and Figure S4). Specifically, 4 of 12 *Gata4*$^{fl/+}$;*R26*^{CreERT2} mice ($P = 0.116$) and 1 of 8 *Nkx2-5*$^{fl/+}$;*R26*^{CreERT2} mice ($P = 0.5$) experienced AF compared to 0 of 9 *R26*^{CreERT2} mice and both showed statistically less AF inducibility than *Tbx5* haploinsufficiency ($P = 0.0074$) (Figure 1G, I and Supplemental Figure 4B).

Remarkably, atrial arrhythmicity caused by reduced *Tbx5* dose was rescued by reduced *Gata4* dose. Specifically, the increased *P*-wave duration observed in *Tbx5* haploinsufficient mice was rescued in combined *Gata4/Tbx5* haploinsufficient mice ($P = 0.0163$ *Gata4/Tbx5* compound heterozygote versus *Tbx5*$^{fl/+}$;*R26*^{CreERT2}) (Figure 1C). *Gata4/Tbx5* compound heterozygotes were not susceptible to AF induction by intracardiac burst pacing. Only 1 of 12 *Gata4*$^{fl/+}$;*Tbx5*$^{fl/+}$;*R26*^{CreERT2} mice reproducibly paced into AF, demonstrating rescue of AF inducibility compared to 11 of 18 for *Tbx5*$^{fl/+}$;*R26*^{CreERT2} mice ($P = 0.0068$), and no greater propensity for AF induction compared to *R26*^{CreERT2} controls (0 of 8 *R26*^{CreERT2}, $P = 0.999$) (Figure 1H, I).

Nkx2-5 haploinsufficiency had no discernable effect on atrial rhythm, by itself or in combination with *Tbx5* or *Gata4* haploinsufficiency. We analyzed adult-specific *Tbx5/Nkx2-5* and *Gata4/Nkx2-5* compound heterozygotes and *Gata4/Tbx5/Nkx2-5* triple heterozygotes for atrial conduction deficits or arrhythmia inducibility. No significant *P*-wave duration or PR interval differences were detected in any of these genotypes compared to their respective single or double haploinsufficient controls (Supplemental Figure 1B, C). Furthermore, no significant differences in atrial arrhythmia inducibility were observed in *Gata4/Nkx2-5* (P = 0.999 versus $Gata4^{fl/+};R26^{CreERT2}$ and $P = 0.999$ versus $Nkx2\text{-}5^{fl/+};R26^{CreERT2}$) or *Tbx5/Nkx2-5* ($P = 0.361$ versus $Tbx5^{fl/+};R26^{CreERT2}$ and $P = 0.323$ versus $Nkx2\text{-}5^{fl/+};R26^{CreERT2}$) compound heterozygotes compared to their respective single heterozygote controls or in *Gata4/Tbx5/Nkx2-5* triple heterozygotes compared to *Gata4/Tbx5* double heterozygote controls (P = 0.999) (Supplemental Figure 4). Specifically, 1 of 12 $Gata4^{fl/+};Nkx2\text{-}5^{fl/+};R26^{CreERT2}$ mice paced into AF compared to control littermates, suggesting that GATA4 and NKX2-5 do not interact together in the adult heart for control of atrial rhythm (Supplemental Figure 4D and F). $Tbx5^{fl/+};Nkx2\text{-}5^{fl/+};R26^{CreERT2}$ mice were susceptible to AF induction by intracardiac burst pacing, with prevalence identical to that of *Tbx5* heterozygotes, indicating that TBX5 and NKX2-5 do not interact synergistically or antagonistically in the adult atrium (Supplemental Figure 4C and F). Lastly, mice lacking one copy of *Gata4*, *Tbx5* and *Nkx2-5* ($Tbx5^{fl/+};Gata4^{fl/+};Nkx2\text{-}5^{fl/+};R26^{CreERT2}$) were not vulnerable to AF induction (Supplemental Figure 4E and F). Thus, the AF susceptibility observed in *Tbx5/Nkx2-5* compound heterozygotes was rescued by reducing *Gata4* gene dosage, similar to $Tbx5^{fl/+};Gata4^{fl/+};R26^{CreERT2}$ mice. In each genetic context, *Nkx2-5* was dispensable, causing no worsening or improvement of atrial rhythm in adult mice compared to littermate controls.

Abnormal atrial electric activity observed in Tbx5 heterozygotes is normalized in Gata4/Tbx5 compound heterozygotes.

We sought to define the cellular basis by which reduced *Gata4* dose rescued the atrial conduction deficits and arrhythmia propensity caused by reduced *Tbx5* dose. We previously showed that adult-specific *Tbx5* haploinsufficiency caused prolonged atrial cardiomyocyte (CM) action potentials (APs) and abnormal spontaneous depolarizations of atrial myocytes, electrophysiological deficits that can cause or contribute to AF [47]. We hypothesized that *Gata4* haploinsufficiency may rescue the cellular electrophysiology defects caused by *Tbx5* haploinsufficiency. APs from atrial myocytes isolated from $Tbx5^{fl/+};R26^{CreERT2}$ mice 2 weeks after TM treatment were significantly prolonged, specifically in phases 2 and 3 of the AP, and time to 90% repolarization (APD90), compared to $R26^{CreERT2}$ atrial myocytes ($P = 0.0029$) (Figure 2A, B, E). EADs and DADs were frequently observed in $Tbx5^{fl/+};R26^{CreERT2}$ atrial myocytes but never in control littermates (9 of 14 $Tbx5^{fl/+};R26^{CreERT2}$ versus 0 of 9 $R26^{CreERT2}$ atrial myocytes, $P = 0.003$), consistent with our previous study (Figure 2F-H) [47]. Adult-specific G*ata4* haploinsufficiency caused no aberrations in AP measurements or inappropriate afterdepolarizations (Figure 2C, E and H). Remarkably, decreased *Gata4* dose rescued the cellular electrophysiology abnormalities observed in $Tbx5^{fl/+};R26^{CreERT2}$ mice. Atrial AP duration was rescued in $Gata4^{fl/+};Tbx5^{fl/+};R26^{CreERT2}$ myocytes (P=0.0006) (Figure 2B, D, E). Additionally, propensity of EADs and DADs was rescued in $Gata4^{fl/+};Tbx5^{fl/+};R26^{CreERT2}$ compared to $Tbx5^{fl/+};R26^{CreERT2}$ atrial myocytes ($P = 0.018$), and $Gata4^{fl/+};Tbx5^{fl/+};R26^{CreERT2}$ atrial myocytes showed no increased propensity for inappropriate depolarizations compared to $R26^{CreERT2}$ control atrial myocytes ($P = 0.493$) (Figure 2H). We conclude that the cellular electrophysiology defects caused by reduced *Tbx5* dose were rescued by reduced *Gata4* dose (Figure 2I).

Atrial myocyte ectopic activity, implicated as a mechanism of AF induction, can result from abnormal calcium handling. We therefore investigated altered expression of genes controlling cardiomyocyte calcium flux as a potential molecular mechanism for paroxysmal AF induction in *Tbx5* heterozygote mice. We focused on calcium handling genes involved in phase 2 and 3 of the AP, given our observation of specific deficits during these AP phases in *Tbx5* adult haploinsufficient mice (Figure 2). Adult-specific *Tbx5* heterozygote mice showed significantly diminished left atrial expression of *Atp2a2* and *Ryr2* compared to $R26^{CreERT2}$ mice ($P = 0.0038$ for *Atp2a2*; $P = 0.0163$ for *Ryr2*, respectively), whereas expression of other calcium handling genes, including *Sln*, *Pln*, *Slc8a1* and *Cacna1c* were not significantly altered (Figure 3A and). Interestingly, *Atp2a2* and *Ryr2* expression was normalized in *Gata4/Tbx5* compound heterozygotes ($P = 0.0232$ for *Atp2a2*; $P = 0.0323$ for *Ryr2*, respectively) (Figure 3A). In addition, we also assessed expression of potassium handling genes previously linked to AF. RNA expression of *Kcnj3* ($P = 0.0443$), *Kcnj5* ($P = 0.0039$) and *Kcnh2* ($P = 0.0182$) showed significant reduction in left atrial tissue of $Tbx5^{fl/+};R26^{CreERT2}$ compared to control littermates (Supplemental Figure 5), whereas expression of *Kcna5*, *Kcnd3*, *Kcnk2*, *Kcnn3* and *Kcnq1*, were unchanged. However, *Kcnj3*, *Kcnj5* or *Kcnh2* gene expression were not normalized in $Gata4^{fl/+};Tbx5^{fl/+};R26^{CreERT2}$ mice ($P = 0.7001$ for *Kcnj3*, $P = 0.4254$ for *Kcnj5* and $P = 0.5286$ for *Kcnh2*, respectively). Overall, these results suggested that atrial arrhythmogenesis in adult *Tbx5* heterozygous mice may be mediated by altered SR calcium flux, mediated by reduced expression of *Atp2a2* and *Ryr2*.

We previously demonstrated that TBX5 drives atrial expression of *Pitx2*, and that TBX5 and PITX2 oppositely modulate the expression of cardiac rhythm effector genes, including *Ryr2* and *Atp2a2* [47]. This suggested that the rescue of *Tbx5* haploinsufficiency by Gata4 haploinsufficiency could occur through diminished *Pitx2* levels. *Pitx2* mRNA expression

remained unchanged in *Tbx5*$^{fl/+}$;*R26*^{CreERT2} and *Gata4*$^{fl/+}$;*R26*^{CreERT2} mice 2 weeks after TM treatment, as previously described ($P = 0.7049$ *Tbx5*$^{fl/+}$;*R26*^{CreERT2} compared to *R26*^{CreERT2} and $P = 0.7261$ *Gata4*$^{fl/+}$;*R26*^{CreERT2} compared to *R26*^{CreERT2}) (Figure 3B) [47]. Levels of *Pitx2* mRNA were slightly higher in *Gata4*$^{fl/+}$;*Tbx5*$^{fl/+}$;*R26*^{CreERT2} mice compared to wildtype littermates ($P = 0.0117$); however this increase was not significant compared to *Tbx5*$^{fl/+}$;*R26*^{CreERT2} or *Gata4*$^{fl/+}$;*R26*^{CreERT2} mice ($P = 0.1208$ versus *Tbx5*$^{fl/+}$;*R26*^{CreERT2} and $P = 0.1135$ versus *Gata4*$^{fl/+}$;*R26*^{CreERT2} mice, respectively). This observation suggested that the rescue of *Tbx5* haploinsufficiency by *Gata4* haploinsufficiency was not mediated by a reduction of *Pitx2* expression.

We hypothesized that TBX5 and GATA4 directly co-regulate expression of *Atp2a2* and *Ryr2*. To test this hypothesis, we defined regions with overlapping chromatin occupancy for both TBX5 and GATA4 from published ChIP datasets (Figure 3C-D, Supplemental Figure 6 and 7) [173]. Candidate cis-regulatory elements (CRE) were refined by open chromatin regions from HL-1 cardiomyocyte ATAC-seq dataset [99]. We functionally interrogated these CREs for enhancer activity in the presence of TBX5 and/or GATA4. The *Atp2a2* enhancer (mm9 Chr5: 122970476-122971591) demonstrated activation in response to *TBX5* expression in HEK293T cells, as previously described (Figure 3E) [99]. *GATA4* similarly activated the enhancer and co-expression of TBX5 and GATA4 had no additive or synergistic effects, by in vitro luciferase reporter assay in HEK293T cells (Figure 3E). In contrast, the *Ryr2* enhancer was activated by TBX5 ($P = 0.0013$) but not GATA4 alone ($P = 0.5923$) in HEK293T cells (Figure 3F). Remarkably, co-expression of GATA4 suppressed TBX5-dependent transactivation of this *Ryr2* enhancer ($P = 0.0681$ compared to TBX5 alone), suggesting antagonistic interactions of TBX5 and GATA4 on this CRE. We further tested the *Ryr2* CRE in HL-1 cardiomyocytes, which possesses expression of cardiac transcription factors, including TBX5 and GATA4 [174]. This enhancer previously demonstrated

TBX5-dependent activity in HL-1 cells, and consistently, this enhancer alone showed activation in HL-1 cardiomyocytes (Figure 3G) [99]. Interestingly, mutation of the four GATA binding motifs within this enhancer caused an increase of enhancer activity in HL-1 cardiomyocytes ($P = 0.0010$ versus WT enhancer) (Fig 3G). These observations indicated that GATA4 represses TBX5-dependent activity of the *Ryr2* enhancer.

Reduced SR load and SERCA function caused by Tbx5 haploinsufficiency is rescued by Gata4 haploinsufficiency

Abnormal CM membrane depolarizations, including DADs, can be induced by Ca^{2+} driven Na^{+}/Ca^{2+} exchanger (NCX1) activity in the setting of reduced SERCA-mediated SR Ca^{2+} uptake, causing membrane depolarization [175]. We therefore hypothesized that the ectopic depolarizations caused by *Tbx5* haploinsufficiency would be associated with depressed SERCA function and slowed SR Ca^{2+} uptake. To test this hypothesis, we measured SR load and SERCA activity in *Tbx5* heterozygote atrial myocytes, 2 weeks after TM treatment. We used fluo4 AM to study cytosolic calcium handling kinetics and fura2 AM to study diastolic calcium levels. We defined SR Ca^{2+} uptake by loading myocytes with Fluo-4 AM and pacing with a train of field stimuli to achieve a steady state load followed by application of caffeine to synchronize ryanodine receptor opening, resulting in a maximum release of SR calcium into the cytosol (Figure 4A-D). We observed reduced caffeine-induced calcium transient amplitudes in $Tbx5^{fl/+};R26^{CreERT2}$ in comparison with $R26^{CreERT2}$ mice, indicating reduced SR calcium levels (P <0.0001) (Figure 4A, B and E). To assess SERCA activity, we measured $[Ca]_i$ decay rate after caffeine in the absence of external sodium (NCX inactive), allowing measurement of isolated SR uptake. Consistent with reduced left atrial expression of *Atp2a2*, we observed decreased SERCA activity in *Tbx5* haploinsufficient mice (P <0.0001) (Figure 4A, B and F and Supplemental Figure 8). Furthermore, no significant

differences were observed in resting cytosolic calcium between *Tbx5*$^{fl/+}$;*R26*^{CreERT2} and *R26*^{CreERT2} cardiomyocytes (1.001 *Tbx5*$^{fl/+}$;*R26*^{CreERT2} versus 0.992 *R26*^{CreERT2}, P =0.515) (Supplemental Figure 8). This suggest that the observed differences in SERCA function is not due to alterations in cytosolic calcium levels or calcium buffering capacity, but rather to TBX5-depedent regulation of SERCA. Overall, our findings indicate that *Tbx5* haploinsufficiency causes reduced SERCA function, providing a molecular mechanism for ectopic CM depolarizations (Figure 4G).

Decreased *Gata4* dose rescued abnormal SERCA function observed in *Tbx5* haploinsufficient mice. Specifically, SR calcium load in *Gata4*$^{fl/+}$;*Tbx5*$^{fl/+}$;*R26*^{CreERT2} myocytes was not different from *R26*^{CreERT2} control cardiomyocytes (P = 0.312), and *Gata4*$^{fl/+}$;*Tbx5*$^{fl/+}$;*R26*^{CreERT2} myocytes showed significantly increased SR load compared to *Tbx5*$^{fl/+}$;*R26*^{CreERT2} cardiomyocytes (P = 0.0070) (Figure 4B, D and E). Furthermore, SERCA activity was normalized in *Gata4*$^{fl/+}$;*Tbx5*$^{fl/+}$;*R26*^{CreERT2} myocytes as observed by a normal decay rate upon removal of caffeine, compared to *Tbx5*$^{fl/+}$;*R26*^{CreERT2} cardiomyocytes (P = 0.0145) (Figure 4B, D and F). Additional analysis of the calcium dependence of SERCA activity showed decreased activity at all level of cytosolic calcium in *Tbx5*$^{fl/+}$;*R26*^{CreERT2} compared to *R26*^{CreERT2}, and this was normalized in *Gata4*$^{fl/+}$;*Tbx5*$^{fl/+}$;*R26*^{CreERT2} (Supplemental Figure 8). We conclude that the atrial calcium homeostasis defects caused by reduced *Tbx5* dose were rescued by reduced *Gata4* dose, providing a molecular mechanism for the physiological rescue (Figure 4G)

Modulation of SERCA function eliminates TF-driven arrhythmogenic phenotype.

The observation that reduced *Gata4* dose rescued the defects caused by reduced *Tbx5* dose at the level of cardiac rhythm control, cellular electrophysiology, gene expression, and reduced SR calcium flux suggested that the pathophysiology of reduced *Tbx5* dose on atrial rhythm control may be entirely mediated by reduced SR calcium uptake.

PLN inhibits SERCA activity in its non-phosphorylated state. *Pln* is essential for atrial calcium homeostasis and human genetic variants at *PLN* associate with AF risk, suggesting that PLN activity contributes to AF susceptibility [3, 176]. We hypothesized that reducing *Pln* gene levels may restore SERCA activity and rescue atrial calcium abnormalities caused by reduced *Tbx5* dose. We compared SR uptake, SERCA function, and AF inducibility in adult-specific littermate *Tbx5* haploinsufficient, *Pln* haploinsufficient or *Tbx5*/*Pln* double haploinsufficient mice 2 weeks following TM treatment. We observed depressed SR load (P <0.0001) and SERCA activity (P = 0.0221) in atrial cardiomyocytes from $Tbx5^{fl/+};R26^{CreERT2}$ mice compared to those from $R26^{CreERT2}$ littermate controls, as expected (Figure 5A, B, E and F). *Pln* heterozygote atrial cardiomyocytes showed a significant increase in SR load (P = 0.0304) and SERCA function (P = 0.0003) compared to those from $R26^{CreERT2}$ (Figure 5A, C, E and F). Both SR load (P = 0.0211) and SERCA activity (P =0.0007) were normalized in *Tbx5/Pln* compound heterozygotes (Figure 5L).

We hypothesized that normalization of SERCA function and SR load in *Tbx5/Pln* compound heterozygotes may rescue the AF predisposition caused by decreased *Tbx5* dose. *Tbx5* heterozygotes were highly susceptible to atrial arrhythmias, consistent with our previous observations (Figure 1E and H). AF was induced in 4 of 6 $Tbx5^{fl/+};R26^{CreERT2}$ mice compared to 0 of 10 for $R26^{CreERT2}$ controls (P = 0.008) (Figure 5H and K). *Pln* heterozygotes demonstrated no AF inducibility (0 of 8 mice; P = 0.999) (Figure 5I and K). Remarkably, $Tbx5^{fl/+};Pln^{+/-};R26^{CreERT2}$ adult mice were not susceptible to AF induction by intracardiac pacing (0 of 7 $Tbx5^{fl/+};Pln^{+/-};R26^{CreERT2}$ mice; P = 0.021 versus $Tbx5^{fl/+};R26^{CreERT2}$) (Figure 5G-K). Overall, we conclude that decreased *Pln* gene dose normalizes SERCA activity and rescues AF susceptibility caused by *Tbx5* haploinsufficiency, indicating that diminished SERCA activity is a primary deficit causing arrhythmogenesis in the setting of *Tbx5* haploinsufficiency (Figure 5L).

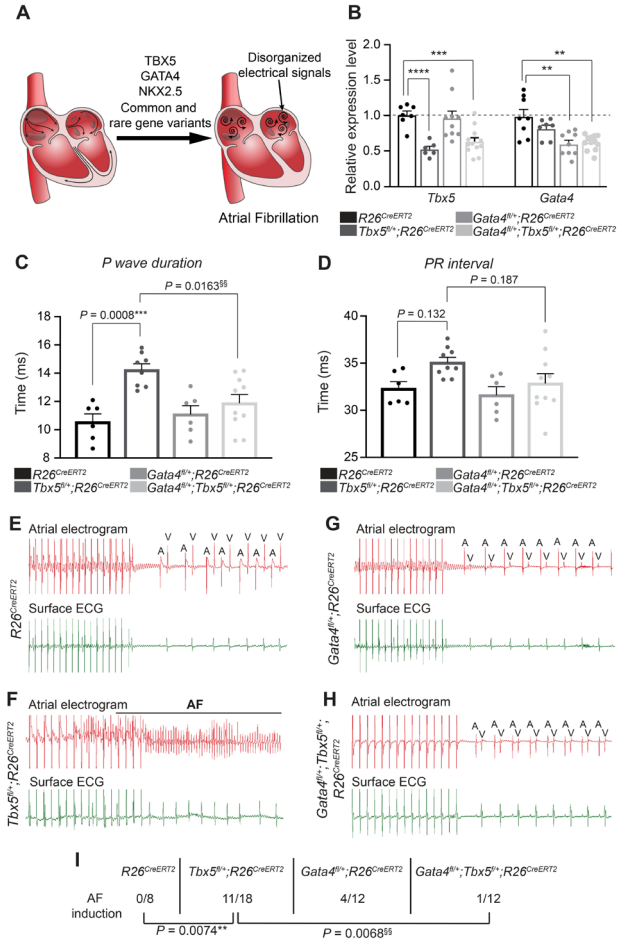

Figure 3-1. Gata4 haploinsufficiency rescues atrial arrhythmias caused by Tbx5 haploinsufficiency.

(**A**) Common and rare gene variants in the transcription factors *TBX5*, *GATA4* and *NKX2-5* have been linked to increased AF susceptibility. (**B**) Relative transcript expression by qPCR in the left atrium of $Tbx5^{fl/+};R26^{CreERT2}$, $Gata4^{fl/+};R26^{CreERT2}$ and *Gata4/Tbx5* compound heterozygotes 2 weeks after TM treatment. Data are represented as means ± SEM normalized to GAPDH and relative to $R26^{CreERT2}$ mice (set as 1) (n=7-8 $R26^{CreERT2}$, n=6-7 $Tbx5^{fl/+};R26^{CreERT2}$, n=9-10 $Gata4^{fl/+};R26^{CreERT2}$, n=12 $Gata4^{fl/+};Tbx5^{fl/+};R26^{CreERT2}$). Experiments were performed in technical duplicates. *P* values were determined by one-way ANOVA followed by Tukey post-hoc test. (**C and D**) *P*-wave duration and PR interval calculated from ambulatory telemetry ECG recordings from $R26^{CreERT2}$ (n=6), $Tbx5^{fl/+};R26^{CreERT2}$ (n=8-9), $Gata4^{fl/+};R26^{CreERT2}$ (n=6) and $Gata4^{fl/+};Tbx5^{fl/+};R26^{CreERT2}$ (n=10) mice. $Tbx5^{fl/+};R26^{CreERT2}$ adult mice displayed significant increase in *P*-wave duration (**C**) and prolongation of the PR interval compared to $R26^{CreERT2}$ littermate controls (**D**). *P* values were determined by one-way ANOVA followed by post-hoc Tukey test. (**E-H**) Intracardiac atrial electrogram recordings and corresponding surface ECG of $R26^{CreERT2}$ (n=8), $Tbx5^{fl/+};R26^{CreERT2}$ (n=18), $Gata4^{fl/+};R26^{CreERT2}$ (n=12) and $Gata4^{fl/+};Tbx5^{fl/+};R26^{CreERT2}$ (n=12) mice. *Tbx5* heterozygotes displayed irregular atrial electrogram, consistent with lack of *P*-wave on surface ECG, which is representative of AF (**F**). A, atrial electrical signal; V, far field ventricular electrical signal. (**I**) Pacing induction by intra-atrial pacing of mice in D-G. AF was reproducibly induced

Figure 3-1, continued.

in 11 of 18 *Tbx5* heterozygotes (60%) in contrast to 1 of 12 *Gata4/Tbx5* compound heterozygotes, indicating rescue of atrial arrhythmias. *P* values were determined by Fisher's exact test.

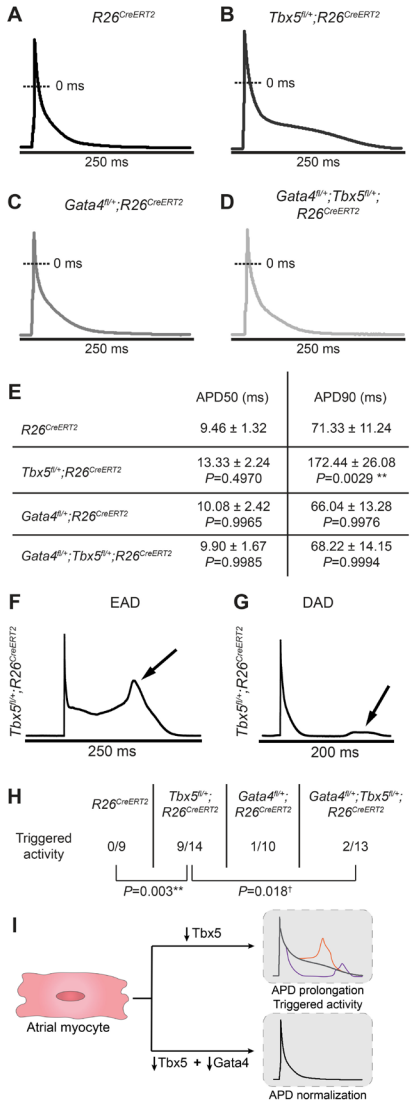

Figure 3-2. Abnormal atrial cardiomyocyte electrical activity caused by Tbx5 haploinsufficiency is rescued by Gata4 haploinsufficiency.

(**A-D**) Representative AP recordings from atrial myocytes isolated from $R26^{CreERT2}$, $Tbx5^{fl/+};R26^{CreERT2}$, $Gata4^{fl/+};R26^{CreERT2}$ and $Gata4^{fl/+};Tbx5^{fl/+};R26^{CreERT2}$ mice 2 weeks after receiving TM. Prolongation of phase 2 and 3 of the AP was observed exclusively in $Tbx5^{fl/+};R26^{CreERT2}$ mice (**B**) but not in $Gata4^{fl/+};Tbx5^{fl/+};R26^{CreERT2}$ littermates (**D**), suggesting rescue of AP abnormalities. (**E**) Corresponding properties of AP from mice in A-D. *Tbx5* heterozygotes showed significant prolongation of APD90 in comparison to $R26^{CreERT2}$ controls. These defects were completely rescued in *Gata4/Tbx5* compound heterozygote mice (APD90, $P = 0.006$). APD50, APD at 50% repolarization; APD90, APD at 90% repolarization; Data represent mean ± SEM (n=3-5 animals per genotype; n=9 cardiomyocytes $R26^{CreERT2}$, n=14 $Tbx5^{fl/+};R26^{CreERT2}$, n=10 $Gata4^{fl/+};R26^{CreERT2}$ and n=13 $Gata4^{fl/+};Tbx5^{fl/+};R26^{CreERT2}$). P values of APD50 and APD90 were determined by one-way ANOVA followed by Tukey post-hoc test. (**F**, **G**) Representative tracings of early after depolarizations (EAD) and delayed after depolarizations (DAD) in $Tbx5^{fl/+};R26^{CreERT2}$ atrial myocytes. (**H**) Representative abnormal depolarization events (EAD and DAD) observed in atrial myocytes. Reduced *Gata4* gene dosage rescued abnormal triggers observed in *Tbx5* haploinsufficient atrial myocytes. Total number of ectopic depolarization events were recorded in

Figure 3-2, continued.

R26^{CreERT2} (*n*=9), *Tbx5*$^{fl/+}$;*R26*^{CreERT2} (*n*=14), *Gata4*$^{fl/+}$;*R26*^{CreERT2} (*n*=10) and *Gata4*$^{fl/+}$;*Tbx5*$^{fl/+}$;*R26*^{CreERT2} (*n*=13) atrial myocytes from $n > 4$ for each genotype. *P* values of triggers were determined by Fisher's exact test. (I) Schematic representation of the cellular conduction deficits caused by *Tbx5* haploinsufficiency, including AP prolongation and triggered activity and normalization by reduced *Gata4* dose.

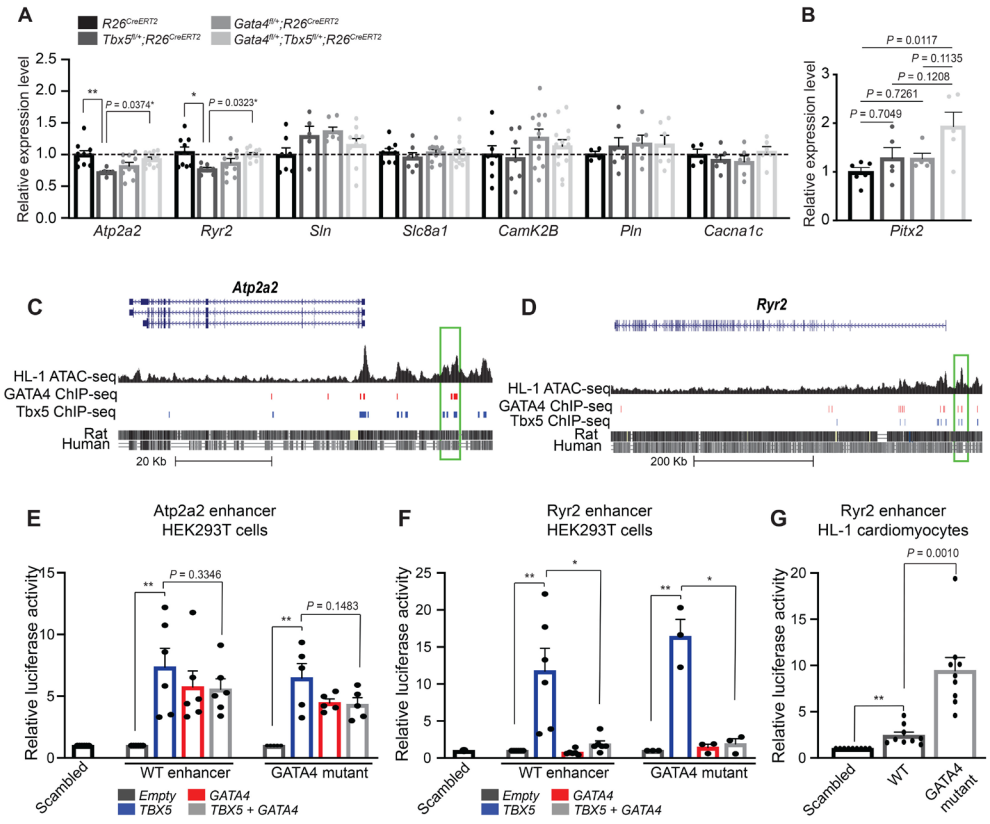

Figure 3-3. Antagonistic interactions between TBX5 and GATA4 on *Atp2a2* and *Ryr2* expression and on a *Ryr2* enhancer.

(**A**) Relative gene expression by qPCR of known AF calcium genes and calcium interacting proteins from left atrium of $R26^{CreERT2}$ (n=6-10) $Tbx5^{fl/+};R26^{CreERT2}$ (n=5-7), $Gata4^{fl/+};R26^{CreERT2}$ (n=7-10) and $Gata4^{fl/+};Tbx5^{fl/+};R26^{CreERT2}$ (n=9-13) mice 2 weeks after TM treatment. *Tbx5* heterozygotes showed 20% decrease in *Atp2a2* and *Ryr2* gene expression, which was normalized in *Gata4/Tbx5* compound heterozygotes. Data are normalized to GAPDH and relative to $R26^{CreERT2}$. *P* values were determined by one-way ANOVA followed by Tukey post-hoc test. (**B**) Relative transcript expression of *Pitx2* by qPCR in the left atrium of *Tbx5* heterozygotes, *Gata4* heterozygotes and *Gata4/Tbx5* compound heterozygotes 2 weeks after TM treatment. Data are represented as means ± SEM normalized to GAPDH and relative to $R26^{CreERT2}$ mice (set as 1) (n=6 $R26^{CreERT2}$, n=5 $Tbx5^{fl/+};R26^{CreERT2}$, n=5 $Gata4^{fl/+};R26^{CreERT2}$ and n=5 $Gata4^{fl/+};Tbx5^{fl/+};R26^{CreERT2}$). Experiments were performed in technical duplicates. *P* value was determined by one-way ANOVA followed by post-hoc Tukey test. (**C** and **D**) *Atp2a2* and *Ryr2* genomic locus (Mm9) aligned with published ATAC-seq dataset from HL-1 cardiomyocytes and ChIP-seq dataset for TBX5 and GATA4. Green rectangle denotes the cis-regulatory regions with overlapping open chromatin as well as TBX5 and GATA4 binding motifs. (**E-G**) In vitro luciferase response assay of *Atp2a2* and *Ryr2* candidate enhancers in HEK293T cells co-transfected with TBX5 and/or GATA4 or HL-1 atrial cardiomyocytes and corresponding GATA mutant enhancer. Data are means ± SEM, normalized to scrambled vector. Experiments were performed in technical triplicates (n = 5 for *Atp2a2* enhancer; n = 4 for *Ryr2* in HEK293T cells and n = 5 for *Ryr2* in HL-1 cardiomyocytes). *P* values were determined by one-way ANOVA followed by Tukey post-hoc test.

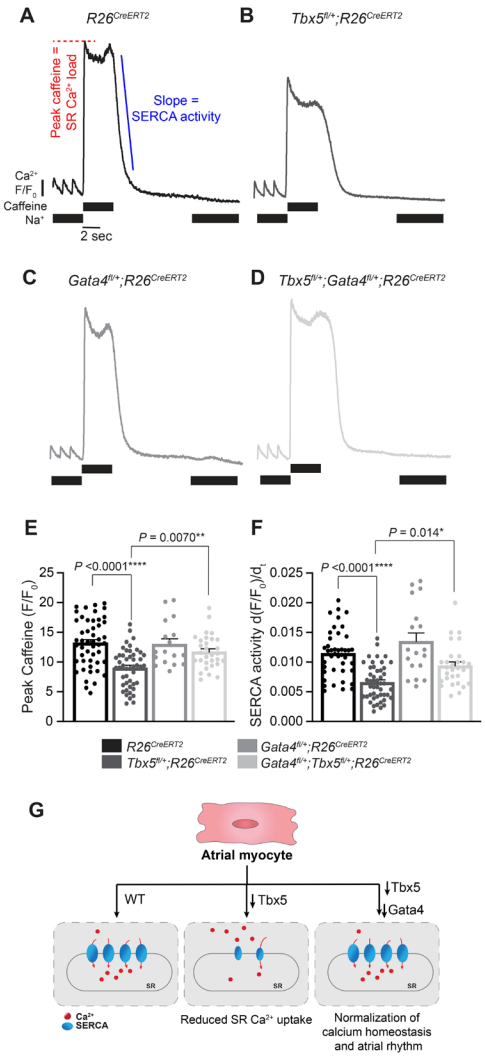

Figure 3-4. Reduced SERCA function caused by Tbx5 haploinsufficiency is rescued by Gata4 haploinsufficiency in atrial myocytes.

(**A-D**) Representative SERCA2 traces after steady state field stimulation at 1 Hz and application of caffeine in the absence of Na_o provides a measurement of SR load. Removal of caffeine, in the absence of external Nao provides a measure of SERCA2 mediated SR calcium uptake. (**E**) SR load, determined from peak caffeine transients was diminished in *Tbx5*$^{fl/+}$;*R26*^{CreERT2} compared to *R26*^{CreERT2} and was completely rescued in *Gata4*$^{fl/+}$;*Tbx5*$^{fl/+}$;*R26*^{CreERT2} mice (n=49 *R26*^{CreERT2}, n=47 *Tbx5*$^{fl/+}$;*R26*^{CreERT2}, n=18 *Gata4*$^{fl/+}$;*R26*^{CreERT2} and n=30 *Gata4*$^{fl/+}$;*Tbx5*$^{fl/+}$;*R26*^{CreERT2} atrial myocytes from 3-5 mice for each genotype). *P* values were determined by one-way ANOVA followed by post-hoc Tukey test. (**F**) SERCA activity, determined from the maximal rate of calcium decay was diminished in *Tbx5*$^{fl/+}$;*R26*^{CreERT2} compared to *R26*^{CreERT2} and normalized by *Gata4* haploinsufficiency. *P* values were determined by one-way ANOVA followed by post-hoc Tukey test. (**G**) Schematic representation of calcium homeostasis in control atrial myocytes, how it is disrupted by *Tbx5* haploinsufficiency and rescued by decreasing *Gata4* gene dosage.

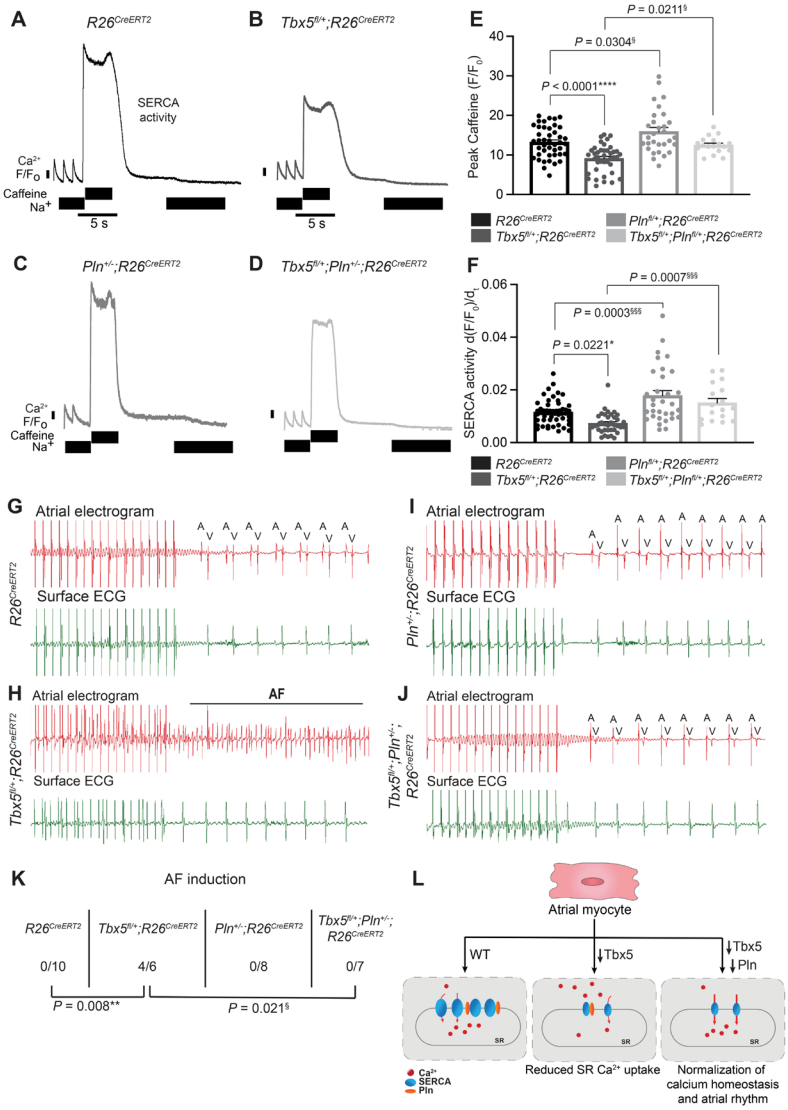

Figure 3-5. Normalization of SERCA2 function eliminates AF susceptibility in *Tbx5*$^{fl/+}$*;R26*^{CreERT2}.

(**A-D**) Representative SERCA2 traces of *R26*^{CreERT2} (**A**), *Tbx5*$^{fl/+}$*;R26*^{CreERT2} (**B**), *Pln*$^{+/-;}$*R26*^{CreERT2} (**C**), and *Tbx5*$^{fl/+}$*;Pln*$^{+/-}$*;R26*^{CreERT2} (**D**) atrial myocytes. (**E, F**) Representative SR load and SERCA2 measurements from A-D. SR load (**E**) and SERCA2 function (**F**) was low in *Tbx5*$^{fl/+}$*;R26*^{CreERT2} and normalized in *Tbx5/Pln* compound heterozygous mice. (*n*=43 *R26*^{CreERT2}, n=40 *Tbx5*$^{fl/+}$*;R26*^{CreERT2}, *n*=30 *Pln*$^{+/-}$*;R26*^{CreERT2}, and *n*=18 *Tbx5*$^{fl/+}$*;Pln*$^{+/-}$*;R26*^{CreERT2} for SR load and SERCA2 measurements, 3-4 mice per genotype were analyzed). (**G-J**) Intracardiac atrial electrogram recordings and corresponding surface ECG of *R26*^{CreERT2} (*n*=9), *Tbx5*$^{fl/+}$*;R26*^{CreERT2} (*n*=6), *Pln*$^{+/-}$*;R26*^{CreERT2} (*n*=8) and *Pln*$^{+/-}$*;Tbx5*$^{fl/+}$*; R26*^{CreERT2} (*n*=7) mice. *Tbx5* heterozygotes displayed irregular atrial electrogram, representative of AF (**H**). A, atrial electrical signal; V, far field ventricular electrical signal. (**K**) Pacing induction by intra-atrial pacing of mice in G-J. AF was reproducibly induced in 4 of 6 *Tbx5* heterozygotes (60%) in contrast to 0 of 7 *Pln/Tbx5* compound heterozygotes, indicating complete rescue of atrial arrhythmias. *P* values were determined by Fisher's exact test; **P* < 0.05. (L) Schematic representation of calcium homeostasis in control atrial myocytes, how it is disrupted by *Tbx5* haploinsufficiency and rescued by decreasing *Pln* gene dosage.

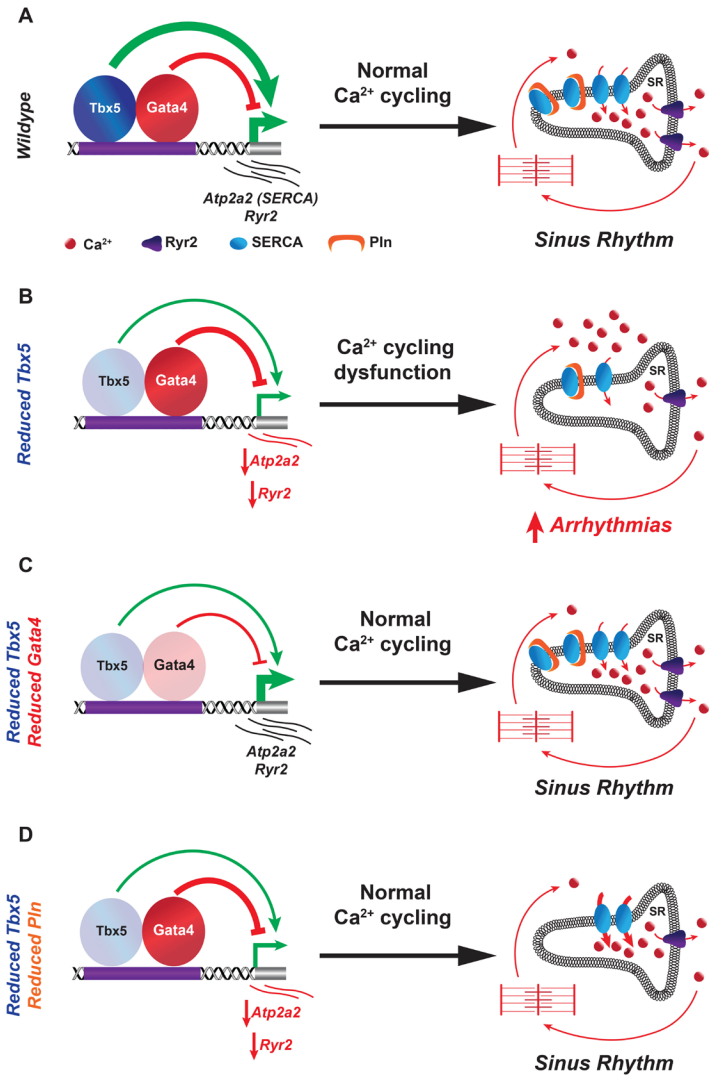

Figure 3-6. TBX5 and GATA4 are key regulators of atrial calcium homeostasis.

Schematic representation of proteins involved in Ca^{2+} handling of atrial myocytes. In the healthy atrium, calcium homeostasis is maintained through a tight balance between Ca^{2+} fluxes across the membrane. Reducing *Tbx5* gene dosage in the adult heart results in depressed *Atp2a2* expression and SERCA2 function, affecting SR Ca^{2+} influx. Abnormal Ca^{2+} handling leads to Ca^{2+} accumulation in the cytosol, contributing to ectopic atrial activity, prolonged APs and atrial arrhythmias observed with adult-specific *Tbx5* haploinsufficiency. Reducing *Gata4* gene dosage rescues *Atp2a2* expression, SERCA2 function and SR Ca^{2+} uptake, restoring sinus rhythm. SERCA2 and its inhibitory protein PLN play a fundamental role in Ca^{2+} handling within atrial myocytes. Reducing *Pln* gene dosage, as a means to modulate SERCA2 function, normalizes SERCA2 activity and SR Ca^{2+} uptake, resulting in restoration of sinus rhythm in combined *Tbx5/Pln* haploinsufficiency. NCX, sodium-calcium (Na^{+}/Ca^{2+}) exchanger; PLN, phospholamban; SERCA, sarco/endoplasmic reticulum Ca^{2+}-ATPase; SR, sarcoplasmic reticulum.

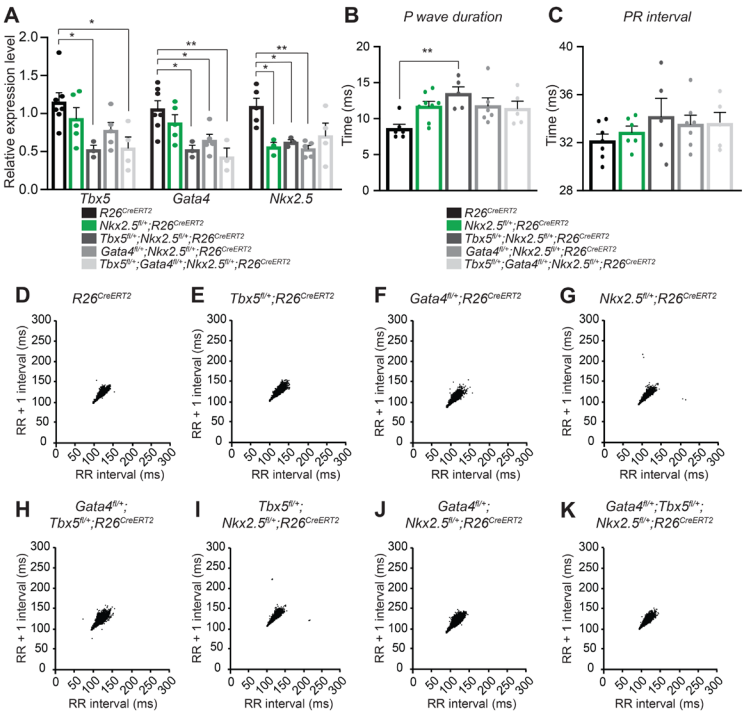

Supplemental Figure 3-1.1. Combined *Gata4* (or *Tbx5*) and *Nkx2-5* haploinsufficiency does not affect adult atrial rhythm.

(**A**) Relative transcript expression by qPCR in the left atrium of *Nkx2.5* heterozygotes, *Tbx5/Nkx2.5* and *Gata4/Nkx2.5* compound heterozygotes and *Gata4/Tbx5/Nkx2.5* triple heterozygotes 2 weeks after TM treatment. Data are represented as means ± SEM normalized to GAPDH and relative to $R26^{CreERT2}$ mice (set as 1) (n=5-7 $R26^{CreERT2}$, n=3-4 $Nkx2.5^{fl/+};R26^{CreERT2}$, n=3-4 $Tbx5^{fl/+};Nkx2.5^{fl/+};R26^{CreERT2}$, n=4 $Gata4^{fl/+};Nkx2.5^{fl/+};R26^{CreERT2}$ and n=4 $Tbx5^{fl/+};Gata4^{fl/+};Nkx2.5^{fl/+};R26^{CreERT2}$). Experiments were performed in technical duplicates. P value was determined by one-way ANOVA followed by post-hoc Tukey test; $*P < 0.05$ was considered significant. (**B, C**) P-wave duration and PR interval calculated from ambulatory telemetry ECG recordings from $R26^{CreERT2}$ (n=12), $Nkx2.5^{fl/+};R26^{CreERT2}$ (n=8), $Tbx5^{fl/+};Nkx2.5^{fl/+};R26^{CreERT2}$ (n=5), $Gata4^{fl/+};Nkx2.5^{fl/+};R26^{CreERT2}$ (n=4) and $Gata4^{fl/+};Tbx5^{fl/+};Nkx2.5^{fl/+};R26^{CreERT2}$ (n=5) mice. P values were determined ANOVA followed by post-hoc Tukey test. (**D-G**) Representative Poincare plot of RR interval (RRn) against the subsequent beat (RRn + 1) (n=7 for $R26^{CreERT2}$, n=5 $Tbx5^{fl/+};R26^{CreERT2}$, n=6 $Gata4^{fl/+};R26^{CreERT2}$, n=6 $Nkx2.5^{fl/+};R26^{CreERT2}$, n=7 $Gata4^{fl/+};Tbx5^{fl/+};R26^{CreERT2}$, n=5 $Tbx5^{fl/+};Nkx2.5^{fl/+};R26^{CreERT2}$, n=6 $Gata4^{fl/+};Nkx2.5^{fl/+};R26^{CreERT2}$ and n=5 $Gata4^{fl/+};Tbx5^{fl/+};Nkx2.5^{fl/+};R26^{CreERT2}$ mice).

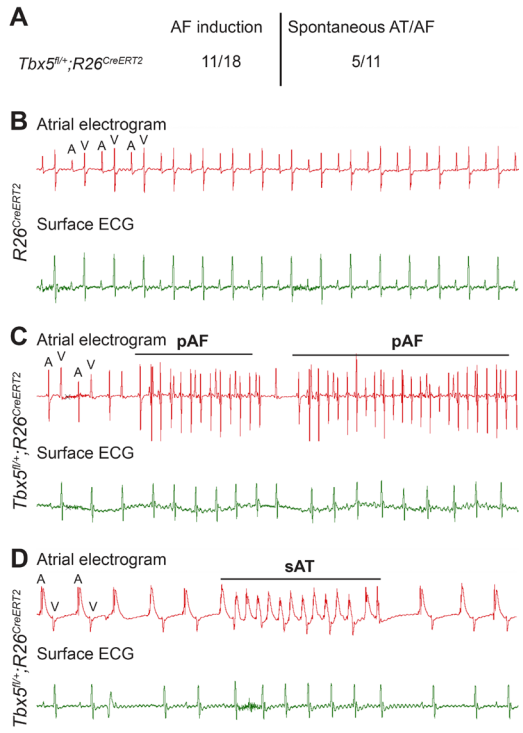

Supplemental Figure 3-1.2. Adult *Tbx5* heterozygotes have spontaneous atrial arrhythmias under anesthesia.

(**A**) Pacing induction by intra-atrial pacing of $Tbx5^{fl/+};R26^{CreERT2}$ mice showing episodes of spontaneous AF or AT. 5 of 11 (45%) $Tbx5^{fl/+};R26^{CreERT2}$ mice developed spontaneous atrial arrhythmias (**B-D**) Intracardiac atrial electrogram recordings and corresponding surface ECG of $R26^{CreERT2}$ (**B**), and$Tbx5^{fl/+};R26^{CreERT2}$ mice (**C, D**) with paroxysmal AF (**C**) or spontaneous atrial tachycardia (**D**) 2 weeks post-TM treatment. Paroxysmal AF was observed in 3 of 11 and $Tbx5^{fl/+};R26^{CreERT2}$ mice while spontaneous AT occurred in 2 of 11 $Tbx5^{fl/+};R26^{CreERT2}$ mice. A, atrial electrical signal; AF, atrial fibrillation; AT, atrial tachycardia; pAF, paroxysmal AF; sAT, spontaneous atrial tachycardia; V, far field ventricular electrical signal.

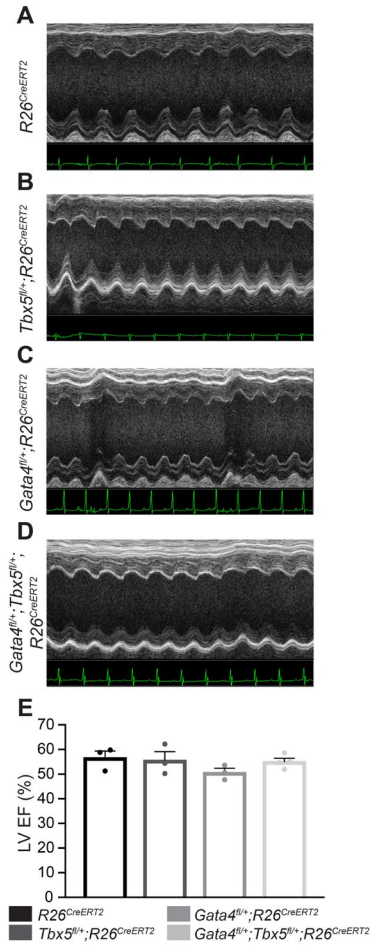

Supplemental Figure 3-1.3. Left ventricular function of *Tbx5*$^{fl/+}$;*R26*^{CreERT2} adult mice is not changed.

(**A-D**) M-mode echocardiography from *R26*^{CreERT2} (**A**), *Tbx5*$^{fl/+}$;*R26*^{CreERT2} (**B**), *Gata4*$^{fl/+}$;*R26*^{CreERT2} (**C**) and *Tbx5*$^{fl/+}$;*Gata4*$^{fl/+}$;*R26*^{CreERT2} (**D**) mice 2 weeks post-TM treatment. Surface ECGs are represented at the bottom. N = 3-4 mice per genotype. (**E**) Left ventricular ejection fraction (LVEF) was calculated from the M-mode images. P values were calculated from ANOVA followed by post-hoc Tukey test.

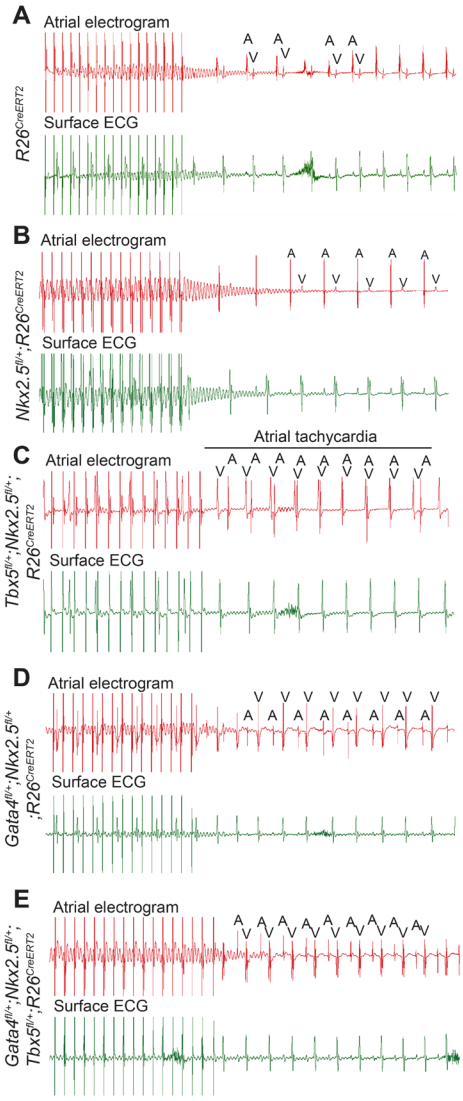

F

	AF induction
R26^{CreERT2}	0/9
Nkx2.5$^{fl/+}$;*R26*^{CreERT2}	1/8
Tbx5$^{fl/+}$;*Nkx2.5*$^{fl/+}$;*R26*^{CreERT2}	3/8
Gata4$^{fl/+}$;*Nkx2.5*$^{fl/+}$;*R26*^{CreERT2}	1/12
Gata4$^{fl/+}$;*Nkx2.5*$^{fl/+}$;*Tbx5*$^{fl/+}$;*R26*^{CreERT2}	0/6

Supplemental Figure 3-1.4. Combined *Gata4* (or *Tbx5*) and *Nkx2.5* haploinsufficiency does not increase susceptibility to AF.

(**A-F**) Intracardiac atrial electrogram recordings and corresponding surface ECG of R26^{CreERT2} (n=9), Nkx2.5$^{fl/+}$;R26^{CreERT2} (n=8), Tbx5$^{fl/+}$;Nkx2.5$^{fl/+}$;R26^{CreERT2} (n=8), Gata4$^{fl/+}$;Nkx2.5$^{fl/+}$;R26^{CreERT2} (n=12) Gata4$^{fl/+}$;Tbx5$^{fl/+}$;Nkx2.5$^{fl/+}$;R26^{CreERT2} (n=6) mice. A, atrial electrical signal; V, far field ventricular electrical signal. (**F**) Pacing induction by intra-atrial pacing of mice in A-H. P values were determined by Fisher's exact test; *P < 0.05 and **P < 0.01.

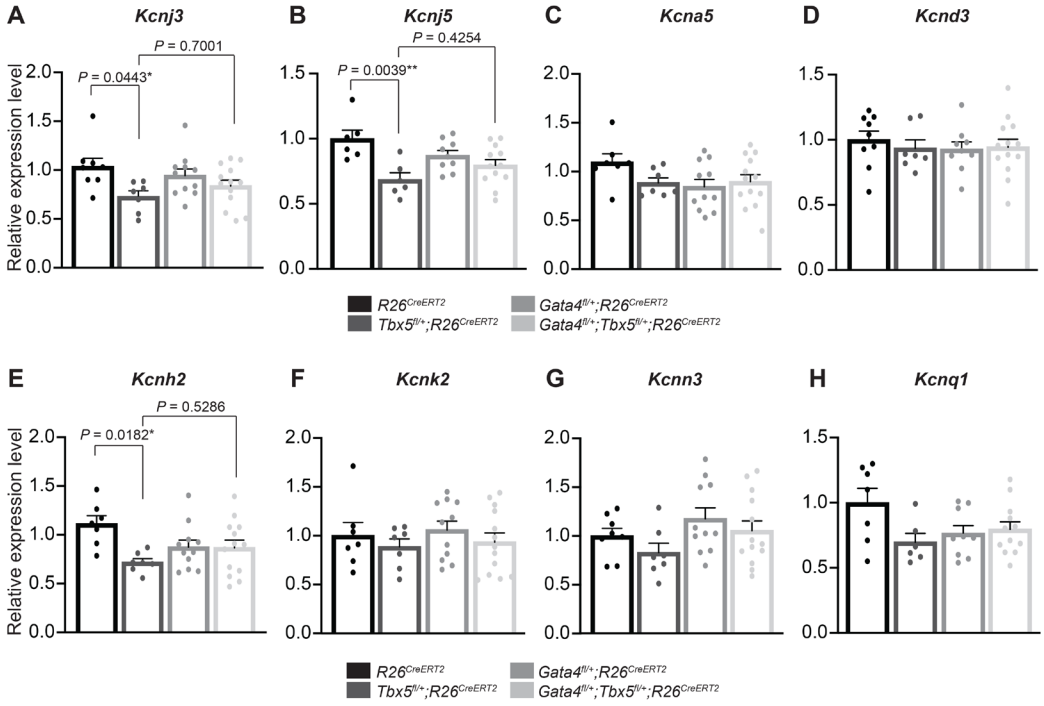

Supplemental Figure 3-3.1. Decreased expression of potassium channels in *Tbx5* heterozygotes is not rescued by *Gata4* haploinsufficiency.

(**A-H**) Relative transcript expression by qPCR of known AF potassium genes from left atrium of $R26^{CreERT2}$ (n=6) $Tbx5^{fl/+};R26^{CreERT2}$ (n=5), $Gata4^{fl/+};R26^{CreERT2}$ (n=7) and $Gata4^{fl/+};Tbx5^{fl/+};R26^{CreERT2}$ (n=9) mice 2 weeks after TM treatment. $Tbx5^{fl/+};R26^{CreERT2}$ mice showed a 20-30% reduction in *Kcnj3*, *Kcnj5* and *Kcnh2* gene expression, and was not normalized in $Gata4^{fl/+};Tbx5^{fl/+};R26^{CreERT2}$ mice. Data are normalized to GAPDH and relative to $R26^{CreERT2}$. P values were analyzed with one-way ANOVA followed by post-hoc Tukey test.

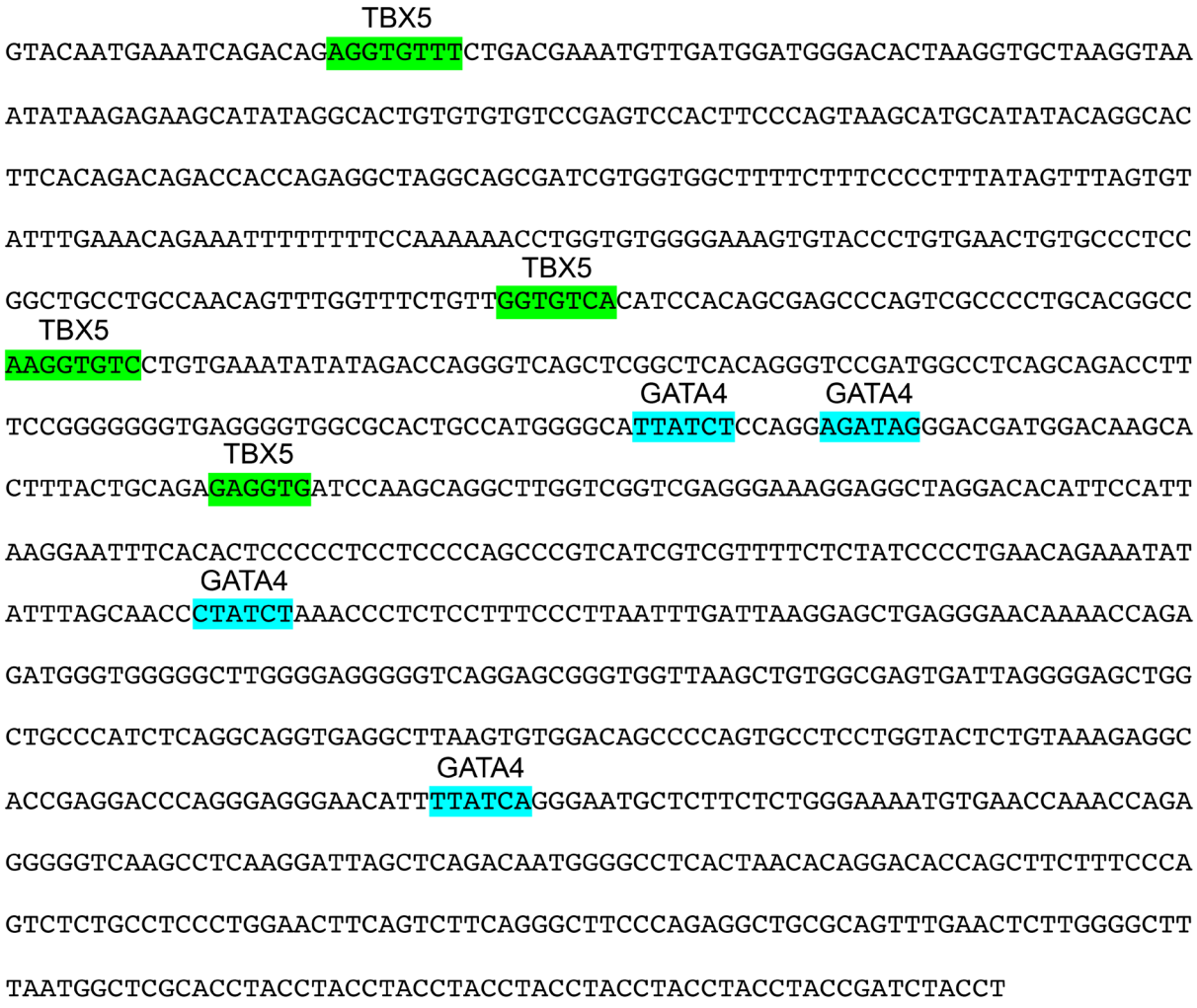

Supplemental Figure 3-3.2. Nucleotide sequence of the 5'-upstream region of the mouse *Atp2a2* gene.

Atp2a2 enhancer located 19Kb upstream of the start site (mm9 Chr5: 122970476-122971591) with GATA and TBX canonical binding sites shown in blue and green.

AGAGGGTCCCAAAGGAACACATCCTATCGCCGGAGCAAGACGAGCAGCTGCTAGGTTGACGGGACAATCA

TCACATACCTTCCCTTGTCCCTTTCCCCGTCCTCCCAGGAGCTCACACGTGCTTTCTCTTTACCCAGCAG

CAAGACACTATTCTTTACATTATTAGCATCCTGAGTTTCTGGACCTCCCTGTTGGAGACAACAGGACAAC

AGCACCAGCTGATTTCTAAGGCCCATTTCTTGATTCAGTGTGGACTTTGTCAGCTACAATGGGAAGCCAG

GAAGTGACACCGAGGGTCATTCATACCAGTAAGACCCATCATGAGGGAAAACCTTATACTGGTATTTGGT

CCATCACAATGGCCAAAATACGTGGCATGAACAACTTAAAAAATAAAACTATTGGCTTCTAGATCCAGAG

GTTTCAGTGTAGGACAGCAGGGCAGGCAGAGAGGAGAGGCTTGGTCCAGAGCAACAGTAGTCTGTAGCAA

AGTTTGCTCATGTGGTAGGAGACTAGGAAACAGAGAACGGGGCCAGAACTCAGGGCTGAGTATTACCTTT

AAAAGCCCACCCCTATTCCATTTCACCAGGTAGGCCCTAACTCCTAAAGGTCCCATGCCCCAGCAAATAG

TGCCATCATCCAGGGAACAATCATTTAAAGCATAAGCCTATGGGGACATTTTAGATCCAAACCACGATAC

TCCTTTTCCCCTCCCCCCTCCATGCATCTCCTGTGTCCTGCATACATACAGAACCAAGTTCTGGACACTG

GATA4

AGAATGCCCAAGTCTGAGACCTCCGTGGAAGATAAAAGTTGGGATTACAGCTATTTTTCTTAATTTCTTA

TCCATTGGGAATCTGGTTTGGGGGTTCATTTGAATAGGACCCTAGGAACTAGATATGGGATGACAGACTC

TBX5

CCTCCTTTGAAAGCACTCACAAGTCAATAAAGAATAGAGATCAGCAACTCCATGGCAGTGAGGTGTGTGC

TTAATCTAGTGATATCCAGAGAGGCTGTGCCCTGCCACATACCAGAGCCCTGCAGAACAAGACCCACAGG

GATA4

ACTTTGCTGATAAGGACAAGAGGCTTAGCAGTGACAAATCGTGACGCACATCATTATCTTCATGACCCCA

TGCTGCAAAGCAGCTCTACTACACTGAAGGAAACTTACTGCTAACACTGTACTGGTTGCATTTGTCACTG

AGAAGCCCCTGTTGGGATACCCTGGGCTCCTGTGTTTCCCTACTAGGCAATGAAGATCATGCCTTCTCCA

TCTCTGGAAGGACGACTGTGAGATTTAACTACTCAACCTTCTCTGTGTGTCTCTCTGACTTTGTCTCTGT

CCTCCTGCCCCAGTTACTCTCAGATCTACCATCCAGGAGAAGAGGGCTCTGTCTGCTCCCTGGGCACTGG

CTATGCTGGAGGGTCAGGAGGCAAAAGGAGTCTGCAAACATCTAGAAAGCATCAGAGAAACCACTACTGG

GTTTTGCTTGTCTACAGGGGCAGTGGTGGTCACGGAAAATGAAAAATTAATTAGGAGAACATGACTGCTG

GATTTCCTTTATTCTTGAACCAAATCAAATCAATACAGTTCTCAGATCCTGCCAATAAAAGGCAAAGACC

GATA4

TAATTGTGCCTGACTTGGGAACTGCCAAGAAACAGAACCACAAGATATCTAGGGCAGGACAGAGATAAGG

CAATCCTAAGAGCCCAGTGACCAGCTTGGCTAGCTGGAATAGCAAACTTTATACTCAGTGAGAGACCCTG

TBX5

ACCTCCCCCACCCTCCGTCACACCAATTAAAAAACAAAAAAGAAGTGGATGGCTATGAGGATGACATCGT

GGTTAAGCCTAAGTGTGAAGACTAAAGCTTGGAGCCTTCCCTTGGAAAGATCCCAGAGCATATCCTTGAG

Supplemental Figure 3-3.3. Nucleotide sequence of the 5'-upstream region of the mouse *Ryr2* gene.

Ryr2 enhancer located 24Kb upstream of the start site (mm9 Chr13: 12223550-12226563) with GATA and TBX canonical binding sites shown in blue and green.

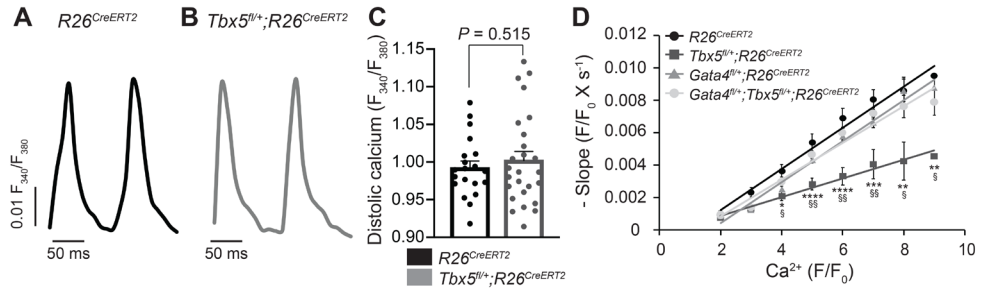

Supplemental Figure 3-4. Diastolic calcium levels are unaltered in *Tbx5*$^{fl/+}$*;R26*^{CreERT2}.

(**A**, **B**) Representative diastolic calcium traces after Fura-2 AM staining. (**C**) $[Ca]_I$, determined by dividing fluorescence emission following 340 nm excitation by 380 nm excitation, was unchanged in *Tbx5*$^{fl/+}$*;R26*^{CreERT2} compared to littermate controls (n = 3 mice per genotype). (D) SERCA activity was decreased at all levels of calcium *Tbx5*$^{fl/+}$*;R26*^{CreERT2} compared to littermate controls and normalized in *Gata4/Tbx5* compound heterozygotes. *P* values were calculated using an ANOVA followed by post-hoc Tukey test. (* *Tbx5*$^{fl/+}$*;R26*^{CreERT2} versus *R26*^{CreERT2} mice; § *Tbx5*$^{fl/+}$*;R26*^{CreERT2} versus *Gata4*$^{fl/+}$*;Tbx5*$^{fl/+}$*;R26*^{CreERT2} mice).

Gene	Primers	
	Forward	**Reverse**
Tbx5	GGCATGGAAGGAATCAAGGT	CTAGGAAACATTCTCCTCCCTGC
Gata4	AAACGGAAGCCCAAGAACCTGAAT	GAGCTGGCCTGCGATGTCTAGGTG
Nkx2.5	ACATTTTACCCGGGAGCC	GGCTTTGTCCAGCTCCAC
Ryr2	CAAATCCTTCTGCTGCCAAG	CGAGGATGAGATCCAGTTCC
Atp2a2	CTGGTGATATAGTGGAAATTGCTG	GGTCAGGGACAGGGTCAGTA
Sln	CTGAGGTCCTTGGTAGCCTG	GGTGTGTCAGGCATTGTGAG
NCX	TTCTCATACTCCTCGTCATCG	TTGAGGACACCTGTGGAGTG
CamK2B	ACCCTCTACTTTCTCTCCTCC	ACTTTGGTGTCTTCGTCCTC
Pln	TTATGCCAGGACGGCAAAAG	CACTGTGACGATCACCGAAG
Cacna1c	CTACAGAAACCCATGTGAGCAT	CAGCCACGTTGTCAGTGTTG
Kcnj3	GCTGGCAACTACACTCCCTG	AACATGCAGCCGATGAGGAA
Kcnj5	TGTAAGAGCTCCGTGCTTGG	TGTGGAGATGTCTCGTGCTC
Kcna5	AAAATTGGAGACGATGACGG	ATGAGGCCCATCACTGTAGG
Kcnd3	GGGTGGCAGGCAGGTTAGA	CCTGCTGCTCCCGTCGTA
Kcnh2	ATGGCTCAGATCCAGGCAGTTA	CAAGGAGAGCGGTCAGGTAATG
Kcnk2	TGGCTACGGGTGATCTCTAAG	GCTGGAACTTGTCGTAGATCTC
Kcnn3	CAAGAATGCCGCCGCCAATGTC	CCAGGCTGCCAATCTGCTTTTC
Kcnq1	GAGGATAGGAGGCCAGACCA	AAGTACTGCATGCGCCTGAT

Discussion

We report that TBX5 and GATA4, both implicated in human AF, genetically interact in mice for atrial rhythm control with unanticipated results. Surprisingly, reducing *Gata4* gene dosage rescued defects caused by *Tbx5* haploinsufficiency, including atrial arrhythmias, prolonged APs, abnormal ectopic cellular depolarizations, sarcoplasmic reticulum Ca^{2+} load and SERCA

calcium flux. Rescue of both P-wave prolongation and ectopic cardiomyocyte depolarizations suggests that *Gata4* haploinsufficiency may rescue both the vulnerable substrate and arrhythmia trigger propensity caused by *Tbx5* haploinsufficiency. The identification of SERCA function as the nexus of the *Tbx5/Gata4* genetic interaction suggested the more general hypothesis that calcium flux deficits caused by *Tbx5* haploinsufficiency were the primary mechanism for the observed atrial rhythm disturbance. This hypothesis is supported by the ability of reduced dose of phospholamban (*pln*), encoding a direct binding SERCA inhibitor, to also rescue the *Tbx5* heterozygote phenotype. By providing insights into the co-regulation of atrial rhythm and calcium homeostasis by TBX5 and GATA4, this work illuminates complex genetic interactions that will undergird efforts towards personalized care in human rhythm control. The work also identifies SERCA calcium flux as the pathophysiologic basis of increased AF risk caused by decreased *Tbx5* dose, and therefore a possible pathophysiologic mechanism germane to AF risk more generally.

We defined a calcium handling network underlying cardiomyocyte prolonged action potentials and ectopy observed with decreased *Tbx5* dose and rescued by reduced *Gata4* dose. We hypothesized that normalization of SERCA expression caused normalization of AP duration and elimination of ectopic depolarization events. Consistently, reduction in *Atp2a2* expression, SERCA activity and SR Ca^{2+} load observed in *Tbx5* haploinsufficient mice were all rescued by *Gata4* haploinsufficiency (Figure 4). Recent studies investigating the cellular mechanisms of AF have suggested that abnormal atrial calcium handling contributes to AF pathogenesis, contributing to trigger formation [87, 88, 175, 177]. While SR calcium content is affected by both SERCA uptake and RYR2-mediated calcium leak, our previous study suggested that Ryr2 binding was not affected in *Tbx5* knockout mice, suggesting a primary role of SERCA in TBX5-dependent calcium dysfunction [45]. Consistent with this model, increased SERCA activity by reduced PLN*, a* SERCA

inhibitor, rescued the *Tbx5* haploinsufficient phenotype (Figure 5). Human *PLN* mutations have been previously linked to AF and cardiomyopathy [178-180]. Reductions in SERCA2 expression/activity or enhancement of the inhibitory effects of PLN are also hallmarks of heart failure (HF) [181, 182]. Interestingly, PLN inhibition has been shown to alleviate cardiomyopathy in several animal models and improve cardiomyocyte contractility in patients with HF [183-185]. Here we show that decreased *Pln* dose can rescue the arrhythmogenic phenotype caused by *Tbx5* haploinsufficiency, by restoring SERCA function and normalizing SR Ca^{2+} content (Figure 4 and 6). Zhu *et al* observed rescue of heart failure and ventricular SERCA function following ablation of PLN in $Tbx5^{vdel/+}$ mice [186]. TBX5 therefore regulates SERCA in both the atria and ventricles for both cardiac function and rhythm. The observation that decreased *Pln* normalizes SR Ca^{2+} uptake and SERCA activity in a mouse model of AF provides a direct molecular link between calcium flux perturbations observed in HF and AF risk, which are strongly associated, regardless of genetic background. These observations suggest that PLN inhibition, and more generally the modulation of SR calcium flux, may be considered as possible therapeutic approaches for the treatment of AF in HF.

Understanding of the genetic basis of cardiac rhythm control has benefited greatly from highly powered genome-wide association studies, which have identified over 100 loci contributing to the heritability of AF. A mechanistic and actionable understanding of how the identified loci affect cardiac rhythm control requires the transition from genetic implication to functional investigation [187]. The implication of the cardiogenic TFs *TBX5, GATA4* and *NKX2-5* by GWAS is an exciting feature, suggesting a shared transcriptional kernel in cardiac development and adult cardiac rhythm control. In the context of cardiac development, *Tbx5*, *Gata4*, and *Nkx2-5* interact genetically in a synergistic fashion, their encoded TFs physically associate, and they cooperatively

drive embryonic cardiac gene expression (33-44). These detailed studies provided a clear paradigm for the cooperative interaction between these TFs in adult rhythm control. Remarkably, we find that these TFs interact very differently in the adult mouse: *Tbx5* and *Gata4* act oppositely, and *Nkx2-5* has no appreciable impact.

Understanding how TBX5 and GATA4 levels are integrated at the molecular level to afford genetic rescue of the *Tbx5* mutant phenotype by reduced *Gata4* activity will be essential for AF risk prediction. We identified an enhancer at *Ryr2* that molecularly integrates GATA4 and TBX5 with opposite activity. Previous work has characterized multiple promoters or enhancers co-regulated by TBX5 and GATA4, and in each case positive interactions were observed, either additive or synergistic [153, 156-161]. However, GATA4 has been reported to possess repressive molecular activity on cardiac enhancers in a few cases. For example, GATA4 recruits Hdac1/2 to deacetylate specific atrioventricular canal loci, thereby repressing AV canal identity during cardiac chamber development [157]. GATA4 can also cooperate with β-catenin on TCFL2-enahncers in the adult heart, to maintain normal homeostasis through repression of TCFL2-driven loci [188]. Therefore, GATA4 harbors repressive potential in some contexts in the heart. Here, we identified a novel repressive role for GATA4 at an enhancer of *Ryr2*, on which GATA4 opposes TBX5-dependent activation (Figure 3). We observed that TBX5 activation and GATA4 antagonism of the Ryr2 enhancer was dependent on GATA-binding sites in HL-1 cells but not HEK293T cells. One possibility for these different results is the distinct physiological conditions of these cell lines. Because HEK cells lack endogenous expression of TBX5 and GATA4, TF overexpression may overcome the effect of the binding site mutation because TBX5 and GATA4 physically interact [153]. In contrast, HL-1 cells, possessing endogenous physiologic expression of the cardiogenic kernel of TFs, including TBX5 and GATA4, may be more sensitive to the necessity of the GATA

binding sites. It remains to be elucidated how GATA4 antagonizes TBX5-dependent function in the adult atrium, perhaps by recruiting repressive chromatin remodeling enzymes or cardiac co-repressors. None-the-less, our observations provide a model for the integration of TBX5 and GATA4 dose on gene expression by the opposite modulation of single target gene enhancers. Understanding the molecular mechanisms underlying the opposite action of TBX5 and GATA4 on cardiac gene expression will improve our understanding of the molecular basis of adult cardiac rhythm control.

This work unveiled complex genetic interactions between genes individually implicated in AF by human genetic studies. The opposite sign with which decreased Gata4 dose impacted AF risk in the context of decreased Tbx5 dose indicates the importance of unveiling specific genetic interactions between genetic risk loci for understanding the combined impact of genetic variants across genomes for disease risk prediction. Human genetic studies have been underpowered for the identification of multigenic interactions to date, highlighting the importance of gene-gene interactions studies in model systems like those included in this study. This work suggests that interaction studies between genetic risk loci will be an essential component of understanding personalized risk from genetic association studies.

Chapter IV: ZO-1 regulates intercalated disc composition and atrioventricular node conduction

Note: The following section titled "A calcium transport mechanism for atrial fibrillation" is reproduced verbatim, with the exception of figure renumbering from my published article (Dai et al., Circulation Research. 2020;127:e28–e43)

Authors: Wenli Dai, Rangarajan D. Nadadur, Jaclyn A. Brennan, Heather L. Smith ,Kaitlyn M. Shen, Margaret Gadek, Brigitte Laforest, Mingyi Wang, Joanna Gemel, Ye Li, Jing Zhang, Bruce D. Ziman, Jiajie Yan, Xun Ai, Eric C. Beyer, Edward G. Lakata, Narayanan Kasthuri, Igor R. Efimov, Michael T. Broman, Ivan P. Moskowitz, Le Shen[§] and Christopher R. Weber[§]

[§] Co-corresponding authorship

Abstract

Rationale: Zona occludens 1 (ZO-1), encoded by the Tight Junction Protein 1 (TJP1) gene, is a regulator of paracellular permeability in epithelia and endothelia. ZO-1 interacts with the actin cytoskeleton, gap and adherens junction proteins, and localizes to intercalated discs in cardiomyocytes. However, the contribution of ZO-1 to cardiac physiology remains poorly defined. Objective: We aim to determine the role of ZO-1 in cardiac function. Methods and Results: Inducible cardiomyocyte-specific Tjp1 deletion mice (Tjp1fl/fl; Myh6Cre/Esr1*) were generated by crossing the Tjp1 floxed mice and Myh6Cre/Esr1* transgenic mice. Tamoxifen-induced loss of ZO-1 led to atrioventricular (AV) block without changes in heart rate, as measured by electrocardiogram (ECG) and ex vivo optical mapping. Mice with tamoxifen-induced conduction system specific deletion of Tjp1 (Tjp1fl/fl; Hcn4CreERt2) developed AV block while tamoxifen-induced conduction system deletion of Tjp1 distal to the AV node (Tjp1fl/fl; Kcne1CreERt2) did not demonstrate conduction defects. Western blot and immunostaining analyses of AV nodes showed that ZO-1 loss decreased connexin (Cx) 40

expression and intercalated disc localization. Consistent with the mouse model study, immunohistochemical staining showed that ZO-1 is abundantly expressed in the human AV node, and colocalizes with Cx40. Ventricular conduction was not altered despite decreased localization of ZO-1 and Cx43 at the ventricular intercalated disc and slightly decreased left ventricular ejection fraction, suggesting ZO-1 is differentially required for AV node and ventricular conduction. Conclusion: ZO-1 is a key protein responsible for maintaining appropriate AV node conduction through maintaining gap junction protein localization.

Introduction

ZO-1, encoded by the *TJP1* gene, is a cytoplasmic scaffolding protein critical to the function of the apical junctional complex[70, 189, 190]. Its essential function as a regulator of paracellular permeability is well recognized[190, 191]. In addition to binding to transmembrane proteins that dictate paracellular permeability[192-194], ZO-1 can bind to the actin cytoskeleton and the adherens junction component, α-catenin[192, 195-198]. Although ZO-1 is widely expressed in multiple cell types, its function has mostly been studied in epithelial and endothelial cells[72, 191, 199].

While its function in the heart remains poorly defined[200], ZO-1 is known to be enriched at the myocardial intercalated disc[37, 73, 75, 201], which contains multiple components, including gap junctions, adherens junctions, and desmosomes[37]. ZO-1 has been shown to bind to multiple intercalated disc proteins, including Coxsackie and adenovirus receptor (CAR)[77] and gap junction proteins Connexin (Cx) 35, 36 , 43, 45 and 40[73, 78-80, 202], and vinculin[203]. In addition, loss of ZO-1 binding partners Cx43, CAR, α-catenin, or vinculin in cardiomyocytes all disrupt heart function[204-208] and loss of CAR results in decreased ZO-1 localization at the intercalated disc[205, 206]. Taken together, these data suggest ZO-1 may be required for intercalated disc structure and function.

Given previous studies suggesting the importance of ZO-1 at the intercalated disc[37, 76], we sought to understand how ZO-1 might affect cardiac physiology. To circumvent the embryonic lethality of constitutive total body ZO-1 knockout[209], we developed inducible heart-specific *Tjp1* deletion mouse models that allow for interrogation of the role for ZO-1 in the adult myocardium and conduction system. We show that ZO-1 is critical to AV nodal conduction and only

modestly contributes to ventricular myocardial function. These data shed insight into the role of ZO-1 and potentially other ZO-1 associated proteins in heart physiology.

Methods

Generation of adult, cardiac specific ZO-1 deficient mice: All protocols were approved by The University of Chicago Institutional Animal Care and Use Committee. *Tjp1* floxed mice (*Tjp1*$^{tm2c(KOMP)Wtsi}$, MGI:6272009) were described previously[71, 210]. These mice were bred with mice expressing a tamoxifen inducible Cre recombinase driven by the *Myh6* (B6.FVB(129)-A1cfTg(Myh6-cre/Esr1*)1Jmk/J, MGI:3050453)[211], *Hcn4* (Tg(Hcn4-cre/ERT2)1Yzhao, MGI:5562295)[212] , or *Kcne1* (Tg(Kcne1-cre/ERT2)1Imos, MGI:5301931)[213] promoter. To induce recombination, both male and female mice were injected with tamoxifen at 6-8 weeks of age as previously described[138]. *Tjp1*$^{fl/fl}$ littermates with no Cre were also dosed with tamoxifen and used as controls.

Gene expression analysis: Left ventricular tissue was harvested from anesthetized mice. RNA extraction, reverse transcription, and quantitative real time PCR was performed as previously described[47]. Mouse *Tjp1* expression was measured by quantitative real-time PCR with exon 3 spanning primers specific to the deletion, F: 5'-TTTCAGAGTGGGGAAACCTCC-3', R: 5'-CACTCTTCCTTAGCTGCTGAAC-3'. Transcript abundance was normalized to *Gapdh*.

Western blot analysis: Following heart harvest, left ventricular and AV node was identified and dissected under a dissecting microscope. These tissues were processed and tissue homogenates were made as previously described[214]. Bradford assay was used to determine the protein concentration of the homogenates and 25 □g of protein was loaded onto 5% (homemade) or 4-20% (Bio-rad) acrylamide gels for separation by SDS-PAGE. Immunoblotting and detection

were performed as previously described[214]. Mouse anti-ZO-1 antibody (Thermo Fisher, Waltham, MA, Catalog # 339100) and Rabbit anti-GAPDH (Cell Signaling Technology, Catalog #5174) were used at 1:1000 dilution. CAR (Santa Cruz Biotechnology, Catalog #sc-373791), Cx40 (Thermo Fisher Scientific, Catalog # 37-8900), β-catenin (Cell Signaling Technology, Catalog #9562), and HCN4 (Abcam, Catalog #ab32675) were used at 1:300 dilution. Mouse, Rat, and Rabbit HRP conjugated secondary antibodies were used at 1:1000 dilution (Cell Signaling Technology, Catalog #7076, 7077, 7074 respectively).

Electrocardiogram recordings: ECGs were recorded as previously described[45, 47, 168]. Briefly, mice were implanted with subcutaneous telemetry transmitters and recorded over 48 hours (ETA-F10; Data Science International, St. Paul, MN)[168]. Arrhythmia analysis and measurement of ECG intervals were carried out using Ponemah Physiology Platform software (Data Science International, St. Paul, MN).

In vivo electrophysiology: *In vivo* electrophysiology was performed as previously described[47]. A right internal jugular venous approach was used on anesthetized mice to make recordings from the atrium, His bundle and ventricle via a Scisense 1.9 F octapolar catheter with 0.5 mm spacing (Transonic, Ithica, NY) connected to ADI BioAmp and PowerLab apparatus (ADInstruments, Colorado Springs, CO). Data were recorded using LabChart Software (ADInstruments). Atrial and ventricular pacing protocols were driven by a custom Python-based pacing program. Effective refractory periods were measured using 8-beat S1 drive trains followed by a single extra-stimulus.

Echocardiography: Echocardiography was performed on anesthetized mice as previously described[47]. The heart was imaged with a Vevo 770 ultrasound (VisualSonics, Toronto, Canada)

using a 30 MHz high-frequency transducer. Two-dimensional images were recorded in the parasternal long- and short-axis projections at the mid-papillary muscle level in both views. Left ventricular internal diameters, septal wall thickness, and posterior wall thickness were measured in at least three beats from each projection and averaged, and fractional shortening was calculated, and used to calculate left ventricular ejection fraction.

Ex vivo optical mapping: Optical mapping was performed as previously described[47] using an approved George Washington University animal protocol. Hearts were isolated and prepared as previously described[215]. Briefly, a midsternal incision was performed on the mice, and hearts were excised and mounted on a Langendoff apparatus for retrograde perfusion and superfusion with warmed (37 °C) and oxygenated (95% O_2/ 5% CO_2) Tyrode's solution (in mM: 128.2 NaCl, 4.7 KCl, 1.05 $MgCl_2$, 1.3 $CaCl_2$, 1.19 NaH_2PO_4, 20 $NaHCO_3$, 11.1 Glucose). Each isolated heart was pinned at the apex to bottom of the chamber to prevent stream-induced movement. After pinning the right atrial and left atrial appendages, the excitation-contraction uncoupler blebbistatin (10 μM, Bio-techne, Minneapolis, MN) was used to eliminate motion artifacts from the optical signals. Langendorff-perfused hearts were stained in line with perfusion with the voltage-sensitive dye di-4-ANEPPS (30 μl of a 2.6 mM stock solution dissolved in DMSO). Epicardial depolarization was measured by illuminating the tissue preparation with a 520 nm LED light. Emitted light was recorded through a 650 nm long-pass filter by a MiCAM Ultima-L CMOS camera (SciMedia) with high spatial (100 x 100 pixels, 230 ± 20 μm/pixel) and temporal (1000–3000 frames/s) resolution. The acquired fluorescent signal was analyzed with custom-developed software[216].

Immunofluorescence staining: 5 μm thick cryosections of mouse left ventricular tissue or 10 μm AV node containing tissue were fixed (1% PFA), washed (1xPBS), quenched (50 mM NH_4Cl),

permeabilized (0.5% NP-40), and stained with primary antibody as previously described[217]. Antibodies were used against the following intercalated disc proteins: ZO-1 (Thermo Fisher Scientific, Catalog # 339100), ZO-2 (Thermo Fisher Scientific, Catalog #71-1400), Cx43 (Cell signaling technology, Catalog # 3512), JUP (Abcam Catalog #ab11799), Nav1.5 (Abcam, Catalog #ab56240), β-catenin (Cell Signaling Technology, Catalog #9562), N-cadherin (Thermo Fisher Scientific, Catalog #333900), CAR (Santa Cruz Biotechnology, Catalog #sc-373791), Cx45 (Thermo Fisher Scientific, Catalog #PA5- 77357), Cx40 (Thermo Fisher Scientific, Catalog # 37-8900), CD31 (Antio-Proteomie, Catalog # mAP-0032). The sections were then stained with Alexa Fluor dye conjugated secondary antibodies (Jackson ImmunoResearch Laboratories, Inc, Catalog #s 711-586-152,715-546-151), phalloidin (Thermo Fisher Scientific, Catalog# A22287), and Hoechst 33342 (Thermo Fisher Scientific, Catalog# 953557). ProLong Gold (Thermo Fisher Scientific, Catalog# P36934) was used for mounting. Fluorescence images were taken using an IX81 Olympus microscope (Olympus, Waltham, MA) with 20x or 40x air or oil immersion objectives. Quantification was performed in MetaMorph Image Analysis Software (Molecular Devices, San Jose, CA) with linescan of the fluorescence signal across the width of the intercalated disc. Blinded imaging and quantification were performed using identical exposures and matched imaging and processing conditions.

Immunohistochemistry: Immunohistochemical staining for ZO-1 was performed using anti-ZO-1 (Thermo Scientific, Cat#339100, mouse monoclonal antibody, Clone: ZO-1-1A12,) on formalin fixed paraffin embedded mouse heart sections. After deparaffinization and rehydration, tissue sections were treated with antigen retrieval solution (Agilent, Santa Clara, CA) in a steamer for 20 minutes. MOM blocking kit (Vector Laboratories, Burlingame, CA) was used. Anti-ZO-1 antibody (1:50) was applied on tissue sections for one hour incubation at room temperature in a

humidity chamber. Following PBS wash, the antigen-antibody binding was detected with Envision+ system (Agilent) and DAB+ chromogen (Agilent). Tissue sections were counterstained with hematoxylin and mounted. Hematoxylin and eosin stain[218] and trichrome stain (Millipore-Sigma, St. Louis, MO) were performed using standard protocols. Slides were imaged using a Leica DM2000 Microscope (Leica Microsystems, Wetzlar, Germany) with a ProgRes C14^{plus} color digital camera (Jenoptik, Jena, Germany).

Use of human atrial tissue: Human heart tissue was collected from organ donors (that were not used for heart transplantation, but had no history of major cardiovascular diseases and had normal cardiac function) provided by Illinois Gift of Hope Organ & Tissue Donor Network (GOH). The studies were approved by the Human Study Committee of Rush University. The AV node containing region was dissected out and fixed with formalin. Immunofluoresence and IHC staining of AV node slides were performed using anti ZO-1 (described above) and anti-Cx40 (Thermo Fisher Scientific, Catalog # 37-8900) antibodies with the secondary antibodies described above. Immunofluoresence images were obtained using an Olympus IX81 Inverted Widefield Microscope (Olympus, Waltham, MA).

Transmission Electron Microscopy: AV node and surrounding tissues were dissected from mice two weeks post tamoxifen treatment. Tissues were fixed, embedded, sectioned and mounted onto carbon grids as previously described with the following differences[219]. For primary fixation, 2% glutaraldehyde and 4% paraformaldehyde in 0.1M sodium cacodylate buffer was used. 1% Osmium Tetroxide was used for secondary fixation. Polymerization was done at 60ºC for 48 hours in a vacuum oven. 60 nm thickness sections were cut and mounted on carbon-coated copper grids. Brief staining in 100% Uranyl Acetate and Lead Citrate was performed. Semi-thin

sections used for Toluidine blue staining were cut at 300 nm. Images were taken with a JEM-1400 Plus electron microscope (JEOL, Tokyo, Japan).

Statistics: Data are reported as mean ± standard error of the mean (SEM). Statistical analyses were performed for paired comparisons using a two-tailed Student's t-tests unless otherwise noted. For count-based quantification of heart-block occurrence, a two-tailed Fisher's exact test was used. Statistical significance is designated as *p<0.05, **p<0.01, and ***p<0.001 in the figures.

Results

Generation of adult cardiac-specific Tjp1 knockout mice

ZO-1 is widely expressed in multiple cell types and is a known regulator of paracellular permeability in epithelial and endothelial cells[70, 72, 189-191, 199]. Although ZO-1 localization at the intercalated disc is well-documented[37, 73, 201, 220, 221], the function of ZO-1 in the heart remains poorly defined. Since complete loss of ZO-1 is embryonic lethal at day E11.5 due to vascular defects[209], we generated inducible tissue-specific knockout models to study cardiac-specific ZO-1 function. *Tjp1* floxed mice were bred with cardiomyocyte-specific (Myh6 promoter) Cre/Esr1* transgenic mice (Fig. 1A) [71, 211].

We first assessed *Tjp1* deletion efficiency in the heart. qRT-PCR showed $Tjp1^{fl/fl;}$ $Myh6^{Cre/Esr1*}$ heart tissue have decreased *Tjp1* exon3 containing mRNA (46 ± 4% decrease, p=1e-5) relative to $Tjp1^{fl/fl}$ controls two weeks post-tamoxifen injection (Fig. 1B). In contrast, liver expression of *Tjp1* mRNA was unchanged between $Tjp1^{fl/fl;}$ $Myh6^{Cre/Esr1*}$ and $Tjp1^{fl/fl}$ mice. In the left ventricle, ZO-1 protein was reduced by 69 ± 10% (p=0.007) by western blot (Fig. 1C). The partial loss of *Tjp1* mRNA and ZO-1 protein in the left ventricle could be due to 1)

incomplete *Tjp1* locus recombination resulting in incomplete knockout or 2) the presence of non-cardiomyocyte cells (such as endothelial cells and fibroblasts) not affected by cardiomyocyte specific MerCreMer protein activity. To differentiate between these two possibilities, we next performed immunofluorescence staining for ZO-1 protein to determine its myocardial-specific expression. ZO-1 expression remained abundant in endothelial cells, as identified by CD31 (Fig. 1D arrow heads). ZO-1 protein expression at the intercalated discs was significantly reduced (73 ± 8% decrease, p=2e-7) (Fig. 1D,E arrows, F) as measured by peak intensity of immunofluorescence staining of ZO-1 at the intercalated disc. These findings support that incomplete *Tjp1* knockout is due to a combination of both factors discussed above. There were no observed differences in cardiomyocyte actin organization or cell morphology.

Loss of ZO-1 disrupts cardiac conduction

To study the physiologic role of ZO-1 in the heart, we first monitored mice longitudinally by electrocardiogram (ECG) under anesthesia. Five d after tamoxifen treatment, $Tjp1^{fl/fl}$; $Myh6^{Cre/Esr1*}$ mice had significantly prolonged PR interval (80 ± 10% prolongation, p=2e-6) (Fig. 2A, B), indicating 1st degree AV block. By 10 d post-tamoxifen, 4 of 11 mice (p=0.04, Fisher's exact test) displayed complete dissociation of atrial and ventricular depolarization, indicating heart block with junctional escape rhythm compared to none in control mice (Fig. 2C). Ambulatory telemetric electrocardiogram recordings were performed to assess RR and PR interval variation. At one week post-tamoxifen injection, Poincaré plots of the PR interval showed distinct separation between $Tjp1^{fl/fl}$; $Myh6^{Cre/Esr1*}$ and $Tjp1^{fl/fl}$ control mice (Fig. 2D) and average PR interval was significantly prolonged in $Tjp1^{fl/fl}$; $Myh6^{Cre/Esr1*}$ mice (Fig. 2E). In contrast, dispersion of RR interval was similar and average RR interval and heart rate was unchanged (Fig. 2F,G). By two weeks post-tamoxifen injection, PR interval was not only

prolonged, but highly variable, consistent with 3rd degree heart block with junctional escape rhythm. RR intervals remained unchanged (Fig. 2H-K). Neither P wave (10.2 ± 0.8 ms *vs*. 12.3 ± 0.7 ms, p=0.18) nor QRS complex durations (8.9 ± 0.4 ms *vs*. 10.4 ± 0.5 ms, p=0.13) were altered between $Tjp1^{fl/fl}$ and $Tjp1^{fl/fl}; Myh6^{Cre/Esr1*}$ mice. Additionally, tamoxifen-injected $Myh6^{Cre/Esr1*}$ control mice also did not exhibit PR interval prolongation (PR=32.7 ± 14 ms). To confirm the specific location of the conduction defect, intracardiac electrophysiology studies were performed. Ten d after tamoxifen injection, the time interval from atrial to bundle of His depolarization was increased (A-H Interval, p=0.003, Fig. 2L, M), but the interval from bundle of His depolarization to ventricular depolarization was unchanged (H-V Interval, p=0.3, Fig. 2L, N). The minimum cycle duration that is capable of maintaining 1:1 atrial to ventricular conduction time (Fig. 2O; AV Wenckebach time) was prolonged (p=0.02). Together, A-H interval and AV Wenckebach prolongation are indicative of slowed AV nodal conduction. Intracardiac pacing studies showed normal atrial and ventricular refractory periods (AERP p=0.5, VERP p=0.25, not shown). These data suggest that removal of ZO-1 causes slowed AV nodal conduction, but does not alter atrial myocardial conduction, ventricular myocardial conduction, or RR interval.

To assess epicardial depolarization patterns, we performed optical mapping studies. Propagation of epicardial depolarization in isolated hearts from mice 20 d post-tamoxifen treatment was measured. The overall pattern of atrial and ventricular depolarization was not different between $Tjp1^{fl/fl}$ and $Tjp1^{fl/fl}; Myh6^{Cre/Esr1*}$ hearts with only one focus of depolarization initiation occurring at or near the sinoatrial node in both genotypes (Fig. 3A). There were no significant differences observed in atrial and ventricular activation times (Fig. 3A, B). However,

an increase in AV conduction time was observed, consistent with electrophysiology studies (Fig. 3 and Fig. 2A, B, L, M, O).

Tjp1 deletion is associated with modestly decreased heart function.

Given the observed changes in conduction, we next asked whether loss of cardiomyocyte *Tjp1* would cause decreased heart function. We measured left ventricular ejection fraction by echocardiography over the course of 10 weeks. Ejection fraction was unchanged in $Tjp1^{fl/fl}$; $Myh6^{Cre/Esr1*}$ compared to $Tjp1^{fl/fl}$ controls in the first 10 d post-tamoxifen. Beginning at 20 d post-tamoxifen treatment, average ejection fraction in $Tjp1^{fl/fl}$; $Myh6^{Cre/Esr1*}$ mice was slightly decreased compared to $Tjp1^{fl/fl}$ controls (16 ± 4%, p=5e-5). (Supplement 1A, B). 40 d post-tamoxifen injection, the decreased ejection fraction in $Tjp1^{fl/fl}$; $Myh6^{Cre/Esr1*}$ mice persisted without additional decrease in ejection fraction (Supplement 1B). A repeated measures mixed ANOVA was performed and ejection fraction between $Tjp1^{fl/fl}$ and $Tjp1^{fl/fl}$; $Myh6^{Cre/Esr1*}$ mice was significantly different (p=5e-4 and partial eta squared = 0.952). The heart rate was not significantly different at any time point (Supplement 1B). Left ventricular systolic and diastolic diameters are shown in Supplement 2A-F. The small and persistent decrease in ejection fraction in $Tjp1^{fl/fl}$; $Myh6^{Cre/Esr1*}$ mice at >20 d is due predominantly to increased internal diameter during systole without reduction in diastolic diameter (Supplement 2D). The change in ejection fraction was not accompanied by gross or microscopic changes, including heart size (Supplement 1C), heart weight (Supplement 1D), or fibrosis as determined by trichrome staining (Supplement 1E) 12 weeks after tamoxifen injection. Thus, loss of ZO-1 causes only a small but significant change in cardiac function without evidence of gross or histological alterations.

ZO-1 loss disrupts AV nodal Cx40 and CAR localization and perinodal Cx43 localization

Due to AV nodal dysfunction following *Tjp1* deletion, we assessed AV node morphology and ZO-1 expression in $Tjp1^{fl/fl}$ and $Tjp1^{fl/fl}; Myh6^{Cre/Esr1*}$ mice. Using trichrome staining, we identified the AV node, which was not organizationally disrupted in $Tjp1^{fl/fl}; Myh6^{Cre/Esr1*}$ mice (Fig. 4A). In $Tjp1^{fl/fl}$ mice, immunohistochemical staining showed ZO-1 was highly expressed at the AV node. ZO-1 staining intensity was decreased by 49 ± 10% (p=0.01, n=3 for each group) in AV nodes in $Tjp1^{fl/fl}; Myh6^{Cre/Esr1*}$ mice (Fig. 4B). Next, we assessed expression and localization of proteins important to AV nodal conduction. HCN4 staining was high in the region identified as the AV node via trichrome stain (Fig. 4C,D), further confirming its functional specialization. Cx40 and CAR stained the AV node strongly, whereas Cx43 was absent from the AV node, but was strongly expressed in the adjacent myocardium (perinodal region) (Fig 4E,F). Cx40 and CAR co-staining with the intercalated disc marker β-catenin showed that Cx40 and CAR are enriched at intercalated discs of AV nodes (Supplement 3). Cx40 staining intensity within the intercalated discs of the AV node was decreased by 70 ± 8% in $Tjp1^{fl/fl}; Myh6^{Cre/Esr1*}$ mice (p=0.05, n=3 animals per genotype) (Fig. 4G). Cx43 staining intensity at the intercalated discs of perinodal myocardium was decreased by 65 ± 4% in $Tjp1^{fl/fl}; Myh6^{Cre/Esr1*}$ mice (p=0.002, n=3 animals per genotype) (Fig. 4H). CAR stained AV nodal cells in a punctate and membranous pattern at cell-to-cell junctions, and staining intensity was decreased by 39 ± 6% in $Tjp1^{fl/fl}; Myh6^{Cre/Esr1*}$ mice (p=0.01, n=3 animals per genotype) (Fig. 4I). Cx45, $Na_V1.5$, β-catenin and N-cadherin staining intensity were not changed in the AV node (Supplement 4).

To determine whether overall Cx40 and CAR protein abundance is altered, we performed western blot for ZO-1, Cx40, and CAR using homogenates of dissected AV nodes. AV nodal tissue dissection was confirmed by enrichment of HCN4 in AV nodal tissue relative to ventricular tissue (Fig. 4J). We observed that ZO-1 and Cx40 protein abundance was decreased

by 50 ± 6% (p=.009) and 59 ± 11% (p=.04) respectively in dissected AV nodal regions of *Tjp1*$^{fl/fl}$*; Myh6*$^{Cre/Esr1*}$ mice at 2 weeks of age (Fig. 4K,L). CAR protein abundance also showed a downward trend, but it did not reach statistical significance, (Fig. 4K,L). Similar to immunofluorescence staining results, β-catenin protein abundance was also not changed (Fig. 4K,L). We further tested if similar changes could also occur in ventricular myocardium distant from the AV node. At the ventricular intercalated disc, Cx43 and CAR localization was significantly decreased, but β-catenin distribution was unaltered, as assessed by immunofluorescent staining (Supplement 5).

We next examined whether changes in AV node protein localization and total expression would yield discernable AV node ultrastructural changes. Transmission electron microscopy (TEM) was performed on AV node containing sections, as determined by Toluidine blue staining (Supplement 6 A,B). No discernable differences in overall AV node architecture or in the appearance of the intercalated disc were noted between *Tjp1*$^{fl/fl}$*; Myh6*$^{Cre/Esr1*}$ and control mice at 2 weeks of age (Supplement 6 C,D)

ZO-1 and Cx40 colocalize in human AV nodes

Similar to our observation of high ZO-1 abundance in mouse AV nodes, we found ZO-1 is also highly expressed in AV nodes of humans (Fig. 5A,B). It is also expressed at intercalated discs of atrial and ventricular cardiomyocytes (Fig. 5A,B). Since Cx40 is a major AV node connexin[222, 223], and Cx40 is decreased in *Tjp1*$^{fl/fl}$*; Myh6*$^{Cre/Esr1*}$, we stained for Cx40 in human AV node samples. ZO-1 colocalizes with Cx40 in both the AV node and atrial myocardial tissue but is not found in the ventricle (Fig. 5C). Taken together, our human and mouse studies suggest abundant ZO-1 expression in the AV node.

Conduction system-specific ZO-1 loss is sufficient to drive heart block.

Upon determining that ZO-1 is abundantly expressed in mouse and human AV nodal tissues, we next tested the contribution of ZO-1 to cardiac conduction specifically by genetic dissection. We generated conduction system specific (*Tjp1*$^{fl/fl}$*; Hcn4*^{CreERt2}) and AV bundle-His-Purkinje specific (*Tjp1*$^{fl/fl}$*; Kcne1*^{CreERt2}) *Tjp1* deletion mouse models. *Tjp1*$^{fl/fl}$*; Hcn4*^{CreERt2} mice developed increased PR interval (148 ± 7% increase, p=6e-6) and dissociation of atrial and ventricular depolarization 2 weeks after the start of tamoxifen treatment (Fig. 6A-C). In contrast, *Tjp1*$^{fl/fl}$*; Kcne1*^{CreERt2} mice did not demonstrate any heart block (Fig. 6A-C). In line with this finding, the abundant ZO-1 expression found in the AV node was not observed in the AV bundle (Supplement 7). Furthermore, despite the conduction system defects in the *Tjp1*$^{fl/fl}$*; Hcn4*^{CreERt2} mice, there was no evidence of depressed myocardial function (Fig. 7D), in contrast to our observations in *Tjp1*$^{fl/fl}$*; Myh6*$^{Cre/Esr1*}$ mice (Supplement 1 A, B). These results show that ZO-1 expression in the conduction system proximal to the His bundle is critical to conduction. Furthermore, the data suggest myocardial dysfunction is independent of the conduction system defects in cardiac specific *Tjp1* deleted mice.

Discussion

Healthy cardiac conduction and function relies on the coordinated electrical activity of distinct populations of cardiomyocytes. Electrical activity initiated at the SA node must propagate through atrial myocardium, the AV node, His-Purkinje system, and into ventricular myocardium. Disruption of cell-cell conduction results in cardiac arrhythmias and cardiomyopathies, a leading cause of morbidity and mortality worldwide[38, 224-226]. Intercalated disc proteins have been recognized as important regulators of cardiac conduction due to their

function in maintaining electrical and physical coupling between cells. Here we show inducible loss of the intercalated disc protein ZO-1 in cardiomyocytes of adult mice impedes AV node conduction and modestly affects ejection fraction.

Mice with induced cardiomyocyte specific *Tjp1* deletion *(Tjp1$^{fl/fl}$; Myh6$^{Cre/Esr1*}$* mice with tamoxifen injection) exhibit an AV nodal conduction defect with normal atrial and ventricular conduction (Figs. 2,3). This interpretation is based on electrophysiological and optical mapping studies demonstrating increased PR interval, increased AH intervals, increased AV Wenckebach time, and AV conduction time but unchanged HV interval, P wave, QRS complex duration, and atrial and ventricular activation time in *Tjp1$^{fl/fl}$; Myh6$^{Cre/Esr1*}$* mice (Figs. 2,3). To assess 1) if the AV block is intrinsic to the conduction system or secondary to myocardial changes, and 2) to assess potential region-specific requirements of ZO-1 in the conduction system, we generated two additional inducible tissue-specific knockout models. Similar to induced cardiomyocyte specific *Tjp1* knockout (*Tjp1$^{fl/fl}$; Myh6$^{Cre/Esr1*}$*), tamoxifen-induced overall conduction system *Tjp1* knockout (*Tjp1$^{fl/fl}$; Hcn4^{CreERt2}*) resulted in AV block without decreased ejection fraction (Fig. 6), suggesting AV block is not secondary to myocardial changes. In contrast, tamoxifen-induced *Tjp1* knockout distal to the AV node (*Tjp1$^{fl/fl}$; Kcne1^{CreERt2}*) did not manifest heart block. Taken together with our observation that ZO-1 is highly expressed in the AV node, but in the fast conducting AV-bundle, such high expression was not apparent (Supplement 7), these results support that ZO-1 loss in the conduction system above the bundle of His is responsible for PR prolongation and ZO-1 expression is critical to normal AV nodal conduction.

Given the observed AV node dysfunction following ZO-1 loss, we hypothesized that ZO-1 is important to the organization of proteins at the intercalated disc that facilitate cell-cell conduction. Immunofluorescent microscopy and western blot studies showed decreased

expression of Cx40[223, 227] and to a lesser extent, CAR[205, 206], in the AV node in *Tjp1*$^{fl/fl;}$ *Myh6*$^{Cre/Esr1}$ mice. This is in line with previous biochemical data demonstrating that connexins, CAR, and ZO-1 can reside within the same protein complex. Connexins contain a C-terminal PDZ binding sequence that directly binds to the PDZ domains of ZO-1[73, 80, 228-230]. CAR contains a PDZ binding C-terminal motif and can precipitate with ZO-1[77, 205, 231, 232]. Furthermore, genetic deletion of Cx40[223, 227] and CAR[205, 206] both slow AV nodal conduction. Together these data suggest ZO-1 plays a key role in maintaining the connexin-ZO-1-CAR complex at the intercalated disc.

It is notable that although PR interval was altered in cardiac and conduction system specific *Tjp1* deleted mice, there was no change in RR interval or heart rate. This observation of AV block with normal heart rate is in contrast to some models in which PR interval prolongation is associated with increased RR interval[233, 234]. Interestingly, PR prolongation with normal heart rate is also observed in *Cxadr* (CAR)[205, 206] and *Gja5* (Cx40)[223] knockout mice. Our finding that CAR localization at the intercalated disc is affected by *Tjp1* knockout along with biochemical interactions between ZO-1, CAR, and Cx40 (discussed above) and altered ZO-1 distribution in *Cxadr* knockout mice provide increasing evidence for functional interactions between these proteins. Together, these observations coalesce into a model in which ZO-1, CAR, and Cx40 physically associate to co-regulate AV nodal conduction.

Although atrial and ventricular conduction speed were normal in *Tjp1*$^{fl/fl;}$ *Myh6*$^{Cre/Esr1}$ mice, changes in ventricular intercalated disc organization and protein staining were still observed. By immunofluorescence microscopy, there was decreased Cx43 and CAR localization at the ventricular intercalated disc. These observations are consistent with previous findings that partial connexin loss is not sufficient to induce altered myocardial conduction[235, 236, 237], and

Cxadr (CAR) deletion in cardiomyocytes also does not significantly affect atrial and ventricular conduction, despite decreased connexin and ZO-1 localization at intercalated discs of ventricular cardiomyocytes[205, 206]. Our finding that *Tjp1* knockout mice have prolonged AV nodal conduction times but normal ventricular conduction times suggests that AV nodal and ventricular cardiomyocyte conduction have different molecular requirements. Our observations support that AV nodal conduction may be particularly vulnerable to defects in the connexin-ZO-1-CAR complex (Fig. 7).

We demonstrate that ZO-1 loss in myocardial tissue is associated with modestly decreased ejection fraction. In contrast, neither of the conduction specific knockout models demonstrated this phenotype (Fig. 6D). This suggests that loss of ZO-1 can independently affect conduction and ejection fraction, and decreased functional output is due directly to loss of ZO-1 in the myocardium and not secondary to conduction defects. We did not observe a progressive loss of ejection fraction and sudden death of the $Tjp1^{fl/fl;}$ $Myh6^{Cre/Esr1*}$ mice, which could be explained by the presence of compensatory mechanisms that may be important for preserving myocardial function following loss of ZO-1. For example, ZO-2, a closely related protein to ZO-1, may play a role in such compensatory mechanisms. ZO-1 and ZO-2 both work to regulate epithelial function, including tight junction function and apical membrane organization[238-240]. Although we could readily detect ZO-2 expression in cardiac endothelial cells, we failed to detect ZO-2 at the intercalated disc 10 d following ZO-1 knockout (Supplement 8), long term studies are needed to understand whether ZO-2 along with other protein expression and localization are altered and limit ZO-1 induced myocardial changes.

Recently, *TJP1* variations have been associated with arrhythmogenic cardiomyopathy in patients[241], but AV nodal dysfunction was not observed in the 4 probands studied by Bartoli *et*

al[241]. We do not currently know why such a difference exists, and further investigation will be requiredto determine the potential role of ZO-1 on AV nodal function in humans with arrhythmogenic cardiomyopathy. Another difference between our ZO-1 knockout mouse model and the patients of Bartoli et al[241] is the absence of fibrofatty replacement of myocardial tissue up to 12 weeks after *Tjp1* deletion in the mice. This difference may be due to the adult onset, cardiomyocyte specific nature of the ZO-1 loss in our mouse model compared to patients carrying pathogenic *TJP1* variants, who have altered ZO-1 function in all cell types, throughout their life. Since ZO-1 may influence many aspects of cardiac (e.g. coronary vasculature) as well as other organ system development and physiological function, the clinical symptoms may be influenced by all of these cell types and organs. Long term studies will be required to further evaluate whether histological features of arrhythmogenic cardiomyopathy can manifest in mice following knockout of *Tjp1*.

ZO-1 has been implicated in other forms of cardiomyopathy without *Tjp1* mutations. For example, expression of a pathogenic mutant of transmembrane protein 43 (TMEM43) associated with arrhythmogenic cardiomyopathy causes loss of ZO-1 at the intercalated disc-like cell-cell junctions, and decreases cell-cell conduction velocity in HL-1 cells[54]. Furthermore, our analysis of published Gene Expression Omnibus datasets suggest *TJP1* expression is altered in hearts of cardiomyopathy patients (GDS2205 and GDS1362), and isoproterenol treated mice (GDS3684). Together, these findings suggest ZO-1 expression or localization change can influence cardiomyopathy pathogenesis.

In conclusion, we demonstrate ZO-1 is necessary for maintaining gap junction protein expression and localization, and loss of ZO-1 results in AV node dysfunction, and when deleted from myocytes throughout the heart, results in modest decrease in cardiac function.

Understanding how ZO-1 function is altered in patients with cardiomyopathy and other heart diseases will be important and may provide novel therapeutic approaches.

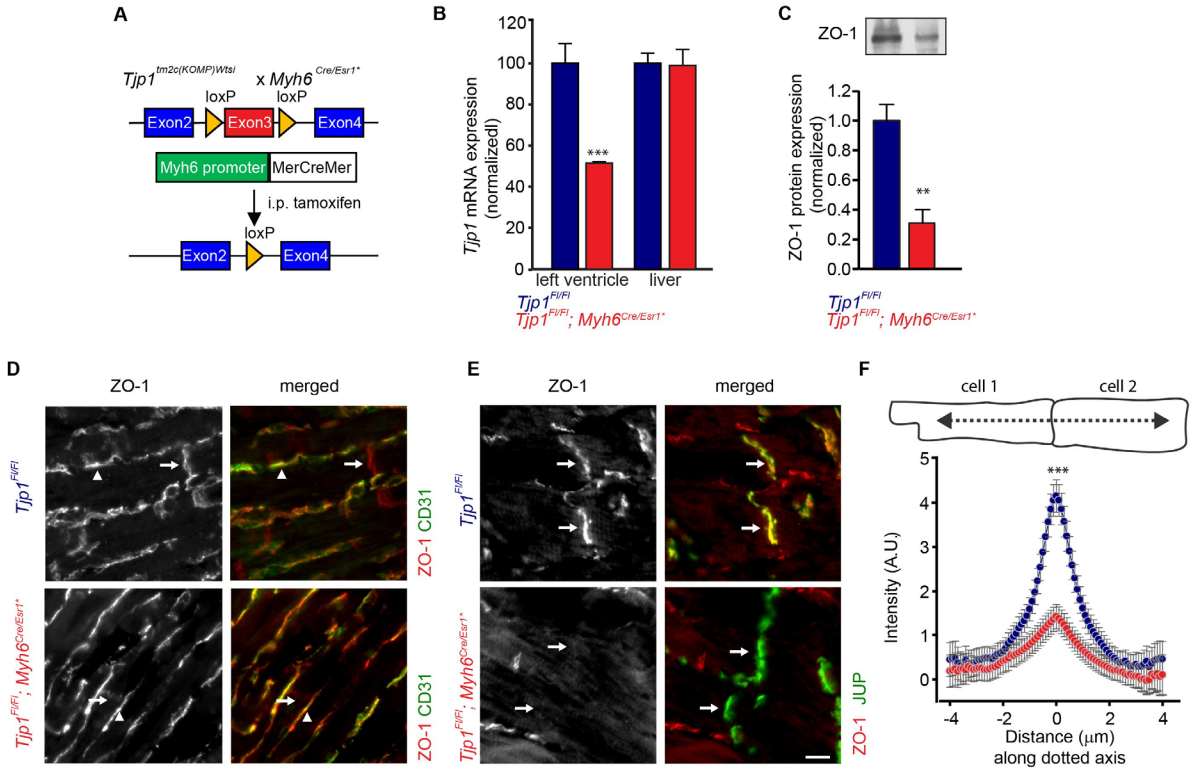

Figure 4-1. Inducible cardiomyocyte-specific Tjp1 deletion reduces ZO-1 expression at intercalated discs.

A. Breeding and treatment scheme for Tjp1 deletion (Tjp1fl/fl; Myh6Cre/Esr1*). B. Exon 3 specific Tjp1 mRNA levels in left ventricle and liver, as determined by qRT-PCR (n=4-5 animals per genotype). C. Western blot of left ventricular lysate (n=4 animals per genotype). D. Representative images of immunofluorescent staining of ZO-1 in left ventricular tissue. CD31 was used to label endothelial cells. Arrows: intercalated disc, Arrow heads: endothelial cells. E. Representative images of immunofluorescent staining of ZO-1 in left ventricular tissue. Junction plakoglobin (JUP) was co-stained with ZO-1 to mark intercalated discs. Arrow: intercalated disc E. Immunofluorescent staining along lines perpendicular to the intercalated disc are shown (n=3 mice per genotype, 2-3 regions within the ventricle per animal, 8-10 intercalated discs per region) (Red: Tjp1fl/fl; Myh6Cre/Esr1*, Blue: Tjp1fl/fl, ***P<0.001, ** P<0.01). All studies were performed at 10 d post-tamoxifen injection. (Scale bar = 10 μm)

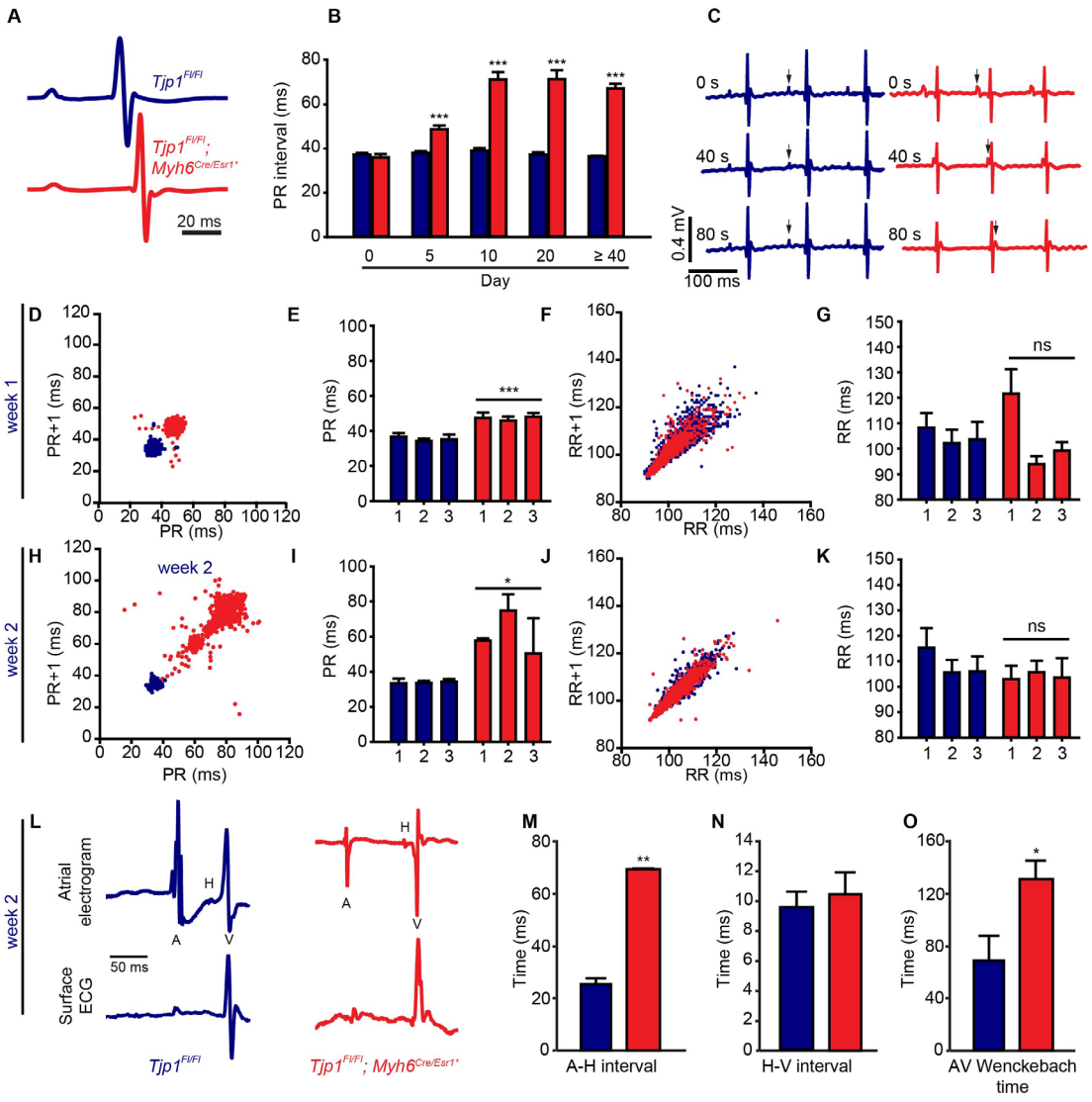

Figure 4-2. *Tjp1*$^{fl/fl}$*; Myh6*$^{Cre/Esr1*}$ mice have altered cardiac electrophysiology.

A. Averaged telemetry signals 5 d after tamoxifen injection. B. Time course of PR interval following tamoxifen injection (n=6-11 animals per genotype). C. Sampling of 3 time points within a representative ECG trace in *Tjp1*$^{fl/fl}$ and *Tjp1*$^{fl/fl}$*; Myh6*$^{Cre/Esr1*}$ mice. (arrows: P waves) D, H. Representative Poincaré plots, showing beat-to-beat PR interval variability, from *Tjp1*$^{fl/fl}$*; Myh6*$^{Cre/Esr1*}$ and *Tjp1*$^{fl/fl}$ mice 5 or 10 d post tamoxifen treatment. E, I. PR intervals for three individual mice per genotype 5 or 10 d post tamoxifen treatment. F, J. Representative Poincaré plots, showing beat-to-beat RR interval variability, from *Tjp1*$^{fl/fl}$*; Myh6*$^{Cre/Esr1*}$ and *Tjp1*$^{fl/fl}$ mice 5 or 10 d post tamoxifen treatment. G, K. RR intervals for three individual mice per genotype 5 or 10 d post tamoxifen treatment. L. Representative atrial electrogram and simultaneous surface ECG recordings (n=4-5 animals per genotype). M. Atrial to His conduction time (n=4-5 animals per genotype). N. His to ventricular conduction time (n=4-5 animals per genotype). O. AV Wenckebach time (n=4-5 animals per genotype). (Red: *Tjp1*$^{fl/fl}$*; Myh6*$^{Cre/Esr1*}$, Blue: *Tjp1*$^{fl/fl}$, ***P<0.001, ** P<0.01, *P<0.05)

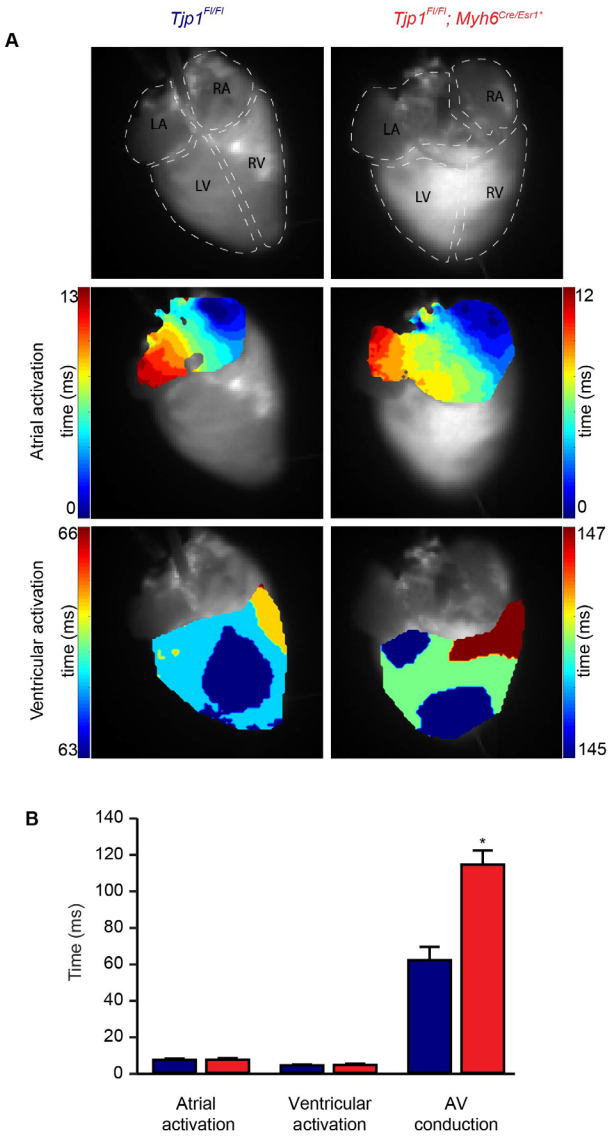

Figure 4-3 Identification of prolonged AV conduction time by optical mapping.

A. Representative activation maps of atria and ventricle in *Tjp1*$^{fl/fl}$ (left) and *Tjp1*$^{fl/fl}$*; Myh6*$^{Cre/Esr1*}$ (right) mice. B. Atrial, ventricular, AV conduction times (n=5-6 mice of each genotype). All studies were performed 20 d post-tamoxifen injection. (Red: *Tjp1*$^{fl/fl}$*; Myh6*$^{Cre/Esr1*}$, Blue: *Tjp1*$^{fl/fl}$, *P<0.05)

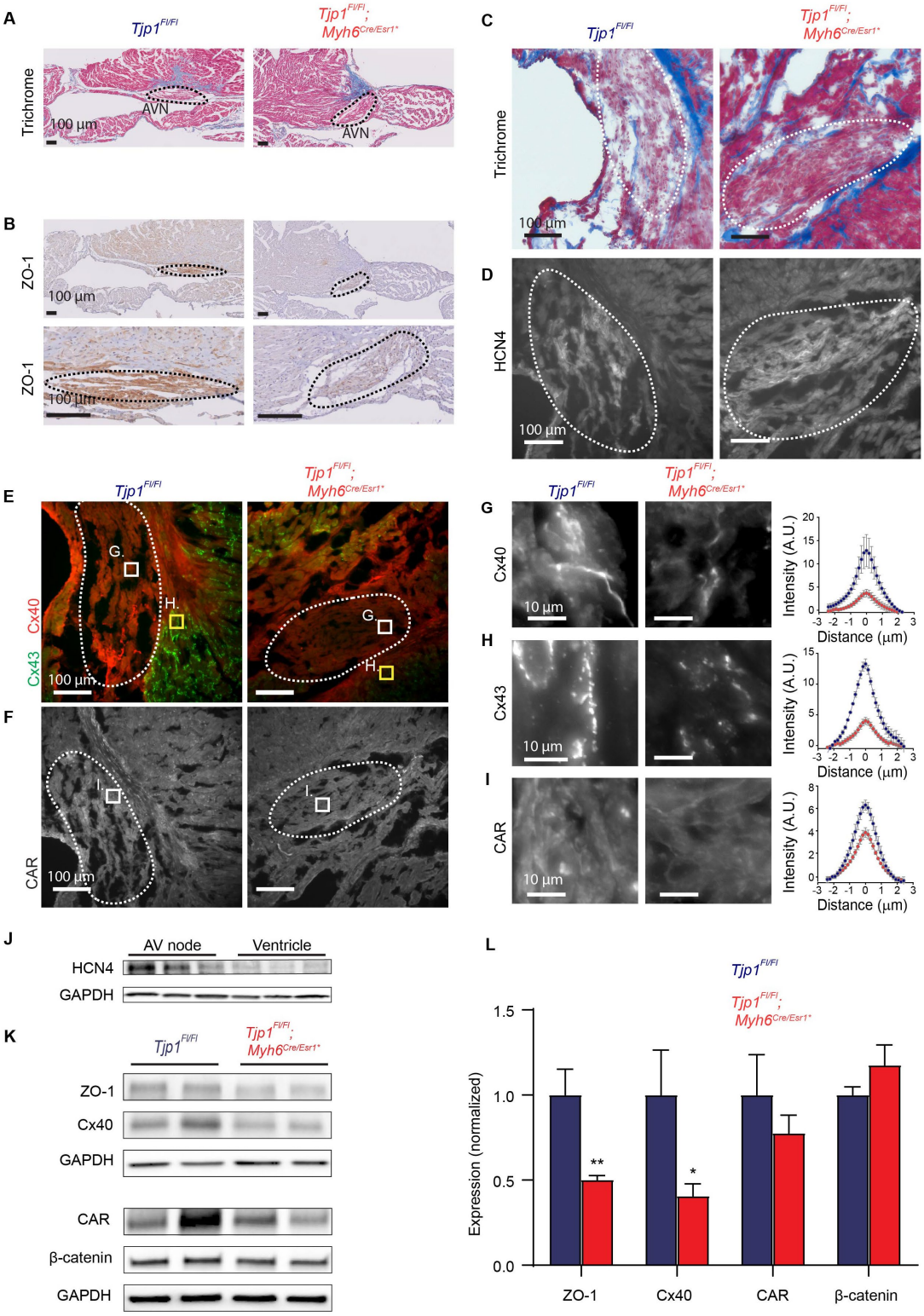

Figure 4-4. ZO-1 loss disrupts AV node protein localization and abundance.

Figure 4-4, continued.

A. Representative trichrome stain of mouse AV nodes. B. Representative immunohistochemical staining for ZO-1 in AV nodes (Low and high magnification images of the same AV node). C-D. Representative trichrome (C) and HCN4 immunofluorescent (D) staining for AV node identification. E-F. Immunofluorescent staining of Cx40 (E), Cx43 (E), and CAR (F) at low power (scale bar = 100 μm). G-I. Representative high power images from boxed region of images in E-F (Cx40 in panel G, within AV node, Cx43 in panel H, in perinodal area, CAR in panel I, within AV node, scale bar = 10 μm) and quantification of intercalated disc staining of Cx40 (G, within AV node), Cx43 (G, perinodal area), and CAR (I, within AV node). Quantification of immunofluorescent staining along lines perpendicular to the intercalated disc are shown. N = 3 for each group, 8 intercalated disc region measurements per mouse). AV nodes are circled by dashed lines. J. Western blot images of HCN4 expression in AV node tissues compared to ventricular tissue in the same $Tjp1^{fl/fl}$ mice (N=3). K. Representative western blot images of AV node ZO-1, Cx40, CAR, and β-catenin and corresponding GAPDH loading control. L. Quantification of western blot from 4 mice per genotype (Red: $Tjp1^{fl/fl}; Myh6^{Cre/Esr1*}$, Blue: $Tjp1^{fl/fl}$, ***P<0.001, ** P<0.01, *P<0.05, N.S. P>0.05. All studies were performed 10 d post-tamoxifen injection.

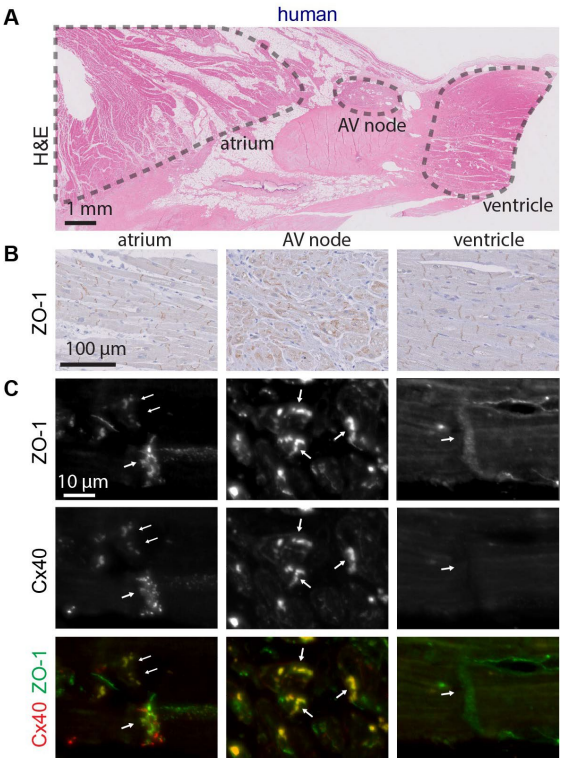

Figure 4-5. ZO-1 colocalizes with Cx40 in human AV nodes.

A. Representative H&E stain of a normal human AV node (scale bar = 1 mm). B. Immunohistochemical staining of ZO-1 in normal human atrium, AV node, and ventricle (scale bar = 100 µm). C. Immunofluorescence staining of ZO-1 and Cx40 in human atrium, AV node, and ventricle (scale bar = 10 µm).

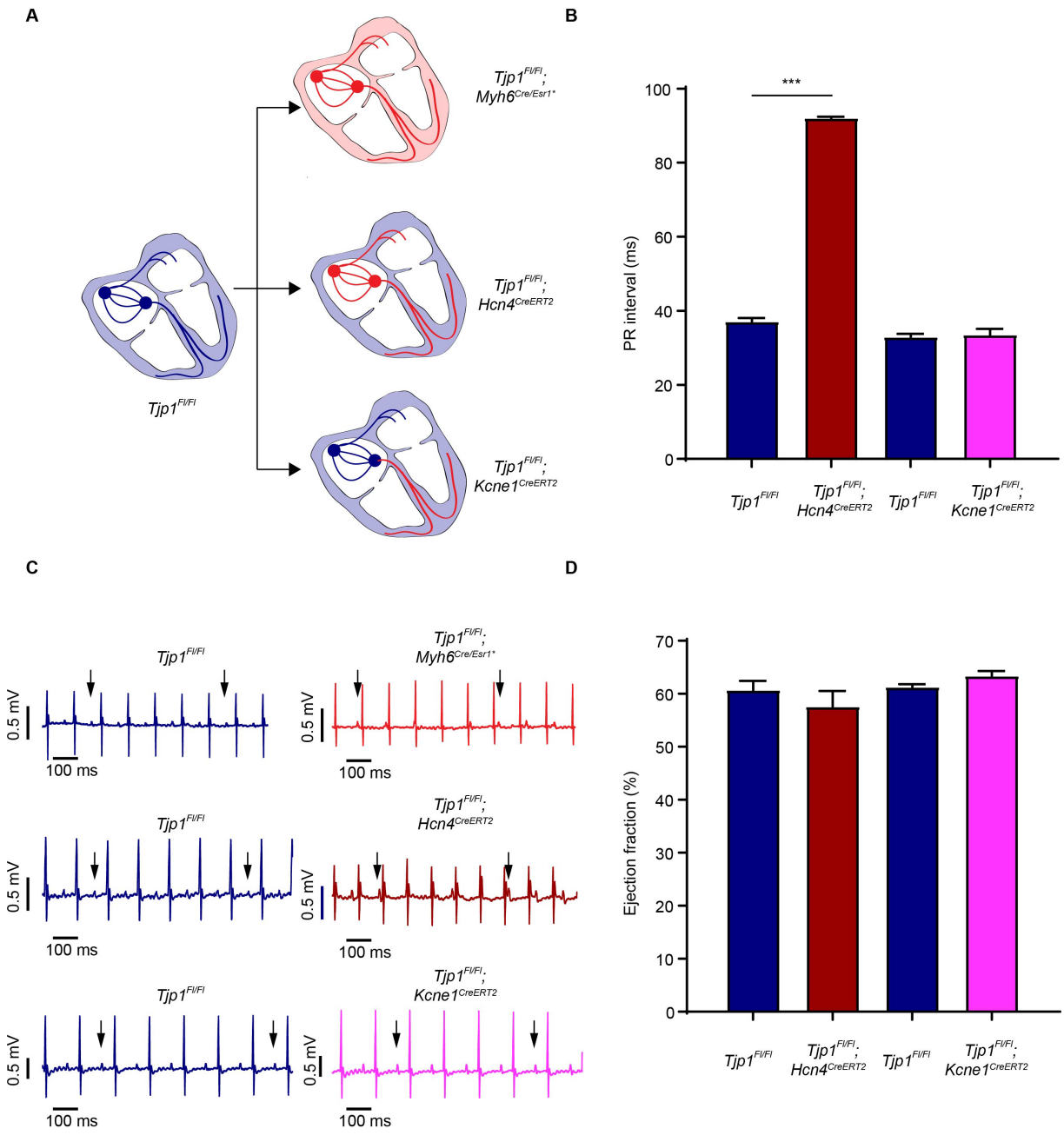

Figure 4-6. PR prolongation is due to ZO-1 loss proximal to the bundle of His.

A. Schematics of locations of ZO-1 deletion in *Tjp1*$^{fl/fl}$*; Myh6*$^{Cre/Esr1*}$, *Tjp1*$^{fl/fl}$*; Hcn4*^{CreERt2}, and *Tjp1*$^{fl/fl}$*; Kcne1*^{CreERt2} mouse lines. B. PR intervals of *Tjp1*$^{fl/fl}$*; Hcn4*^{CreERt2}, and *Tjp1*$^{fl/fl}$*; Kcne1*^{CreERt2} mice. C. Representative surface ECG recordings in *Tjp1*$^{fl/fl}$*; Myh6*$^{Cre/Esr1*}$, *Tjp1*$^{fl/fl}$*; Hcn4*^{CreERt2}, and *Tjp1*$^{fl/fl}$*; Kcne1*^{CreERt2} mice. D. Ejection fraction in *Tjp1*$^{fl/fl}$*; Hcn4*^{CreERt2}, and *Tjp1*$^{fl/fl}$*; Kcne1*^{CreERt2} mice. All studies were performed 10 d post-tamoxifen injection. (***P<0.001)

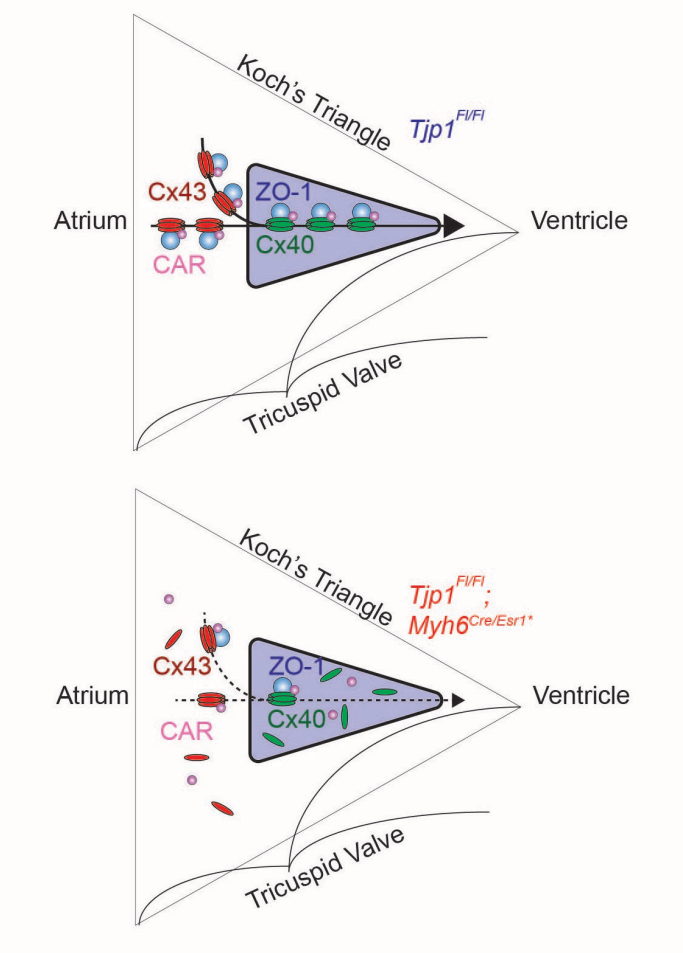

Figure 4-7. ZO-1 maintains AV nodal Cx40-ZO-1-CAR complex to facilitate atrial to ventricular conduction.

Electrical conduction from the atrium to ventricle passes through the AV node (purple triangle). A. Cx40-ZO-1-CAR protein complex exist at the cell-cell junctions within the AV node to maintain normal AV nodal conduction. B. When ZO-1 expression is lost in AV nodal cells, Cx40 and CAR cannot concentrate at cell-cell junctions, decreasing cell-cell conductance, leading to impeded AV nodal conduction (AV node purple, ZO-1 blue, Cx40 green, Cx43 red, CAR magenta).

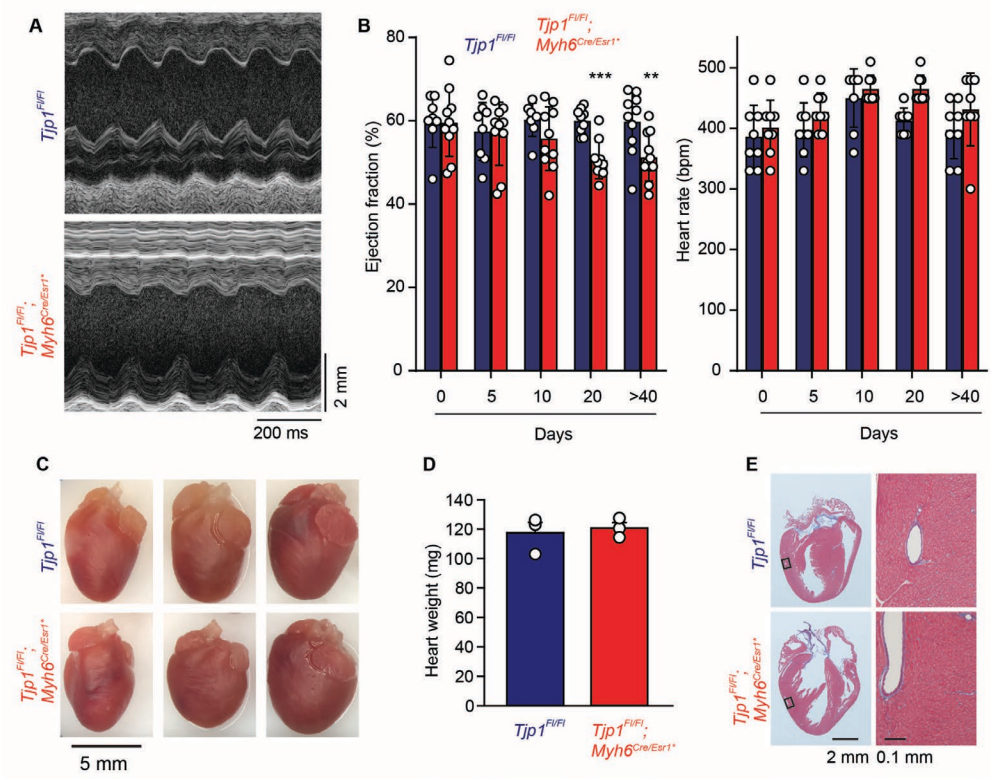

Supplemental Figure 4-1.1. *Tjp1*$^{fl/fl}$*; Myh6*$^{Cre/Esr1*}$ mice have modestly decreased cardiac function without evidence of gross or histologic changes.

A. Representative M-mode echocardiographs 10 d post tamoxifen injection. B. Time course of ejection fraction and heart rate in *Tjp1*$^{fl/fl}$ and *Tjp1*$^{fl/fl}$*; Myh6*$^{Cre/Esr1*}$ mice following tamoxifen injection (n=8-10 animals per genotype). C. Hearts from of a cohort of 3 *Tjp1*$^{fl/fl}$ (top) and *3 Tjp1*$^{fl/fl}$*; Myh6*$^{Cre/Esr1*}$ (bottom) 42 d after tamoxifen injection. D. Heart weights of 3 *Tjp1*$^{fl/fl}$ and *3 Tjp1*$^{fl/fl}$*; Myh6*$^{Cre/Esr1*}$ 42 d after tamoxifen injection. E. Low and high power images of trichrome stained *Tjp1*$^{fl/fl}$ and *Tjp1*$^{fl/fl}$*; Myh6*$^{Cre/Esr1*}$ hearts. Left panels: low magnification; Right panels: high magnification of boxed regions in left panels. (Red: *Tjp1*$^{fl/fl}$*; Myh6*$^{Cre/Esr1*}$, Blue: *Tjp1*$^{fl/fl}$, *P<0.05)

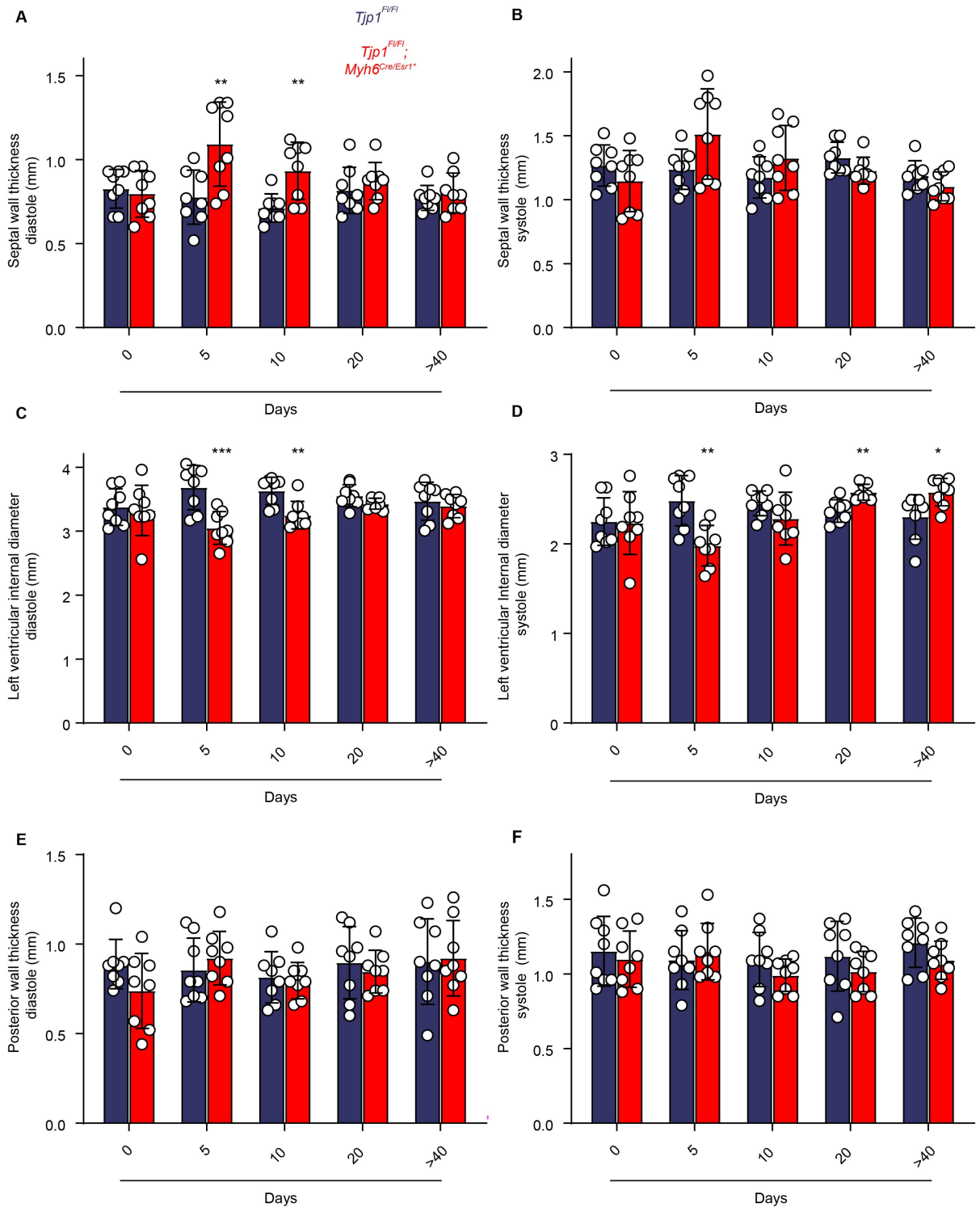

Supplemental Figure 4-1.2. Cardiac dimension changes in *Tjp1*$^{fl/fl}$*; Myh6*$^{Cre/Esr1*}$ mice following tamoxifen induced knockout.

Supplemental Figure 4-1.2, continued.

Time course of echocardiogram parameters in *Tjp1*$^{fl/fl}$ and *Tjp1*$^{fl/fl}$*; Myh6*$^{Cre/Esr1*}$ mice following tamoxifen injection (n=8 animals per genotype) A. Septal wall thickness during diastole. B. Septal wall thickness during systole. C. Left ventricular internal diameter during diastole. D. Left ventricular internal diameter during systole E. Posterior wall thickness during diastole. F. Posterior wall thickness during systole.

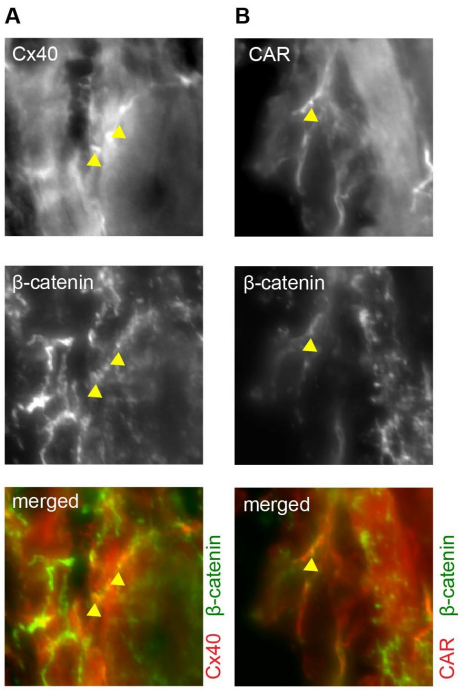

Supplemental Figure 4-4.1. Connexin 40 and CAR colocalize with β-catenin in the AV node.

Representative immunofluorescence staining of *Tjp1*$^{fl/fl}$ AV nodes. A. Cx40 B. CAR. Arrows indicate regions of co-localization. All studies were performed 10 d post-tamoxifen injection.

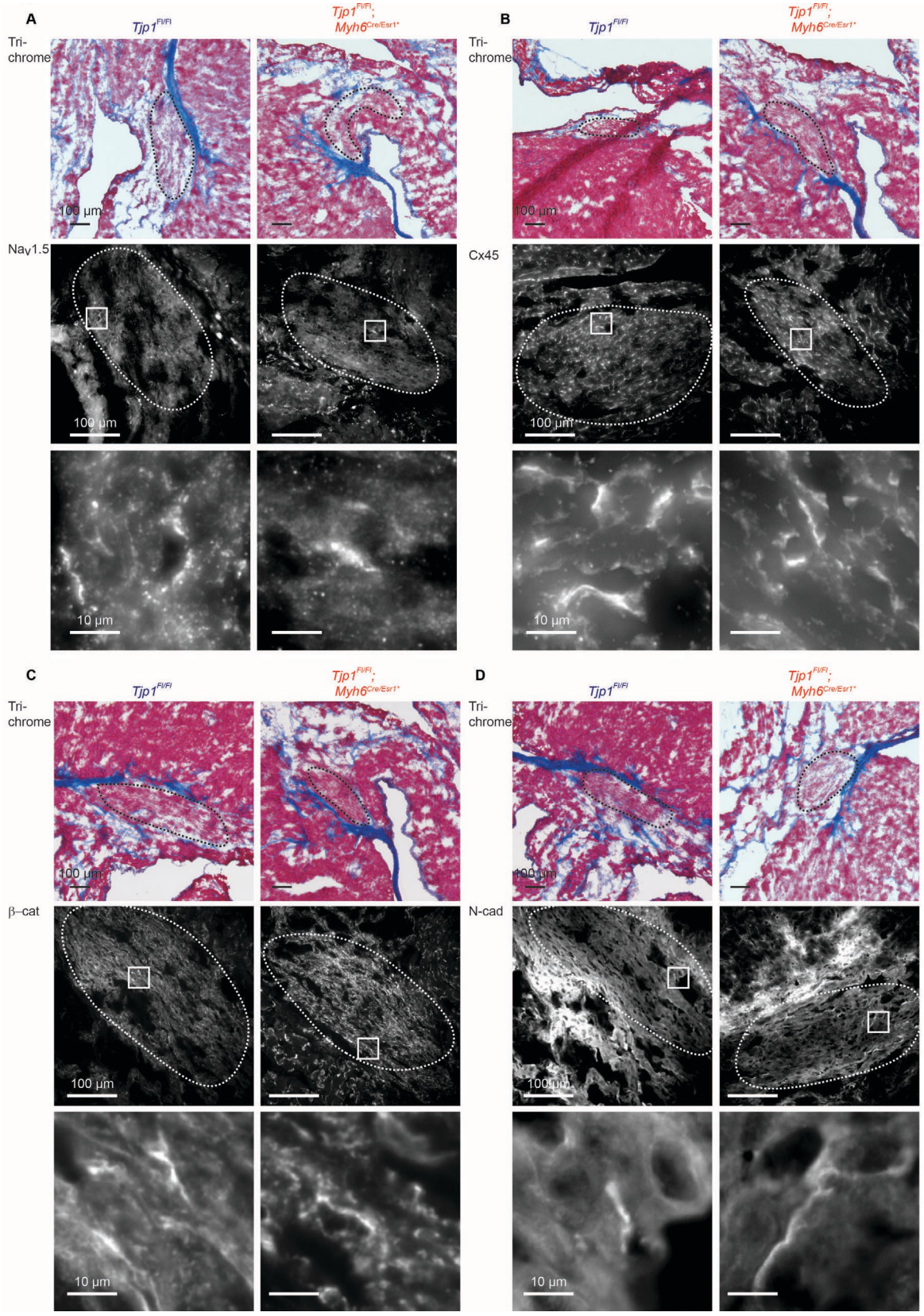

Supplemental Figure 4-4.2. Tjp1 deletion does not alter nodal expression of NaV1.5, Cx45, β-catenin or N-cadherin.

Supplemental Figure 4-4.2, continued.

Representative trichrome and immunofluorescence staining of AV nodes. A. $Na_V1.5$, B. Cx45, C. β-catenin, D. N-cadherin. All studies were performed 10 d post-tamoxifen injection. For each stain, trichrome was used to visualize the node (top) and low power (middle) and high power (bottom) images are shown. High power images reflect boxed areas within the circled AV nodal regions.

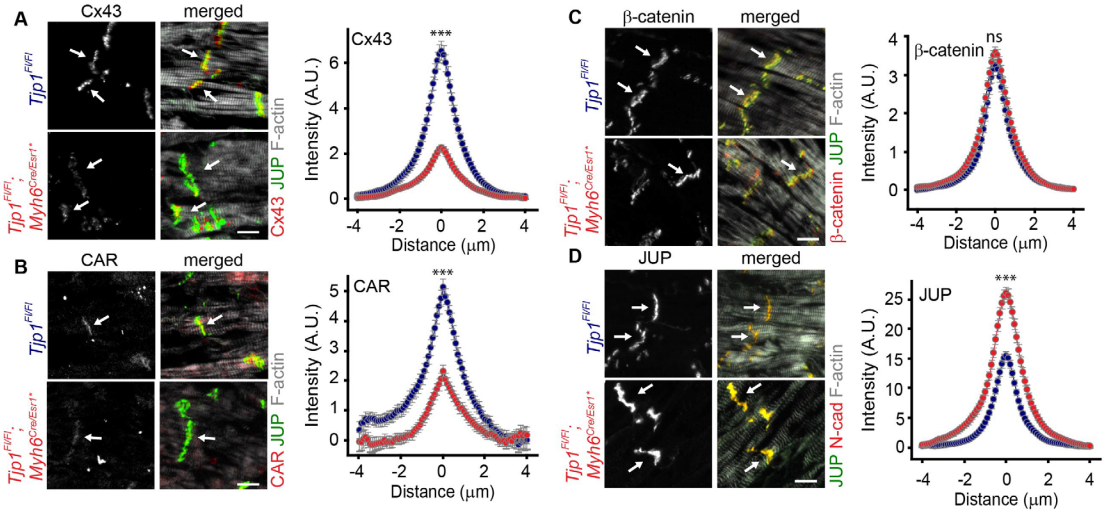

Supplemental Figure 4-4.3. *Tjp1* deletion alters protein localization at the intercalated disc of ventricular cardiomyocytes.

Representative images immunofluorescent staining and quantification of immunofluorescent staining along lines perpendicular to the intercalated disc are shown. A. Cx43 (red), JUP (green), B. CAR (red), JUP (green), C. β-catenin (β-cat; red), JUP (green), D. JUP (green), N-cad (red). Phalloidin stains (F-actin) are shown in grey. (Red: $Tjp1^{fl/fl}$; $Myh6^{Cre/Esr1*}$, Blue: $Tjp1^{fl/fl}$, ***P<0.001, N.S. P>0.05) All studies were performed 10 d post-tamoxifen injection (Scale bars = 10 μm).

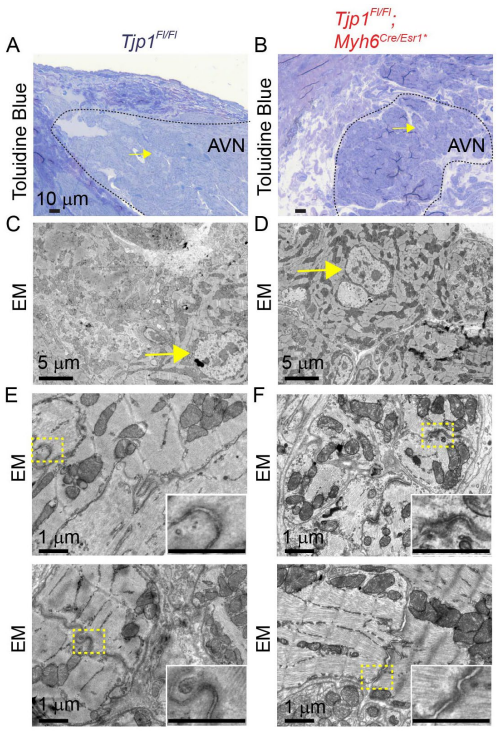

Supplemental Figure 4-4.4. AV node ultrastructure was not significantly altered by *Tjp1* deletion.

A-B. Representative images of Toluidine blue stained sections of AV node containing tissues; bars: 10 µm. Arrows indicate large AV nodal cell nuclei with prominent nucleoli. C-D. Representative TEM images of AV nodes. Arrows indicate large AV nodal cell nuclei with prominent nucleoli. Bars =5 µm E-F. Representative TEM images of AV nodes. Magnified views of boxed intercalated disc containing region are shown in insets. Representative EM images from two mice of each genotype are shown. Bars =1 µm. Samples were collected 10 d post-tamoxifen injection.

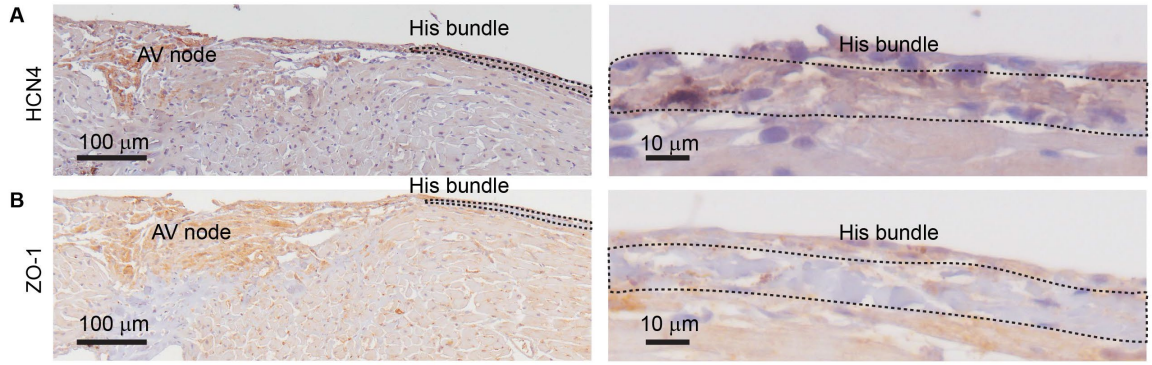

Supplemental Figure 4-7. ZO-1 is abundantly expressed in AV node, but not the His bundle in *Tjp1*$^{fl/fl}$ mice.

A. Immunohistochemical staining of HCN4 in AV node and His bundle in *Tjp1*$^{fl/fl}$ mice. B. Immunohistochemical staining of ZO-1 in AV node and His bundle. (left panels: scale bars = 100 μm, right panels: scale bars = 10 μm) His bundles are circled by dashed lines.

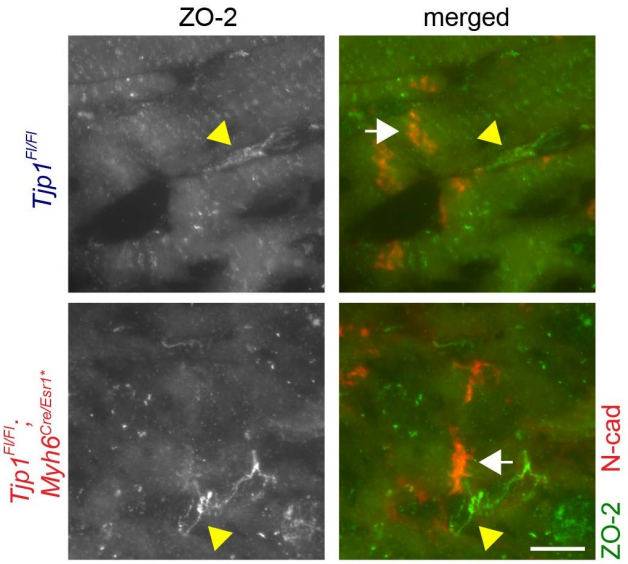

Supplement 4-7. Low ZO-2 expression in ventricular cardiomyocytes.

ZO-2 and N-cadherin staining in *Tjp1*$^{fl/fl}$ and *Tjp1*$^{fl/fl}$*; Myh6*$^{Cre/Esr1*}$ ventricular tissue sections. N-cadherin staining highlights intercalated discs (white arrows), with no colocalization with ZO-2. ZO-2 staining is present in cardiac endothelial cells (yellow arrowheads). Studies were performed 10 d post-tamoxifen injection (Scale bar = 10 μm).

Discussion

Healthy cardiac conduction and function relies on the coordinated electrical activity of distinct populations of cardiomyocytes. Electrical activity initiated at the SA node must propagate through atrial myocardium, the AV node, His-Purkinje system, and into ventricular myocardium. Disruption of cell-cell conduction results in cardiac arrhythmias and cardiomyopathies, a leading cause of morbidity and mortality worldwide[38, 224-226]. Intercalated disc proteins have been recognized as important regulators of cardiac conduction due to their function in maintaining electrical and physical coupling between cells. Here we show inducible loss of the intercalated disc protein ZO-1 in cardiomyocytes of adult mice impedes AV node conduction and modestly affects ejection fraction.

Mice with induced cardiomyocyte specific *Tjp1* deletion *(Tjp1$^{fl/fl}$; Myh6$^{Cre/Esr1*}$* mice with tamoxifen injection) exhibit an AV nodal conduction defect with normal atrial and ventricular conduction (Figs. 2,3). This interpretation is based on electrophysiological and optical mapping studies demonstrating increased PR interval, increased AH intervals, increased AV Wenckebach time, and AV conduction time but unchanged HV interval, P wave, QRS complex duration, and atrial and ventricular activation time in *Tjp1$^{fl/fl}$; Myh6$^{Cre/Esr1*}$* mice (Figs. 2,3). To assess 1) if the AV block is intrinsic to the conduction system or secondary to myocardial changes, and 2) to assess potential region-specific requirements of ZO-1 in the conduction system, we generated two additional inducible tissue-specific knockout models. Similar to induced cardiomyocyte specific *Tjp1* knockout (*Tjp1$^{fl/fl}$; Myh6$^{Cre/Esr1*}$*), tamoxifen-induced overall conduction system *Tjp1* knockout (*Tjp1$^{fl/fl}$; Hcn4^{CreERt2}*) resulted in AV block without decreased ejection fraction (Fig. 6), suggesting AV block is not secondary to myocardial changes. In contrast, tamoxifen-induced *Tjp1* knockout distal to the AV node (*Tjp1$^{fl/fl}$; Kcne1^{CreERt2}*) did not manifest heart block.

Taken together with our observation that ZO-1 is highly expressed in the AV node, but in the fast conducting AV-bundle, such high expression was not apparent (Supplement 7), these results support that ZO-1 loss in the conduction system above the bundle of His is responsible for PR prolongation and ZO-1 expression is critical to normal AV nodal conduction.

Given the observed AV node dysfunction following ZO-1 loss, we hypothesized that ZO-1 is important to the organization of proteins at the intercalated disc that facilitate cell-cell conduction. Immunofluorescence microscopy and western blot studies showed decreased expression of Cx40[223, 227] and to a lesser extent, CAR[205, 206], in the AV node in *Tjp1*$^{fl/fl;}$ *Myh6*$^{Cre/Esr1}$ mice. This is in line with previous biochemical data demonstrating that connexins, CAR, and ZO-1 can reside within the same protein complex. Connexins contain a C-terminal PDZ binding sequence that directly binds to the PDZ domains of ZO-1[73, 80, 228-230]. CAR contains a PDZ binding C-terminal motif and can precipitate with ZO-1[77, 205, 231, 232]. Furthermore, genetic deletion of Cx40[223, 227] and CAR[205, 206] both slow AV nodal conduction. Together these data suggest ZO-1 plays a key role in maintaining the connexin-ZO-1-CAR complex at the intercalated disc.

It is notable that although PR interval was altered in cardiac and conduction system specific *Tjp1* deleted mice, there was no change in RR interval or heart rate. This observation of AV block with normal heart rate is in contrast to some models in which PR interval prolongation is associated with increased RR interval[233, 234]. Interestingly, PR prolongation with normal heart rate is also observed in *Cxadr* (CAR)[205, 206] and *Gja5* (Cx40)[223] knockout mice. Our finding that CAR localization at the intercalated disc is affected by *Tjp1* knockout along with biochemical interactions between ZO-1, CAR, and Cx40 (discussed above) and altered ZO-1 distribution in *Cxadr* knockout mice provide increasing evidence for functional interactions between these

proteins. Together, these observations coalesce into a model in which ZO-1, CAR, and Cx40 physically associate to co-regulate AV nodal conduction.

Although atrial and ventricular conduction speed were normal in *Tjp1*$^{fl/fl}$*; Myh6*$^{Cre/Esr1}$ mice, changes in ventricular intercalated disc organization and protein staining were still observed. By immunofluorescence microscopy, there was decreased Cx43 and CAR localization at the ventricular intercalated disc. These observations are consistent with previous findings that partial connexin loss is not sufficient to induce altered myocardial conduction[235, 236, 237], and *Cxadr* (CAR) deletion in cardiomyocytes also does not significantly affect atrial and ventricular conduction, despite decreased connexin and ZO-1 localization at intercalated discs of ventricular cardiomyocytes[205, 206]. Our finding that *Tjp1* knockout mice have prolonged AV nodal conduction times but normal ventricular conduction times suggests that AV nodal and ventricular cardiomyocyte conduction have different molecular requirements. Our observations support that AV nodal conduction may be particularly vulnerable to defects in the connexin-ZO-1-CAR complex (Fig. 7).

We demonstrate that ZO-1 loss in myocardial tissue is associated with modestly decreased ejection fraction. In contrast, neither of the conduction specific knockout models demonstrated this phenotype (Fig. 6D). This suggests that loss of ZO-1 can independently affect conduction and ejection fraction, and decreased functional output is due directly to loss of ZO-1 in the myocardium and not secondary to conduction defects. We did not observe a progressive loss of ejection fraction and sudden death of the *Tjp1*$^{fl/fl}$*; Myh6*$^{Cre/Esr1*}$ mice, which could be explained by the presence of compensatory mechanisms that may be important for preserving myocardial function following loss of ZO-1. For example, ZO-2, a closely related protein to ZO-1, may play a role in such compensatory mechanisms. ZO-1 and ZO-2 both work to regulate

epithelial function, including tight junction function and apical membrane organization[238-240]. Although we could readily detect ZO-2 expression in cardiac endothelial cells, we failed to detect ZO-2 at the intercalated disc 10 d following ZO-1 knockout (Supplement 8), long term studies are needed to understand whether ZO-2 along with other protein expression and localization are altered and limit ZO-1 induced myocardial changes.

Recently, *TJP1* variations have been associated with arrhythmogenic cardiomyopathy in patients[241], but AV nodal dysfunction was not observed in the 4 probands studied by Bartoli *et al*[241]. We do not currently know why such a difference exists, and further investigation will be requiredto determine the potential role of ZO-1 on AV nodal function in humans with arrhythmogenic cardiomyopathy. Another difference between our ZO-1 knockout mouse model and the patients of Bartoli et al[241] is the absence of fibrofatty replacement of myocardial tissue up to 12 weeks after *Tjp1* deletion in the mice. This difference may be due to the adult onset, cardiomyocyte specific nature of the ZO-1 loss in our mouse model compared to patients carrying pathogenic *TJP1* variants, who have altered ZO-1 function in all cell types, throughout their life. Since ZO-1 may influence many aspects of cardiac (e.g. coronary vasculature) as well as other organ system development and physiological function, the clinical symptoms may be influenced by all of these cell types and organs. Long term studies will be required to further evaluate whether histological features of arrhythmogenic cardiomyopathy can manifest in mice following knockout of *Tjp1*.

ZO-1 has been implicated in other forms of cardiomyopathy without *Tjp1* mutations. For example, expression of a pathogenic mutant of transmembrane protein 43 (TMEM43) associated with arrhythmogenic cardiomyopathy causes loss of ZO-1 at the intercalated disc-like cell-cell junctions, and decreases cell-cell conduction velocity in HL-1 cells[54]. Furthermore, our analysis

of published Gene Expression Omnibus datasets suggest *TJP1* expression is altered in hearts of cardiomyopathy patients (GDS2205 and GDS1362), and isoproterenol treated mice (GDS3684). Together, these findings suggest ZO-1 expression or localization change can influence cardiomyopathy pathogenesis.

In conclusion, we demonstrate ZO-1 is necessary for maintaining gap junction protein expression and localization, and loss of ZO-1 results in AV node dysfunction, and when deleted from myocytes throughout the heart, results in modest decrease in cardiac function. Understanding how ZO-1 function is altered in patients with cardiomyopathy and other heart diseases will be important and may provide novel therapeutic approaches.

Chapter V: Discussion

Summary and implications of cellular mechanism studies in Tbx5 knockout mice

In the past decade, GWAS and other genomics studies have identified transcriptional networks that regulate cardiac rhythm. In addition to identification of the network members, mechanistic studies are required to determine how transcription factor changes result in atrial fibrillation. Our data along with others have linked transcription factor regulation of calcium handling to cardiac rhythm control. We find that *Tbx5* knockout mice develop spontaneous AF and isolated atrial cardiomyocytes from these mice display prolonged action potentials and increased propensity for EADs and DADs. Further, we find this triggered activity is caused by abnormal calcium handling, specifically decreased SERCA activity concurrent with increased NCX and L-type calcium activity. Rescue of SERCA activity through phospholamban knockout not only rescued action potential duration and decreased propensity for triggered activity, but also prevented spontaneous AF in *Tbx5* knockout mice.

Our findings help to illustrate that AF can be the manifestation of a number of different underlying cellular defects. Here, we discuss several ways in which our findings add to breadth of cellular changes that have been observed in AF. First, commonly atrial fibrillation is thought to be associated with shortened action potentials as was found in many early models of AF[242], but we find that *Tbx5* knockout mice actually exhibit prolonged action potentials. Our findings are in line with previous examples of prolonged action potentials in both human and animal atrial fibrillation[243-249]. Overall, these data support the paradigm that AF is caused by an arrhythmogenic substrate and ectopic trigger leading to reentrant arrhythmia. In *Tbx5* knockout mice, the arrhythmogenic trigger is provided by EADs and DADs while decreased conduction speed[47] and increased dispersion of refractoriness from the AP prolongation may both be

arrhythmogenic substrates. Second, we observed DADs in *Tbx5* knockout atrial myocytes despite a decreased SR load. Classically, DADs are thought to be associated with SR calcium overload, which then generates a calcium wave that triggers increased NCX activity, leading to a DAD[250]. In this case, DADs are likely still triggered by increased NCX activity, but driven by increased driving force during diastole as less calcium can be returned to the SR via SERCA and thus needs to extruded via NCX to maintain homeostasis

Third, we observe unaltered amplitude of calcium transients in *Tbx5* knockout atrial myocytes despite a decreased SR load and SERCA activity. This is likely due to the prolonged action potential, which increases the time during which the cell is depolarized and thus calcium is released from the SR, resulting in the same overall same total amplitude of the calcium transient. Further, the increased L-type calcium current in *Tbx5* knockout myocytes may also facilitate increased SR release from RyR2. When *Tbx5* knockout cells were stimulated by a constant duration square pulse, which normalizes the AP duration, calcium transient amplitudes were decreased. Overall, our studies demonstrate the need to examine the specific mechanism underlying individual cases of AF as treatments that target one aspect of atrial fibrillation such as drugs increasing AP duration would not be appropriate in the case of *TBX5* loss-of-function associated AF. Further, it is important to consider the interplay between different calcium handling components as changing one component can result in compensatory changes in other components.

Ryanodine regulation by Tbx5

RNA sequencing and western blot experiments in *Tbx5* knockout atrial myocytes showed significantly decreased RyR2 expression, but a ryanodine binding assay indicated RyR2 function is actually preserved over the physiological range of calcium. This indicates the presence of

compensatory mechanisms that may maintain RyR2 function in this context. We discuss here several potential avenues of exploration to elucidate the regulation of RyR2 in the context of *Tbx5* loss. First, to directly measure SR calcium leak, intracellular calcium can be measured using Fluo-4AM in 0 Na^+/0 Ca^{2+} tyrode solution with the addition of tetracaine to block RyR2 mediated calcium leak compared to total SR calcium content as measured by caffeine induced calcium release. Second, we could examine modulation of RyR2 in the setting of *Tbx5* loss. Ryr2 can be regulated by numerous proteins, but one important form of regulation is phosphorylation and dephosphorylation of RyR2 subunits by kinases PKA PKG, and CamKII, and phosphatases PP1, PP2A, and PDE4D3. CaMKII is of particular interest because its phosphorylation of RyR2 promotes increased open probability and increased calcium release or leak at baseline. CaMKII has a critical role in adjusting intracellular calcium content through the phosphorylation of multiple calcium handling moieties including L-type calcium channel, phospholamban, and RyR2. CaMKII is activated by the binding of a complex consisting of calcium bound to calmodulin, a calcium sensor, which releases the autoinhibitory domain from the catalytic domain, and allowing for kinase activity. Interestingly, CaMKII creates molecular memory through autophosphorylation, which increases the binding affinity of calmodulin to CaMKII and thus prevents dissociation and prolongs kinase activity even when intracellular calcium is decreased. This memory as an acute response is a beneficial compensatory mechanism in cases such as a fight-or-flight response or sudden pressure or volume stresses to the heart. However, in cases such as heart failure, CaMKII upregulation can be maladaptive as it results in decreased contractile force and can be arrhythmogenic[251-254]. PKA is activated by increased cytosolic cAMP levels upon activation of beta-adrenergic receptors. Like CaMKII, PKA can also phosphorylate L-type calcium channels, phospholamban, and RyR2. It has been shown that PKA

phosphorylation of RyR2 S2808 synchronizes RyR2 calcium release with calcium flux through L-type calcium channel, regulates propagation of calcium waves, and sensitizes RyR2 to luminal calcium[255]. It would be valuable to understand the extent of CaMKII and PKA phosphorylation by first assessing using western blot the expression of phosphorylated RyR2 S2808 and S2814 and Cav1.2. We observed previously that Pln S17 was unchanged in *Tbx5* knockout mice, but Pln S16 was significantly increased, suggesting PKA activity may play an important role in compensating for decreased RyR2 expression[256]. Following this, addition of isoproterenol could be used to induce a beta-adrenergic response after which RyR2 mediated SR leak can be evaluated to determine the sensitivity of *Tbx5* knockout atrial myocytes to PKA. This could be compared to measurement of SR leak upon addition of CaMKII inhibitor KN93 to dissect out the effects of the two compensatory pathways[257].

Therapeutic potential for mechanistic findings in Tbx5 knockout mice

Our data along with others strongly suggest that AF is likely a manifestation of multiple different cellular mechanisms that may include disturbances in calcium handling, sodium channels, and potassium channels. As health care moves toward a personalized medicine model of disease treatment, it will hopefully become more feasible to determine the mechanism for the observed AF in each patient via high throughput genomics and proteomics. Concurrent with the advances in diagnostics, it will also be important to develop a broader range of therapeutics specific to individual mechanisms. In the case of *Tbx5* loss associated AF, several avenues of pharmacologic treatments can be considered. Drugs such as Istaroxime, which simultaneously increases SERCA activity while decreasing NCX flux may be beneficial in restoring SR load, decreasing APD, and reducing propensity for EADs and DADs. Additionally, since the APD is prolonged in *Tbx5* deficient myocytes, increasing repolarizing force by increasing potassium

currents with Zacopride could be an alternative method of preventing triggered activity. Increased repolarizing force would shorten the AP and reduce late L-type calcium. In general, new therapeutics that can restore calcium homeostasis could be valuable in treating AF.

Tbx5 regulation in development compared to adulthood

Our studies combined with previous work demonstrating the critical role of *Tbx5* in cardiogenesis[56, 132] illustrate that it is a continued requirement for normal cardiac rhythm and function throughout life. Here we synthesize the known regulatory roles of *Tbx5* in development and adulthood. *Tbx5* is expressed throughout most of the heart in both development and adulthood, with notable exceptions being the AV valves, the left ventricular endocardium, developing right ventricular chamber, and the developing outflow tract[258]. Further, its expression is much higher in the atria compared to the ventricle[133]. During development, Tbx5 is known to play a key role in ventricular septum morphology via its unilateral expression on the left side[259], atrial septum morphology, acting upstream of *Sonic hedgehog* signaling[260], and formation of the ventricular conduction system via its regulation of transcriptional repressor *Id2*[163]. Embryos with heterozygous *Tbx5* deletion had significantly decreased expression of connexin 40 and atrial natriuretic factor, but connexin 43 and L-type calcium channel gene transcripts were unchanged[100]. In the adult *Tbx5* homozygous deletion model, *Cacna1c* transcript levels were unchanged, *Gja5* transcript levels were also significantly decreased. Interestingly, in the adult *Tbx5* knockout model, *Gja1* was significantly decreased but ANF was unchanged, and L-type calcium current was significantly increased. Further, we and others observe significant changes in calcium handling genes *Atp2a2, Ryr2,* and *Pln* in our adult *Tbx5* homozygous and heterozygous knockout mice, which was not previously observed in embryonic loss of *Tbx5* gene dosage[261]. These differences suggest that although the effect of *Tbx5* on its downstream targets

remains unchanged from development to adulthood, some key alterations such as transcriptional regulation of calcium handling are likely critical in the maintenance of cardiac rhythm. Direct studies examining the specific changes in the network of *Tbx5* targets through different developmental stages, adulthood, and through the aging process could provide valuable insight into the changing role of *Tbx5* through life. These studies if performed utilizing previously established models of controlled *Tbx5* gene dosage could be particularly valuable in dissecting how the sensitivity of gene targets to *Tbx5* dosage changes over time[261].

Complexity of Gata4 and Tbx5 interaction

Our findings that *Gata4* haploinsufficiency rescues *Tbx5* haploinsufficiency caused AF provides another example of the complexity of the transcriptional gene network that regulates cardiac rhythm. Previously, it was found that *Tbx5* and *Pitx2*, both of which have been implicated in AF, form an incoherent feed forward loop where *Tbx5* drives expression of *Pitx2*, but *Pitx2* has the opposite effect on downstream targets as *Tbx5*[47]. A *Tbx5* dependent cis-regulatory element was identified in the *Pitx2* AF GWAS signal. Thus, loss of *Pitx2* is able to rescue *Tbx5* loss induced AF. While *Gata4* haploinsufficiency rescued AF symptoms, *Tbx5* and *Gata4* do not appear to directly regulate each other. *Tbx5* haploinsufficient atrial myocytes did not show altered *Gata4* expression and likewise *Gata4* haploinsufficiency did not alter *Tbx5* expression levels. Instead, both *Gata4* and *Tbx5* appear to act on downstream calcium handling moieties, specifically *Atp2a2* and *Ryr2*. Interestingly, *Gata4* haploinsufficiency did not directly increase *Atp2a2* and *Ryr2* transcript levels compared to littermate controls, but both of these genes were significantly increased in *Gata4/Tbx5* double haploinsufficient myocytes compared to *Tbx5* haploinsufficient littermate controls. We also observed that *Gata4* haploinsufficiency did not decrease *Pitx2* transcript levels, thus suggesting against *Pitx2* mediated mechanism of rescue.

However, it is interesting to note that unlike *Tbx5* homozygous knockout animals, *Tbx5* heterozygous knockout animals did not show a decrease in *Pitx2* in our study or previous studies. Thus, it may be valuable to evaluate in the context of homozygous *Gata4* knockout and compound *Tbx5/Gata4* homozygous knockout whether *Pitx2* may play a role. In our luciferase assay assessing *Atp2a2* enhancer activity, we observed activation by *Tbx5* and *Gata4* individually, but no evidence of a synergistic effect, which differs from our functional data that SERCA activity is decreased in *Tbx5* heterozygous myocytes but unchanged in *Gata4* heterozygous myocytes. Several factors could contribute to this discrepancy. First, there could be a thus far unidentified cis-regulatory element that may show different enhancer activity than the one identified in this study. Second, regulation of SERCA function by *Gata4* may be through means other than direct *Atp2a2* transcript activity, such as through phospholamban or microRNAs, both of which could be interesting areas of future study. In contrast to *Atp2a2*, the *Ryr2* enhancer was activated by *Tbx5*, but suppressed in the presence of both *Gata4* and *Tbx5*, suggesting antagonistic regulatory interactions between the two transcription factors. To follow up on this observation, it may be valuable to compare RyR2 function via ryanodine binding assays or RyR2 mediated leak measurements to determine the functional effect of this antagonistic relationship between *Gata4* and *Tbx5*. Further, it may also be valuable to perform RNA-sequencing and ATAC sequencing experiments in *Gata4* heterozygous and homozygous animals to determine the breadth of *Gata4* targets. Follow-up studies on these targets could provide novel insight into the full picture of interaction between *Gata4* and *Tbx5*.

The undetermined role of Nkx2.5

Nkx2.5 haploinsufficiency alone or compounded with *Tbx5* and *Gata4* insufficiency did not result in AF although *Nkx2.5* has been implicated in AF by GWAS and many studies have

demonstrated synergistic activation of cardiac enhancers and promoters by *Tbx5*, *Nkx2.5*, and *Gata4*. Further, these three transcription factors physically associate during development. Thus, it is remarkable that in adulthood, the synergistic effect between these transcription factors does not appear to exist. It would be valuable to understand why and how such a change occurs. Several aspects to consider include if the expression and localization of *Nkx2.5* and its gene product changes over time, if there are additional regulatory elements that may repress *Nkx2.5* binding during adulthood, over what time course does this change in functional interaction with other transcription factors occur, and whether this is conserved across species. We may also consider the use of a homozygous *Nkx2.5* deletion model in the case that the heterozygous deletion is insufficient to produce an observable functional effect or if there are compensatory mechanisms that mask the effect of heterozygous deletion. Since *Nkx2.5* is implicated by GWAS in human AF, it may be important to consider the role of *Nkx2.5* loss in the context of clinical risk factors for AF such as hypertension, heart failure, coronary disease, obesity, and diabetes. Although in this study *Nkx2.5* haploinsufficiency did not cause AF symptoms, more studies are necessary to determine the role of *Nkx2.5* in adult cardiac rhythm regulation.

Transcription factors at the intercalated disc

Transcription factors such as *Tbx5* and *Gata4* have been shown to regulate intercalated disc proteins, particularly connexins. For example, loss of *Tbx5* results in decreased connexin 43, connexin 40, as well as ZO-1. Further, strong *Tbx5* and *Gata4* expression is found at the human intercalated disk as visualized by immunohistochemical staining[262]. This is of interest because it suggests that transcription factors may play a role at the intercalated disc itself instead of just in the nucleus. We consider here some potential avenues of exploration regarding the interaction of intercalated disc proteins with transcription factors. First, it may be valuable to determine the

proportion of intercalated disc compared to nuclear Tbx5 and Gata4 via a fractionation assay. Following this, it would be useful to perform more detailed characterization of transcription factor complexes at the intercalated disc using co-immunoprecipitation assays and super resolution microscopy. Such studies could address questions such as which proteins directly interact with Tbx5 and Gata4 at the intercalated disc, what is the distribution of transcription factors among the components of the intercalated disc (gap junction, adherens junction, or desmosome), and whether transcription factor localization and expression varies across different heart regions (atria, ventricle, conduction tissue). Additionally, studies using FRAP could be used to determine the rate of transcription factor turnover at the intercalated disc. Such studies could reveal a new functional role of Tbx5 and Gata4 at the intercalated disc.

Intercalated disc proteins in cellular signaling

In a similar vein as the observation that transcription factors can be localized at the intercalated disc, recent studies revealed intercalated disc proteins β-catenin and plakophilin-2 can have dual functions as structural elements as well as transcription factors regulating calcium handling or Wnt signaling[263, 264]. Both β-catenin and plakophilin-2 can be found at the intercalated disc as well as in the nucleus, where they can interact with nuclear proteins. Loss of plakophilin-2 results in reduced *Ryr2, Cacna1c*, and calsequestrin-2 suggesting that intercalated disc proteins can regulate cardiac rhythm via both structural and signaling mechanisms. It is interesting to consider if other proteins that can shuttle between the intercalated disc, cytosol, and nucleus may also have roles in cell signaling. For example, ZO-1 interacts with small GTPases, ion channels[37, 265, 266], transcription factors[267, 268], and signaling molecules[269-271] can shuttle between the nucleus and cytoplasm, suggesting it may play a role in intrinsic cell functioning in addition to its role at the ID. Additionally, we observed perinuclear localization of ZO-1 in areas

with fibrofatty replacement in patients with arrhythmogenic cardiomyopathy compared to adjacent regions where ZO-1 was mostly localized at the intercalated disc. Further studies are needed to investigate if there is a role for ZO-1 in cell signaling.

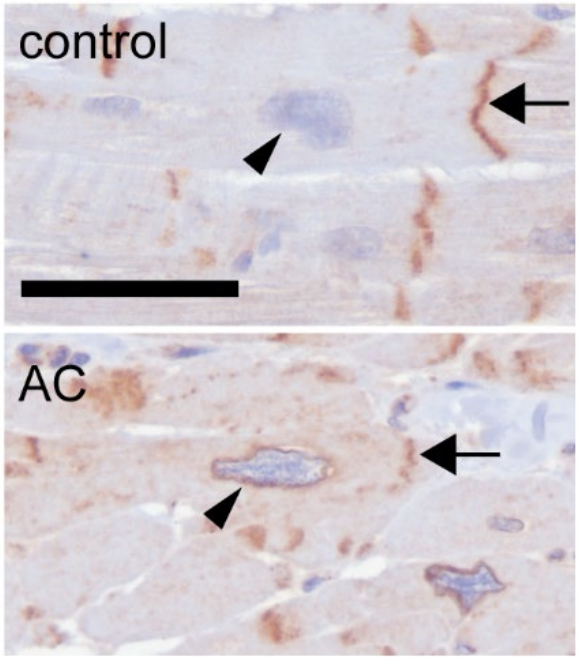

Figure 5-1. Perinuclear ZO-1 distribution

In humans with AC cardiomyocytes exhibit ZO-1 redistribution from the ID (arrow) to perinuclear regions (arrowhead) in regions of fibrofatty change. Scale bar 50 μm.

Relationship between Tbx5 and ZO-1

Tbx5 was previously found to be a regulator of several intercalated disc proteins, particularly connexins and desmoplakin. ZO-1 also appears to be regulated in part by Tbx5, as *Tbx5* knockout animals show a 32% decrease in *Tjp1* transcript levels[47]. Interesting in *Tjp1* knockout animals, *Tbx5* was actually increased. This suggests that *Tjp1* and *Tbx5* may be in the same pathway, perhaps with *Tbx5* acting upstream of *Tjp1* and serving in a compensatory role following loss of *Tjp1*. It is also of note that both *Tjp1* deleted and $Tbx5^{del/+}$ animals show PR prolongation[100, 132], suggesting that a relationship between ZO-1 and TBX5 could be particularly important in the AV node.

AV node arrhythmia resulting from ZO-1 loss

Upon deletion of *Tjp1* from the myocardium, PR prolongation was consistently observed beginning less than one-week post-tamoxifen treatment. The PR prolongation increased in severity over time, and by day 10, dissociation of the P-wave and QRS complex was observed. Further, the AH interval and AV Wenckebach time, a measurement of the refractory time of the AV node, were both significantly increased, all suggestive of AV node dysfunction. Traditional AV node block is also accompanied by slow ventricular rate or skipped beats. In ZO-1 knockout mice however, there were no qualitative differences in the distribution of RR interval in the Poincaré plot, which would be altered if there were skipped beats, or the average RR interval was larger. Interestingly, this exact phenotype was also observed in CAR knockout mice, where PR interval was prolonged but the heart rate was either unchanged or higher than littermate controls[205, 206]. This suggests that while there is a conduction blockage between the SA and AV node, the automaticity of the AV node or its surrounding conduction tissue may be higher, resulting in junctional escape rhythm, which was observed during the dissociation of the P-wave and QRS complex, and the consistent ventricular rhythm that is independent of the atrial rhythm. The mechanism by which loss of ZO-1 or CAR can result in decreased conduction, but increased automaticity is of interest for future studies.

We consider here several approaches to begin evaluating the mechanism by which ZO-1 and proteins within the connexome can regulate conduction and automaticity in the AV node. First, it is important to determine if there are any sinus node conduction defects that may drive PR prolongation. *Gjd3* driven Cre recombinase could be used to delete *Tjp1* specifically in the AV node to confirm that AV node specific ZO-1 loss is indeed responsible for the PR prolongation[272]. Our data showed that ZO-1 loss in the AV node results in loss of Cx40 protein

expression as visualized by immunofluorescence and quantified by western blot. We were not able to detect changes in Cx45 or Cx30.2 by immunofluorescence. However, more in-depth characterization of the localization and characteristics of these connexins could prove valuable. For example, while the distribution of connexins in a gap junction plaque compared to the perinexus has been examined in ventricular cardiomyocytes, such studies have not been done in the AV node. The localization of each connexin type within the context of the AV node ultrastructure could be examined by careful immuno-gold labelling with electron microcopy of AV node tissue in *Tjp1* deleted hearts compared to littermate controls. Using different size immune-gold particles, we could label multiple connexins at once to understand their localization with respect to each other or with respect to ZO-1. Since the organization of the AV node is particularly complex, with one AV node cell making contacts with many cells in different orientations, it is particularly valuable to have a method to examine protein localization and ultrastructure over numerous cells. Serial electron microscopy could be a valuable tool to help elucidate the role of ZO-1 in regulating AV node structure and cell-cell junctions. Additionally, 3D fluorescence microscopy could also be utilized to visualize the distribution of each connexin through the entire AV node in both *Tjp1* deleted animals and their littermate controls.

Given previous work demonstrating that Cx30.2 is a regulator of AV node conduction, and specifically that its loss results in increased conduction speed[64], one hypothesis is that loss of ZO-1 could result in loss of Cx30.2 localization in a manner that results in increased automaticity. Testing this hypothesis would require generation and validation of a Cx30.2 antibody that shows strong signal in the AV node. In the CAR knockout mice, dye coupling experiments revealed increased dye coupling between cells upon loss of CAR, which indicates

increased ability to exchange ions and small molecules between cells. Given our data along with others[205, 206] indicate that ZO-1 and CAR reside in the same complex, it is possible that ZO-1 loss could also result in increased dye coupling in the ventricular slices. Dye coupling experiments could also be conducted in AV node slices to determine if the same remains true. The results of such an experiment could provide insight into a mechanism by which abnormal, increased coupling between cells could facilitate increased automaticity.

Differential effect of ZO-1 loss on AV node compared to ventricular myocardium

In contrast to the pronounced AV node dysfunction, atrial and ventricular activation times and conduction velocity remained unchanged, despite a decrease in Cx43 at ventricular intercalated discs. This difference was also observed in CAR knockout models[205, 206]. We consider here several ideas for why there is phenotypic discrepancy between the AV node and atria/ventricle.

First, previous work has suggested that connexin protein expression must be reduced by 70% to 95% in the ventricle before conduction velocity is decreased[273]. Additionally, studies of heart failure in canines revealed that loss of Cx43 significantly precedes conduction velocity slowing, but relocalization of Cx43 from the intercalated disc to the lateral membrane as well as dephosphorylation correlated closely with decreased conduction velocity[274]. These data suggest that in *Tjp1* deletion alone in the ventricle is likely insufficient to reduce Cx43 protein levels to the threshold required for conduction velocity loss. However, in the AV node the threshold of connexin reduction for conduction slowing may be lower. Further, since AV node conduction is reliant on a combination of Cx40, Cx30.2, and Cx45, with Cx30.2 and Cx45 providing higher intercellular resistance[64, 275-277]. ZO-1 loss may not only affect total connexin expression, but also the ratio of these connexins, which may be a potential secondary means of regulation that could

make the AV node more sensitive to ZO-1 loss. Finally, we observed a significantly increased density of ZO-1 in the AV node of both human and mice hearts compared to surrounding atrial and ventricular tissue, suggesting a higher intrinsic level of ZO-1 is required in the AV node. Follow-up experiments quantifying Cx43, Cx 40, Cx45, and Cx30.3 protein expression, localization, phosphorylation state over time following *Tjp1* deletion in atrial, ventricular, and AV node tissue would be necessary to fully dissect out the location specific role of ZO-1. Additional experiments in which *Tjp1* deletion was coupled with a pharmacological method of connexin dephosphorylation could be a potential strategy of testing the hypothesis that changes in connexin phosphorylation state in addition to protein expression reduction are required for altered ventricular conduction speed.

In addition to differences in connexin requirements, structural differences unique to the AV node may result in conduction differences such that a minor loss of cell-cell communication has a much more detrimental effect than the same loss in ventricular tissue. The AV node is highly complex and contains several different regions, which are both structurally and electrophysiologically distinct. It has been established that there are two functional pathways of conduction through the AV node, the fast pathway and the slow pathway, although the anatomic pathways are less clear[278-280]. Generally, the fast pathway is thought to be located in the cells surrounding or within the compact node, while the slow pathway travels through the inferior nodal extension. During normal conduction, the depolarizing wave travels from the atrium into both the fast and slow pathways, but the fast pathway wave front arrives at the bundle of His first. The slow pathway wave encounters tissue that has already been activated by the fast pathway, so it is blocked from being conducted further into the bundle of His[281]. Anatomically, cells of the fast pathway are longer with a larger diameter compared to those of the slow

pathway. The molecular composition of the AV node is also complex in the distribution of connexin type expressed. Cx43 is highly expressed surrounding the AV node, but becomes significantly less abundant closer to the compact node, and is important for the slow pathway, while Cx40 expression is highest within the compact node is a main component of the fast pathway. Cx45 and Cx30.2 are expressed throughout the AV node region, but at comparatively lower levels than connexin 40[280]. We observed a decrease in both Cx40 AV node expression as well as localization at AV node intercalated discs following deletion of *Tjp1*. This data along with the observed PR prolongation in *Tjp1* deleted mice suggests that ZO-1 may be important in regulating the fast pathway in the AV node. Careful examination of cell morphology, protein localization, and measurement of conduction velocity between the fast and slow pathway would be required to determine the specific effect of ZO-1 on AV node functional and structural pathways. This would be challenging in a mouse model due to the small size of the AV node. Thus, a rabbit model of *Tjp1* deletion may be better suited for these studies. Alternatively, AV node conduction could be modeled computationally incorporating our observed changes in connexin expression to dissect out the role of ZO-1 in regulating conduction of the different regions of the AV node. Overall, a greater understanding of differences in the role of intercalated disc proteins within the AV node compared to surrounding atrial or ventricular myocardium could help shape new clinical outcomes for patients with AV node dysfunction.

ZO-1 complex components

Tight junction composition has been examined extensively in epithelial and endothelial cells with dozens of transmembrane and tight junction associated proteins having been identified over the years. ZO-1 was the first to be identified in 1986, and since then has been found to bind a long list of proteins including claudins, occludin, JAM family of proteins, tricellulin, CAR,

Bves, Neph family of proteins, connexins, the other members of the zonula occludens family, AF6, α-catenin, ARVCF (PDZ domains), α-actinin-4, α-spectrin, d F-actin, ZONAB, tuba, Shroom2, Csk, Gα(12), phosphoinositide[70]. Our data provides evidence that ZO-1 also interacts with CAR, Cx40 and Cx43 in the cardiac gap junctions. However unlike epithelial tight junctions, which require ZO-1 for their formation, cardiac gap junctions were still observed by immunofluorescence and immune-gold electron microscopy staining ten days following *Tjp1* deletion although connexin expression at the intercalated disc was decreased. This along with other studies suggest that the requirement for ZO-1 in gap junction formation may be different from that for tight junction formation. While ZO-1 interaction with critical tight junction protein claudin is required for its polymerization, *in vitro* studies showed blocking the PDZ mediated interaction between ZO-1 and Cx43 led to increased plaque size, suggesting the role of ZO-1/ Cx43 interaction is to regulate the population of connexins available for incorporation into the gap junction plaque[75]. In addition to its direct interaction with Cx43, ZO-1's regulatory role may be through its interactions with multiple other proteins including vinculin, CAR, and N-cadherin. This hypothesis is supported by our data and other studies in Cx43, vinculin, CAR, and N-cadherin knockout mice. Loss of vinculin, CAR, Cx43, and N-cadherin all resulted in decreased expression of ZO-1 and Cx43, accompanied by cardiomyocyte necrosis or increased propensity for arrhythmias. This suggests a complex role of ZO-1 in the regulation of the intercalated disc that relies on more than its direct interaction with one protein. Further studies will be required to dissect out the role of specific protein interactions in the regulation of the intercalated disc. To understand the scope of regulation by ZO-1, an RNA sequencing experiment comparing *Tjp1* deleted cardiomyocytes with littermate controls could be performed. Following this, double knockout of ZO-1 with its interaction partners including vinculin, CAR, N-cadherin, connexins,

as well as targets identified by the RNA sequencing can be assessed to determine if interactions between intercalated disc proteins are synergistic. Further, in vitro experiments assessing the effect direct interaction of ZO-1 with its interaction partners using peptide inhibitors of the binding regions could yield insight into the specific role of ZO-1 binding at the intercalated disc.

Conclusion

In summary, we have investigated the mechanisms of arrhythmogenesis from several angles. First, we defined a novel calcium-dependent mechanism of atrial fibrillation following transcription factor Tbx5 insufficiency. Next, we examined the coregulatory relationship between transcription factors Tbx5 and Gata4 in maintaining atrial rhythm. Finally, we assessed the role of Tbx5 downstream intercalated disc protein, ZO-1, in arrhythmogenesis and find that it is important for AV node function.

References

1. Weng LC, Preis SR, Hulme OL, Larson MG, Choi SH, Wang B, Trinquart L, McManus DD, Staerk L, Lin H, Lunetta KL, Ellinor PT, Benjamin EJ, Lubitz SA. Genetic predisposition, clinical risk factor burden, and lifetime risk of atrial fibrillation. *Circulation*. 2018;137:1027-1038

2. Nishida K, Datino T, Macle L, Nattel S. Atrial fibrillation ablation: Translating basic mechanistic insights to the patient. *J Am Coll Cardiol*. 2014;64:823-831

3. Fatkin D, Santiago CF, Huttner IG, Lubitz SA, Ellinor PT. Genetics of atrial fibrillation: State of the art in 2017. *Heart Lung Circ*. 2017;26:894-901

4. WEIDMANN S. The electrical constants of purkinje fibres. *J Physiol*. 1952;118:348-360

5. Carmeliet E. Conduction in cardiac tissue. Historical reflections. *Physiol Rep*. 2019;7:e13860

6. Vassalle M. Automaticity and automatic rhythms. *Am J Cardiol*. 1971;28:245-252

7. Vassalle M. The relationship among cardiac pacemakers. Overdrive suppression. *Circ Res*. 1977;41:269-277

8. Antzelevitch C, Burashnikov A. Overview of basic mechanisms of cardiac arrhythmia. *Card Electrophysiol Clin*. 2011;3:23-45

9. van Eif VWW, Devalla HD, Boink GJJ, Christoffels VM. Transcriptional regulation of the cardiac conduction system. *Nat Rev Cardiol*. 2018;15:617-630

10. De Ponti R, Marazzato J, Bagliani G, Leonelli FM, Padeletti L. Sick sinus syndrome. *Card Electrophysiol Clin*. 2018;10:183-195

11. Andrade J, Khairy P, Dobrev D, Nattel S. The clinical profile and pathophysiology of atrial fibrillation: Relationships among clinical features, epidemiology, and mechanisms. *Circ Res*. 2014;114:1453-1468

12. Delaney JA, Yin X, Fontes JD, Wallace ER, Skinner A, Wang N, Hammill BG, Benjamin EJ, Curtis LH, Heckbert SR. Hospital and clinical care costs associated with atrial fibrillation for medicare beneficiaries in the cardiovascular health study and the framingham heart study. *SAGE Open Med*. 2018;6:2050312118759444

13. Boriani G, Biffi M, Capucci A, Botto G, Broffoni T, Ongari M, Trisolino G, Rubino I, Sanguinetti M, Branzi A, Magnani B. Conversion of recent-onset atrial fibrillation to sinus rhythm: Effects of different drug protocols. *Pacing Clin Electrophysiol*. 1998;21:2470-2474

14. Xu J, Luc JG, Phan K. Atrial fibrillation: Review of current treatment strategies. *J Thorac Dis*. 2016;8:E886-E900

15. Danias PG, Caulfield TA, Weigner MJ, Silverman DI, Manning WJ. Likelihood of spontaneous conversion of atrial fibrillation to sinus rhythm. *J Am Coll Cardiol*. 1998;31:588-592

16. Copley DJ, Hill KM. Atrial fibrillation: A review of treatments and current guidelines. *AACN Adv Crit Care*. 2016;27:120-128

17. Frommeyer G, Eckardt L. Drug-induced proarrhythmia: Risk factors and electrophysiological mechanisms. *Nat Rev Cardiol*. 2016;13:36-47

18. Cappato R, Calkins H, Chen SA, Davies W, Iesaka Y, Kalman J, Kim YH, Klein G, Natale A, Packer D, Skanes A. Prevalence and causes of fatal outcome in catheter ablation of atrial fibrillation. *J Am Coll Cardiol*. 2009;53:1798-1803

19. Cheng EP, Liu CF, Yeo I, Markowitz SM, Thomas G, Ip JE, Kim LK, Lerman BB, Cheung JW. Risk of mortality following catheter ablation of atrial fibrillation. *J Am Coll Cardiol*. 2019;74:2254-2264

20. Liżewska-Springer A, Dąbrowska-Kugacka A, Lewicka E, Drelich Ł, Królak T, Raczak G. Echocardiographic predictors of atrial fibrillation recurrence after catheter ablation: A literature review. *Cardiol J*. 2018

21. Lubitz SA, Ozcan C, Magnani JW, Kääb S, Benjamin EJ, Ellinor PT. Genetics of atrial fibrillation: Implications for future research directions and personalized medicine. *Circ Arrhythm Electrophysiol*. 2010;3:291-299

22. Iwasaki YK, Nishida K, Kato T, Nattel S. Atrial fibrillation pathophysiology: Implications for management. *Circulation*. 2011;124:2264-2274

23. Tse G. Mechanisms of cardiac arrhythmias. *J Arrhythm*. 2016;32:75-81

24. Roden DM, Balser JR, George AL, Anderson ME. Cardiac ion channels. *Annu Rev Physiol*. 2002;64:431-475

25. Bers DM. Cardiac excitation-contraction coupling. *Nature*. 2002;415:198-205

26. January CT, Riddle JM. Early afterdepolarizations: Mechanism of induction and block. A role for l-type ca2+ current. *Circ Res*. 1989;64:977-990

27. Szabo B, Sweidan R, Rajagopalan CV, Lazzara R. Role of na+:Ca2+ exchange current in cs(+)-induced early afterdepolarizations in purkinje fibers. *J Cardiovasc Electrophysiol*. 1994;5:933-944

28. Patterson E, Lazzara R, Szabo B, Liu H, Tang D, Li YH, Scherlag BJ, Po SS. Sodium-calcium exchange initiated by the ca2+ transient: An arrhythmia trigger within pulmonary veins. *J Am Coll Cardiol*. 2006;47:1196-1206

29. Pogwizd SM, Schlotthauer K, Li L, Yuan W, Bers DM. Arrhythmogenesis and contractile dysfunction in heart failure: Roles of sodium-calcium exchange, inward rectifier potassium current, and residual beta-adrenergic responsiveness. *Circ Res*. 2001;88:1159-1167

30. Gilmour RF, Moïse NS. Triggered activity as a mechanism for inherited ventricular arrhythmias in german shepherd dogs. *J Am Coll Cardiol*. 1996;27:1526-1533

31. Burashnikov A, Antzelevitch C. Reinduction of atrial fibrillation immediately after termination of the arrhythmia is mediated by late phase 3 early afterdepolarization-induced triggered activity. *Circulation*. 2003;107:2355-2360

32. Weiss JN, Garfinkel A, Karagueuzian HS, Chen PS, Qu Z. Early afterdepolarizations and cardiac arrhythmias. *Heart Rhythm*. 2010;7:1891-1899

33. Fozzard HA, Schoenberg M. Strength-duration curves in cardiac purkinje fibres: Effects of liminal length and charge distribution. *J Physiol*. 1972;226:593-618

34. Plotnikov AN, Shlapakova I, Szabolcs MJ, Danilo P, Lorell BH, Potapova IA, Lu Z, Rosen AB, Mathias RT, Brink PR, Robinson RB, Cohen IS, Rosen MR. Xenografted adult human mesenchymal stem cells provide a platform for sustained biological pacemaker function in canine heart. *Circulation*. 2007;116:706-713

35. Xie Y, Sato D, Garfinkel A, Qu Z, Weiss JN. So little source, so much sink: Requirements for afterdepolarizations to propagate in tissue. *Biophys J*. 2010;99:1408-1415

36. Zipes DP. Mechanisms of clinical arrhythmias. *Heart Rhythm*. 2004;1:4C-18C

37. Vermij SH, Abriel H, van Veen TA. Refining the molecular organization of the cardiac intercalated disc. *Cardiovasc Res*. 2017;113:259-275

38. Landstrom AP, Dobrev D, Wehrens XHT. Calcium signaling and cardiac arrhythmias. *Circulation research*. 2017;120:1969-1993

39. Lubitz SA, Yi BA, Ellinor PT. Genetics of atrial fibrillation. *Heart Fail Clin*. 2010;6:239-247

40. Fox CS, Parise H, D'Agostino RB, Lloyd-Jones DM, Vasan RS, Wang TJ, Levy D, Wolf PA, Benjamin EJ. Parental atrial fibrillation as a risk factor for atrial fibrillation in offspring. *JAMA*. 2004;291:2851-2855

41. Ellinor PT, Yoerger DM, Ruskin JN, MacRae CA. Familial aggregation in lone atrial fibrillation. *Hum Genet*. 2005;118:179-184

42. Arnar DO, Thorvaldsson S, Manolio TA, Thorgeirsson G, Kristjansson K, Hakonarson H, Stefansson K. Familial aggregation of atrial fibrillation in iceland. *Eur Heart J*. 2006;27:708-712

43. Darbar D, Roden DM. Genetic mechanisms of atrial fibrillation: Impact on response to treatment. *Nat Rev Cardiol*. 2013;10:317-329

44. Mahida S. Transcription factors and atrial fibrillation. *Cardiovasc Res*. 2014;101:194-202

45. Dai W, Laforest B, Tyan L, Shen KM, Nadadur RD, Alvarado FJ, Mazurek SR, Lazarevic S, Gadek M, Wang Y, Li Y, Valdivia HH, Shen L, Broman MT, Moskowitz IP, Weber CR. A calcium transport mechanism for atrial fibrillation in tbx5-mutant mice. *Elife*. 2019;8

46. Laforest B, Dai W, Tyan L, Lazarevic S, Shen KM, Gadek M, Broman MT, Weber CR, Moskowitz IP. Atrial fibrillation risk loci interact to modulate ca2+-dependent atrial rhythm homeostasis. *J Clin Invest*. 2019;129:4937-4950

47. Nadadur RD, Broman MT, Boukens B, Mazurek SR, Yang X, van den Boogaard M, Bekeny J, Gadek M, Ward T, Zhang M, Qiao Y, Martin JF, Seidman CE, Seidman J, Christoffels V, Efimov IR, McNally EM, Weber CR, Moskowitz IP. Pitx2 modulates a tbx5-dependent gene regulatory network to maintain atrial rhythm. *Science translational medicine*. 2016;8:354ra115

48. Syeda F, Kirchhof P, Fabritz L. Pitx2-dependent gene regulation in atrial fibrillation and rhythm control. *J Physiol*. 2017;595:4019-4026

49. Chen J, Xu S, Li W, Wu L, Wang L, Li Y, Zhou W. Nkx2.5 insufficiency leads to atrial electrical remodeling through wnt signaling in hl-1 cells. *Exp Ther Med*. 2019;18:4631-4636

50. Wang Y, Morishima M, Zheng M, Uchino T, Mannen K, Takahashi A, Nakaya Y, Komuro I, Ono K. Transcription factors csx/nkx2.5 and gata4 distinctly regulate expression of ca2+ channels in neonatal rat heart. *J Mol Cell Cardiol*. 2007;42:1045-1053

51. Luo X, Yang B, Nattel S. Micrornas and atrial fibrillation: Mechanisms and translational potential. *Nat Rev Cardiol*. 2015;12:80-90

52. Friedman RC, Farh KK, Burge CB, Bartel DP. Most mammalian mrnas are conserved targets of micrornas. *Genome Res*. 2009;19:92-105

53. Luo X, Pan Z, Shan H, Xiao J, Sun X, Wang N, Lin H, Xiao L, Maguy A, Qi XY, Li Y, Gao X, Dong D, Zhang Y, Bai Y, Ai J, Sun L, Lu H, Luo XY, Wang Z, Lu Y, Yang B, Nattel S. Microrna-26 governs profibrillatory inward-rectifier potassium current changes in atrial fibrillation. *J Clin Invest*. 2013;123:1939-1951

54. Lu Y, Zhang Y, Wang N, Pan Z, Gao X, Zhang F, Shan H, Luo X, Bai Y, Sun L, Song W, Xu C, Wang Z, Yang B. Microrna-328 contributes to adverse electrical remodeling in atrial fibrillation. *Circulation*. 2010;122:2378-2387

55. van den Berg NWE, Kawasaki M, Berger WR, Neefs J, Meulendijks E, Tijsen AJ, de Groot JR. Micrornas in atrial fibrillation: From expression signatures to functional implications. *Cardiovasc Drugs Ther*. 2017;31:345-365

56. Steimle JD, Moskowitz IP. Tbx5: A key regulator of heart development. *Curr Top Dev Biol*. 2017;122:195-221

57. Tucker NR, Ellinor PT. Emerging directions in the genetics of atrial fibrillation. *Circ Res*. 2014;114:1469-1482

58. Mahida S, Ellinor PT. New advances in the genetic basis of atrial fibrillation. *J Cardiovasc Electrophysiol*. 2012;23:1400-1406

59. Chinchilla A, Daimi H, Lozano-Velasco E, Dominguez JN, Caballero R, Delpón E, Tamargo J, Cinca J, Hove-Madsen L, Aranega AE, Franco D. Pitx2 insufficiency leads to atrial electrical and structural remodeling linked to arrhythmogenesis. *Circ Cardiovasc Genet*. 2011;4:269-279

60. Pérez-Hernández M, Matamoros M, Barana A, Amorós I, Gómez R, Núñez M, Sacristán S, Pinto Á, Fernández-Avilés F, Tamargo J, Delpón E, Caballero R. Pitx2c increases in atrial myocytes from chronic atrial fibrillation patients enhancing iks and decreasing ica,l. *Cardiovasc Res*. 2016;109:431-441

61. Wang J, Klysik E, Sood S, Johnson RL, Wehrens XH, Martin JF. Pitx2 prevents susceptibility to atrial arrhythmias by inhibiting left-sided pacemaker specification. *Proc Natl Acad Sci U S A*. 2010;107:9753-9758

62. Kirchhof P, Kahr PC, Kaese S, Piccini I, Vokshi I, Scheld HH, Rotering H, Fortmueller L, Laakmann S, Verheule S, Schotten U, Fabritz L, Brown NA. Pitx2c is expressed in the adult left atrium, and reducing pitx2c expression promotes atrial fibrillation inducibility and complex changes in gene expression. *Circ Cardiovasc Genet*. 2011;4:123-133

63. Noorman M, van der Heyden MA, van Veen TA, Cox MG, Hauer RN, de Bakker JM, van Rijen HV. Cardiac cell-cell junctions in health and disease: Electrical versus mechanical coupling. *J Mol Cell Cardiol*. 2009;47:23-31

64. Kreuzberg MM, Willecke K, Bukauskas FF. Connexin-mediated cardiac impulse propagation: Connexin 30.2 slows atrioventricular conduction in mouse heart. *Trends Cardiovasc Med*. 2006;16:266-272

65. Lo CW. Role of gap junctions in cardiac conduction and development: Insights from the connexin knockout mice. *Circ Res*. 2000;87:346-348

66. Jansen JA, Noorman M, Musa H, Stein M, de Jong S, van der Nagel R, Hund TJ, Mohler PJ, Vos MA, van Veen TA, de Bakker JM, Delmar M, van Rijen HV. Reduced heterogeneous expression of cx43 results in decreased nav1.5 expression and reduced sodium current that accounts for arrhythmia vulnerability in conditional cx43 knockout mice. *Heart Rhythm*. 2012;9:600-607

67. Agullo-Pascual E, Cerrone M, Delmar M. Arrhythmogenic cardiomyopathy and brugada syndrome: Diseases of the connexome. *FEBS Lett*. 2014;588:1322-1330

68. Rampazzo A, Calore M, van Hengel J, van Roy F. Intercalated discs and arrhythmogenic cardiomyopathy. *Circ Cardiovasc Genet*. 2014;7:930-940

69. Stevens TL, Wallace MJ, Refaey ME, Roberts JD, Koenig SN, Mohler PJ. Arrhythmogenic cardiomyopathy: Molecular insights for improved therapeutic design. *J Cardiovasc Dev Dis*. 2020;7

70. Shen L, Weber CR, Raleigh DR, Yu D, Turner JR. Tight junction pore and leak pathways: A dynamic duo. *Annu Rev Physiol*. 2011;73:283-309

71. Odenwald MA, Choi W, Kuo WT, Singh G, Sailer A, Wang Y, Shen L, Fanning AS, Turner JR. The scaffolding protein zo-1 coordinates actomyosin and epithelial apical specializations. *J Biol Chem*. 2018;293:17317-17335

72. Tornavaca O, Chia M, Dufton N, Almagro LO, Conway DE, Randi AM, Schwartz MA, Matter K, Balda MS. Zo-1 controls endothelial adherens junctions, cell-cell tension, angiogenesis, and barrier formation. *J Cell Biol*. 2015;208:821-838

73. Toyofuku T, Yabuki M, Otsu K, Kuzuya T, Hori M, Tada M. Direct association of the gap junction protein connexin-43 with zo-1 in cardiac myocytes. *J Biol Chem*. 1998;273:12725-12731

74. Giepmans BN, Moolenaar WH. The gap junction protein connexin43 interacts with the second pdz domain of the zona occludens-1 protein. *Curr Biol*. 1998;8:931-934

75. Hunter AW, Barker RJ, Zhu C, Gourdie RG. Zonula occludens-1 alters connexin43 gap junction size and organization by influencing channel accretion. *Mol Biol Cell*. 2005;16:5686-5698

76. Palatinus JA, O'Quinn MP, Barker RJ, Harris BS, Jourdan J, Gourdie RG. Zo-1 determines adherens and gap junction localization at intercalated disks. *Am J Physiol Heart Circ Physiol*. 2011;300:H583-594

77. Cohen CJ, Shieh JT, Pickles RJ, Okegawa T, Hsieh JT, Bergelson JM. The coxsackievirus and adenovirus receptor is a transmembrane component of the tight junction. *Proc Natl Acad Sci U S A*. 2001;98:15191-15196

78. Kausalya PJ, Reichert M, Hunziker W. Connexin45 directly binds to zo-1 and localizes to the tight junction region in epithelial mdck cells. *FEBS Lett*. 2001;505:92-96

79. Flores CE, Li X, Bennett MV, Nagy JI, Pereda AE. Interaction between connexin35 and zonula occludens-1 and its potential role in the regulation of electrical synapses. *Proc Natl Acad Sci U S A*. 2008;105:12545-12550

80. Li X, Olson C, Lu S, Kamasawa N, Yasumura T, Rash JE, Nagy JI. Neuronal connexin36 association with zonula occludens-1 protein (zo-1) in mouse brain and interaction with the first pdz domain of zo-1. *Eur J Neurosci*. 2004;19:2132-2146

81. Nishida K, Nattel S. Atrial fibrillation compendium: Historical context and detailed translational perspective on an important clinical problem. *Circulation research*. 2014;114:1447-1452

82. Khramtsova EA. The role of claudin-2 and its regulation in the development of intestinal inflammation. *Order No. 3638604, The University of Chicago*. 2014

83. Christophersen IE, Ravn LS, Budtz-Joergensen E, Skytthe A, Haunsoe S, Svendsen JH, Christensen K. Familial aggregation of atrial fibrillation: A study in danish twins. *Circulation. Arrhythmia and electrophysiology*. 2009;2:378-383

84. McDermott DA, Hatcher CJ, Basson CT. Atrial fibrillation and other clinical manifestations of altered tbx5 dosage in typical holt-oram syndrome. *Circulation research*. 2008;103:e96

85. Sinner MF, Tucker NR, Lunetta KL, Ozaki K, Smith JG, Trompet S, Bis JC, Lin H, Chung MK, Nielsen JB, Lubitz SA, Krijthe BP, Magnani JW, Ye J, Gollob MH, Tsunoda T, Muller-Nurasyid M, Lichtner P, Peters A, Dolmatova E, Kubo M, Smith JD, Psaty BM, Smith NL, Jukema JW, Chasman DI, Albert CM, Ebana Y, Furukawa T, Macfarlane PW, Harris TB, Darbar D, Dorr M, Holst AG, Svendsen JH, Hofman A, Uitterlinden AG, Gudnason V, Isobe M, Malik R, Dichgans M, Rosand J, Van Wagoner DR, Consortium M, Consortium AF, Benjamin EJ, Milan DJ, Melander O, Heckbert SR, Ford I, Liu Y, Barnard J, Olesen MS, Stricker BH, Tanaka T, Kaab S, Ellinor PT. Integrating genetic, transcriptional, and functional analyses to identify 5 novel genes for atrial fibrillation. *Circulation*. 2014;130:1225-1235

86. Dobrev D. Atrial ca2+ signaling in atrial fibrillation as an antiarrhythmic drug target. *Naunyn Schmiedebergs Arch Pharmacol*. 2010;381:195-206

87. Voigt N, Li N, Wang Q, Wang W, Trafford AW, Abu-Taha I, Sun Q, Wieland T, Ravens U, Nattel S, Wehrens XH, Dobrev D. Enhanced sarcoplasmic reticulum ca2+ leak and increased na+-ca2+ exchanger function underlie delayed afterdepolarizations in patients with chronic atrial fibrillation. *Circulation*. 2012;125:2059-2070

88. Voigt N, Heijman J, Wang Q, Chiang DY, Li N, Karck M, Wehrens XHT, Nattel S, Dobrev D. Cellular and molecular mechanisms of atrial arrhythmogenesis in patients with paroxysmal atrial fibrillation. *Circulation*. 2014;129:145-156

89. Vest JA, Wehrens XH, Reiken SR, Lehnart SE, Dobrev D, Chandra P, Danilo P, Ravens U, Rosen MR, Marks AR. Defective cardiac ryanodine receptor regulation during atrial fibrillation. *Circulation*. 2005;111:2025-2032

90. Shanmugam M, Molina CE, Gao S, Severac-Bastide R, Fischmeister R, Babu GJ. Decreased sarcolipin protein expression and enhanced sarco(endo)plasmic reticulum ca2+ uptake in human atrial fibrillation. *Biochemical and biophysical research communications*. 2011;410:97-101

91. Neef S, Dybkova N, Sossalla S, Ort KR, Fluschnik N, Neumann K, Seipelt R, Schondube FA, Hasenfuss G, Maier LS. Camkii-dependent diastolic sr ca2+ leak and elevated diastolic ca2+ levels in right atrial myocardium of patients with atrial fibrillation. *Circulation research*. 2010;106:1134-1144

92. Macquaide N, Tuan HT, Hotta J, Sempels W, Lenaerts I, Holemans P, Hofkens J, Jafri MS, Willems R, Sipido KR. Ryanodine receptor cluster fragmentation and redistribution in persistent atrial fibrillation enhance calcium release. *Cardiovascular research*. 2015;108:387-398

93. Liang X, Xie H, Zhu PH, Hu J, Zhao Q, Wang CS, Yang C. Ryanodine receptor-mediated ca2+ events in atrial myocytes of patients with atrial fibrillation. *Cardiology*. 2008;111:102-110

94. Lenaerts I, Bito V, Heinzel FR, Driesen RB, Holemans P, D'Hooge J, Heidbuchel H, Sipido KR, Willems R. Ultrastructural and functional remodeling of the coupling between ca2+ influx and sarcoplasmic reticulum ca2+ release in right atrial myocytes from experimental persistent atrial fibrillation. *Circulation research*. 2009;105:876-885

95. Hove-Madsen L, Llach A, Bayes-Genis A, Roura S, Rodriguez Font E, Aris A, Cinca J. Atrial fibrillation is associated with increased spontaneous calcium release from the sarcoplasmic reticulum in human atrial myocytes. *Circulation*. 2004;110:1358-1363

96. Greiser M, Lederer WJ, Schotten U. Alterations of atrial ca(2+) handling as cause and consequence of atrial fibrillation. *Cardiovascular research*. 2011;89:722-733

97. El-Armouche A, Boknik P, Eschenhagen T, Carrier L, Knaut M, Ravens U, Dobrev D. Molecular determinants of altered ca2+ handling in human chronic atrial fibrillation. *Circulation*. 2006;114:670-680

98. Brundel BJ, van Gelder IC, Henning RH, Tuinenburg AE, Deelman LE, Tieleman RG, Grandjean JG, van Gilst WH, Crijns HJ. Gene expression of proteins influencing the calcium homeostasis in patients with persistent and paroxysmal atrial fibrillation. *Cardiovascular research*. 1999;42:443-454

99. Yang XH, Nadadur RD, Hilvering CR, Bianchi V, Werner M, Mazurek SR, Gadek M, Shen KM, Goldman JA, Tyan L, Bekeny J, Hall JM, Lee N, Perez-Cervantes C, Burnicka-Turek O, Poss KD, Weber CR, de Laat W, Ruthenburg AJ, Moskowitz IP.

Transcription-factor-dependent enhancer transcription defines a gene regulatory network for cardiac rhythm. *Elife*. 2017;6

100. Bruneau BG, Nemer G, Schmitt JP, Charron F, Robitaille L, Caron S, Conner DA, Gessler M, Nemer M, Seidman CE, Seidman JG. A murine model of holt-oram syndrome defines roles of the t-box transcription factor tbx5 in cardiogenesis and disease. *Cell*. 2001;106:709-721

101. Ventura A, Kirsch DG, McLaughlin ME, Tuveson DA, Grimm J, Lintault L, Newman J, Reczek EE, Weissleder R, Jacks T. Restoration of p53 function leads to tumour regression in vivo. *Nature*. 2007;445:661-665

102. Luo W, Grupp IL, Harrer J, Ponniah S, Grupp G, Duffy JJ, Doetschman T, Kranias EG. Targeted ablation of the phospholamban gene is associated with markedly enhanced myocardial contractility and loss of beta-agonist stimulation. *Circulation research*. 1994;75:401-409

103. Alvarado FJ, Chen X, Valdivia HH. Ablation of the cardiac ryanodine receptor phospho-site ser2808 does not alter the adrenergic response or the progression to heart failure in mice. Elimination of the genetic background as critical variable. *Journal of molecular and cellular cardiology*. 2017;103:40-47

104. Federico M, Portiansky EL, Sommese L, Alvarado FJ, Blanco PG, Zanuzzi CN, Dedman J, Kaetzel M, Wehrens XHT, Mattiazzi A, Palomeque J. Calcium-calmodulin-dependent protein kinase mediates the intracellular signalling pathways of cardiac apoptosis in mice with impaired glucose tolerance. *The Journal of physiology*. 2017;595:4089-4108

105. Sikkel MB, Francis DP, Howard J, Gordon F, Rowlands C, Peters NS, Lyon AR, Harding SE, MacLeod KT. Hierarchical statistical techniques are necessary to draw reliable conclusions from analysis of isolated cardiomyocyte studies. *Cardiovascular research*. 2017;113:1743-1752

106. Grandi E, Pandit SV, Voigt N, Workman AJ, Dobrev D, Jalife J, Bers DM. Human atrial action potential and ca2+ model: Sinus rhythm and chronic atrial fibrillation. *Circ Res*. 2011;109:1055-1066

107. Heijman J, Voigt N, Nattel S, Dobrev D. Cellular and molecular electrophysiology of atrial fibrillation initiation, maintenance, and progression. *Circulation research*. 2014;114:1483-1499

108. Bers DM, Grandi E. Human atrial fibrillation: Insights from computational electrophysiological models. *Trends in cardiovascular medicine*. 2011;21:145-150

109. Blaustein MP, Lederer WJ. Sodium/calcium exchange: Its physiological implications. *Physiological reviews*. 1999;79:763-854

110. Li L, Louch WE, Niederer SA, Andersson KB, Christensen G, Sejersted OM, Smith NP. Calcium dynamics in the ventricular myocytes of serca2 knockout mice: A modeling study. *Biophysical journal*. 2011;100:322-331

111. Di Pino A, Caruso E, Costanzo L, Guccione P. A novel ryr2 mutation in a 2-year-old baby presenting with atrial fibrillation, atrial flutter, and atrial ectopic tachycardia. *Heart rhythm*. 2014;11:1480-1483

112. King JH, Zhang Y, Lei M, Grace AA, Huang CL, Fraser JA. Atrial arrhythmia, triggering events and conduction abnormalities in isolated murine ryr2-p2328s hearts. *Acta physiologica*. 2013;207:308-323

113. Xu L, Eu JP, Meissner G, Stamler JS. Activation of the cardiac calcium release channel (ryanodine receptor) by poly-s-nitrosylation. *Science*. 1998;279:234-237

114. Fischer TH, Herting J, Mason FE, Hartmann N, Watanabe S, Nikolaev VO, Sprenger JU, Fan P, Yao L, Popov AF, Danner BC, Schondube F, Belardinelli L, Hasenfuss G, Maier LS, Sossalla S. Late ina increases diastolic sr-ca2+-leak in atrial myocardium by activating pka and camkii. *Cardiovascular research*. 2015;107:184-196

115. Bhupathy P, Babu GJ, Periasamy M. Sarcolipin and phospholamban as regulators of cardiac sarcoplasmic reticulum ca2+ atpase. *Journal of molecular and cellular cardiology*. 2007;42:903-911

116. Zaman JA, Harling L, Ashrafian H, Darzi A, Gooderham N, Athanasiou T, Peters NS. Post-operative atrial fibrillation is associated with a pre-existing structural and electrical substrate in human right atrial myocardium. *International journal of cardiology*. 2016;220:580-588

117. Bourfiss M, Te Riele AS, Mast TP, Cramer MJ, JF VDH, TA VANV, Loh P, Dooijes D, Hauer RN, Velthuis BK. Influence of genotype on structural atrial abnormalities and atrial fibrillation or flutter in arrhythmogenic right ventricular dysplasia/cardiomyopathy. *Journal of cardiovascular electrophysiology*. 2016;27:1420-1428

118. Dai J, Zhang H, Chen Y, Chang Y, Yuan Q, Ji G, Zhai K. Characterization of ca+ handling proteins and contractile proteins in patients with lone atrial fibrillation. *International journal of cardiology*. 2016;202:749-751

119. Lugenbiel P, Wenz F, Govorov K, Schweizer PA, Katus HA, Thomas D. Atrial fibrillation complicated by heart failure induces distinct remodeling of calcium cycling proteins. *PloS one*. 2015;10:e0116395

120. Lima-Leopoldo AP, Leopoldo AS, da Silva DC, do Nascimento AF, de Campos DH, Luvizotto RA, de Deus AF, Freire PP, Medeiros A, Okoshi K, Cicogna AC. Long-term obesity promotes alterations in diastolic function induced by reduction of phospholamban phosphorylation at serine-16 without affecting calcium handling. *Journal of applied physiology*. 2014;117:669-678

121. Lima-Leopoldo AP, Sugizaki MM, Leopoldo AS, Carvalho RF, Nogueira CR, Nascimento AF, Martinez PF, Luvizotto RA, Padovani CR, Cicogna AC. Obesity induces upregulation of genes involved in myocardial ca2+ handling. *Brazilian journal of medical and biological research = Revista brasileira de pesquisas medicas e biologicas*. 2008;41:615-620

122. Jost N, Nagy N, Corici C, Kohajda Z, Horvath A, Acsai K, Biliczki P, Levijoki J, Pollesello P, Koskelainen T, Otsomaa L, Toth A, Papp JG, Varro A, Virag L. Orm-10103, a novel specific inhibitor of the na+/ca2+ exchanger, decreases early and delayed afterdepolarizations in the canine heart. *British journal of pharmacology*. 2013;170:768-778

123. Nagy N, Kormos A, Kohajda Z, Szebeni A, Szepesi J, Pollesello P, Levijoki J, Acsai K, Virag L, Nanasi PP, Papp JG, Varro A, Toth A. Selective na(+) /ca(2+) exchanger inhibition prevents ca(2+) overload-induced triggered arrhythmias. *British journal of pharmacology*. 2014;171:5665-5681

124. Ferrandi M, Barassi P, Tadini-Buoninsegni F, Bartolommei G, Molinari I, Tripodi MG, Reina C, Moncelli MR, Bianchi G, Ferrari P. Istaroxime stimulates serca2a and accelerates calcium cycling in heart failure by relieving phospholamban inhibition. *British journal of pharmacology*. 2013;169:1849-1861

125. Parikh A, Mantravadi R, Kozhevnikov D, Roche MA, Ye Y, Owen LJ, Puglisi JL, Abramson JJ, Salama G. Ranolazine stabilizes cardiac ryanodine receptors: A novel mechanism for the suppression of early afterdepolarization and torsades de pointes in long qt type 2. *Heart rhythm*. 2012;9:953-960

126. Kormos A, Nagy N, Acsai K, Vaczi K, Agoston S, Pollesello P, Levijoki J, Szentandrassy N, Papp JG, Varro A, Toth A. Efficacy of selective ncx inhibition by orm-10103 during simulated ischemia/reperfusion. *European journal of pharmacology*. 2014;740:539-551

127. Bai T, Hu X, Zheng Y, Wang S, Kong J, Cai L. Resveratrol protects against lipopolysaccharide-induced cardiac dysfunction by enhancing serca2a activity through promoting the phospholamban oligomerization. *American journal of physiology. Heart and circulatory physiology*. 2016;311:H1051-H1062

128. Chong E, Chang SL, Hsiao YW, Singhal R, Liu SH, Leha T, Lin WY, Hsu CP, Chen YC, Chen YJ, Wu TJ, Higa S, Chen SA. Resveratrol, a red wine antioxidant, reduces atrial fibrillation susceptibility in the failing heart by pi3k/akt/enos signaling pathway activation. *Heart rhythm*. 2015;12:1046-1056

129. Nielsen JB, Thorolfsdottir RB, Fritsche LG, Zhou W, Skov MW, Graham SE, Herron TJ, McCarthy S, Schmidt EM, Sveinbjornsson G, Surakka I, Mathis MR, Yamazaki M, Crawford RD, Gabrielsen ME, Skogholt AH, Holmen OL, Lin M, Wolford BN, Dey R, Dalen H, Sulem P, Chung JH, Backman JD, Arnar DO, Thorsteinsdottir U, Baras A, Odushlaine C, Holst AG, Wen X, Hornsby W, Dewey FE, Boehnke M, Kheterpal S, Lee

S, Kang HM, Holm H, Kitzman J, Shavit JA, Jalife J, Brummett CM, Teslovich TM, Carey DJ, Gudbjartsson DF, Stefansson K, Abecasis GR, Hveem K, Willer C. 2018

130. Dobrev D, Nattel S. New insights into the molecular basis of atrial fibrillation: Mechanistic and therapeutic implications. *Cardiovasc Res*. 2011;89:689-691

131. Mauritz C, Schwanke K, Reppel M, Neef S, Katsirntaki K, Maier LS, Nguemo F, Menke S, Haustein M, Hescheler J, Hasenfuss G, Martin U. Generation of functional murine cardiac myocytes from induced pluripotent stem cells. *Circulation*. 2008;118:507-517

132. Moskowitz IP, Pizard A, Patel VV, Bruneau BG, Kim JB, Kupershmidt S, Roden D, Berul CI, Seidman CE, Seidman JG. The t-box transcription factor tbx5 is required for the patterning and maturation of the murine cardiac conduction system. *Development*. 2004;131:4107-4116

133. Bruneau BG, Logan M, Davis N, Levi T, Tabin CJ, Seidman JG, Seidman CE. Chamber-specific cardiac expression of tbx5 and heart defects in holt-oram syndrome. *Dev Biol*. 1999;211:100-108

134. Pfeufer A, van Noord C, Marciante KD, Arking DE, Larson MG, Smith AV, Tarasov KV, Muller M, Sotoodehnia N, Sinner MF, Verwoert GC, Li M, Kao WH, Kottgen A, Coresh J, Bis JC, Psaty BM, Rice K, Rotter JI, Rivadeneira F, Hofman A, Kors JA, Stricker BH, Uitterlinden AG, van Duijn CM, Beckmann BM, Sauter W, Gieger C, Lubitz SA, Newton-Cheh C, Wang TJ, Magnani JW, Schnabel RB, Chung MK, Barnard J, Smith JD, Van Wagoner DR, Vasan RS, Aspelund T, Eiriksdottir G, Harris TB, Launer LJ, Najjar SS, Lakatta E, Schlessinger D, Uda M, Abecasis GR, Muller-Myhsok B, Ehret GB, Boerwinkle E, Chakravarti A, Soliman EZ, Lunetta KL, Perz S, Wichmann HE, Meitinger T, Levy D, Gudnason V, Ellinor PT, Sanna S, Kaab S, Witteman JC, Alonso A, Benjamin EJ, Heckbert SR. Genome-wide association study of pr interval. *Nat Genet*. 2010;42:153-159

135. Holm H, Gudbjartsson DF, Arnar DO, Thorleifsson G, Thorgeirsson G, Stefansdottir H, Gudjonsson SA, Jonasdottir A, Mathiesen EB, Njolstad I, Nyrnes A, Wilsgaard T, Hald EM, Hveem K, Stoltenberg C, Lochen ML, Kong A, Thorsteinsdottir U, Stefansson K. Several common variants modulate heart rate, pr interval and qrs duration. *Nat Genet*. 2010;42:117-122

136. Tan N, Chung MK, Smith JD, Hsu J, Serre D, Newton DW, Castel L, Soltesz E, Pettersson G, Gillinov AM, Van Wagoner DR, Barnard J. Weighted gene coexpression network analysis of human left atrial tissue identifies gene modules associated with atrial fibrillation. *Circ Cardiovasc Genet*. 2013;6:362-371

137. Zang X, Zhang S, Xia Y, Li S, Fu F, Li X, Wang F, Zhang R, Tian X, Gao L, Zhang J, Yang Y, Tu X, Wang Q. Snp rs3825214 in tbx5 is associated with lone atrial fibrillation in chinese han population. *PLoS One*. 2013;8:e64966

138. Oka T, Maillet M, Watt AJ, Schwartz RJ, Aronow BJ, Duncan SA, Molkentin JD. Cardiac-specific deletion of gata4 reveals its requirement for hypertrophy, compensation, and myocyte viability. *Circulation research*. 2006;98:837-845

139. Bisping E, Ikeda S, Kong SW, Tarnavski O, Bodyak N, McMullen JR, Rajagopal S, Son JK, Ma Q, Springer Z, Kang PM, Izumo S, Pu WT. Gata4 is required for maintenance of postnatal cardiac function and protection from pressure overload-induced heart failure. *Proc Natl Acad Sci U S A*. 2006;103:14471-14476

140. Heineke J, Auger-Messier M, Xu J, Oka T, Sargent MA, York A, Klevitsky R, Vaikunth S, Duncan SA, Aronow BJ, Robbins J, Crombleholme TM, Molkentin JD. Cardiomyocyte gata4 functions as a stress-responsive regulator of angiogenesis in the murine heart. *J Clin Invest*. 2007;117:3198-3210

141. Yang YQ, Wang MY, Zhang XL, Tan HW, Shi HF, Jiang WF, Wang XH, Fang WY, Liu X. Gata4 loss-of-function mutations in familial atrial fibrillation. *Clin Chim Acta*. 2011;412:1825-1830

142. Jiang JQ, Shen FF, Fang WY, Liu X, Yang YQ. Novel gata4 mutations in lone atrial fibrillation. *Int J Mol Med*. 2011;28:1025-1032

143. Posch MG, Boldt LH, Polotzki M, Richter S, Rolf S, Perrot A, Dietz R, Ozcelik C, Haverkamp W. Mutations in the cardiac transcription factor gata4 in patients with lone atrial fibrillation. *Eur J Med Genet*. 2010;53:201-203

144. Boldt LH, Posch MG, Perrot A, Polotzki M, Rolf S, Parwani AS, Huemer M, Wutzler A, Ozcelik C, Haverkamp W. Mutational analysis of the pitx2 and nkx2-5 genes in patients with idiopathic atrial fibrillation. *Int J Cardiol*. 2010;145:316-317

145. Huang RT, Xue S, Xu YJ, Zhou M, Yang YQ. A novel nkx2.5 loss-of-function mutation responsible for familial atrial fibrillation. *Int J Mol Med*. 2013;31:1119-1126

146. Xie WH, Chang C, Xu YJ, Li RG, Qu XK, Fang WY, Liu X, Yang YQ. Prevalence and spectrum of nkx2.5 mutations associated with idiopathic atrial fibrillation. *Clinics (Sao Paulo)*. 2013;68:777-784

147. Briggs LE, Takeda M, Cuadra AE, Wakimoto H, Marks MH, Walker AJ, Seki T, Oh SP, Lu JT, Sumners C, Raizada MK, Horikoshi N, Weinberg EO, Yasui K, Ikeda Y, Chien KR, Kasahara H. Perinatal loss of nkx2-5 results in rapid conduction and contraction defects. *Circ Res*. 2008;103:580-590

148. Pashmforoush M, Lu JT, Chen H, Amand TS, Kondo R, Pradervand S, Evans SM, Clark B, Feramisco JR, Giles W, Ho SY, Benson DW, Silberbach M, Shou W, Chien KR. Nkx2-5 pathways and congenital heart disease; loss of ventricular myocyte lineage specification leads to progressive cardiomyopathy and complete heart block. *Cell*. 2004;117:373-386

149. Chung IM, Rajakumar G. Genetics of congenital heart defects: The nkx2-5 gene, a key player. *Genes (Basel)*. 2016;7

150. Jay PY, Harris BS, Maguire CT, Buerger A, Wakimoto H, Tanaka M, Kupershmidt S, Roden DM, Schultheiss TM, O'Brien TX, Gourdie RG, Berul CI, Izumo S. Nkx2-5 mutation causes anatomic hypoplasia of the cardiac conduction system. *J Clin Invest*. 2004;113:1130-1137

151. Jay PY, Rozhitskaya O, Tarnavski O, Sherwood MC, Dorfman AL, Lu Y, Ueyama T, Izumo S. Haploinsufficiency of the cardiac transcription factor nkx2-5 variably affects the expression of putative target genes. *FASEB J*. 2005;19:1495-1497

152. Furtado MB, Wilmanns JC, Chandran A, Tonta M, Biben C, Eichenlaub M, Coleman HA, Berger S, Bouveret R, Singh R, Harvey RP, Ramialison M, Pearson JT, Parkington HC, Rosenthal NA, Costa MW. A novel conditional mouse model for nkx2-5 reveals transcriptional regulation of cardiac ion channels. *Differentiation*. 2016;91:29-41

153. Garg V, Kathiriya IS, Barnes R, Schluterman MK, King IN, Butler CA, Rothrock CR, Eapen RS, Hirayama-Yamada K, Joo K, Matsuoka R, Cohen JC, Srivastava D. Gata4 mutations cause human congenital heart defects and reveal an interaction with tbx5. *Nature*. 2003;424:443-447

154. Ang YS, Rivas RN, Ribeiro AJ, Srivas R, Rivera J, Stone NR, Pratt K, Mohamed TM, Fu JD, Spencer CI, Tippens ND, Li M, Narasimha A, Radzinsky E, Moon-Grady AJ, Yu H, Pruitt BL, Snyder MP, Srivastava D. Disease model of gata4 mutation reveals transcription factor cooperativity in human cardiogenesis. *Cell*. 2016;167:1734-1749 e1722

155. Maitra M, Schluterman MK, Nichols HA, Richardson JA, Lo CW, Srivastava D, Garg V. Interaction of gata4 and gata6 with tbx5 is critical for normal cardiac development. *Dev Biol*. 2009;326:368-377

156. Nadeau M, Georges RO, Laforest B, Yamak A, Lefebvre C, Beauregard J, Paradis P, Bruneau BG, Andelfinger G, Nemer M. An endocardial pathway involving tbx5, gata4, and nos3 required for atrial septum formation. *Proc Natl Acad Sci U S A*. 2010;107:19356-19361

157. Stefanovic S, Barnett P, van Duijvenboden K, Weber D, Gessler M, Christoffels VM. Gata-dependent regulatory switches establish atrioventricular canal specificity during heart development. *Nat Commun*. 2014;5:3680

158. Takeuchi JK, Ohgi M, Koshiba-Takeuchi K, Shiratori H, Sakaki I, Ogura K, Saijoh Y, Ogura T. Tbx5 specifies the left/right ventricles and ventricular septum position during cardiogenesis. *Development*. 2003;130:5953-5964

159. Ding B, Liu CJ, Huang Y, Hickey RP, Yu J, Kong W, Lengyel P. P204 is required for the differentiation of p19 murine embryonal carcinoma cells to beating cardiac myocytes: Its

expression is activated by the cardiac gata4, nkx2.5, and tbx5 proteins. *J Biol Chem*. 2006;281:14882-14892

160. Linhares VL, Almeida NA, Menezes DC, Elliott DA, Lai D, Beyer EC, Campos de Carvalho AC, Costa MW. Transcriptional regulation of the murine connexin40 promoter by cardiac factors nkx2-5, gata4 and tbx5. *Cardiovasc Res*. 2004;64:402-411

161. Misra C, Chang SW, Basu M, Huang N, Garg V. Disruption of myocardial gata4 and tbx5 results in defects in cardiomyocyte proliferation and atrioventricular septation. *Hum Mol Genet*. 2014;23:5025-5035

162. Kasahara H, Benson DW. Biochemical analyses of eight nkx2.5 homeodomain missense mutations causing atrioventricular block and cardiac anomalies. *Cardiovasc Res*. 2004;64:40-51

163. Moskowitz IP, Kim JB, Moore ML, Wolf CM, Peterson MA, Shendure J, Nobrega MA, Yokota Y, Berul C, Izumo S, Seidman JG, Seidman CE. A molecular pathway including id2, tbx5, and nkx2-5 required for cardiac conduction system development. *Cell*. 2007;129:1365-1376

164. Postma AV, van de Meerakker JB, Mathijssen IB, Barnett P, Christoffels VM, Ilgun A, Lam J, Wilde AA, Lekanne Deprez RH, Moorman AF. A gain-of-function tbx5 mutation is associated with atypical holt-oram syndrome and paroxysmal atrial fibrillation. *Circ Res*. 2008;102:1433-1442

165. Luna-Zurita L, Stirnimann CU, Glatt S, Kaynak BL, Thomas S, Baudin F, Samee MA, He D, Small EM, Mileikovsky M, Nagy A, Holloway AK, Pollard KS, Muller CW, Bruneau BG. Complex interdependence regulates heterotypic transcription factor distribution and coordinates cardiogenesis. *Cell*. 2016;164:999-1014

166. Watt AJ, Battle MA, Li J, Duncan SA. Gata4 is essential for formation of the proepicardium and regulates cardiogenesis. *Proc Natl Acad Sci U S A*. 2004;101:12573-12578

167. Wheeler MT, Allikian MJ, Heydemann A, Hadhazy M, Zarnegar S, McNally EM. Smooth muscle cell-extrinsic vascular spasm arises from cardiomyocyte degeneration in sarcoglycan-deficient cardiomyopathy. *J Clin Invest*. 2004;113:668-675

168. Arnolds DE, Liu F, Fahrenbach JP, Kim GH, Schillinger KJ, Smemo S, McNally EM, Nobrega MA, Patel VV, Moskowitz IP. Tbx5 drives scn5a expression to regulate cardiac conduction system function. *The Journal of clinical investigation*. 2012;122:2509-2518

169. Pradhan L, Gopal S, Li S, Ashur S, Suryanarayanan S, Kasahara H, Nam HJ. Intermolecular interactions of cardiac transcription factors nkx2.5 and tbx5. *Biochemistry*. 2016;55:1702-1710

170. Molkentin JD, Lin Q, Duncan SA, Olson EN. Requirement of the transcription factor gata4 for heart tube formation and ventral morphogenesis. *Genes Dev*. 1997;11:1061-1072

171. Kuo CT, Morrisey EE, Anandappa R, Sigrist K, Lu MM, Parmacek MS, Soudais C, Leiden JM. Gata4 transcription factor is required for ventral morphogenesis and heart tube formation. *Genes Dev*. 1997;11:1048-1060

172. Lyons I, Parsons LM, Hartley L, Li R, Andrews JE, Robb L, Harvey RP. Myogenic and morphogenetic defects in the heart tubes of murine embryos lacking the homeo box gene nkx2-5. *Genes Dev*. 1995;9:1654-1666

173. He A, Kong SW, Ma Q, Pu WT. Co-occupancy by multiple cardiac transcription factors identifies transcriptional enhancers active in heart. *Proc Natl Acad Sci U S A*. 2011;108:5632-5637

174. White SM, Constantin PE, Claycomb WC. Cardiac physiology at the cellular level: Use of cultured hl-1 cardiomyocytes for studies of cardiac muscle cell structure and function. *Am J Physiol Heart Circ Physiol*. 2004;286:H823-829

175. Nattel S, Dobrev D. Electrophysiological and molecular mechanisms of paroxysmal atrial fibrillation. *Nat Rev Cardiol*. 2016;13:575-590

176. Christophersen IE, Rienstra M, Roselli C, Yin X, Geelhoed B, Barnard J, Lin H, Arking DE, Smith AV, Albert CM, Chaffin M, Tucker NR, Li M, Klarin D, Bihlmeyer NA, Low SK, Weeke PE, Muller-Nurasyid M, Smith JG, Brody JA, Niemeijer MN, Dorr M, Trompet S, Huffman J, Gustafsson S, Schurmann C, Kleber ME, Lyytikainen LP, Seppala I, Malik R, Horimoto A, Perez M, Sinisalo J, Aeschbacher S, Theriault S, Yao J, Radmanesh F, Weiss S, Teumer A, Choi SH, Weng LC, Clauss S, Deo R, Rader DJ, Shah SH, Sun A, Hopewell JC, Debette S, Chauhan G, Yang Q, Worrall BB, Pare G, Kamatani Y, Hagemeijer YP, Verweij N, Siland JE, Kubo M, Smith JD, Van Wagoner DR, Bis JC, Perz S, Psaty BM, Ridker PM, Magnani JW, Harris TB, Launer LJ, Shoemaker MB, Padmanabhan S, Haessler J, Bartz TM, Waldenberger M, Lichtner P, Arendt M, Krieger JE, Kahonen M, Risch L, Mansur AJ, Peters A, Smith BH, Lind L, Scott SA, Lu Y, Bottinger EB, Hernesniemi J, Lindgren CM, Wong JA, Huang J, Eskola M, Morris AP, Ford I, Reiner AP, Delgado G, Chen LY, Chen YI, Sandhu RK, Li M, Boerwinkle E, Eisele L, Lannfelt L, Rost N, Anderson CD, Taylor KD, Campbell A, Magnusson PK, Porteous D, Hocking LJ, Vlachopoulou E, Pedersen NL, Nikus K, Orho-Melander M, Hamsten A, Heeringa J, Denny JC, Kriebel J, Darbar D, Newton-Cheh C, Shaffer C, Macfarlane PW, Heilmann-Heimbach S, Almgren P, Huang PL, Sotoodehnia N, Soliman EZ, Uitterlinden AG, Hofman A, Franco OH, Volker U, Jockel KH, Sinner MF, Lin HJ, Guo X, ISGC MCot, Neurology Working Group of the CC, Dichgans M, Ingelsson E, Kooperberg C, Melander O, Loos RJF, Laurikka J, Conen D, Rosand J, van der Harst P, Lokki ML, Kathiresan S, Pereira A, Jukema JW, Hayward C, Rotter JI, Marz W, Lehtimaki T, Stricker BH, Chung MK, Felix SB, Gudnason V, Alonso A, Roden DM, Kaab S, Chasman DI, Heckbert SR, Benjamin EJ, Tanaka T, Lunetta KL, Lubitz SA,

Ellinor PT, Consortium AF. Large-scale analyses of common and rare variants identify 12 new loci associated with atrial fibrillation. *Nat Genet*. 2017;49:946-952

177. Nattel S, Shiroshita-Takeshita A, Brundel BJ, Rivard L. Mechanisms of atrial fibrillation: Lessons from animal models. *Prog Cardiovasc Dis*. 2005;48:9-28

178. Liu GS, Morales A, Vafiadaki E, Lam CK, Cai WF, Haghighi K, Adly G, Hershberger RE, Kranias EG. A novel human r25c-phospholamban mutation is associated with super-inhibition of calcium cycling and ventricular arrhythmia. *Cardiovasc Res*. 2015;107:164-174

179. Schmitt JP, Kamisago M, Asahi M, Li GH, Ahmad F, Mende U, Kranias EG, MacLennan DH, Seidman JG, Seidman CE. Dilated cardiomyopathy and heart failure caused by a mutation in phospholamban. *Science*. 2003;299:1410-1413

180. van der Zwaag PA, van Rijsingen IA, Asimaki A, Jongbloed JD, van Veldhuisen DJ, Wiesfeld AC, Cox MG, van Lochem LT, de Boer RA, Hofstra RM, Christiaans I, van Spaendonck-Zwarts KY, Lekanne dit Deprez RH, Judge DP, Calkins H, Suurmeijer AJ, Hauer RN, Saffitz JE, Wilde AA, van den Berg MP, van Tintelen JP. Phospholamban r14del mutation in patients diagnosed with dilated cardiomyopathy or arrhythmogenic right ventricular cardiomyopathy: Evidence supporting the concept of arrhythmogenic cardiomyopathy. *Eur J Heart Fail*. 2012;14:1199-1207

181. Hayward C, Banner NR, Morley-Smith A, Lyon AR, Harding SE. The current and future landscape of serca gene therapy for heart failure: A clinical perspective. *Hum Gene Ther*. 2015;26:293-304

182. Sikkel MB, Hayward C, MacLeod KT, Harding SE, Lyon AR. Serca2a gene therapy in heart failure: An anti-arrhythmic positive inotrope. *Br J Pharmacol*. 2014;171:38-54

183. Morihara H, Yamamoto T, Oiwa H, Tonegawa K, Tsuchiyama D, Kawakatsu I, Obana M, Maeda M, Mohri T, Obika S, Fujio Y, Nakayama H. Phospholamban inhibition by a single dose of locked nucleic acid antisense oligonucleotide improves cardiac contractility in pressure overload-induced systolic dysfunction in mice. *J Cardiovasc Pharmacol Ther*. 2017;22:273-282

184. Hoshijima M, Ikeda Y, Iwanaga Y, Minamisawa S, Date MO, Gu Y, Iwatate M, Li M, Wang L, Wilson JM, Wang Y, Ross J, Jr., Chien KR. Chronic suppression of heart-failure progression by a pseudophosphorylated mutant of phospholamban via in vivo cardiac raav gene delivery. *Nat Med*. 2002;8:864-871

185. Kaneko M, Hashikami K, Yamamoto S, Matsumoto H, Nishimoto T. Phospholamban ablation using crispr/cas9 system improves mortality in a murine heart failure model. *PLoS One*. 2016;11:e0168486

186. Zhu Y, Gramolini AO, Walsh MA, Zhou YQ, Slorach C, Friedberg MK, Takeuchi JK, Sun H, Henkelman RM, Backx PH, Redington AN, Maclennan DH, Bruneau BG. Tbx5-

dependent pathway regulating diastolic function in congenital heart disease. *Proc Natl Acad Sci U S A*. 2008;105:5519-5524

187. Roberts JD. Noncoding genetic variation and gene expression: Deciphering the molecular drivers of genome-wide association study signals in atrial fibrillation. *Circ Genom Precis Med*. 2018;11:e002109

188. Iyer LM, Nagarajan S, Woelfer M, Schoger E, Khadjeh S, Zafiriou MP, Kari V, Herting J, Pang ST, Weber T, Rathjens FS, Fischer TH, Toischer K, Hasenfuss G, Noack C, Johnsen SA, Zelarayan LC. A context-specific cardiac beta-catenin and gata4 interaction influences tcf7l2 occupancy and remodels chromatin driving disease progression in the adult heart. *Nucleic Acids Res*. 2018;46:2850-2867

189. Stevenson BR, Siliciano JD, Mooseker MS, Goodenough DA. Identification of zo-1: A high molecular weight polypeptide associated with the tight junction (zonula occludens) in a variety of epithelia. *J Cell Biol*. 1986;103:755-766

190. Fanning AS, Anderson JM. Zonula occludens-1 and -2 are cytosolic scaffolds that regulate the assembly of cellular junctions. *Ann N Y Acad Sci*. 2009;1165:113-120

191. Rodgers LS, Beam MT, Anderson JM, Fanning AS. Epithelial barrier assembly requires coordinated activity of multiple domains of the tight junction protein zo-1. *J Cell Sci*. 2013;126:1565-1575

192. Fanning AS, Jameson BJ, Jesaitis LA, Anderson JM. The tight junction protein zo-1 establishes a link between the transmembrane protein occludin and the actin cytoskeleton. *J Biol Chem*. 1998;273:29745-29753

193. Itoh M, Furuse M, Morita K, Kubota K, Saitou M, Tsukita S. Direct binding of three tight junction-associated maguks, zo-1, zo-2, and zo-3, with the cooh termini of claudins. *J Cell Biol*. 1999;147:1351-1363

194. Ebnet K, Schulz CU, Meyer Zu Brickwedde MK, Pendl GG, Vestweber D. Junctional adhesion molecule interacts with the pdz domain-containing proteins af-6 and zo-1. *J Biol Chem*. 2000;275:27979-27988

195. Furuse M, Itoh M, Hirase T, Nagafuchi A, Yonemura S, Tsukita S. Direct association of occludin with zo-1 and its possible involvement in the localization of occludin at tight junctions. *J Cell Biol*. 1994;127:1617-1626

196. Maiers JL, Peng X, Fanning AS, DeMali KA. Zo-1 recruitment to α-catenin--a novel mechanism for coupling the assembly of tight junctions to adherens junctions. *J Cell Sci*. 2013;126:3904-3915

197. Fanning AS, Ma TY, Anderson JM. Isolation and functional characterization of the actin binding region in the tight junction protein zo-1. *FASEB J*. 2002;16:1835-1837

198. Itoh M, Nagafuchi A, Moroi S, Tsukita S. Involvement of zo-1 in cadherin-based cell adhesion through its direct binding to alpha catenin and actin filaments. *J Cell Biol*. 1997;138:181-192

199. Itoh M, Nakadate K, Matsusaka T, Hunziker W, Sugimoto H. Effects of the differential expression of zo-1 and zo-2 on podocyte structure and function. *Genes Cells*. 2018;23:546-556

200. Roberts JD. Tjp1 mutations in arrhythmogenic cardiomyopathy. *Circ Genom Precis Med*. 2018;11:e002337

201. Bruce AF, Rothery S, Dupont E, Severs NJ. Gap junction remodelling in human heart failure is associated with increased interaction of connexin43 with zo-1. *Cardiovasc Res*. 2008;77:757-765

202. Nagasawa K, Chiba H, Fujita H, Kojima T, Saito T, Endo T, Sawada N. Possible involvement of gap junctions in the barrier function of tight junctions of brain and lung endothelial cells. *J Cell Physiol*. 2006;208:123-132

203. Zemljic-Harpf AE, Godoy JC, Platoshyn O, Asfaw EK, Busija AR, Domenighetti AA, Ross RS. Vinculin directly binds zonula occludens-1 and is essential for stabilizing connexin-43-containing gap junctions in cardiac myocytes. *J Cell Sci*. 2014;127:1104-1116

204. Eckardt D, Theis M, Degen J, Ott T, van Rijen HV, Kirchhoff S, Kim JS, de Bakker JM, Willecke K. Functional role of connexin43 gap junction channels in adult mouse heart assessed by inducible gene deletion. *J Mol Cell Cardiol*. 2004;36:101-110

205. Lim BK, Xiong D, Dorner A, Youn TJ, Yung A, Liu TI, Gu Y, Dalton ND, Wright AT, Evans SM, Chen J, Peterson KL, McCulloch AD, Yajima T, Knowlton KU. Coxsackievirus and adenovirus receptor (car) mediates atrioventricular-node function and connexin 45 localization in the murine heart. *J Clin Invest*. 2008;118:2758-2770

206. Lisewski U, Shi Y, Wrackmeyer U, Fischer R, Chen C, Schirdewan A, Jüttner R, Rathjen F, Poller W, Radke MH, Gotthardt M. The tight junction protein car regulates cardiac conduction and cell-cell communication. *J Exp Med*. 2008;205:2369-2379

207. Li J, Goossens S, van Hengel J, Gao E, Cheng L, Tyberghein K, Shang X, De Rycke R, van Roy F, Radice GL. Loss of αt-catenin alters the hybrid adhering junctions in the heart and leads to dilated cardiomyopathy and ventricular arrhythmia following acute ischemia. *J Cell Sci*. 2012;125:1058-1067

208. Zemljic-Harpf AE, Ponrartana S, Avalos RT, Jordan MC, Roos KP, Dalton ND, Phan VQ, Adamson ED, Ross RS. Heterozygous inactivation of the vinculin gene predisposes to stress-induced cardiomyopathy. *Am J Pathol*. 2004;165:1033-1044

209. Katsuno T, Umeda K, Matsui T, Hata M, Tamura A, Itoh M, Takeuchi K, Fujimori T, Nabeshima Y, Noda T, Tsukita S. Deficiency of zonula occludens-1 causes embryonic

lethal phenotype associated with defected yolk sac angiogenesis and apoptosis of embryonic cells. *Mol Biol Cell*. 2008;19:2465-2475

210. Testa G, Schaft J, van der Hoeven F, Glaser S, Anastassiadis K, Zhang Y, Hermann T, Stremmel W, Stewart AF. A reliable lacz expression reporter cassette for multipurpose, knockout-first alleles. *Genesis*. 2004;38:151-158

211. Sohal DS, Nghiem M, Crackower MA, Witt SA, Kimball TR, Tymitz KM, Penninger JM, Molkentin JD. Temporally regulated and tissue-specific gene manipulations in the adult and embryonic heart using a tamoxifen-inducible cre protein. *Circ Res*. 2001;89:20-25

212. Wu M, Peng S, Zhao Y. Inducible gene deletion in the entire cardiac conduction system using hcn4-creert2 bac transgenic mice. *Genesis*. 2014;52:134-140

213. Arnolds DE, Moskowitz IP. Inducible recombination in the cardiac conduction system of mink: Creert² bac transgenic mice. *Genesis*. 2011;49:878-884

214. Gemel J, Su Z, Gileles-Hillel A, Khalyfa A, Gozal D, Beyer EC. Intermittent hypoxia causes nox2-dependent remodeling of atrial connexins. *BMC Cell Biol*. 2017;18:7

215. Glukhov AV, Flagg TP, Fedorov VV, Efimov IR, Nichols CG. Differential k(atp) channel pharmacology in intact mouse heart. *J Mol Cell Cardiol*. 2010;48:152-160

216. Laughner JI, Ng FS, Sulkin MS, Arthur RM, Efimov IR. Processing and analysis of cardiac optical mapping data obtained with potentiometric dyes. *Am J Physiol Heart Circ Physiol*. 2012;303:H753-765

217. Weber CR, Raleigh DR, Su L, Shen L, Sullivan EA, Wang Y, Turner JR. Epithelial myosin light chain kinase activation induces mucosal interleukin-13 expression to alter tight junction ion selectivity. *J Biol Chem*. 2010;285:12037-12046

218. Cardiff RD, Miller CH, Munn RJ. Manual hematoxylin and eosin staining of mouse tissue sections. *Cold Spring Harb Protoc*. 2014;2014:655-658

219. Graham L, Orenstein JM. Processing tissue and cells for transmission electron microscopy in diagnostic pathology and research. *Nat Protoc*. 2007;2:2439-2450

220. Barker RJ, Price RL, Gourdie RG. Increased association of zo-1 with connexin43 during remodeling of cardiac gap junctions. *Circ Res*. 2002;90:317-324

221. Hervé JC, Bourmeyster N, Sarrouilhe D, Duffy HS. Gap junctional complexes: From partners to functions. *Prog Biophys Mol Biol*. 2007;94:29-65

222. Temple IP, Inada S, Dobrzynski H, Boyett MR. Connexins and the atrioventricular node. *Heart Rhythm*. 2013;10:297-304

223. Simon AM, Goodenough DA, Paul DL. Mice lacking connexin40 have cardiac conduction abnormalities characteristic of atrioventricular block and bundle branch block. *Curr Biol*. 1998;8:295-298

224. Severs NJ, Coppen SR, Dupont E, Yeh HI, Ko YS, Matsushita T. Gap junction alterations in human cardiac disease. *Cardiovascular research*. 2004;62:368-377

225. van Weerd JH, Christoffels VM. The formation and function of the cardiac conduction system. *Development*. 2016;143:197-210

226. Arnolds DE, Chu A, McNally EM, Nobrega MA, Moskowitz IP. The emerging genetic landscape underlying cardiac conduction system function. *Birth defects research. Part A, Clinical and molecular teratology*. 2011;91:578-585

227. Kirchhoff S, Nelles E, Hagendorff A, Krüger O, Traub O, Willecke K. Reduced cardiac conduction velocity and predisposition to arrhythmias in connexin40-deficient mice. *Curr Biol*. 1998;8:299-302

228. Laing JG, Manley-Markowski RN, Koval M, Civitelli R, Steinberg TH. Connexin45 interacts with zonula occludens-1 and connexin43 in osteoblastic cells. *J Biol Chem*. 2001;276:23051-23055

229. Nielsen PA, Beahm DL, Giepmans BN, Baruch A, Hall JE, Kumar NM. Molecular cloning, functional expression, and tissue distribution of a novel human gap junction-forming protein, connexin-31.9. Interaction with zona occludens protein-1. *J Biol Chem*. 2002;277:38272-38283

230. Bouvier D, Kieken F, Kellezi A, Sorgen PL. Structural changes in the carboxyl terminus of the gap junction protein connexin 40 caused by the interaction with c-src and zonula occludens-1. *Cell Commun Adhes*. 2008;15:107-118

231. Coyne CB, Voelker T, Pichla SL, Bergelson JM. The coxsackievirus and adenovirus receptor interacts with the multi-pdz domain protein-1 (mupp-1) within the tight junction. *J Biol Chem*. 2004;279:48079-48084

232. Sollerbrant K, Raschperger E, Mirza M, Engstrom U, Philipson L, Ljungdahl PO, Pettersson RF. The coxsackievirus and adenovirus receptor (car) forms a complex with the pdz domain-containing protein ligand-of-numb protein-x (lnx). *J Biol Chem*. 2003;278:7439-7444

233. Fabritz L, Kirchhof P, Fortmüller L, Auchampach JA, Baba HA, Breithardt G, Neumann J, Boknik P, Schmitz W. Gene dose-dependent atrial arrhythmias, heart block, and brady-cardiomyopathy in mice overexpressing a(3) adenosine receptors. *Cardiovasc Res*. 2004;62:500-508

234. Baruscotti M, Bucchi A, Viscomi C, Mandelli G, Consalez G, Gnecchi-Rusconi T, Montano N, Casali KR, Micheloni S, Barbuti A, DiFrancesco D. Deep bradycardia and

heart block caused by inducible cardiac-specific knockout of the pacemaker channel gene hcn4. *Proc Natl Acad Sci U S A*. 2011;108:1705-1710

235. Thomas SP, Kucera JP, Bircher-Lehmann L, Rudy Y, Saffitz JE, Kléber AG. Impulse propagation in synthetic strands of neonatal cardiac myocytes with genetically reduced levels of connexin43. *Circ Res*. 2003;92:1209-1216

236. Morley GE, Vaidya D, Samie FH, Lo C, Delmar M, Jalife J. Characterization of conduction in the ventricles of normal and heterozygous cx43 knockout mice using optical mapping. *J Cardiovasc Electrophysiol*. 1999;10:1361-1375

237. Akar FG, Spragg DD, Tunin RS, Kass DA, Tomaselli GF. Mechanisms underlying conduction slowing and arrhythmogenesis in nonischemic dilated cardiomyopathy. *Circ Res*. 2004;95:717-725

238. Van Itallie CM, Fanning AS, Bridges A, Anderson JM. Zo-1 stabilizes the tight junction solute barrier through coupling to the perijunctional cytoskeleton. *Mol Biol Cell*. 2009;20:3930-3940

239. Fanning AS, Van Itallie CM, Anderson JM. Zonula occludens-1 and -2 regulate apical cell structure and the zonula adherens cytoskeleton in polarized epithelia. *Mol Biol Cell*. 2012;23:577-590

240. Spadaro D, Tapia R, Jond L, Sudol M, Fanning AS, Citi S. Zo proteins redundantly regulate the transcription factor dbpa/zonab. *J Biol Chem*. 2014;289:22500-22511

241. De Bortoli M, Postma AV, Poloni G, Calore M, Minervini G, Mazzotti E, Rigato I, Ebert M, Lorenzon A, Vazza G, Cipriani A, Bariani R, Perazzolo Marra M, Husser D, Thiene G, Daliento L, Corrado D, Basso C, Tosatto SCE, Bauce B, van Tintelen JP, Rampazzo A. Whole-exome sequencing identifies pathogenic variants in tjp1 gene associated with arrhythmogenic cardiomyopathy. *Circ Genom Precis Med*. 2018;11:e002123

242. Veenhuyzen GD, Simpson CS, Abdollah H. Atrial fibrillation. *CMAJ*. 2004;171:755-760

243. Narayan SM, Franz MR, Clopton P, Pruvot EJ, Krummen DE. Repolarization alternans reveals vulnerability to human atrial fibrillation. *Circulation*. 2011;123:2922-2930

244. Pau D, Workman AJ, Kane KA, Rankin AC. Electrophysiological and arrhythmogenic effects of 5-hydroxytryptamine on human atrial cells are reduced in atrial fibrillation. *J Mol Cell Cardiol*. 2007;42:54-62

245. Narayan SM, Bode F, Karasik PL, Franz MR. Alternans of atrial action potentials during atrial flutter as a precursor to atrial fibrillation. *Circulation*. 2002;106:1968-1973

246. Sánchez C, Bueno-Orovio A, Wettwer E, Loose S, Simon J, Ravens U, Pueyo E, Rodriguez B. Inter-subject variability in human atrial action potential in sinus rhythm versus chronic atrial fibrillation. *PLoS One*. 2014;9:e105897

247. Li N, Timofeyev V, Tuteja D, Xu D, Lu L, Zhang Q, Zhang Z, Singapuri A, Albert TR, Rajagopal AV, Bond CT, Periasamy M, Adelman J, Chiamvimonvat N. Ablation of a ca2+-activated k+ channel (sk2 channel) results in action potential prolongation in atrial myocytes and atrial fibrillation. *J Physiol*. 2009;587:1087-1100

248. Dautova Y, Zhang Y, Sabir I, Grace AA, Huang CL. Atrial arrhythmogenesis in wild-type and scn5a+/delta murine hearts modelling lqt3 syndrome. *Pflugers Arch*. 2009;458:443-457

249. Olson TM, Alekseev AE, Liu XK, Park S, Zingman LV, Bienengraeber M, Sattiraju S, Ballew JD, Jahangir A, Terzic A. Kv1.5 channelopathy due to kcna5 loss-of-function mutation causes human atrial fibrillation. *Hum Mol Genet*. 2006;15:2185-2191

250. Venetucci LA, Trafford AW, O'Neill SC, Eisner DA. The sarcoplasmic reticulum and arrhythmogenic calcium release. *Cardiovasc Res*. 2008;77:285-292

251. Bers DM. Ca^{2+}-calmodulin-dependent protein kinase ii regulation of cardiac excitation-transcription coupling. *Heart Rhythm*. 2011;8:1101-1104

252. Beckendorf J, van den Hoogenhof MMG, Backs J. Physiological and unappreciated roles of camkii in the heart. *Basic Res Cardiol*. 2018;113:29

253. Uchinoumi H, Yang Y, Oda T, Li N, Alsina KM, Puglisi JL, Chen-Izu Y, Cornea RL, Wehrens XHT, Bers DM. Camkii-dependent phosphorylation of ryr2 promotes targetable pathological ryr2 conformational shift. *J Mol Cell Cardiol*. 2016;98:62-72

254. Van Petegem F. Ryanodine receptors: Structure and function. *J Biol Chem*. 2012;287:31624-31632

255. Ullrich ND, Valdivia HH, Niggli E. Pka phosphorylation of cardiac ryanodine receptor modulates sr luminal ca2+ sensitivity. *J Mol Cell Cardiol*. 2012;53:33-42

256. Mattiazzi A, Kranias EG. The role of camkii regulation of phospholamban activity in heart disease. *Front Pharmacol*. 2014;5:5

257. Terentyev D, Belevych AE, Terentyeva R, Martin MM, Malana GE, Kuhn DE, Abdellatif M, Feldman DS, Elton TS, Györke S. Mir-1 overexpression enhances ca(2+) release and promotes cardiac arrhythmogenesis by targeting pp2a regulatory subunit b56alpha and causing camkii-dependent hyperphosphorylation of ryr2. *Circ Res*. 2009;104:514-521

258. Hatcher CJ, Goldstein MM, Mah CS, Delia CS, Basson CT. Identification and localization of tbx5 transcription factor during human cardiac morphogenesis. *Dev Dyn*. 2000;219:90-95

259. Franco D, Meilhac SM, Christoffels VM, Kispert A, Buckingham M, Kelly RG. Left and right ventricular contributions to the formation of the interventricular septum in the mouse heart. *Dev Biol*. 2006;294:366-375

260. Xie L, Hoffmann AD, Burnicka-Turek O, Friedland-Little JM, Zhang K, Moskowitz IP. Tbx5-hedgehog molecular networks are essential in the second heart field for atrial septation. *Dev Cell*. 2012;23:280-291

261. Mori AD, Zhu Y, Vahora I, Nieman B, Koshiba-Takeuchi K, Davidson L, Pizard A, Seidman JG, Seidman CE, Chen XJ, Henkelman RM, Bruneau BG. Tbx5-dependent rheostatic control of cardiac gene expression and morphogenesis. *Dev Biol*. 2006;297:566-586

262. Uhlen M, Zhang C, Lee S, Sjöstedt E, Fagerberg L, Bidkhori G, Benfeitas R, Arif M, Liu Z, Edfors F, Sanli K, von Feilitzen K, Oksvold P, Lundberg E, Hober S, Nilsson P, Mattsson J, Schwenk JM, Brunnström H, Glimelius B, Sjöblom T, Edqvist PH, Djureinovic D, Micke P, Lindskog C, Mardinoglu A, Ponten F. A pathology atlas of the human cancer transcriptome. *Science*. 2017;357

263. Gessert S, Kühl M. The multiple phases and faces of wnt signaling during cardiac differentiation and development. *Circ Res*. 2010;107:186-199

264. Cerrone M, Montnach J, Lin X, Zhao YT, Zhang M, Agullo-Pascual E, Leo-Macias A, Alvarado FJ, Dolgalev I, Karathanos TV, Malkani K, Van Opbergen CJM, van Bavel JJA, Yang HQ, Vasquez C, Tester D, Fowler S, Liang F, Rothenberg E, Heguy A, Morley GE, Coetzee WA, Trayanova NA, Ackerman MJ, van Veen TAB, Valdivia HH, Delmar M. Plakophilin-2 is required for transcription of genes that control calcium cycling and cardiac rhythm. *Nat Commun*. 2017;8:106

265. Berryman MA, Goldenring JR. Clic4 is enriched at cell-cell junctions and colocalizes with akap350 at the centrosome and midbody of cultured mammalian cells. *Cell Motil Cytoskeleton*. 2003;56:159-172

266. Song X, Zhao Y, Narcisse L, Duffy H, Kress Y, Lee S, Brosnan CF. Canonical transient receptor potential channel 4 (trpc4) co-localizes with the scaffolding protein zo-1 in human fetal astrocytes in culture. *Glia*. 2005;49:418-429

267. Matter K, Balda MS. Signalling to and from tight junctions. *Nat Rev Mol Cell Biol*. 2003;4:225-236

268. Balda MS, Matter K. The tight junction protein zo-1 and an interacting transcription factor regulate erbb-2 expression. *EMBO J*. 2000;19:2024-2033

269. Dodane V, Kachar B. Identification of isoforms of g proteins and pkc that colocalize with tight junctions. *J Membr Biol*. 1996;149:199-209

270. de Almeida JB, Holtzman EJ, Peters P, Ercolani L, Ausiello DA, Stow JL. Targeting of chimeric g alpha i proteins to specific membrane domains. *J Cell Sci*. 1994;107 (Pt 3):507-515

271. Denker BM, Saha C, Khawaja S, Nigam SK. Involvement of a heterotrimeric g protein alpha subunit in tight junction biogenesis. *J Biol Chem*. 1996;271:25750-25753

272. Bhattacharyya S, Duan J, Wang L, Li B, Bhakta M, Fernandez-Perez A, Hon GC, Munshi NV. Using gjd3-creegfp mice to examine atrioventricular node morphology and composition. *Sci Rep*. 2019;9:2106

273. van Rijen HV, Eckardt D, Degen J, Theis M, Ott T, Willecke K, Jongsma HJ, Opthof T, de Bakker JM. Slow conduction and enhanced anisotropy increase the propensity for ventricular tachyarrhythmias in adult mice with induced deletion of connexin43. *Circulation*. 2004;109:1048-1055

274. Akar FG, Nass RD, Hahn S, Cingolani E, Shah M, Hesketh GG, DiSilvestre D, Tunin RS, Kass DA, Tomaselli GF. Dynamic changes in conduction velocity and gap junction properties during development of pacing-induced heart failure. *Am J Physiol Heart Circ Physiol*. 2007;293:H1223-1230

275. Gros DB, Jongsma HJ. Connexins in mammalian heart function. *Bioessays*. 1996;18:719-730

276. Söhl G, Willecke K. Gap junctions and the connexin protein family. *Cardiovasc Res*. 2004;62:228-232

277. Severs NJ, Dupont E, Coppen SR, Halliday D, Inett E, Baylis D, Rothery S. Remodelling of gap junctions and connexin expression in heart disease. *Biochim Biophys Acta*. 2004;1662:138-148

278. MOE GK, PRESTON JB, BURLINGTON H. Physiologic evidence for a dual a-v transmission system. *Circ Res*. 1956;4:357-375

279. Medkour D, Becker AE, Khalife K, Billette J. Anatomic and functional characteristics of a slow posterior av nodal pathway: Role in dual-pathway physiology and reentry. *Circulation*. 1998;98:164-174

280. George SA, Faye NR, Murillo-Berlioz A, Lee KB, Trachiotis GD, Efimov IR. At the atrioventricular crossroads: Dual pathway electrophysiology in the atrioventricular node and its underlying heterogeneities. *Arrhythm Electrophysiol Rev*. 2017;6:179-185

281. Hucker WJ, Nikolski VP, Efimov IR. Optical mapping of the atrioventricular junction. *J Electrocardiol*. 2005;38:121-125